UNIVERSITÉ
LAVAL

Modelling and Model-Based Optimization of N-Removal WRRFs: Reactive Settling, Conventional & Short-Cut N-Removal Processes

Thèse

Gamze Kirim

Doctorat en génie des eaux
Philosophiæ doctor (Ph. D.)

Québec, Canada

Modelling and Model-Based Optimization of N-Removal WRRFs:
Reactive Settling, Conventional & Short-Cut N-Removal Processes

Thèse
Génie des eaux

Gamze KIRIM

Sous la direction de:

Peter. A. VANROLLEGHEM, directeur de recherche
Elena TORFS, codirectrice de recherche

Résumé

La détérioration des ressources en eau et la grande quantité d'eau polluée générée dans les sociétés industrialisées donnent une importance fondamentale aux procédés de traitement des eaux usées pour préserver les ressources, conformément à l'objectif 6 des 17 objectifs de développement durable des Nations Unies. Le rejet de nutriments tels que l'ammoniac par les eaux usées est un problème important, l'élimination de l'azote (N) est donc l'un des processus critiques de toute station de récupération des ressources en eau (StaRRE). L'objectif de ce projet de recherche doctoral est d'améliorer la compréhension des mécanismes d'élimination de l'azote dans le traitement biologique des eaux usées grâce à la modélisation, et d'optimiser les StaRRE existantes pour réduire la consommation d'énergie et de ressources. Dans ce cadre, 3 études différentes ont été réalisées.

Tout d'abord, un modèle de décanteur réactif unidimensionnel a été développé. Celui-ci prédit le comportement de décantation de boues à des concentrations élevées de boues ainsi que les conversions biocinétiques dans le processus de décantation secondaire (DS). Il a été constaté qu'une description précise des réactions biocinétiques dans la DS impose des défis de calibration élevés pour le modèle de décantation, car ce dernier doit capturer les profils de concentration complets de la biomasse active dans la couverture de boues. Le modèle calibré a pu prédire avec précision les profils de concentration des effluents et du lit de boues dans la DS. Le modèle développé peut être utilisé pour le contrôle et la simulation des StaRRE afin d'obtenir de meilleures prédictions des concentrations d'effluents et des boues de retour, et aussi de calculer correctement le bilan massique d'azote d'une StaRRE.

Deuxièmement, un modèle à l'échelle de l'usine a été mis en place pour un système de pré-dénitrification conventionnel pour la StaRRE pilEAUte à l'échelle pilote. Une méthodologie de calibration du modèle par étapes a été adoptée en fusionnant les principaux protocoles de calibration de modèle, tout en mettant l'accent sur le modèle biocinétique. Le modèle de la StaRRE pilEAUte, y compris le décanteur réactif développé, a été calibré et validé pour simuler les variables de modèle sélectionnées, puis utilisé pour une analyse de scénarios plus approfondie de l'optimisation de la consommation d'énergie et des ressources. Les résultats de l'analyse des scénarios ont montré le potentiel d'optimisation du système conventionnel d'élimination d'azote grâce à 'la réduction de 'l'aération et du retour interne des nitrates. Ils ont également démontré que la dénitrification dans le décanteur secondaire peut avoir une contribution significative à la capacité globale d'élimination d'azote d'une StaRRE lorsque la liqueur mixte peut traverser le lit de boues.

Troisièmement, l'étude visait à évaluer l'applicabilité des stratégies de commande continu et intermittent du rapport de l'ammoniac par rapport aux NOX-N (commande AvN) sur la StaRRE pilEAUte. Les stratégies de commande de l'aération par AvN sont appliquées en amont d'un réacteur de désammonification, qui est un

processus d'élimination efficace d'azote avec un besoin de ressources réduit (en termes d'aération et carbone) par rapport aux systèmes conventionnels. Les deux stratégies de commande testées pourraient être réalisées grâce à une commande automatique. Cependant, le maintien du rapport AvN dans l'effluent à la valeur souhaitée (1) dépend fortement des conditions opérationnelles telles que les variations de l'affluent, le temps de rétention des boues et la fiabilité des capteurs.

Même si la recherche est guidée par les études de StaRRE à l'échelle pilote', les méthodologies développées pour démontrer et modéliser les processus et les conditions opérationnelles économes en énergie et en ressources sont applicables et transférables à d'autres études de cas à plein échelle.

Abstract

Deterioration of water resources and the large amount of polluted water generated in industrialized societies gives fundamental importance to wastewater treatment processes to preserve resources in accordance with goal 6 of the 17 sustainable development goals of the United Nations. Discharge of nutrients such as ammonia with wastewater is a significant issue, thus nitrogen (N) removal is one of the critical processes of any water resource recovery facilities (WRRF). The objective of this PhD research project was to improve the understanding of N-removal mechanisms in biological treatment of wastewater through modelling and to optimize existing WRRFs to reduce energy and resource consumption. Within this context, 3 different studies were carried out.

First, a one dimensional reactive settler model was developed that predicts the settling behaviour at high sludge concentrations together with biokinetic conversions in the secondary settling process. It was found that an accurate description of biokinetic reactions in the SST puts high calibration requirements on the settling model as it must properly capture the full concentration profiles of active biomass in the sludge blanket. The calibrated model was able to accurately predict the effluent and sludge blanket concentration profiles in the SST. The developed model can be used for control and simulation of WRRFs for better predictions of SST effluent and underflow concentrations and also properly calculate the nitrogen mass balance of a WRRF.

Second, a plant-wide model was set up for a conventional pre-denitrification system for the pilot-scale pilEAUte WRRF. A step-wise model calibration methodology was adopted by merging main existing model calibration protocols while placing emphasis on the biokinetic model. The pilEAUte model, including the developed reactive settler, was calibrated and validated to simulate the selected model variables and used for further scenario analysis for energy and resource optimization. The scenario analysis results showed the optimization potential of conventional N removal systems through application of reduced aeration and internal nitrate recycling. It also demonstrated that denitrification in the secondary settler can contribute significantly to the overall N removal capacity of the WRRF when mixed liquor can pass through the sludge blanket.

Third, it was aimed to evaluate the applicability of continuous and intermittent Ammonia vs NO_X-N (AvN) control strategies on the pilEAUte WRRF. The AvN aeration control strategies are applied prior to a deammonification stage which is a short-cut N removal process with reduced resource (aeration and carbon) requirements in comparison to conventional systems. Both strategies could be achieved through automatic control. However, keeping the AvN ratio in the effluent on the desired value highly depends on operational conditions such as influent variations, sludge retention time and the sensor's measurement reliability.

Even though this research is driven by case studies applied to a pilot-scale WRRF, the developed methodologies to demonstrate and model the energy and resource-efficient processes and operational conditions are applicable and transferable to other full-scale case studies.

Contents

List of Figures

List of Tables

List of Abbreviations

AOB:	Ammonia oxidizing bacteria
AvN:	Ammonia vs NO_X-N control
ASM:	Activated sludge model
BD model:	Bürger-Diehl model
BOD:	Biochemical oxygen demand
CFD:	Computational fluid dynamics
COD:	Chemical oxygen demand
DO:	Dissolved oxygen
GHG:	Greenhouse gas
GMP:	Good modelling practice
HB:	Heterotrophic bacteria
IR:	Internal recycle
NOB:	Nitrite-oxidizing bacteria
ODE:	Ordinary differential equation
PAO:	Phosphorus accumulating organisms
SBH:	Sludge blanket height
SBR:	Sequencing batch reactor
SND:	Simultaneous nitrification and denitrification
SRT:	Sludge retention time
SST:	Secondary settling tank
TIN:	Total inorganic nitrogen
TKN:	Total Kjeldahl nitrogen
TN:	Total nitrogen
TSS:	Total suspended solids
VSS:	Volatile suspended solids
WRRF:	Water resource recovery facility

Acknowledgements

This academic journey has been a surging and enjoyable adventure in my life. This big leap would not be possible to achieve without the support and guidance of many people. I would like to express my gratitude to the people who have contributed to the completion of this work. I would like to thank all of you from the bottom of my heart and hope to work with you again in future.

I would like to express my sincere gratitude to my supervisor Prof. *Peter A. Vanrolleghem* who gave me the opportunity to be one of his PhD students in the model*EAU* research team and his continuous support during my PhD. It was a great pleasure to work with you and learn from you Peter! Thank you so much for this great experience and the occasion to work at the pilEAUte! Also, I am extremely grateful for all your support to my extracurricular activities and the invaluable network that I gained during my PhD through the International Water Association, the Young Water Professionals Canada, the Modelling and Integrated Assessment Specialist Group and more. I would also like to thank to my co-supervisor Dr. *Elena Torfs* who guided me since the first day of my PhD. Thank you so much Elena for all your support, insights and contributions all along the way. Your support was really influential in shaping my experimental campaigns, model development and evaluating my results.

I would also like to express my gratitude towards the members of my jury Prof. Paul Lessard, Prof. Ulf Jeppsson and Dr. Charles Bott, whose in-depth comments and feedback were not only very much appreciated but also greatly improved the final version of this PhD dissertation.

I would also like to thank the former and the current model*EAU* research team members, especially to *Romain Philippe, Andreia Amaral, and Sovanna Tik*. It had been such a pleasure to work with you all and it will always be remembered. Thanks for the research discussions, your support and friendship! Also, thanks to the pilEAUte team which gave me the opportunity to lead, learn and teamwork!Thanks to my dearest friends *Oluş Uyar* and *Dafni Synodinou* for being my family in Québec! I am very lucky that I have you guys in my life and thank you for all your support! And then there is *Titouan Royal* as well who was a great company and source of motivation. Thanks *Titu* for being on my side and encouraging me to finalize this work!

Last but not the least, I would like to thank my family: my parents and to my brother for supporting me spiritually throughout this journey and my life in general.

INTRODUCTION

Water is the most valuable natural resource in the world and the necessity for clean water resources increases rapidly due to the progressive increment of population and urbanization, development of industrial production activities and agriculture, and also climate change. On the other hand, more than half of the global population does not have access to safe sanitation (Unicef 2021), and 80% of the world's wastewater is released into the environment without adequate treatment (World Bank 2020). Therefore, deterioration of water resources and the large amount of polluted water generated in industrialized societies gives fundamental importance to wastewater treatment processes to preserve resources.

Discharge of nutrients with wastewater such as ammonia at high concentrations causes negative effects on receiving water bodies. Many industrial and agricultural activities generate high nitrogen (N) content wastewaters, and ammonium is one of the major pollutants in municipal wastewater. It is highly toxic in aquatic environments and nitrification consumes dissolved oxygen which results in oxygen depletion. Also, it causes eutrophication which is one of the most widespread environmental problems of inland waters (UNEP 2001). Thus, N-removal is a significant issue. Today, a reliable wastewater management system is one of the critical elements of any urban utility's infrastructure insofar as it enables society to have an acceptable quality of life and ensures economic development in industry and trade. Besides this, the recovery of resources from wastewater, especially nutrients and energy, is attracting attention, like the water itself.

National and international regulations enforce the adoption of specific quality indexes for the treated wastewater in many parts of the world. Taking into account current environmental problems, it is not unrealistic to believe that this trend will continue. The Pan-Canadian Strategy for the Management of Municipal Wastewaters and the Municipal Wastewater Treatment Regulations and Environmental Quality Act restrict effluent wastewater quality for Québec in terms of organic material such as biochemical oxygen demand and total suspended solids. These restrictions are also extended by the introduction of a toxicity standard that is often directly related to the presence of ammonia nitrogen in non-ionized form (CCME 2009) (LégisQuébec 2017). Wastewater Systems Effluent Regulations limit wastewater discharges in the scope of the Fisheries Act (SOR/2012-139) in many parts of Canada. It imposes discharge criteria as in the Pan-Canadian Strategy but also requires the maximum concentration of un-ionized ammonia in the effluent to be less than 1.25 mg/L explicitly. As effluent criteria become more stringent and available funds for upgrades/expansions become less available, efficient treatment processes are gaining importance in terms of energy and resource consumption and also effluent water quality.

The challenges in wastewater treatment and discharge criteria lead to the need for process optimization. Researchers are now focusing on the design and optimization of processes through imitation and simulation of

environmental problems with the help of mathematical modelling. Modelling can be used to evaluate different process alternatives or to design process control to improve the operation of existing plants. It can also be helpful for process understanding and for identification of more efficient process modifications (Gernaey et al. 2004). The advantage of having to simultaneously ensure effluent requirements, process safety, investment and operation costs makes modelling a useful tool for designers (Rivas et al. 2008). Accordingly, modelling serves as a time and cost-saving tool for the evaluation of new wastewater treatment concepts and it helps to bridge the gap between lab and full-scale applications (Salem et al. 2002).

The objective of this PhD research project is to improve the understanding of N-removal mechanisms in the biological treatment of wastewater through modelling and optimize existing water resource recovery facilities (WRRFs) to reduce energy and resource consumption. Within this context, three different studies were carried out. First, a one dimensional reactive settler model was developed that predicts the settling behaviour at high sludge concentrations together with biokinetic conversions in the secondary settling process. It is the first modelling work that combines the full set-of ASM1 biokinetics with the 1-D Bürger-Diehl settling model, which includes compression and is supported with pilot-scale measurement campaign data. The developed model can be used for control and simulation of WRRFs with scenario analysis. Second, a plant-wide model was set up for a conventional pre-denitrification system. The model is calibrated and validated with pilot-scale WRRF data and the inclusion of the developed reactive settler model allows it to be used to demonstrate the optimization potential through the use of reactions in the settling tanks. Third, a simultaneous nitrification-denitrification (SND) process was applied in the pilot-scale WRRF to demonstrate the applicability of different aeration control approaches called Ammonia vs NO_X-N (AvN) control.

This PhD dissertation includes 9 chapters as follows.

Introduction: A short introduction to shortly present the need for appropriate wastewater treatment processes and the objectives.

Chapter 1 – Literature Review: The definition of water resource and recovery, energy and resource consumption in WRRFs and how modelling can be used as a tool to optimize the facilities. The chapter also provides an overview of the available mathematical models for biokinetics and the settling process.

Chapter 2 – Problem Statement & Objectives: Explains the motivation of this PhD research project and its main objectives.

Chapter 3 – Materials & Methods: Describes the pilot-scale WRRF as the data source, the modelling methodology applied and the modelling platform that was used in this research project.

Chapter 4 – Development of a 1-D Reactive Settler Model: Describes the developed reactive settler model and its calibration procedure with the results.

Chapter 5 – Modelling of Biological N-removal Processes: Describes the model set-up for the conventional N-removal process and focuses on the calibration methodology.

Chapter 6 – Application of Aeration Control Strategies for Simultaneous N-Removal: Explains the application of the intermittent and continuous AvN control systems in the pilot-scale WRRF.

Chapter 7 – Scenario Analysis: Describes the different scenarios applied in the conventional N-removal process model for process optimization together with their results.

Conclusions & Perspectives: The main results of the PhD research project and future perspectives.

1. LITERATURE REVIEW

1.1 Water Resource and Recovery Concept and Challenges

Wastewater is considered a resource due to the energy and chemicals contained within it. Water resource recovery facilities (WRRFs) - previously called wastewater treatment plants - are no longer waste disposal facilities thanks to the resources that can be recovered, such as clean water production, nutrient recovery & the potential to produce and use renewable energy and implement energy conservation (WEF 2015). WRRFs directly contribute to the circular economy and create valuable products while reducing the amount of waste produced (WEF 2020). The first value that is produced by the WRRFs is the clean, treated effluent which can be reused for beneficial purposes, such as agriculture and irrigation, potable water supply, groundwater replenishment, industrial processes, and environmental restoration (EPA 2021). Biogas is another in-situ source of energy produced in WRRFs with the digestion of organic material of the primary and wasted biological sludge (Metcalf&Eddy 2014). Also, many streams in a WRRF are rich in nitrogen and phosphorus. Different processes for the recovery of nutrients from wastewater are being applied and end products have market potential (Vaneeckhaute et al. 2017; Kehrein et al. 2020).

The energy embodied in wastewater can be divided into three main types. The largest portion of recoverable energy from wastewater is thermal energy which, as low-grade heat, could be captured to heat or cool houses or to generate electricity. Chemical energy is the second type due to the organic matter content of wastewater which can be broken down and transformed into fuels such as biogas. The third one is hydraulic energy that can be captured when water flowing downhill or under pressure can be reused in mechanical systems in the plant (WERF & NYSERDA 2015; NSF, DOE & EPA 2015).

However, many WRRFs are not able to operate optimally due to their design and operation. This situation requires focusing on accurate process application and process optimization in WRRFs to reduce environmental impact, meet the discharge criteria, improve effluent quality and reduce the excess operating costs (Hackworth 2013). On the other hand, as effluent criteria become more stringent with legislation and available funds for upgrades/expansions become less available, efficient treatment processes are gaining importance in terms of energy and chemical consumption and effluent water quality (EPA 1972; EU 2000; SOR/2012-139).

Resource consumption in wastewater treatment also has significant environmental consequences and it is important to view WRRF performance holistically including electricity consumption for aeration and pumping, carbon, alkalinity, or chemical coagulants which are used to improve treatment and sludge handling efficiency (Fitzsimons et al. 2012; World Bank 2019). WRRFs will be obligated to reduce the energy consumption per unit of water treated to be able to become energy-neutral or net energy positive. However, current WRRFs require

several energy-intensive processes, led by aeration (Ramirez 2015). On the other hand, consumption of energy and biokinetic conversion processes lead to the production of GHGs in WRRFs - especially in biological N-removal processes - such as methane, nitrous oxide, and carbon dioxide, thus contributing to global warming (IPCC 2019)

WRRFs capable of removing nitrogen are crucial to treat the wastewater and produce clean and safe effluent through the removal of nutrients, organics, and many pollutants, thus reducing the environmental impacts caused by human activities. However, they still face the challenges mentioned above and thus require optimizing existing processes or apply more efficient treatment processes. All these challenges in wastewater treatment lead to the need for process optimization.

1.2 Energy & Resource Consumption in WRRFs

Wastewater treatment is an energy-intensive process and WRRFs are one of the major energy consumers at the municipal level worldwide (McCormick and Chakrabarti 2013; Capodaglio and Olsson 2020). Energy is required in all stages of treatment, from the collection of raw sewage to the discharge of the effluent and primary energy uses are those directly associated with on-site electrical power and fuel requirements (Daw et al. 2012; Li et al. 2021). The International Energy Agency (2016) estimates a 130% increment in total energy consumption for the water treatment industry until 2040. Therefore, energy consumption is one of the largest expenses in operating a WRRF and operating costs for electricity are now raised as a major concern. Reducing energy costs is not only an economical challenge for the future but also an environmental necessity due to their carbon footprints (EPA 2013). Studies show that especially energy cost is a significant part of the overall operational cost depending on the treatment processes (Kolisch et al. 2008; Trapote et al. 2014; Gikas 2017; WERF 2010).

Energy is consumed throughout the plant, but the most intensive use is during the primary and secondary stages of conventional wastewater treatment (U.S. Department of Energy 2017). Figure 1.1 shows a typical breakdown of the energy consumption of a WRRF using activated sludge (Adapted from (WEF 2010) & (McCormick and Chakrabarti 2013)). Generally, aeration is the largest energy user, followed by pumping actions, sludge handling, and mixing processes.
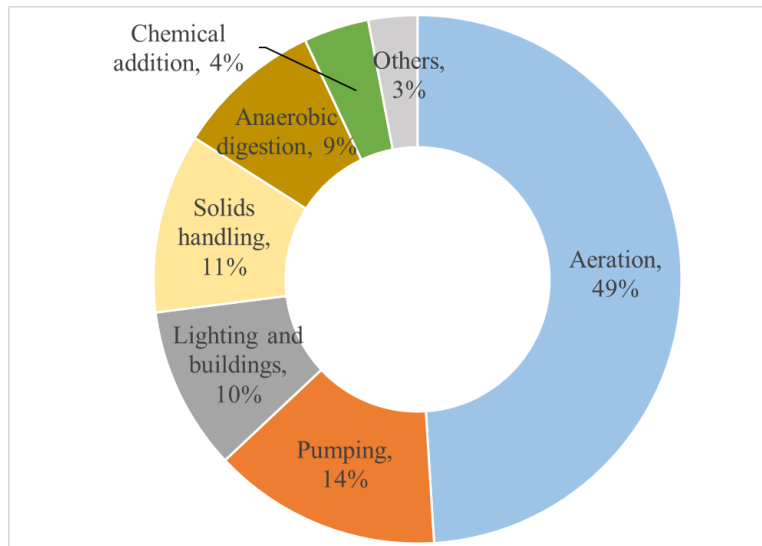
Figure 1.1 Energy Consumption in a Conventional Activated Sludge Plant (WEF 2010; McCormick and Chakrabarti 2013)

Aeration provides oxygen for metabolizing autotrophic and heterotrophic microorganisms that grow and remove pollutants under aerobic conditions and also provide mixing which assures that microorganisms consume organic matter and nutrients in wastewater. The aerobic process is dependent on the dissolved oxygen (DO) concentration in the reactor and it serves as the electron acceptor for the decomposition of organic carbon and oxidation of ammonia. In order to prevent oxygen diffusion from becoming the rate-limiting step, the air is continuously added to the reactor (International Energy Agency 2016). The energy used for aeration can vary 40-65% of the total energy consumption in activated sludge systems including N-removal (Metcalf&Eddy 2014; Olsson 2012; Rosso, et al. 2011). In extended aeration activated sludge systems the energy devoted to aeration can reach 75% of the plant's total energy consumption (Rosso et al. 2008).Thus, it is worth investing in aeration optimisation as it holds enormous saving potential (Amaral et al. 2017).

Energy consumption in aeration systems is related to several key factors such as diffuser type, oxygen transfer rate, oxygen transfer efficiency and DO concentration in the mixed liquor (EPA 2010). Generally, DO concentrations in suspended growth activated sludge systems for organic carbon and N-removal should be between 0.5 to 2.0 mg/L depending on the influent characteristics and the treatment level (WEF 2009); 1.0-2.0 mg/L reported by EPA (2010). If the necessary DO concentration can be decreased, the aeration rate would also decrease thanks to the increased driving force, which results in energy savings.

Short-cut N-removal processes with lower aeration need than the conventional processes are still in the development phase and challenging to apply in mainstream treatment (Cao et al. 2017; Le et al. 2019; Kirim et al. 2022). On the other hand, it is important to improve the general understanding of oxygen transfer for

enhanced aeration efficiency in aerobic biological wastewater treatment (Amaral et al. 2019). Technologies and energy-efficient solutions across the treatment system are urgently needed to reduce the energy requirements of aeration or alternative processes should be provided. Auditing and applying best practices on the less energy-consuming parts of the WRRFs - such as pumping or heating - can also reduce the total energy consumed for wastewater treatment. Still, to become net-energy positive or energy neutral WRRFs, energy reduction efforts should focus on aeration (NSF, DOE & EPA 2015).

Pumping of wastewater (in-plant) is usually the second most energy consuming component of wastewater treatment that may take up to 14% of the total energy consumption (WEF 2010). In a conventional N-removing WRRF, pumping is needed to mainly lift the wastewater to primary treatment units and then to biological treatment units. Also, it includes the transfer of mixed liquor from the biological tanks to secondary clarifiers and sometimes the discharge of effluent to the receiving environment. Sludge pumping activities include sludge recycling, internal sludge recycle, sludge wasting and transfer of sludge in the sludge handling facilities. Pumping-associated energy demand is generally proportional to the volume of wastewater or sludge that must be moved around the plant. These pumps would require less energy if the waste streams are better separated initially to reduce volume and increase their homogeneity (NSF, DOE & EPA 2015). Depending on the adopted system boundaries, some assessments may include energy for pumping wastewater to the plant, while others do not, hence a wide range of reported values exist in literature. Since most of the WRRFs are constructed on flat terrain, pumping cannot be avoided, however, energy consumption can be minimized with the proper design of the internal hydraulic profile (Capodaglio and Olsson 2020).

Especially the internal sludge recycle in pre-denitrification systems cause a significant energy consumption due to the high volumes of mixed liquor to be transferred (Metcalf&Eddy 2014; Qasim and Zhu 2018). Indeed, when N-removal is part of the wastewater treatment process, an internal sludge recycle is often required. Denitrification is essential to remove the nitrate which is produced in the aerated biological reactor. For that reason, the mixed liquor in the activated sludge tank is sent to the anoxic part of the reactor -where fresh COD is supplied from the wastewater- through an internal recycle stream in pre-denitrification configurations. The internal recycle flow rate varies between 1 to 6 times the influent flow rate depending on the treatment process (Metcalf&Eddy 2014; Wang et al. 2009). As a result, the internal recycle can be an important energy consumer due to the required energy for pumping. To reduce the internal sludge recycle energy consumption, alternative tank designs can be applied in WRRFs, which fulfil internal recycle through the recirculation of nitrified mixed liquor within the bioreactor; e.g. Carrousel® and Orbal® systems.

Sludge handling and management require a substantial portion of energy consumption and chemical addition (Chen and Chen 2013; Kato et al. 2019). Sludge handling generally covers thickening, digestion, dewatering

and drying of excess sludge. Sludge treatment is not in the scope of this PhD project, and for that reason, it is not discussed in detail here. However, it is known that the physical unit processes to increase the solids concentration in the activated sludge may consume up to 10% of the overall energy consumption in WRRFs (McCormick and Chakrabarti 2013; WEF 2013; Tao and Chengwen 2012). It is another aspect of operating cost in wastewater treatment and the method of sludge dewatering and disposal can have a significant impact on total energy use in WRRF (Fitzsimons et al. 2012). So, it is quite important to control the excess sludge amount and characterization both for the performance of the activated sludge system and the sludge treatment facilities (WEF 2013; Tao and Chengwen 2012).

Besides energy, chemicals are another resource that is being consumed in wastewater treatment that can either be necessary directly for the chemical treatment of wastewater or improve physical and biological treatment processes (Metcalf&Eddy 2014). Biological N-removal in wastewater with high nitrogen contents can become a major cost factor due to chemical consumption, in particular when the wastewater contains insufficient amounts of biodegradable carbon compounds (Seyfried et al. 2011). It is also possible to achieve N-removal by post-denitrification which necessitates two reactors in series, the first aerobic and the second anoxic. The anoxic reactor receives the nitrate-rich effluent of the first aerated tank and performs denitrification at a relatively slow rate dictated by endogenous decay. Therefore, a very large anoxic volume or carbon addition may be required to reach a high denitrification efficiency (Orhon and Artan 1994). Also, the alkalinity consumption in the nitrification process may necessitate alkalinity addition to the process. Indeed, a significant amount of bicarbonate (HCO$_3^-$) is consumed in the oxidation of ammonia (NH_4^+) to nitrite (NO_3^{-}) (EPA 2002). Stoichiometric calculations indicate 7.14 mg/L of alkalinity destroyed for the oxidation of 1 mg/L NH_4^+-N to NO_3^--N and pH will be reduced (Benninger and Sherrard 1978). A model developed by Gujer and Jenkins (1975) indicates that 8.64 mg/L of bicarbonate will be utilized for each mg/L of NH_4^+-N oxidized. Lack of carbonate alkalinity stops nitrification since the organism is pH-sensitive and rates of nitrification will reduce significantly at pH values below 6.8 (Evans and Sober 2015). It can also be used as a control parameter to limit nitrification in short-cut N-removing processes (Bagchi et al. 2010). Denitrification only partially compensates the alkalinity loss caused by nitrification in pre-denitrification systems, as the alkalinity gain per mg of N is only one-half of the loss caused by nitrification (Metcalf&Eddy 2014). Thus, alkalinity can be a significant source of chemical consumption in N-removing activated sludge systems depending on the ammonia and alkalinity content of wastewater and of course the volume of wastewater to be treated.

1.3 Modelling of Wastewater Treatment Processes

The challenges in wastewater treatment, high energy and resource consumption mentioned in Chapter 1.2, lead to the need for process optimization. Researchers are focusing on the design, control and optimization of the processes through imitation and simulation of environmental problems with the help of mathematical modelling

(Zhang et al. 2009; Kim et al. 2015; Ortiz-Martínez et al. 2021). A model is an approximate representation of a real system that is used to simulate its behaviour. A system or a process can be defined with mathematical models and can be analyzed instead of the real system. Then it is possible to apply what is learnt from the behaviour of the models to the real systems (Gujer 2008). Modelling and dynamic simulation of WRRFs has become a commonly used tool for design, control and optimization of treatment processes with the family of Activated Sludge Models (Henze et al. 2006).

Modelling can be used to evaluate different process alternatives or to design control to improve the operation of existing plants. It can also be helpful for process understanding and an indication of more efficient process modifications (Gernaey et al. 2004). It can identify the conditions to better understand the microbial competition under different operational and environmental conditions to optimize the processes (Shourjeh et al. 2021). Dynamic simulation not only became an important tool for scientific studies but also confirmed its usefulness in general wastewater treatment practice (Langergraber et al. 2004). The advantage of having to simultaneously ensure effluent requirements, process safety, investment, and operation costs make modelling a useful tool for designers (Rivas et al. 2008). Another advantage is the ability to run a large number of different scenarios which would not be possible to try out in practice (due to time, economic and physical constraints). Accordingly, modelling serves as a time and cost-saving tool for the evaluation of new wastewater treatment concepts and it helps to bridge the gap between lab and full-scale applications (Salem et al. 2002).

Despite all innovations related to computational work, it is still not an easy task to develop a well-calibrated and validated model. Modelling of wastewater treatment processes still faces some major challenges such as data collection, calibration, validation, parameter identifiability and uncertainty. Many variables in the dataset can be strongly coupled. The data can be noisy, uncertain, and incomplete which enforce data treatment before one can use them as model inputs (Rieger et al. 2010). Another challenge is that the activated sludge models might be large and over-parameterized (i.e. they have many stoichiometric and kinetic parameters) that suffer identifiability problems. They are also highly nonlinear and dynamic. Model parameters, as well as the model structure, may have to be adjusted according to the WRRFs with different influent characteristics or operation schemes (Zhu et al. 2015). Poorly identifiable parameters make it harder to provide reliable estimates of all parameters simultaneously (Dochain and Vanrolleghem 2001). Thus, providing reliable input data for model calibration and validation without knowing the importance of model parameters and without a proper experimental design may lead to excessive experimental effort and cost.

There are several models that describe the biological processes in activated sludge systems. The Activated Sludge Models (ASMs) developed by the IWA task group on mathematical modelling of the activated sludge

process (Henze et al. 2006) and other mathematical descriptions of biological wastewater treatment processes such as presented by Barker and Dold (1997), are commonly used for simulation of activated sludge systems.

1.4   State-of-the-Art Biokinetic Models Including N-Removal

Nitrogen may exist in seven oxidation states, from -3 to +5, thus is found in many compounds (Sawyer and McCarty 1978). In wastewater, nitrogen may be found in four forms: organic, ammonia or ammonium, nitrite and nitrate nitrogen. Organic nitrogen and ammonia are the main nitrogen components that exist in raw wastewater and decomposition by heterotrophic bacteria, known as ammonification, readily converts organic nitrogen to ammonia nitrogen. Ammonia nitrogen may exist in an aqueous solution either as ammonium ion or unionized ammonia, depending on the pH and expressed by the following equation. When the pH increases, the reaction in Equation 1.1 is displaced to the left (Cheremisinoff 1997).

$$NH_3 + H_2O \leftrightarrow NH_4^+ + OH^-$$
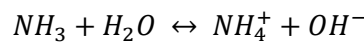
Equation 1.1 Ammonia and pH Dependency

The removal of nitrogen by biological nitrification and denitrification is a two-step process (Metcalf&Eddy 2014). The first step is nitrification which is the conversion of ammonium nitrogen (NH_4-N) to nitrate nitrogen which in itself is a two-step reaction: conversion of ammonium to nitrite (NO_2-N), followed by conversion to nitrate (NO_3-N) by distinct groups of autotrophic bacteria: ammonium-oxidizing bacteria (AOB) and nitrite-oxidizing bacteria (NOB) (Equation 1.2). The second step is denitrification in which nitrate is converted to nitrous oxide (N_2O) or nitrogen gas (N_2) under anoxic conditions by heterotrophic microorganisms (HB) using organic matter as the electron donor (Equation 1.3). N-removal with the coupling of nitrification and denitrification processes is still the conventional method for the design of WRRFs. However, this conventional process has some disadvantages, such as high energy consumption for oxygen supply, need for large tank volumes and often addition of external carbon sources.

$$NH_4^+ + \frac{3}{2} O_2 \rightarrow NO_2^- + 2H^+ + H_2O$$

$$NO_2^- + \frac{1}{2} O_2 \rightarrow NO_3^-$$
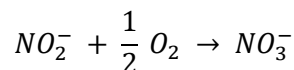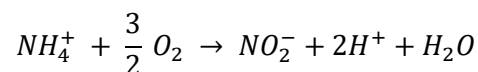
Equation 1.2 Stoichiometry of Nitrification

$$NO_3^- + 6H^+ \rightarrow \frac{1}{2} N_2 + 3H_2O$$
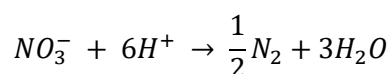
Equation 1.3 Stoichiometry of Denitrification

Several alternative systems for N-removal have been developed in the last decades to reduce aeration costs, external carbon sources and sludge production. Examples include bio-augmentation of nitrification/denitrification, N-removal by nitration and denitration (nitrite shunt), partial nitrification and Anammox, partial denitrification and Anammox processes. These processes are still under development to be applied in mainstream wastewater treatment and scientific studies continue to develop understanding, improve and apply these concepts in full-scale (Chen et al. 2015; Regmi et al. 2015; Jimenez et al. 2015; Valverde Pérez et al. 2016; Salmistraro et al. 2017; Wang et al. 2016; Li et al. 2018; Le et al. 2019; Zhang et al. 2020; Gao and Xiang 2021; Kirim et al. 2022). These innovative processes will be detailed later in this chapter (Chapter 1.5).

Because ammonia oxidation is typically the rate-limiting step under municipal conditions, ASMs describe both nitrification and denitrification as a single step process, with ammonia being directly oxidized to nitrate and nitrate being directly reduced to nitrogen gas. Depending on the aim of the modelling study, modifications and extensions of the state-of-the-art models have been applied to represent novel processes or detail some processes in the model like Anammox (Hao et al. 2002; Volcke et al. 2005), coupled SHARON/Anammox (Volcke et al. 2002; Volcke et al. 2006; Valverde Pérez et al. 2016), 2-step nitrification (Sin et al. 2008a; Kaelin et al. 2009; Ostace et al. 2011), 4-step denitrification including the electron competition (Hiatt and Grady 2008; Pan et al. 2013; Domingo-Félez and Smets 2020), partial nitritation and Anammox (Trojanowicz et al. 2017) and partial denitrification with Anammox (Al-Omari et al. 2021).

In this chapter, a brief overview of the most popular mathematical models for N-removal is given and their specific properties are discussed.

1.4.1 ASM1

The Activated Sludge Model No. 1 (ASM1) which was published by Henze et al. in the year 1987 can be considered as the reference model and is generally still accepted as the state-of-the-art (Hauduc et al. 2013). ASM1 was primarily developed for municipal activated sludge WRRFs to model the removal of organic carbon and nitrogen by simultaneously considering the consumption of oxygen and nitrate as electron acceptors. The model also aims to accurately describe sludge production and oxygen consumption. COD was adopted as the measure of the concentration of organic matter and the wide variety of organic carbon compounds and nitrogenous compounds were condensed into a limited number of fractions based on biodegradability and solubility considerations (Gernaey et al. 2004).

In ASMs the Monod relationship is used to describe the growth rate of both heterotrophic and autotrophic organisms. Nitrification is represented as aerobic growth of autotrophic biomass and ammonia is oxidized to nitrate via a single-step process resulting in the production of autotrophic biomass. Denitrification is the anoxic

growth of heterotrophic biomass in the absence of oxygen. The heterotrophic organisms are capable of using nitrate as an electron acceptor with organic matter as electron donor. The process leads to the production of heterotrophic biomass and nitrogen gas. Also, aerobic growth of autotrophs and anoxic growth of heterotrophs are considered. Two other important reactions are described by the model in relation to nitrogen: hydrolysis of entrapped organic nitrogen and ammonification of soluble organic nitrogen (Henze et al. 2006). During hydrolysis biodegradable particulate organic nitrogen is broken down to soluble organic nitrogen. For ammonification, biodegradable soluble organic nitrogen is converted to ammonia in a first-order process mediated by heterotrophs.

The model assumes the death-regeneration hypothesis to single out the different reactions that take place when organisms die. According to death regeneration, decayed cell material is released again through lysis. One fraction is non-biodegradable and remains as an inert residue while the remaining fraction is considered to be slowly biodegradable and used for cell growth (Jeppsson 1996). The death (decay) regeneration cycle of the heterotrophs and autotrophs are strongly interrelated in ASM1 and it does not include the possibility to differentiate decay rates of autotrophs under aerobic and anoxic conditions.

1.4.2 ASM2 & ASM2d

The Activated Sludge Model No. 2 (ASM2) is an extension of ASM1 and uses the same concepts for N-removal. The main difference is that ASM2 includes additional biological processes to deal with phosphorus removal. Those processes do not have any effect on nitrification and denitrification kinetics. However, hydrolysis of particulate organic nitrogen is no longer included as a separate process and it is assumed that particulate biodegradable organic matter contains a constant fraction of nitrogen. Also, the ammonification process is ignored in ASM2 due to the assumption of fermentable substrates that contain a constant fraction of nitrogen. This assumption was made to eliminate the addition of new processes, components and increase model complexity. In addition to the biological processes, ASM2 includes chemical processes which may be used to model chemical P precipitation (Henze et al. 2006).

The Activated Sludge Model No. 2d (ASM2d) was first published in 1999 as an extension of ASM2. ASM2d is superior to ASM2 for modelling nitrogen and phosphorus dynamics because of the incorporation of denitrification by phosphorus accumulating organisms (PAOs) which is not considered in ASM2.

1.4.3. ASM3

The Activated Sludge Model No. 3 (ASM3) is a modified version of ASM1 representing the removal of organic carbon and nitrogen by correcting some defects of ASM1 such as the ammonia limitation of the heterotrophic growth process. The most remarkable change is that the model includes the storage of organic substrate as a

process. Also, the death-regeneration decay process is exchanged for endogenous respiration (Gujer et al. 1999).

In the model, all conversion processes of the two groups of organisms are clearly separated and the decay processes are described with identical models for both groups. In addition to these, the degradation of soluble and particulate organic nitrogen is integrated into the hydrolysis, decay and growth processes in ASM3 (Henze et al. 2006).

1.4.4. 2-Step Nitrification and 4-Step Denitrification

Because ammonia oxidation is typically the rate-limiting step under municipal conditions, many traditional activated sludge models include nitrification as a single step process. However, this simplification is not suitable for elevated nitrogen conditions or in cases of inhibition, because nitrite is an environmentally important intermediate product of both nitrification and denitrification (Hiatt and Grady 2008). Nitrite accumulation and ammonia inhibition may occur in WRRFs under compelling operating conditions (low dissolved oxygen, low temperature, high temperature, high loadings such as side stream and industrial wastewater treatment processes) and as a consequence nitrite needs to be included in a model of these systems (Sin et al. 2008a). Therefore, many studies in the literature have extended traditional ASMs with 2-step nitrification (Equation 1.2). The model comparison done by Sin and Vanrolleghem (2006) concludes that the common aspect of all these models is that the growth rate is assumed rate-limiting and is used to describe the rate of other substrate conversions via stoichiometric yields similar to the ASM1 convention.

Hiatt & Grady (2008) first published the Activated Sludge Model for Nitrogen (ASMN), which describes the activated sludge process behaviour under elevated nitrogen conditions. The model is an extension of ASM1 and includes 2-step nitrification and the effect of pH and temperature on nitrification. In addition, ASMN includes microbial growth using nitrate (in the absence of ammonia) as the nitrogen source. Denitrification in the model involves four process steps instead of direct reduction of nitrate to nitrogen gas (Equation 1.3). The process includes reduction of nitrate into nitrite, nitrous oxide and nitric oxide as intermediate products where the emission of nitrous oxide has attracted a lot of attention (Equation 1.4).

$$NO_3^- \rightarrow NO_2^- \rightarrow NO \rightarrow N_2O \rightarrow N_2$$
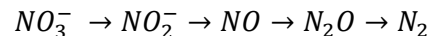
Equation 1.4 Stoichiometry of 4-Step Denitrification

During denitrification, competition among the four reduction steps for electrons occurs. It usually occurs if the electron supply rate from the oxidation process cannot meet the demand for electrons by the four reduction steps and leads to nitrous oxide (N_2O) accumulation which is not desired (Richardson et al. 2009). For that

reason, a denitrification model which considers the electron competition in 4 step-denitrification was first developed by Pan et al. (2013) through the use of different affinity constants with respect to the reduced electron carriers for different enzymes and called as Activated Sludge Model – Indirect coupling of electrons. Later, the Activated Sludge Model – Electron competition was developed which describes denitrification as an analogy to how current intensity varies through a parallel set of resistors in electric circuits (Domingo-Félez and Smets 2020). The model was calibrated with data for different carbon sources.

1.5 Energy & Resource Efficient N-Removal Processes & Modelling

The application of short-cut biological nitrogen removal processes (SBNR) in mainstream wastewater treatment has received considerable attention over the last decade from both academia and industry in order to reduce the overall energy and resource consumption in N-removal. The applicable treatment processes are given in this chapter together with the process control algorithms to achieve them.

1.5.1 Deammonification

Compared to nitrification-denitrification over nitrate, the application of short-cut N removal processes in mainstream wastewater treatment has significant potential to save energy (oxygen demand) and resources (carbon demand) and pursue energy neutrality of WRRFs. A recently developed way to remove nitrogenous compounds is the anammox (anaerobic ammonia oxidation) process in which ammonium is oxidised using nitrite as electron acceptor under anaerobic conditions (Equation 1.5). The process relies on preventing the oxidation of nitrite to nitrate and making nitrite available for anammox (Zhang et al. 2019). Thanks to its outstanding energy-saving potential, anammox-based processes have received considerable attention over the last decade from both academia and industry. The reaction pathways for the conventional N-removal process and the anammox process are schematized in Figure 1.2 which can be achieved by anaerobic ammonium-oxidizing bacteria (AnAOB).

$$NH_4^+ + 1.32\ NO_2^- + 0.066\ HCO_3^- + 13\ H^+$$
$$\rightarrow\ 1.02\ N_2 + 0.26\ NO_3^- + 0.26\ CH_2O_{0.5}N_{0.15} + 2.03\ H_2O$$
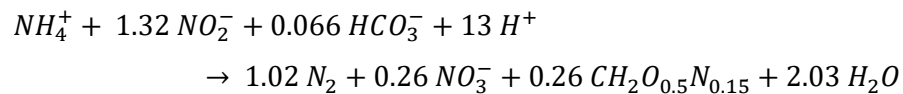
Equation 1.5 Stoichiometry of Anammox Reaction
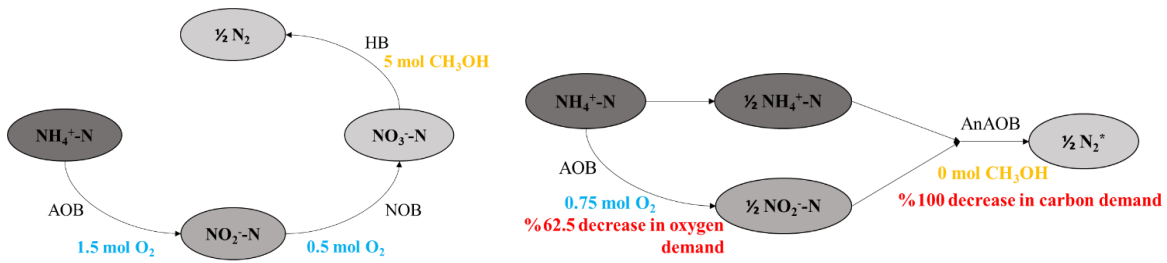
Figure 1.2 Conventional Nitrification/Denitrification Reactions Route vs. Deammonification with Anammox

: General nitrogen turnover is represented in the schema.

1.5.1.1. Partial Nitrification - Anammox

The application of anammox relies on the ability to shunt nitrification at nitrite (Lackner et al. 2014). Partial oxidation of ammonium (nitritation) is required for the successful application of partial nitritation and anammox (PNA) and the overall process is called deammonification. Deammonification provides an efficient biological pathway compared to conventional nitrification/denitrification. The demonstrated advantages of applying deammonification to mainstream treatment are reduction of aeration energy, and reduction in external carbon and alkalinity demands (O'Shaughnessy 2016).

Application of the anammox process together with partial nitrification can reduce the required oxygen input by 60%, eliminate the carbon source demand and reduce the sludge production by 90% in comparison to the conventional N-removing systems (Morales et al. 2015; Miao et al. 2016). Early PNA implementations applied two-stage reactor configurations or made use of already existing nitrite shunt systems like SHARON type reactors (Lackner et al. 2014). The SHARON process (Single reactor High activity Ammonia Removal Over Nitrite) is based on the nitrite shunt which is the partial nitrification of ammonium to nitrite by AOB and the denitrification (Hellinga et al. 1998). The denitrification step in the nitrite-shunt process can be replaced with anammox and becomes more advantageous in terms of the need for external carbon sources. Based on the review of Lackner et al. (2014) the number of partial nitritation/Anammox (PNA) WRRFs had reached over 100 full-scale installations in operation worldwide by 2014. It is expected that the number of installations increased by many more nowadays; however, there is no certain number in the current literature about this. On the other hand, full-scale applications are currently limited to side-stream treatment and only a few successful mainstream applications are reported so far (Cao et al. 2017; O'Shaughnessy 2016; Klaus et al. 2020a).

The successful application of the process could be achieved mainly on side-stream treatment of high-strength NH_4-N wastewater. However, for low-strength domestic and municipal wastewater, it is still a major challenge to maintain stable nitrogen removal performance (Ciudad et al. 2005; Deng et al. 2021). The application of

deammonification for mainstream wastewater treatment is still in laboratory and pilot-scale studies (Kirim et al. 2022). Only a few examples of mainstream full-scale deammonification applications exist such as the Changi Recycling Water Plant in Singapore where the water temperature can be maintained above 28ºC (Cao et al. 2017; Gao and Xiang 2021) and the Strass WRRF in Austria where Anammox seeds are fed to the mainstream to enhance the process (O'Shaughnessy 2016).

The application of PNA on mainstream wastewater treatment strongly relies on process control and the out-selection of NOBs. The main challenge is the high influent COD/N ratio in the raw wastewater which leads to large fractions of heterotrophic bacteria in the system and less active AnAOB and AOB, and thus limited removal rates. (Cao et al. 2017). Also, HB and AOB compete for oxygen in the system which results in the washout of AOBs and destruction of the deammonification process (Zhang et al. 2015). Another main challenge is the difficulties with the suppression of NOB. The out-selection of NOB has been proven to be quite effective in warm nitrogen-rich wastewater streams (Lackner et al. 2014); partly due to the high free ammonia (FA) and free nitrous acid (FNA) concentrations in side-stream liquors which inhibit the growth of NOB (Lackner and Agrawal 2015).

However, FA inhibition is not possible in mainstream treatment due to the lower influent ammonium concentration (Cao et al. 2017). There are also reports of NOB out-selection achieved through side-stream generated FNA exposure (Wang et al. 2016) and more recent studies show that alternating the sludge treatment strategy between FA and FNA can result in a more stable nitrite-shunt with nitrite accumulation above 95% in the mainstream (Duan et al. 2019). The operating conditions to favour AOB and wash out NOB are thoroughly investigated in literature based on DO, pH, temperature and inhibitors. The intrinsic kinetics of these two groups of microorganisms including their maximum growth rate and substrate half-saturations are crucial (Liu et al. 2020). DO affects the diversity and kinetics significantly, thus DO control to manipulate the competition for oxygen between AOB and NOB is one of the main strategies for efficient out-selection of NOB in mainstream conditions (Pérez et al. 2014; Jimenez et al., 2020). The oxygen half-saturation constant for AOB is generally accepted to be lower than the constant for NOB which creates a disadvantage for NOB to compete for oxygen at low concentrations (Sin et al. 2008a; Cao et al. 2017). On the other hand, the predominance of *Nitrobacter* or *Nitrospira* -which are the two main species of NOB- affect the performance of NOB out-selection through DO control. The systems enriched with *Nitrospira* rather than *Nitrobacter* have a higher oxygen affinity, thus have lower oxygen half-saturation than AOBs and can be well adapted to low DO conditions (Regmi et al. 2014a). The use of transient anoxia is another approach to achieve NOB out-selection by causing a lag-time for NOB to transition from anoxic to aerobic condition or nitrite limitation (Zekker et al. 2012; Gilbert et al. 2014). By consuming nitrite in anoxic conditions, heterotrophs restrict substrate availability for NOB in the aerobic phase (Regmi et al. 2014a). Moreover, the AOB growth rate is higher than the NOB's at high temperatures (above 20ºC) in mainstream treatment under limited DO (Regmi et al. 2014a; Yang et al. 2016). This allows operating

the system at a SRT that is suitable for the AOB and wash out the NOB (Blackburne et al. 2008). There are also lab-scale works that support that NOB out-selection can be achieved at lower temperatures depending on the dominant NOB species in the system and the reactor configuration (De Clippeleir et al. 2013; Gilbert et al. 2015; Cao et al. 2017).

Another drawback of the deammonification process is the low growth rate of anammox bacteria and the need for very long sludge retention systems (Valverde Pérez et al. 2016). Anammox bacteria grow about 8 times slower than nitrifying bacteria (Tony Farina 2012). Besides, the optimal ammonium/nitrite influent ratio for the anammox reactor is quite important and may have to increase to 1/1.32, depending on the actual growth yield (Dongenet al. 2001). Also, under the anoxic conditions of the anammox process, part of the produced nitrate can be denitrified to nitrite to affect the ammonium/nitrite ratio needed.

Last but not least, the deammonification process also has to face lower wastewater temperatures and alkalinity reserves, especially in mainstream applications. Lackner et al. (2014) surveyed 14 full-scale PNA plants and reported that temperature variations do not affect the process significantly on side-stream treatment, since the temperature is elevated (above 30ºC). However, the raw wastewater temperature of mainstream treatment is much lower and affects the growth rates. Laureni et al. (2015) stated that reducing the temperature from 29ºC to 12.5ºC resulted in an increment in the doubling time of Anammox bacteria from 18 to 79 days. pH is also a very important environmental condition and different studies recommended optimum pH range for Anammox is between 6.5-8.3 (Tomaszewski et al. 2017).

1.5.1.2 Modelling and Process Control

Overall process control is quite important to adjust the ammonium/nitrite ratio and sustain N-removal by anammox. Microorganism species involved in the processes are sensitive to operational and environmental conditions such as pH, DO level, temperature, SRT and the presence of inhibitors as previously mentioned. Some strategies were applied for process control to optimize N-removal performance (Volcke et al. 2005). Several control strategies were adopted such as low or high DO operation, aerobic SRT, real-time aeration or oxidation-reduction potential control to take advantage of the growth characteristics and the kinetics difference between the microorganisms (Gao and Xiang 2021; Liu et al. 2020). However, the shift and adaptation of microbial communities' growth characteristics to different conditions in mainstream conditions remain a challenge (Agrawal et al. 2018; Gao and Xiang 2021). The control strategies are based on different control loops by considering set points for the key variables in the process, such as pH or dissolved oxygen (O'Shaughnessy 2016). Wu et al. (2016) dealt with the selection of AOB over NOB based on conversion rates by using mathematical modelling to identify the optimal range of influent NH_4-N, alkalinity and operational conditions to achieve partial nitritation successfully based on pH changes. Qi et al. (2016) developed a biofilm model to

simulate the performance of the granular sludge system and determined the optimum range of operational parameters to continuously inhibit the NOB activity. Based on sensitivity analysis, it is found out that the oxygen half-saturation coefficients for AOBs and NOBs are the most influential parameters. Gut et al. (2007) used multivariate data analysis methods for modelling the PNA process to improve process efficiency with an extensive data set. It was observed that a parallel increase in the influent nitrogen load to the partial nitritation and the anammox processes extends the N-removal capacity. Conductivity was mentioned as one of the key parameters for monitoring these systems. Stewart et al. (2017) focused on substrate limitations and microbial behaviour of the deammonification process by using biokinetic models for system design and optimization. Dissolved oxygen, nitrite and ammonium limitation effects on growth of NOBs and Anammox bacteria were investigated and a dual substrate model was developed which allowed improving the process performance by 75% based on simulations of a full-scale mainstream deammonification system.

The mathematical modelling approach of the ASM has proved to be an excellent tool for modelling single-step nitrification-denitrification processes and has triggered further modelling research (Henze et al. 2006). Nevertheless, considering the development of the short-cut processes, nitrite should be considered as an intermediary step in nitrification and denitrification. Modelling the two-step nitrification process is well established where NOB out-selection can be modelled through distinctly defined growth kinetics, substrate affinities, and temperature and pH effects on AOB and NOB (Sin et al. 2008a; Shourjeh et al. 2021). However, most simulation studies so far deal with side-stream conditions associated with high-strength nitrogenous wastewater where NOB out-selection can be achieved much easier with direct pH and temperature effects on the NOB (>1000 mgN/L) (Volcke et al. 2006; Van Hulle et al. 2007; Wett et al. 2010; Volcke et al. 2012; Hubaux et al. 2015). Al-Omari et al. (2015) modelled 2 different control strategies to achieve nitrite shunt for the mainstream deammonification process: Control based on the online measured ammonia and control based on a target ratio of 1 for the Ammonia vs NO_X-N (AvN). Results indicated that the AvN controller is successful for NOB-out selection and it promotes better management of incoming organics and bicarbonate. There are also modelling studies within the same context through bioaugmentation of AOBs from side-stream to mainstream reactors (Cui et al. 2017) and also the treatment of activated sludge with free ammonia to favour AOBs (Wang et al. 2017; Peng et al. 2020). Many studies tackle challenges such as low DO and temperature to enrich AOB biomass and suppress NOBs (Wett et al. 2013; Salmistraro et al. 2017; Wang et al. 2016; Nifong et al. 2015), but the challenges remain.

1.5.1.3 N_2O Emissions

In addition, like conventional N-removal systems, due to high nitrite accumulation and ammonia conversion rates the short-cut processes inevitably generate nitrous oxide (N_2O) as a by-product which is one of the most significant greenhouse gases (Castro-Barros et al. 2016; Li et al. 2020). N_2O production occurs in three different

pathways; i.e. the AOB denitrification, the hydroxylamine oxidation and the heterotrophic denitrifiers denitrification (Li et al. 2020). Process control modelling studies are generally focused on optimizing the deammonification process performance and low emissions separately. Leix et al. (2017), on the other hand, investigated optimizing deammonification performance while simultaneously reducing N_2O emissions. In this study, two models were developed for the prediction of the N-removal rate and N_2O emissions during single-stage deammonification considering pH, feeding and aeration strategy. Zheng et al. (2018) used mathematical modelling to investigate the N_2O emissions by AOBs and enhance the nitrogen removal efficiency by controlling the DO and NO_2-N.

1.5.1.4 Partial Denitrification - Anammox

Due to the challenges with NOB out-selection and stability of the partial nitritation, recent studies propose another route to achieve deammonification in mainstream treatment (Ma et al. 2017; Le et al. 2019; Lu et al. 2021a). The process allows fully autotrophic nitrification of ammonium into nitrate and then partial denitrification to nitrate, followed by anammox (Figure 1.3). Thus, the process is called partial denitrification anammox (PdNA) and does not require NOB out-selection. However, it requires carbon addition to achieve the partial denitrification (Zhang et al. 2019). The PdNA process consumes more resources; aeration and organic matter, than the PNA route, however, the nitrite generating pathway is found more stable (Ma et al. 2017). Also, it is possible to remove the nitrate generated by the anammox process with reduction of it into nitrite, thus achieving lower effluent total nitrogen concentration (Wang et al. 2019; Lu et al. 2021a).
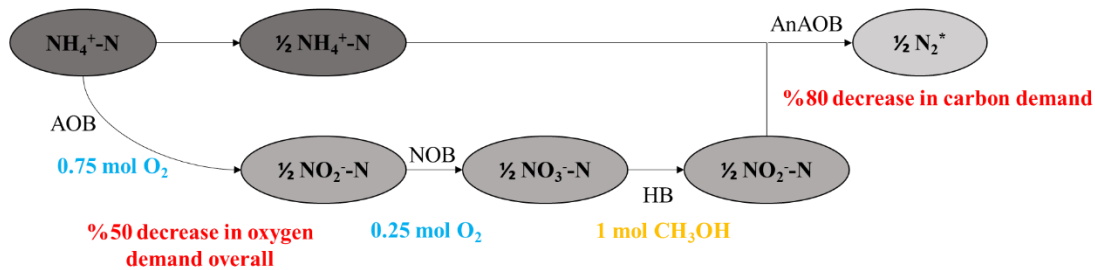
Figure 1.3 Deammonification with Partial Denitrification and Anammox

: General nitrogen turnover is represented in the schema.

With rapidly consumed carbon sources such as acetate, nitrite accumulation has been reported as an indicator of partial denitrification which further led to the use of nitrate residual as the key parameter to control and achieve PdNA (Du et al. 2016; Le et al. 2019). However, the type of carbon source is critically important to create the nitrite sink for the deammonification process and it is found that acetate or glycerol was preferred by the denitrifiers for efficient partial denitrification due to their electron transport pathways (Le et al. 2018). Al-Omari

et al. (2021) could model the PdN selection mechanism by introducing a logistic inhibition term applied on the NO_2-N reduction rate where the electron transport chain is dependent on carbon source and NO_3-N residual. However, the model is only valid for acetate as external carbon source. Also recently, the role of internally stored carbon is being investigated since the endogenous organic matter can also be used to reduce nitrate in partial denitrification (Deng et al. 2021; Lu et al. 2021b).

1.5.1.5 Mainstream Application

Current application types of deammonification implementations for mainstream treatment include a variety of processes in laboratory and pilot scales (Table 1.1 with examples). Processes can be suspended or attached growth or hybrid systems in single-stage or 2-stage reactors (Hoekstra et al. 2018; Le et al. 2019a; Huang et al. 2020). Due to the slow growth rate of anammox bacteria, an anammox retention mechanism is required to allow for SRT separation (Kirim et al., 2022). In a single-stage process, all PNA or PdNA reactions occur in one basin which decreases both the investment and the operational costs (Pérez et al. 2014). Biofilm systems such as granular sludge (Lotti et al. 2015), moving bed biofilm reactors (MBBR) (Gustavsson et al. 2020) or hybrid systems that combine suspended sludge with the biofilm systems such as integrated fixed-film activated sludge system (IFAS) (Cao et al. 2017) are mostly used in these single-stage systems (Ma et al. 2020) to maintain AnAOB. In these attached growth systems, AOB and NOB are usually distributed in the outer aerobic layer of the biofilm while AnAOB exist in the inner part. Thus, a thicker biofilm layer makes AnAOB advantageous for NO_2-N competition with NOB and DO penetration is avoided. On the other hand, when the biofilm has reached the optimal thickness, the N-removal capacity does not improve even if the biofilm keeps developing. Indeed, the thick biofilm is not conducive to the formation of a DO gradient and eventually suppresses the activity of AOB and AnAOB (Liu et al. 2017).

In 2-stage systems, partial nitrition or full-nitrification (aerobic environment) and the deammonification processes (anoxic environment) occur in separate basins. Suspended or biofilm processes can be used in the aerated basin and biofilm-based processes may be used in the anammox basin (Regmi et al. 2014b; Pérez et al. 2015). The processes can be more easily optimized separately in the 2-stage systems and control algorithms can be applied easier.

Mathematical models and model-based control strategies are under development to overcome implementation challenges and to deal with the complexity of mainstream deammonification (Kirim et al. 2022). Through modelling, it is possible to identify the proper conditions for microbial competition under different operational and environmental conditions and to optimize the processes and implement deammonification successfully (Shourjeh et al. 2021). However, the mechanistic models that are currently being used for modelling the nitrogen removal are not sufficiently accurate to model short-cut N removal processes and require specific attention. For example, while the models include the key microbial groups, they do not consider the individual species which

is crucial to reflect the competition among them and predict a community shift. Also, different process configurations such as biofilm systems require specific sub-models such as the mass transport between the bulk liquid and the microorganisms inside the biofilm (Baeten et al. 2019). Thus, the pilot and full-scale applications reported provide invaluable information for model development and to overcome bottlenecks while modelling efforts accelerate the success of practical applications (Kirim et al. 2022).

Table 1.1 Application Types of Deammonification Process in Full-scale

Process	Description	Scale	Application examples
Single-stage PNA	PN and Anammox processes occur in the same reactor. The processes are achieved either by suspended or attached growth system.	Lab-scale	(Lotti et al. 2015) (Han et al. 2016) (Huang et al. 2020)
		Pilot-scale	(Hoekstra et al. 2018)
		Full-scale side-stream	(Klaus 2019)
		Full-scale mainstream	(O'Shaughnessy 2016) (Veuillet et al. 2015)
2-stage PNA	PN and Anammox processes occur in separate reactors. PN is achieved by a suspended growth activated sludge system and the Anammox process can be suspended or biofilm growth systems.	Lab-scale	(Ma et al. 2011) (Dosta et al. 2015)
		Pilot-scale	(Regmi et al. 2014) (Klaus et al. 2020b)
Single-stage PdNA	After the full nitrification of ammonium to nitrate; PdN and Anammox processes are achieved by suspended or attached growth systems in the same reactor.	Pilot-scale	(Du et al. 2017)
2-stage PdNA	After the full nitrification of ammonium to nitrate; PdN and Anammox processes occur in separate reactors. PdN is achieved by a suspended growth activated sludge system and the Anammox process can be suspended or biofilm growth systems.	Lab-scale	(Wang et al. 2019)
		Pilot-scale	(Le et al. 2019) (Klaus 2019)

1.5.2 Simultaneous Nitrification and Denitrification

Nitrification and denitrification processes can occur concurrently in the same reactor at low dissolved oxygen concentrations (Bertanza 1997). The process is so-called simultaneous nitrification and denitrification (SND) and is defined as nitrogen loss in aerated reactors. SND is finding widespread usage especially for the treatment of high strength wastewater in terms of nitrogen content. The process may occur via partial oxidation of ammonium to nitrite or full nitrification to nitrate and then reduction to nitrogen gas and can significantly reduce energy and COD demand for nitrogen removal (Yoo et al. 1999; Zeng et al. 2003). A schematic representation of nitrogen removal through SND is presented in Figure 1.4. In comparison to the conventional nitrification-denitrification system, SND eliminates the need for two separate tank operations, utilizes 22-40% less carbon source, results

in a lower sludge yield, lower alkalinity demand since the consumed alkalinity during nitrification is provided during denitrification and finally less energy requirement due to the reduction in aeration (Ohandja et al. 2008; Yoo et al. 1999; Hirata et al. 2003; Gibbs et al. 2005). However, controllable SND is hard to achieve and the mechanisms are not well understood yet (Jimenez et al. 2020). The optimal DO concentration for effective nitrogen removal via SND varies from 0.2 to 1 mg/L (Schlegel 1992; Jimenez et al. 2010; Lim et al. 2019). Successful application of the nitrite-shunt in mainstream treatment is desired to occur through SND since it has the opportunity to remove the organic matter in the influent. However, it is not easy to achieve because the denitritation relies solely on utilizing the influent COD and thus on the efficiency of carbon pre-treatment process (Kirim et al. 2022).
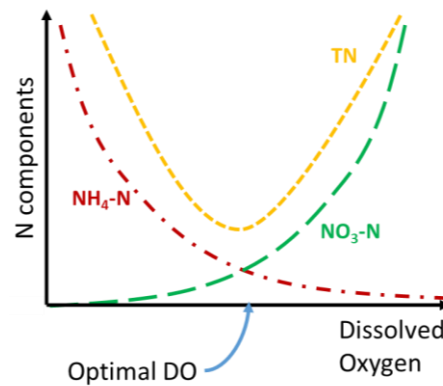
Figure 1.4 Nitrogen Removal through Simultaneous Nitrification and Denitrification

Several mechanisms can be responsible for SND occurrence. One of the main mechanisms is the DO gradient created within the floc, granule or biofilm that provides anoxic conditions for denitrification (Daigger et al. 2007; Layer et al. 2020; Seifi and Fazaelipoor 2012). The second mechanism consists of bioreactor macro environments that anoxic and aerobic zones may develop within the reactor as a result of mixing patterns (Daigger et al. 2007). Diffusion of dissolved oxygen through activated sludge flocs can be achieved either with continuous aeration at low DO concentrations or intermittent aeration by which anoxic zones develop during a brief period of the aerated phase (Jimenez et al. 2010; Layer et al. 2020). It is also possible to achieve the process by favouring different microbial species such as combining heterotrophic nitrifiers and aerobic denitrifiers or denitrifying phosphorus accumulating organisms (Gupta et al. 2022; Zaman et al. 2021).

Keene et al.'s (2017) pilot-scale study demonstrated that an average DO concentration of 0.33 mg/L DO with stable operation can maintain efficient nitrification with nearly 70% of the nitrogen being denitrified, without the need for internal recycling of high nitrate mixed liquor from the aeration basin to the anoxic zone. At the lowest DO conditions used, a 25% reduction is estimated in energy use for aeration compared to conventional biological

nutrient removal. Klaus and Bott (2020) could achieve 88% total inorganic nitrogen removal efficiency through SND at 0.2-0.3 mg/L DO under continuous aeration and determined that carbon availability for denitrification is more likely to be the limiting factor once low DO conditions are met. It is also reported that different carbon sources applied to enhance the SND have a great impact on microbial communities and lead to different nitrogen removal mechanisms. Acetate addition was the most efficient organic source (Wang et al. 2017).

1.5.3 Process Control in N-Removal Processes

In order to check meeting the effluent criteria, to reduce the carbon footprint and to minimize resource consumption for cost-effectiveness in the WRRFs, many performance indicators and control algorithms have been defined (Revollar et al. 2020). To fulfil the effluent quality standards and keep the operational costs low, it is imperative to use control strategies that meet the wastewater treatment process demanding requirements (Ostace et al. 2011). Process control involves maintaining the treatment process at a desired set of conditions by adjusting the selected variables in the plant. The adjustments can be either made manually or by using automatic controllers (Katebi et al. 1999). Aeration control is widely applied for N-removing systems. The nitrification capacity can be varied in relation to DO control either by adjusting the aeration intensity or by adjusting the aerated volume. Return activated sludge, wasted sludge and nitrate recycle or external carbon dosage (for plants with denitrification) are other control handles that may affect the nitrification performance (Åmand et al. 2013). One or more of those control handles can be combined and applied for energy and process optimization purposes (Palatsi et al. 2021). Also, model-based control has been found in literature for nitrogen removing activated sludge systems, especially for control of dissolved oxygen and energy efficiency (Holenda et al. 2008; Revollar et al. 2018).

1.5.3.1 DO Control

The DO concentration is crucial for N-removing systems since it determines the dominant processes in the biological reactor. A high DO inhibits denitrification, whereas a low DO can lead to the limitation of ammonia oxidation (Nourmohammadi et al. 2013). Aeration equipment must be designed to supply the oxygen demand of the microorganisms under a wide range of influent loads, while at the same time assuring that some minimum DO concentration is met. In DO control systems, the output of the aerator is adjusted to meet the changing demands based on the DO measurements in the aeration tank (Figure 1.5) (Metcalf&Eddy 2014). Also, a maximum DO concentration which is defined in the controller properties might help to save energy. A minimum DO concentration of about 0.5 mg/L is required to initiate the nitrification and operation at low DO concentrations below 1.0 mg/L can save energy in nitrogen removing systems through SND or partial nitrification followed by post-treatment such as Anammox (Chapters 1.5.1 & 1.5.2).
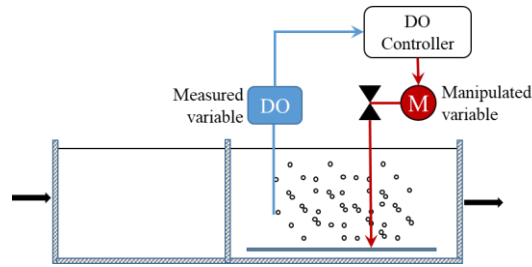
Figure 1.5 DO Controller Mechanism

1.5.3.2 Ammonia-based Aeration Control

Ammonia-based aeration control (ABAC) is a cascade control concept for controlling total ammonia nitrogen in the effluent or influent of activated sludge processes to reduce aeration costs together with eliminating the effluent ammonia peaks (Figure 1.6) (Rieger et al. 2014). ABAC control is composed of an open-loop and closed-loop controller that sets DO set-points in the aeration tank to maintain a predetermined ammonia set-point at the effluent (Medinilla et al. 2020). It tailors the aeration intensity to the ammonia loading and maintains consistent nitrification to meet effluent limits but minimize energy consumption (Schraa et al. 2019). The control of aeration can be implemented either with intermittent aeration or continuous aeration (Klaus and Bott 2020). ABAC can be used to initiate and control SND as well if the DO set-points are low enough (Jimenez et al. 2010).

Schraa et al. (2019) improved the ABAC control strategy by adding a supervisory controller that is used to ensure that the sludge retention time is always optimal for ABAC. By that, the DO set-point for continuous aeration or aerobic fraction in the intermittent aeration is no longer a user input and is determined by the SRT. There are also recent studies that used neural networks and fuzzy logic control schemes for ABAC systems to improve effluent quality (Husin et al. 2019; Kumar and Latha 2021).
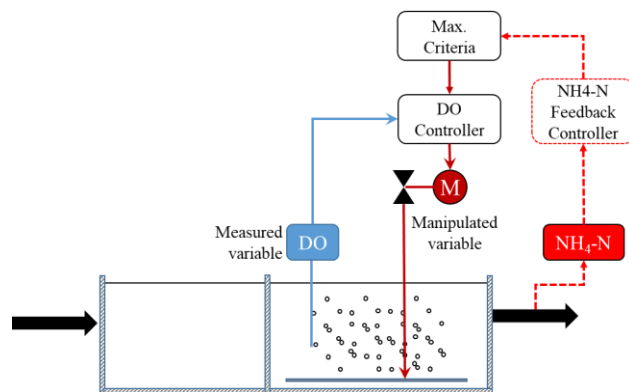
Figure 1.6 ABAC Controller Mechanism

1.5.3.3 Ammonia vs. NO_X-N AvN

Ammonia vs. NO_X-N control, the so-called AvN control, was first developed as an intermittent aeration application for the nitrite-shunt process and achieve NOB out-selection (Regmi et al. 2014a). It is a control algorithm that determines the extent of aeration in the aerobic reactor based on the sum of NO_2-N and NO_3-N (NO_X-N) and the NH_4-N ratio with a set-point of 1, followed by the anammox process (USA Patent No. 20140263041 A1, 2014). It can also be applied through continuous low DO operation and it is considered easier and more practical than intermittent aeration, due to the limitations on the operation of blowers (Klaus and Bott 2020c).
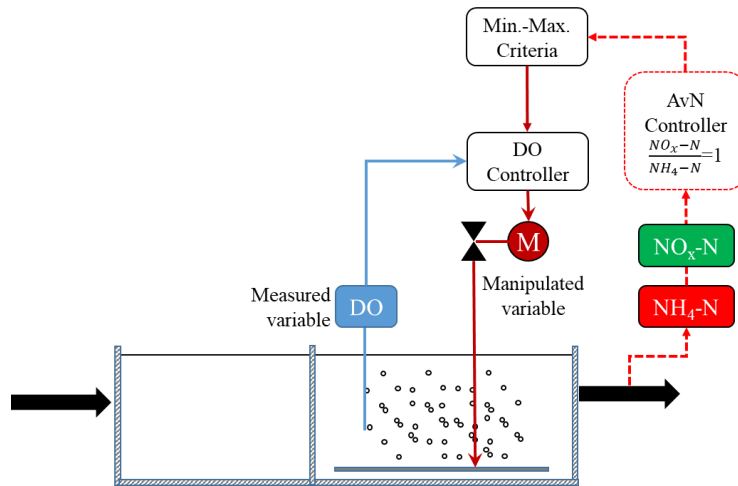
Figure 1.7 AvN Controller Mechanism

The difference and the advantage of AvN control over ABAC is that it is possible to oxidize only the amount of ammonia that can be denitrified by utilizing the carbon amount available in the system which leads to efficient resource usage (Regmi et al. 2014b; Al-Omari et al. 2015). Sadawski (2015) investigated intermittent AvN vs. continuous aeration DO control and ABAC control and found that all control strategies gave similar nitrogen removal performance. However, AvN control effluent was amenable to anammox polishing for additional total inorganic nitrogen (TIN) removal. Also, AvN required less supplemental alkalinity than other strategies. Klaus and Bott (2020c) compared the SND performance of continuous low DO control with continuous and intermittent ABAC and AvN strategies and demonstrated that intermittent aeration application with ABAC and AvN results in the highest TIN removal efficiencies compared to continuous low DO operations (both for ABAC and AvN controls) since it allows for more denitrification in the aerobic zone. On the other hand, it should be noted that low DO concentrations in the conventional activated sludge systems can induce growth of filamentous microorganisms and, thus, sludge bulking problems may occur in the aerated basins and secondary clarifier (Rossetti et al. 2005; Van den Akker et al. 2010; Nittami et al. 2019). Also, nitrogen gas bubbles can be formed due to denitrification in the settler and may lead to rising sludge problems (Metcalf&Eddy 2014).

The AvN control modelling study by Al-Omari (2015) was conducted with scenario analysis, simulating the hypothetical optimized performance and estimated a potential saving of 60% in carbon addition for nitrogen removal by implementing the AvN for full-scale mainstream deammonification. Regmi and Jimenez (2018) modelled the intermittent AvN aeration control in a nitrogen and phosphorus removing WRRF with 76.000 m^3/d capacity. The promising model results showed that effluent ammonia and NO$_X$-N concentration ranging between 2-3.5 mg/L could be achieved. Also, a low NOB/AOB ratio below 0.45 was obtained and the NOB out-selection was thus ensured.

1.6 Modelling Reactive Secondary Settling Process

The activated sludge process basically consists of two consecutive steps: first, the removal of contaminants by microorganisms in a bioreactor which is followed by the separation of the microorganisms from the effluent in a secondary settling tank (SST). The clarification process occurs in the upper zone while thickening occurs near the bottom and the result is the effluent from the top, low in suspended solids and concentrated solids from the bottom for recycling or disposal (Li and Stenstrom 2014). The SST has a crucial function in WRRFs as it directly affects the effluent quality as well as the biomass concentration in the system. As biomass is the driving force for the treatment processes, secondary clarifier operation will affect the performance of the entire facility (Torfs et al. 2015).

Biological reactions occurring in the secondary settler have been mentioned to be an important factor to consider, especially for nitrogen removal (Siegrist et al. 1995). In many full-scale WRRFs, a considerable amount of the overall sludge inventory is stored at the bottom of the settler and it was shown that up to 20% of the incoming total nitrogen can be removed by denitrification in the secondary settling tank (Koch et al. 1999). At long residence times and if incomplete denitrification occurs in the biological reactors, denitrification can indeed take place at the bottom of the settling tank, where the concentration of sludge is high, nitrate levels are still substantial, biomass decay operates, and no oxygen is present (Siegrist et al. 1995). These biokinetic processes and physical settling phenomena occurring in the settler lead to so-called reactive settlers and it is a research topic that warrants further investigation to correctly analyse a WRRF's overall capacity for nitrogen removal.

Several parameters may affect denitrification in the SST, such as the presence of carbon source, dissolved oxygen, nitrate and pH and temperature in the settling tank and the most important one: sludge concentration. It has been found that there is a strong positive correlation between the efficiency of denitrification and both the solids flux and the location of the sludge blanket. These result in increasing the suspended solids concentration (biomass) in the SST (Chavan et al. 2007). The performance of reactive settler models can be improved by including the effect of compression settling (Torfs et al. 2015). On the other hand, strong denitrification during overloaded clarifier conditions can be detrimental to the plant's efficiency, because nitrogen gas bubbles can be

formed due to denitrification leading to the rise of the sludge to the surface of the SST (Metcalf&Eddy 2014). Suspended solids attached to the bubbles result in an increased suspended solids concentration in the clarifier effluent, affecting the overall removal efficiency of the plant with respect to BOD, TSS, TN, and TP. It has been reported that that denitrification may lead to bubble formation when more than 6-8 mg/L NO_3-N is denitrified in the sludge blanket (Henze et al. 1993). Detailed process understanding is thus needed to ensure safe and efficient system operation and control denitrification in the settling tanks.

Thanks to the recent developments in 1-D settling models, the quality and reliability of the numerical solution of the underlying PDE of settling processes have been improved (Plosz et al. 2011; Bürger et al. 2013; Li and Stenstrom 2014; Bürger et al. 2021). In addition, accurate modelling of hindered and compression settling has received increased attention in view of appropriate prediction of the SST performance (De Clercq et al. 2008; Ramin et al. 2014a; Li and Stenstrom 2016; Torfs et al. 2017). Multiple settling velocity functions exist to describe hindered settling under standard operating conditions in SST (Takács et al. 1991; Cho et al. 1993; Plósz et al. 2007; Diehl 2015). At higher sludge concentrations at the bottom of SSTs, sludge compression is known to take place and therefore compression functions have been defined to augment 1-D settling models (e.g. Zhang et al. 2006; De Clercq et al. 2008; Ramin et al. 2014a). Since compression is a force that slows down the hindered settling at high TSS concentrations, the choice of hindered settling function will influence the compression behaviour especially at long residence times leading to elevated sludge concentrations (Torfs et al. 2017).

Despite these recent SST model improvements, model calibration remains challenging and settling parameters are very influential key performance indicators of wastewater treatment such as effluent quality or sludge production (Ramin et al. 2014b; Li and Stenstrom 2016). Thus, accurate predictions of the sludge blanket heught (SBH) and especially the concentration profiles are still a big challenge in SST models. While for traditional activated sludge models, it often suffices to have good calculations of effluent and underflow concentrations, reactive settler models are more demanding: the biological conversion is directly dependent on the local sludge concentrations along with the whole sludge blanket. Hence, in order to develop a reactive SST model and to apply it to properly calculate the nitrogen mass balance, specific attention needs to be paid to the accurate description of the settling process and the calibration of the sludge concentration profile.

Past modelling efforts have mostly focused on modelling the biological processes in the bioreactor and the SST models used are typically simplified. The settling process is usually considered non-reactive, but several studies reported that biological reactions also occur in SSTs (Chapter 1.6.2). Mathematical models that can capture the sedimentation–compression process in settling tanks in combination with biological reactions are urgently needed from a practical perspective to further improve nitrogen removal (Gernaey et al. 2006).

1.6.1 One-Dimensional Settling Models

The one-dimensional (1-D) SST models predict the time-dependent responses to transient process inputs of SSTs (Li and Stenstrom 2014). The mass conservation and transfer are described mathematically in 1-D. Generally, these types of models are applied for the study of operation and control of SSTs as they can be easily combined with biokinetic models for other unit processes in an integrated WRRF model due to their lower computational demand. The 1-D modelling of SSTs is based on the flux theory of Kynch (1952) which assumes that the settling velocity depends on the local sludge concentration and describes sludge transport by a scalar conservation partial differential equation (PDE). The theory states that the transport of particles is the result of a gravitational settling flux combined with a bulk flux due to bulk movement or convective flow.

In WRRF modelling the SST model is coupled to biokinetic mass balance models which typically consist of a set of Ordinary Differential Equations (ODEs). To be able to do this more easily and use the numerical solvers available in typical WRRF modelling software, the PDE which describes the SST process is discretized into a set of ODEs. In this way, the numerical solution can be handled by standard ODE solvers. To achieve this, the settling tank is divided into horizontal layers with a uniform concentration within each layer. This approach is known as the Layer Approach and is the base for 1-D models of SSTs.

1.6.1.1 Takács Settling Model

In the model of Takács et al. (1991) the settler is divided into 10 layers of equal thickness. There are five groups of layers present in the model: the top layer, the layers above the feed point, the feed layer, the layers below the feed point and the bottom layer (Figure 1.8). The model considers 3 phenomena, i.e. feeding, settling and bulk liquid flux, in each layer. The Takács model (1991) is commonly used in many simulation programs (e.g. WEST, GPS-X, BioWin, Simba, SUMO) for modelling of WRRFs. The model performs reasonably well under dry weather conditions. However, under peak flow events (due to rain events) and situations that diverge from normal operating conditions the model's predictions lose realism. Also, the Takács settling model considers the number of layers as a model parameter which is not considered appropriate based on the proposed consistent modelling methodology for SSTs (Bürger et al. 2013). In order to obtain proper predictions of underflow and effluent concentrations and sludge blanket height (SBH) under different flow conditions, a more sophisticated model is required (Torfs et al. 2017).

$$(Q_i + Q_r)X_{in} \qquad Q_i X_1 = Q_i X_{effluent}$$

Top layer — 1
2
3
4
5
6
Feed layer — 7
8
9
Bottom layer — 10

$$Q_r X_{10} = Q_r X_{recycle}$$
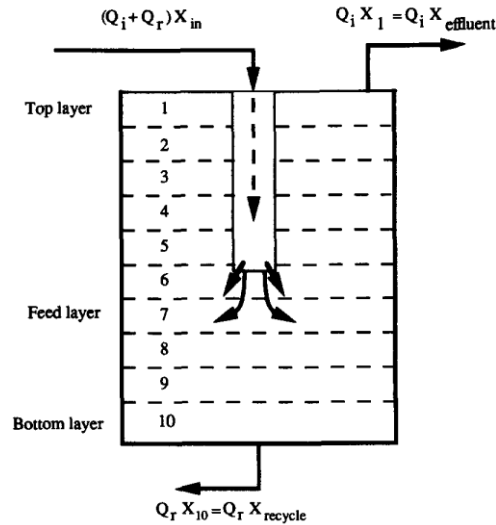
Figure 1.8 Layered Settler Model (Takács et al. 1991)

1.6.1.2 *Bürger-Diehl Settling Model*

The model of Bürger-Diehl (2011) (BD model) is the most recent 1-D SST model which corrects for unsatisfying elements of the commonly used Takács model (1991) and has several superior properties. The BD model ensures the solution of the governing PDE by reliable numerical methods for ODEs and it includes extra functionalities in the model structure to obtain a more detailed description of the sludge settling behaviour. The model considers sludge compression and inlet dispersion phenomena.

These properties are on/off functions that can be set by the user depending on the requirements of the modelling study. The BD model includes several phenomena in a modular way instead of trying to lump different phenomena in a single parameter or function (Bürger et al. 2013). In the BD model, the number of layers can be set by the user. Thus, it can be arranged depending on the level of detail and the aim of the modelling study by considering the computational time and resources available.

These advantages and the flexibility of the user-dependent model terms make the BD model very flexible and more realistic. The compression and dispersion terms can be switched on/off depending on the modeller's needs without affecting the solvability of the model. Moreover, the constitutive functions for hindered settling, compression settling and dispersion in the BD model can easily be updated or replaced whenever further research provides more insight into these phenomena (Bürger et al., 2013; Torfs, 2015).

1.6.2 Reactive Settling Models

The biological reactions occurring in the SST are an important factor to take into consideration when modelling nutrient removal biokinetic processes. The denitrification process can occur due to the high MLSS

concentrations and the anoxic environment in the sludge blanket despite mass transfer limitations such as concentration gradients and preferential pathways (Guerrero et al. 2013).

Several modelling approaches for reactive settling can be found in the literature. Gernaey et al. (2006) and Flores-Alsina et al. (2012) presented reactive settler models in which overall N removal performance was evaluated by comparing nonreactive and reactive settling in SST. Gernaey et al. (2006) combined the standard Takács model with an extra model block in the return sludge line (Figure 1.9). This block provides for an empirical, algebraic elimination of oxygen/nitrate via heterotrophic growth which results in a production of heterotrophic biomass that is transported to the bioreactor. According to that model, the WWTP overall denitrification efficiency improves compared to the non-reactive settling model predictions. However, the model predictions were not found realistic because the organic matter is also removed in the reactor included in the return sludge line. In the same study, a fully reactive settler model was developed based on the Takács model by extending the description of suspended solids sedimentation and transport of soluble components in the layers with the full set of ASM1 equations. As a result, each layer of this reactive settler model acts as an activated sludge tank in the simulations (Figure 1.9). The model predicted a 15.3% and 7.4% improvement of the simulated N removal performance, for steady-state and dynamic conditions respectively. However, the predicted positive effect on the denitrification process resulting from including the reactive settler model is accompanied by a decrease in the nitrification efficiency of the plant. This is caused by increased heterotrophic and autotrophic biomass decay in the settler, and the increased ammonia production due to hydrolysis and ammonification in the settler (Gernaey et al., 2006). Recalibration of the biokinetic model would be needed to obtain the same results.
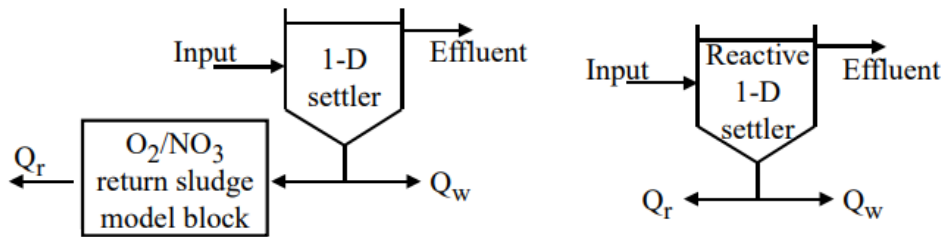
Figure 1.9 Illustration of the Different Reactive Settler Models Adopted in Gernaey et al. (2006)

Flores-Alsina et al. (2012) made the same comparison for 2 different WRRFs but for different biokinetic models, i.e. ASM1, ASM2d and ASM3, integrated with a reactive settler. The general results showed that incorporation of a reactive settler increases the hydrolysis of particulates, reduces the nitrate concentration at the bottom of the clarifier; increases the oxidation of organic matter and increases the decay of biomass. The study also found differences between different biokinetic models for the reactive settler. For example; the death-regeneration in

the ASM1 and ASM2d leads to the generation of a new substrate in the SST, whereas the endogenous respiration in ASM3 affects the biomass differently. Another important observation relates to the fact that the denitrification in the SST is affected by the reduction of dissolved oxygen and the increase of the particulate COD hydrolysis rate in the lower layers of the secondary settler. The consideration of these processes is important because the whole denitrification potential of the WWTP might be underestimated when using a standard non-reactive settler model. Still, the results of Gernaey et al. (2006) and Flores-Alsina et al. (2012) showed that using the Takács settling model coupled with a biokinetic model seems to overestimate the reactive capacity of the settler since the rate expressions to account for biological reactions seem to overestimate the biological growth in the settling tank and mass transport limitations were not considered.

Ostace et al. (2011) and Ostace et al. (2012) considered the reactions in the settling tank as the combination of Takács settling model with an extended ASM1 (with two-step nitrification and two-step denitrification) and ASM3 (two-step nitrification and three-step denitrification) biokinetic models respectively. Guerrero et al. (2013) also used the Takács settling model coupled with ASM3 biokinetics and evaluated the impact of different treatment configurations. However, these studies overestimated the reactive capacity of the settler. To compensate for the over-estimation of the 10-layer reactive settler model, Guerrero et al. (2013) introduced a reduction factor to the kinetics which is not present in the original mass balances. Similar to those studies, Walega et al. (2019) adopted a reactive settler model considering ASM2d biokinetics to make their simulation model more realistic for the secondary settler and achieve a proper nitrogen mass balance and control nutrient removal processes. However, the SST performance and its contribution to the overall nitrogen removal of the plant is not presented in detail.

Another, related application is the reactive settling occurring in sequencing batch reactors (SBRs), for which modelling approaches without PDEs can be found in Kazmi et al. (2001) and Alex et al. (2011). Also, Giberti et al. (2020) developed a dual-layer aeration tank settling model where the biokinetic reactions and settling phenomena occur when the aeration is switched off in the aeration tank based on an empirical relationship to predict the SBH in the aeration tank with ASM1 biokinetics.

In Bürger et al. (2016) the BD settling model is extended with a simplified biological model where only denitrification reactions are considered to describe the last settling stage of a sequencing batch reactor with denitrification. Reactive settling is modelled with a consistent modelling methodology by starting with the mass balances and using appropriate numerical methods for the discretization of the model PDEs. Results of this study indicate that the suggested numerical scheme works well and that the expected denitrification process is simulated correctly. Furthermore, numerical tests with other initial data, resulting in non-monotone concentration profiles and movement of particles upwards, indicate that the numerical method could be extended to the case of continuous sedimentation in SSTs of WRRFs. Bürger et al. (2016) was the first study to combine an advanced

SST model (including hindered and compression settling) with biological reactions. However, a simplified biological submodel was used, and the model was only simulated for a batch case.

Bürger et al. (2018) improved the numerical solution of the developed reactive settler model. In this study, the derived model includes the volume, the mass balances and common constitutive assumptions on the relative velocity between the solid and liquid phases and on the reactions between them. It is possible to insert any suitable constitutive function to model the effects of hindered settling, compression and biochemical reactions with the updated numerical scheme. Thereafter, the study of Bürger et al. (2021) extended the 1-D reactive settler model for varying cross-sectional area and attempted to obtain a numerical method to make its implementation suitable in simulators that are being used for modelling of WRRFs. The developed models presented in these studies were theoretical and not calibrated on experimental data.

1.6.3 CFD Models

CFD models have become increasingly popular in the last decade as tools to improve insights and/or optimization of the settling processes in the SST. Their success results from their ability to predict the performance of a settling tank by modelling the internal flow pattern and transport phenomena of solids and solutes in 2-D or 3-D (Wicklein and Samstag 2009). With proper boundary conditions, CFD models can approximate the velocity vectors and turbulent mixing coefficients with a good accuracy (Ramin 2014). These models are also applied to perform dynamic simulations of wet weather events and the development of wet weather strategies by combining them with whole-plant simulators (Parker et al. 2008; Griborio et al. 2010). The major disadvantage is their high computational needs (Plosz et al. 2011). CFD models are very useful to model the flocculator at the center of a settler and determine its effect on settling phenomena. However, within this PhD research project, rather than mixing behaviour of the activated sludge in the feed zone and the flow pattern, it is aimed to model the biological reactions that take place in the SSTs. For that reason, CFD models will not be used in this PhD project.

2. PROBLEM STATEMENT & OBJECTIVES

Typically, 60% of the energy demand in the water sector goes to wastewater treatment and 40% to drinking water production (in case surface water is the source). In wastewater treatment, nutrient removal and micropollutant removal increase the energy and resource demand further. Nitrification significantly increases the energy consumption of the process due to additional oxygen consumption and it is known that 50% of the process energy is typically used in aeration in N removing WRRFs followed by pumping actions (14%) (McCormick and Chakrabarti 2013). In addition to that, secondary settling processes have been mostly considered as non-reactive and their contribution to the overall nitrogen mass balance of the WRRFs is neglected. However, enhanced denitrification in the SST is important to accurately describe the N mass balance in the plant and to capture the risk of nitrogen gas formation in SSTs. In addition, it would allow us to investigate -for the same N-removal- reducing internal recycle pumping in the biological reactors and lead to savings in energy consumption and costs.

Within this PhD research project, it is aimed to investigate energy and resource-efficient processes and operational conditions for nitrogen removal systems. For this purpose, modelling will be used which serves as an excellent tool for process optimization and moving forward towards energy neutral operation of WRRFs.

Objective 1: Improving the understanding of the reactive settling process and its potential for denitrification

Denitrification in the secondary settling tank can make significant contributions to the overall N mass balance of a WRRF. It is aimed to develop a reliable reactive settling model to improve the understanding of reactive settling processes, the hindered and compression behaviour at high sludge concentrations and to better predict the sludge blanket height and sludge concentration profile over the depth of the settler. This would allow to better determine the biological reaction rates (and in particular the denitrification rate) occurring inside the secondary clarifier and its contribution to overall total inorganic nitrogen removal in the system. This PhD research project aims to develop the first modelling work that combines the full set of ASM1 biokinetics with the 1-D Bürger-Diehl model which includes compression and is supported with a full-scale measurement campaign. The developed model can be used for control and optimization of WRRFs.

Objective 2: Energy and resource optimization in conventional N removal systems

Conventional nitrogen removal (nitrification and denitrification systems) is still the most widely applied N removal process for wastewater treatment which is an energy and resource-intensive process: nitrification needs a lot of oxygen and alkalinity and denitrification requires carbon (either utilizing influent wastewater carbon or

supplemental carbon). In addition, due to the large safety margins of plant design and the different influent characteristics, many N removing WRRFs are not operated optimally. Strict effluent criteria and high operational costs enforce process optimization and application of energy efficient processes in N removing WRRFs. Within this PhD research project, a pilot-scale pre-denitrification N removal WRRF will be modelled and used for scenario analysis to optimize energy consumption for aeration and pumping of sludge. It aims to determine the optimum DO set-points, aeration strategy, sludge and internal recycles for the conventional N removal process by using a well-calibrated and validated model. The reactive settler model will be tested within this plant-wide model and optimal operational conditions will be investigated to improve total inorganic nitrogen removal and optimize sludge and internal recycles for reduction of energy consumption.

Objective 3: Testing the process improvements under aeration with AvN control and short-cut N removal processes

Compared to nitrification-denitrification over nitrate, the application of short-cut N removal processes in mainstream wastewater treatment has significant potential to save energy (oxygen demand) and resources (carbon demand) and pursue energy independence of WRRFs. For that reason, the deammonification process that relies on partial nitritation and anammox (anaerobic ammonia oxidation) has received considerable attention over the last decade in both academia and industry.

Within this PhD research project, it is aimed to evaluate the applicability of continuous and intermittent AvN control strategies on a pilot-scale WRRF and compare their performance. The objective of the AvN control is to maintain an equal concentration of NH_4-N and NO_3-N (NOx-N preferably) in the effluent of the B-stage of an A/B biological wastewater treatment process, by manipulating the extent of aeration in the aerobic reactor compartment (Regime et al. 2015, US Patent 2014/0069864). By maintaining this ratio the effluent can be optimized for downstream anammox treatment, and as such the overall energy budget due to aeration, required to remove COD and N, can be reduced. It is aimed to identify the 2 key operational factors while optimizing simultaneous nitrification denitrification in the aerated reactors: minimum applicable dissolved oxygen concentration and sludge retention time for both AvN control strategies. They are both crucial for the growth kinetics of AOB and NOB thus achieving a stabilized AvN control. In addition, lowing the SRT would lead to less sludge accumulation in the system thus lowering the aeration cost and higher N removal through sludge wasting (N associated growth of microorganisms). Overall, this research aims at finding out if the simultaneous nitrification denitrification performance and effluent concentrations can be sustained over long time for both AvN control strategies.

3. MATERIALS & METHODS

3.1 pilEAUte WWRF & Data Sources

The pilEAUte is a pilot-scale WRRF located in the Adrien-Pouliot Building (Department of Civil Engineering and Water Engineering) at Université Laval. The plant is fed by domestic wastewater originated from the student residence and kinder garden, and rainwater from the parking lot in the university campus. The plant configuration consists of a pumping station, a storage tank, a primary settler and two parallel biological reactors called pilot and co-pilot. Each biological reactor has two anoxic basins followed by three aerobic basins and a secondary clarifier. Every unit of the pilot-scale plant is made of stainless steel and PVC piping is used to transfer the water within the plant.

The pumping station (Figure 3.1) transfers the wastewater from the campus sewer system to the inlet of the pilEAUte. There are 2 Flygt shredder pumps installed in the pumping station which shred the large particles present in the raw wastewater in order to protect the pumps and pipes further down the treatment line.
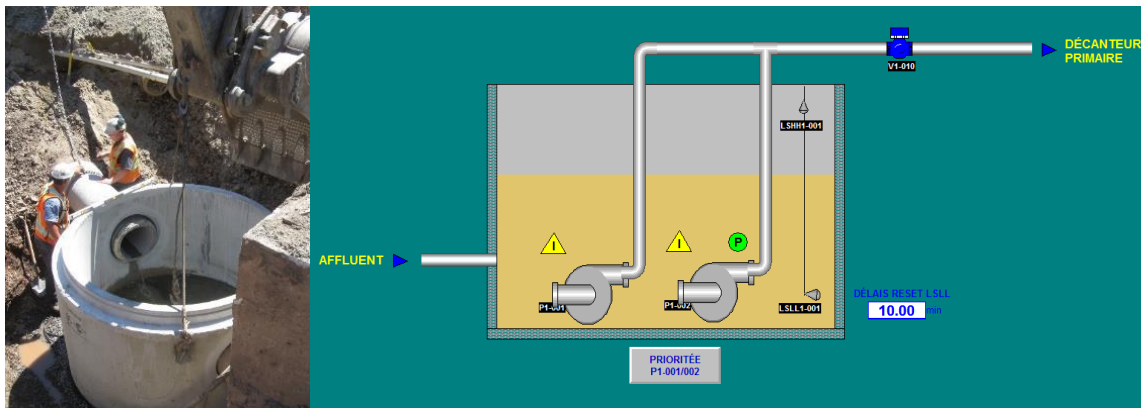
Figure 3.1 pil*EAU*te WRRF Pumping Station

From the pumping station, the wastewater is pumped to a storage tank. The storage tank has a volume of 5 m^3 and is equipped with a mechanical stirrer to maintain homogenized influent. After the equalization in the storage tank, wastewater is conveyed to a primary settler with a dry-screw type pump (brand Mono and Moyno) at a flow rate of 1.1 m^3/h. A Y-strainer (mesh size 7/8 in) is installed on the pipe between the store tank and the primary settler to screen the large solid particles from the influent wastewater to protect the pump. All pumps in the pilEAUte plant are equipped with variable frequency drive (VDF) to adjust the pump's flow or pressure to the actual demand.

The primary settler (volume = 2.8 m³, surface = 1.2 m²) is designed to allow gravity settling of particles in the wastewater. The primary effluent is conveyed to 2 biological reactors called pilot and co-pilot at a flow rate of 0.5 m³/h per reactor (Figure 3.2). The excess primary effluent and the waste primary sludge are returned to the sewer system.
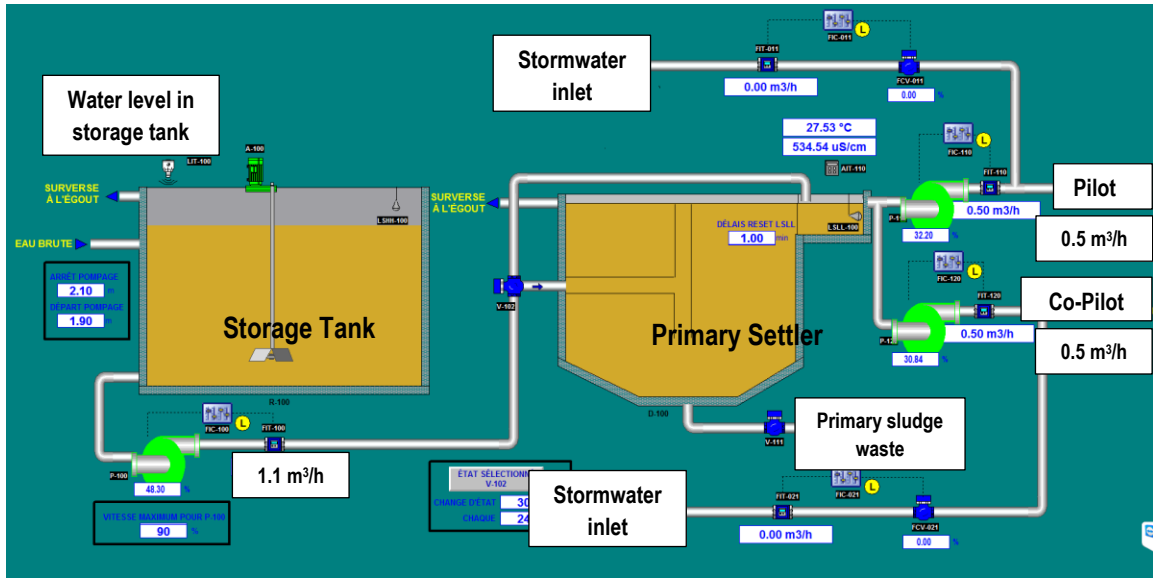
Figure 3.2 Storage Tank and Primary Settler Flow Scheme

Each biological reactor has the same design and is capable of carbon and nitrogen removal using a pre-denitrification configuration (Figure 3.3). The reactors are divided into anoxic and aerobic basins. The anoxic basins (the first 2 basins) of each biological reactor are equipped with mechanical stirrers. The aerobic basins that follow are equipped with industry-standard diffusers at the bottom and aerated with compressed air. It is possible to control the aeration rate for each basin through mass flow controllers connected to the SCADA system. Each basin has separate air flow lines and the air flow can be set with the controllers.

Each biological reactor has an internal recycle from the 5th basin to the 1st basin to sustain pre-denitrification. The internal recycle flow rate is set at default 1.5 m³/h which is 3 times the influent flow rate. Heat exchangers are installed in the internal recycle streams to be able to change the temperature of the mixed liquor. There is also a sludge recycle loop (0.5 m³/h) from the secondary clarifiers to the first basins of the biological reactors to ensure the mixed liquor concentration in the biological reactors. Excess sludge is wasted to ensure a sufficient sludge age for nitrifier growth.
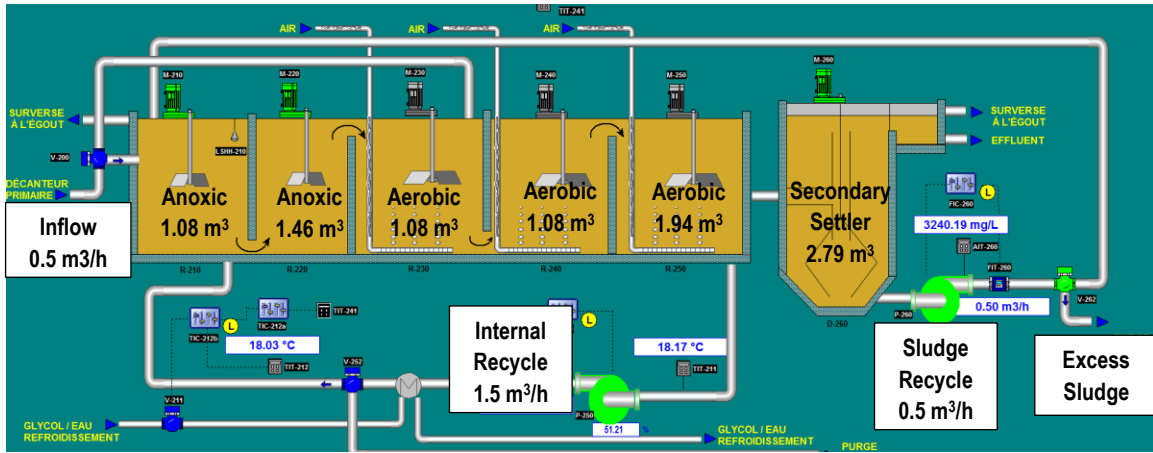
Figure 3.3 Biological Reactors (Pilot and Co-Pilot) Flow Schema

The secondary clarifiers have a total volume of 2.8 m³ each and a surface of 1.2 m². The total height of the clarifiers is 2.5 m and the feeding point is located at 1.1 m above the bottom where the conical shape starts (Figure 3.4). The conical part is equipped with a chain which is hourly rotating against the wall to facilitate sludge transport to the bottom. The inflow of the SST from the biological reactors is 1.0 m³/h and the underflow rate is 0.5 m³/h under standard operational conditions. The effluent and sludge wastage of the secondary clarifier is discharged back to the sewer system.
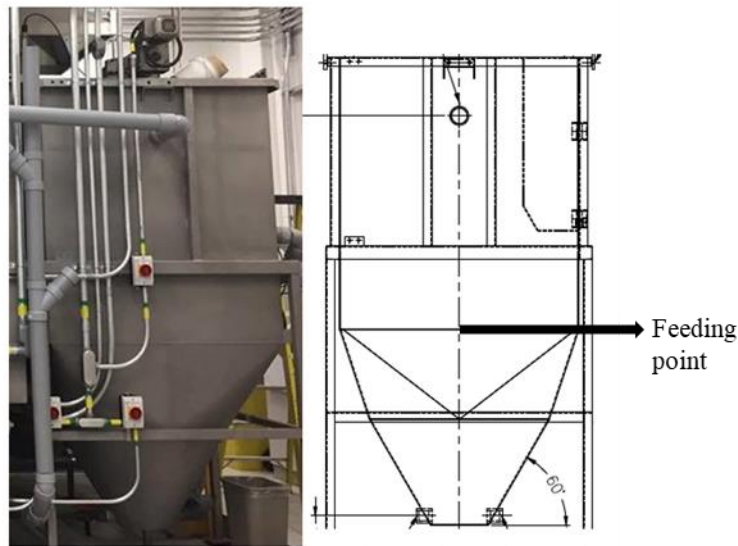
Figure 3.4 pil*EAU*te WRRF Secondary Clarifiers

The pil*EAU*te WRRF described above offers great operational flexibility to run under different conditions. Its set-up allows parallel experimentation on the efficiency of control systems for nutrient removal. It is possible to

bypass the primary clarifier and feed the raw wastewater from the storage tank directly to the biological reactors. Also, the influent flow rate (to the primary settling tank) can be increased to approx. 2 m^3/h. Sludge recycling can be done from pilot to co-pilot and from co-pilot to pilot to allow the mixing of both sludges and provide equal start-up conditions. As can be seen from Figure 3.3, it is possible to pump influent wastewater to the 3rd basin of the biological reactors to allow step-feeding of the system or to operate biological reactors only with nitrification. It is also possible to feed the return sludge and internal recycling to the 3rd basin instead of the 1st basin to allow operational flexibility. With the heat exchangers, it is possible to run the biological reactors at different temperatures. Sludge wastage can be done from both the sludge recycle line (from the secondary clarifier) and from the aeration tank (Ekama 2010). Thus, the pil*EAU*te WRRF is a great workspace to collect data and understand system behaviour under different operational conditions for research studies in the field of WRRF modelling and control. Within the PhD project, the operational flexibility of the pil*EAU*te WRRF was exploited to collect detailed data for modelling and testing different N-removal processes (e.g. conventional nitrification/denitrification, simultaneous nitrification/denitrification and AvN operation).

The monitoring data of the pil*EAU*te are collected by 2 different data acquisition systems: SCADA and mon*EAU*. All data from these sources (including their metadata) are automatically stored in an extensive SQL database called datEAUbase. The database is accessible through a user-friendly interface which allows easy access to data for different sensors and time periods as defined by the user (Plana et al. 2017).

The pil*EAU*te is monitored with sensors at the outlet of the primary clarifier, the biological reactors, the recycle streams and the outlet of the secondary clarifiers (Figure 3.5). Besides these, it is possible to take grab and continuous samples from different points with refrigerated autosamplers. Information about the pil*EAU*te online monitoring system is given in Table 3.1.

Table 3.1 Online Monitoring Equipment of pilEAUte

Location of Sensor	Sensor name	Manufacturer	Monitored Parameters	Principle	Monitoring System
Primary effluent	Spectro::lyser	S::CAN	COD_{total}, $COD_{soluble}$, TSS	UV-VIS spectrophotometry	mon*EAU*
	Ammo::lyser	S::CAN	NH_4-N, K, Temperature, pH	Ion selective electrode	mon*EAU*
	Varion	WTW	NH_4-N, K, Temperature, pH	Ion selective electrode	mon*EAU*
	Conductivity meter (Inductive)	Hach	Conductivity, Temperature	Potentiometric	SCADA
	RODTOX	Hach	BOD_{short_term} and Toxicity	Respirometry	mon*EAU*
Biological reactors – Basin 2	Solitax	Hach	TSS	Infrared duo-scattered light technique	SCADA
Biological reactors – Basin 4	DO meter (LDO)	Hach	Dissolved oxygen, Temperature	Luminescent	SCADA
Biological reactors – Basins 2&5, Secondary effluent	Trescon/Purcon	Hach	NH_4-N, NO_2-N, NO_X-N (NO_2-N & NO_3-N total)	Potentiometric or Photometric	mon*EAU*
Sludge recycle line	Solitax	Hach	TSS	Infrared duo-scattered light technique	SCADA
Secondary effluent	Turbidity meter	WTW	Turbidity	Nephelometric	mon*EAU*
	Varion	WTW	NH_4-N, NO_3-N, K, Cl	Ion selective electrode	mon*EAU*
	pH meter	Hach	pH, Temperature	Potentiometric	mon*EAU*
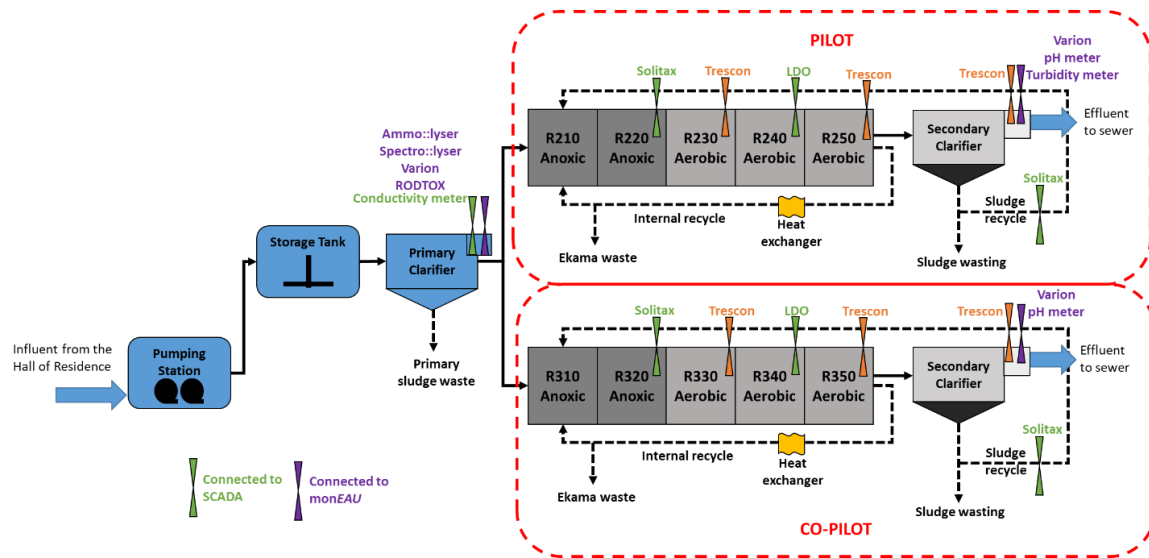
Figure 3.5 Monitoring of pil*EAU*te

3.2 Modelling Methodology

Within this PhD project, the model development was based on the Good Modelling Practice (GMP) Unified Protocol presented by the IWA Task Group on Good Modelling Practise (Rieger et al. 2012). The models were developed in the software platform WEST (DHI, Denmark; Vanhooren et al. 2003).

3.2.1 Modelling Protocol

The GMP Unified Protocol presents a framework to deal with the practical application of commonly used process models such as ASM-type models. The GMP Unified Protocol is based on other wastewater oriented protocols such as STOWA (Hulsbeek et al. 2002), BIOMATH (Vanrolleghem et al. 2003) and WERF (Melcer et al. 2004). It is an approach that unifies the main steps of the existing protocols while extending them with some key elements provided in general guidelines. The general scheme of the GMP Unified Protocol is explained below.

Step 1. Project Definition: This step includes the definition of the objectives of the modelling study and identification of stakeholders and their responsibilities as well as the determination of the budget. The objectives of each model developed in the scope of this Project were already presented in detail in Chapter 2.

Step 2. Data Collection and Reconciliation: This step aims to collect, assess and reconcile data sets necessary for the simulation project. A stepwise procedure to analyse collected data is provided including statistical analyses suggested by the GMP group, engineering expertise and mass balancing. The data required for this modelling study is supplied from the pil*EAU*te WRRF by continuous monitoring specific to the modelling goals. Measurement campaigns were carried out for different modelling purposes (e.g. tracer test for the

hydraulic model, reactive settler model development, aeration control through AvN). Also, existing data from previous measurement campaigns were considered for hydraulic model and influent characterization (e.g. COD and N fractionation).

Step 3. Plant Model Set-Up: This step involves setting up the model of the WRRF by translating real-world data into a simplified mathematical description of reality. It involves setting up the models' layout and determination of the sub-model structures. At this step, model output graphs and tables should also be set-up. The plant model set-up requires checks of the general functionality of the model to ensure it gives sensible outputs.

Within this PhD project, a previous modelling study which analysed the hydraulic situation of the pil*EAU*te will be considered as initial model set-up (Zhao and Vanrolleghem 2015). The biokinetic model selection should also be done at this step by considering the objective of the modelling study and the desired level of detail of the model. In this case, the ASM1 biokinetic model extended with 2 step nitrification and denitrification is to be used as the biokinetic model to represent carbon and N removal processes.

Step 4. Calibration and Validation: Model calibration is the process of modifying the values of the parameters until simulation results match an observed set of data. The process is completed when the model outputs are within an acceptable error to the real data. Validation is the second step that ensures the calibrated model is able to perform predictions with a level of confidence in accordance with the modelling objectives. Overall the aim of the GMP Unified Protocol is to provide a roadmap for the practical application of WRRF models. However, it does not provide answers to the detailed questions that this PhD project poses. For this reason, the calibration step in the GMP protocol is further detailed by using parts of the BIOMATH Calibration Protocol.

The BIOMATH research group from Ghent University (Belgium) proposed a generic calibration procedure (Vanrolleghem et al. 2003), using state-of-the-art parameter estimation methods. The protocol focuses on model calibration by considering hydraulics, settling and aeration individually as well as the interaction between those phenomena. The procedure requires a high level of experimental results and expert knowledge for systems analysis (Rieger et al. 2012). The protocol's targeted users are researchers and other modellers dealing with advanced modelling issues such as parameter estimation and identifiability of parameters, sensitivity and uncertainty analysis (Sin et al. 2005).

The BIOMATH calibration protocol is visualised in Figure 3.6. This calibration procedure is integrated within the GMP Unified Protocol for the calibration step as it is much more detailed and meets the requirements of the PhD project (e.g. the need to model the measured backflows between different basins of the biological reactor, integrating the developed reactive settler model). It requires the calibration of the hydraulic model, the settler model and the biological model to be done sequentially.
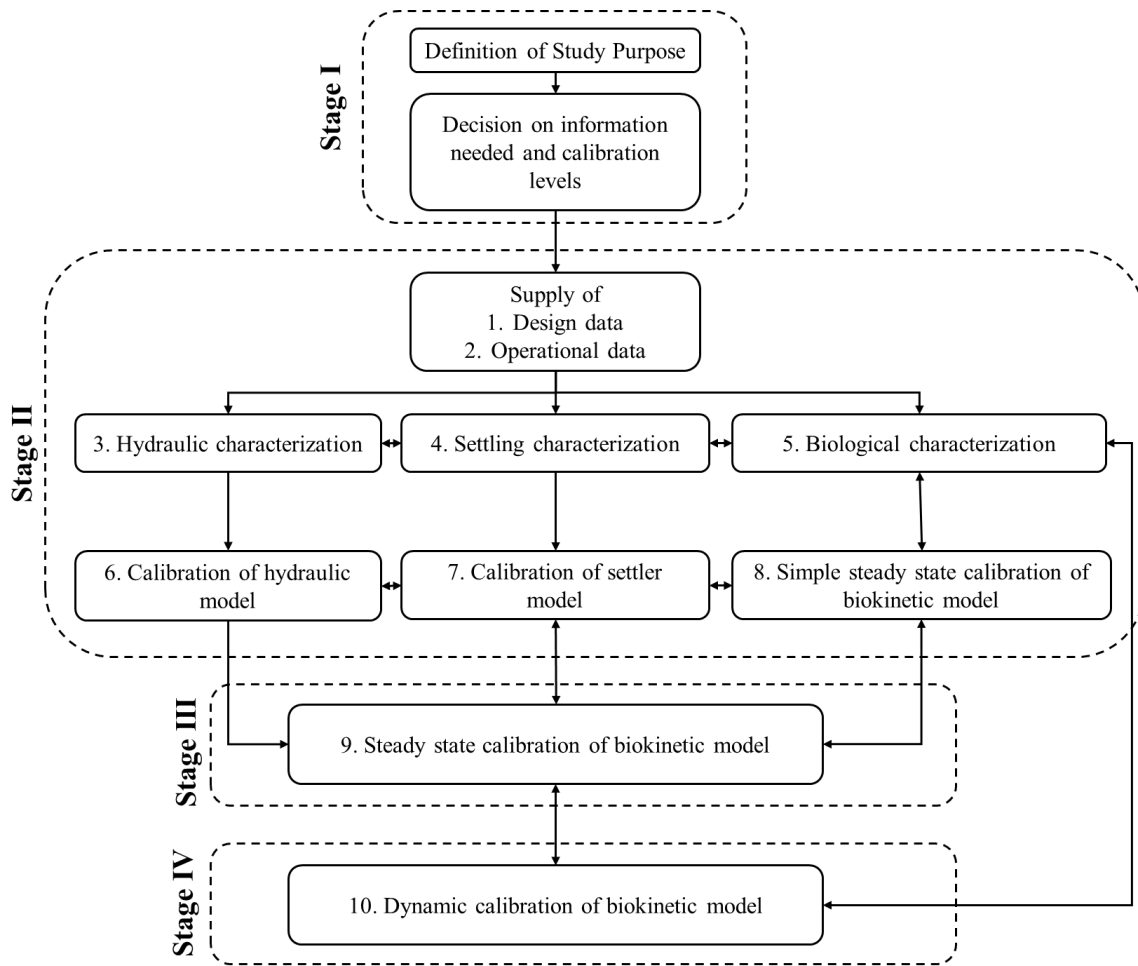
Figure 3.6 BIOMATH Calibration Protocol

The mass transfer characterization is suggested to be done first in the protocol. In the mass transfer characterization two main aspects have to be considered: oxygen transfer characterization and hydraulic characterization of the WRRF. Because one of the aims of the PhD project is energy optimization through aeration control, the determination of parameters related to aeration, especially the oxygen transfer efficiency (k_{La}), is quite important. Regarding the determination of the k_{La} for aeration, first, the influence of operational and biological factors on the oxygen transfer have to be considered, e.g. temperature. Properly quantifying daily air consumption in each aerated basin is considered while constituting the aeration model.

Mass balances of the system for mixing are also checked at this step. The protocol promotes the application of well-designed tracer tests for the hydraulic characterization of the WRRF. Within this PhD project, a tracer test and a hydraulic model had already been developed for the pil*EAU*te WRRF (Zhao and Vanrolleghem 2015). Another tracer test was designed and applied to determine the suspected backflows between the different basins of the biological reactors (Souidi et al. 2018).

Mass balances of sludge, COD and N in the WRRF are to be developed in the next step. They are important as a necessary data quality check (e.g. to properly determine sludge age). In this work, the settling process is to be modelled as a reactive settler. The developed reactive settler model is to be calibrated in terms of its settling characteristics with detailed measurement campaign data (Chapter 4) and is to be integrated into the plant-wide pil*EAU*te models (Chapter 5). The influent characterization, fractionation and hindered settling velocity parameters are obtained from the measurement campaign. A Monte Carlo-based calibration procedure is adopted for the calibration of sludge compression behaviour.

The next step is the biological characterization of the activated sludge and the set-up of the biological model. Mass transfer characterization of the WRRF, influent fractionation and biokinetics characterisation are to be done in this step. The ASM1_AN model developed by Van Hulle (2005), which is implemented in the modelling platform WEST's model library, was chosen as biokinetic model for both the biological reactors and the reactive settler. The ASM1_AN model is an extension of ASM1 with Anammox and two-step nitrification and denitrification (details of the state-of-the-art biokinetic models are presented in Chapter 1.4). The aerobic growth of heterotrophic biomass is described as in ASM1. Autotrophic nitrification of ammonium into nitrite and then nitrate is described as a 2-step process with distinct groups of AOB and NOB. Denitrification of nitrate into nitrite and then N_2 is also described as 2-step process and denitrifying heterotrophs use nitrite and nitrate when oxygen becomes limiting. For the nitrification and denitrification model, ammonia rather than ammonium, and nitrous acid rather than nitrite are used as actual substrates for AOB and NOB growth, respectively. The reason to choose ASM1_AN is that the model includes nitrite as an intermediate variable and the developed model can be further used for modelling of short-cut N removal process (albeit not in the scope of this PhD project).

The calibration of the ASM-type biokinetic model is done by first selecting the identifiable model parameters. Selection of the most influential parameters is done by considering previous literature reports on methods for calibration of nutrient removal WRRF models. In this context, sensitivity analysis allows, based on the target of the modelling exercise, to discriminate between the relatively less influential and the most influential parameters.

Following Mannina et al. (2011), a step-wise Monte Carlo-based calibration protocol was slightly modified to calibrate the biokinetic model (Figure 3.7) (Chapter 5).

- First, a pre-selection of model parameters is done based on engineering expertise and the available data.

- Second, a pre-screening of parameters is done based on local sensitivity analysis (LSA). This allows to determine the influential model parameters on the selected model outputs/variables individually and eliminate non-influential parameters. LSA-based pre-screening of model parameters also reduces the number of model

parameters to be calibrated in this step. The central relative sensitivity (CRS) of each model parameter on the selected model variables is to be calculated and used as the evaluation criterion.

- Third, different parameter subsets are determined prior to calibration, each focusing on a different group of output variables (e.g. N variables (NO_3-N, NO_2-N, NH_4-N), COD variables (COD_S, COD_P)). Monte Carlo simulation and global sensitivity analysis (GSA) are to be applied in this step to determine the parameter subsets. Multivariate linear regression between the sampled resulting model parameters and variables is performed. Standardized regression coefficients (SRC) of each model parameter for each model output individually are to be used as the evaluation criterion. Based on this evaluation, some model parameters might be influential on more than one model variable since those parameters influence more than one process. This means, a model parameter can be included into more than one parameter subset and needed to be recalibrated.

- Finally, the model calibration is performed by a step-wise Monte Carlo-based calibration of the subset of influential parameters on the relevant group of model outputs/variables (Weijers & Vanrolleghem 1997; Mannina et al. 2011). The parameter subset calibration procedure is started with the parameter subset which has the highest number of parameters that is influential only on one group of model variables. That way, the model parameter subsets that have parameters influential on multiple model output groups, are left to be calibrated later. Thus, this calibration protocol (Mannina et al., 2011) allows an appropriate calibration hierarchy for the parameter subsets based on the interdependency of state variables, and determines the optimized parameter values based on multiple model outputs/variables. Monte Carlo simulation is to be applied in this step as well. The Sum of Squared Errors (SSE) between the model predictions and the measurements of the relevant group of variables is to be used as the evaluation criteria (objective function). Each model variable within the group is weighted to calculate one single objective value for each Monte Carlo run. Then, the parameter set of the Monte Carlo run that gives the minimum overall objective value is chosen as the optimal parameter set. If none of the model parameters within the relevant subset is influential for another group of outputs/variables, all parameter values for the subset can be fixed to the calibrated values and the next parameter subset is to be calibrated. If not, the non-influential model parameters are fixed and the influential ones are to be recalibrated within the next parameter subset. When all the parameter subsets are calibrated, the final set of calibrated model parameters is obtained. Then, the calibrated model is used to simulate a different time period than the calibration time period for model validation.

Note that the plant-wide model of the pilEAUte WRRF is to be calibrated and validated with the available monitoring data. Even though the proposed biokinetic model calibration procedure adopts the local and global sensitivity analyses to determine the model parameter subsets and the relevant model variable groups for calibration, practical identifiability issues may arise with the parameter subset calibrations. Practical identifiability

analysis challenges the quality and quantity of the data and is used to verify whether the available data are sufficiently informative to identify model parameters and give them an accurate value (Vanrolleghem et al. 1995). To eliminate this issue and check the quality of the parameter estimations, confidence intervals can be determined with statistical methods such as the Fisher Information Matrix or the generalized likelihood uncertainty estimation (GLUE) (Weijers & Vanrolleghem 1997; Asprey & Macchietto 2000; Mannina et al. 2011).

Step 5. Simulation and Result Interpretation: The calibrated and validated model is used to run simulations to meet the objectives laid out in the Project objectives (Chapter 2). This step includes the scenario analyses for energy and resource optimization in N removing process. The overall modelling protocol adopted within the scope of this PhD Project is presented in Figure 3.8.

3.2.2 Modelling Platform – WEST

The models are built in the modelling and simulation platform WEST (DHI, Denmark; Vanhooren et al. 2003). The simulation platform can be used to model physical, chemical and biological processes in WRRFs, sewer systems and rivers. It is a user-friendly simulator thanks to its extensive and transparent default model library and adequate flexibility to develop customised model libraries. The models included in WEST are programmed in MSL-USER which is an open source modelling language. Thus, it is possible to modify, improve and integrate existing models as well as efficiently introduce new models. The main application areas of WEST in wastewater treatment are process optimization, design and the development of control strategies.
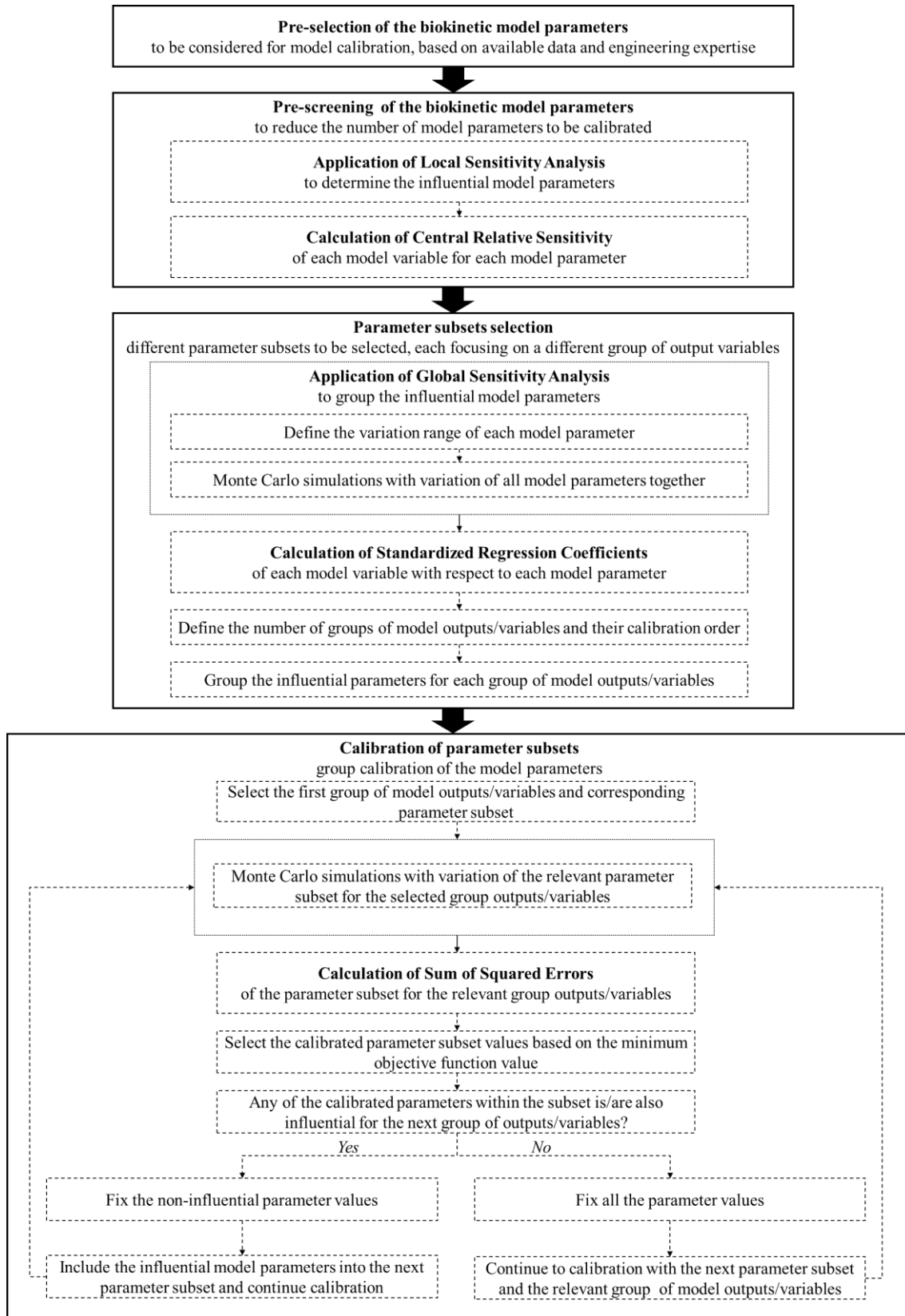
Figure 3.7 Calibration Protocol for the Biokinetic Model (based on Mannina et al. 2011)
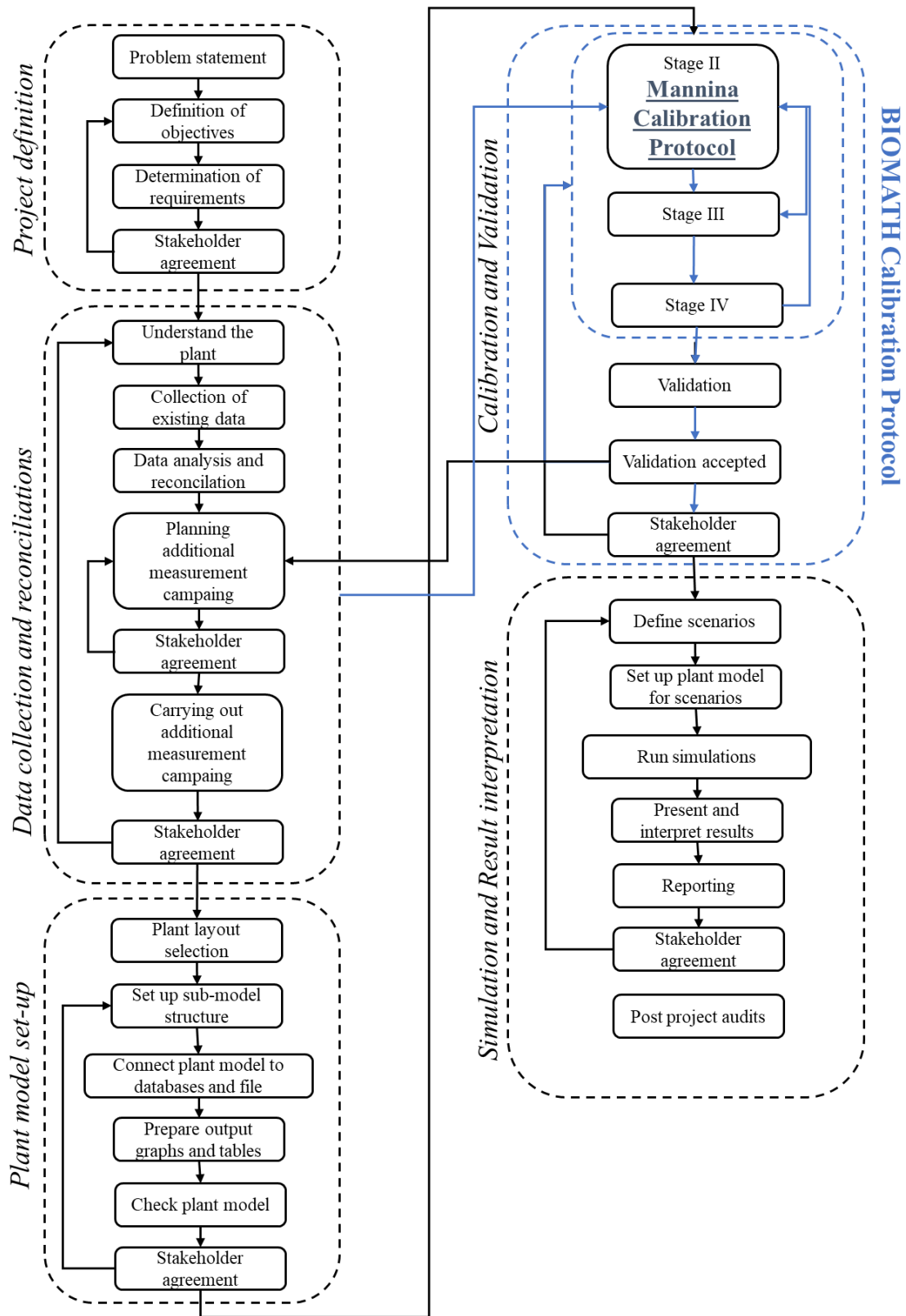
Figure 3.8 General Modelling Methodology of the PhD Project (based on Rieger et al. 2012)

4. DEVELOPMENT of a 1-D REACTIVE SETTLER MODEL

Secondary settling tanks (SSTs) are mainly used for gravity separation of microorganisms from the effluent in water resource recovery facilities (WRRF) and they bring the thickened sludge back to the biological reactors. Through settling and thickening, a significant amount of the overall sludge inventory of the treatment plant can be stored at the bottom of the SST. This accumulated sludge mass can turn the bottom of the settling tank into an additional biological reactor Particularly at long residence times in the settler and with incomplete denitrification in the biological reactors, denitrification can take place at the bottom of the settling tank, where the concentration of sludge is high, nitrate levels are still substantial, oxygen is no longer present and organic matter is available through the decay of biomass or internally stored carbon (Siegrist et al. 1995; Koch et al. 1999; Bürger et al. 2016). Simultaneous occurrence of biokinetic processes and physical settling phenomena in a settler leads to the concept of a so-called reactive settler. Its dynamics should be investigated to correctly determine the effluent and underflow characteristics, and also analyse the contribution of SST denitrification to the overall N removal in a WRRF (for details see Chapter 1.6.2). In addition, strong denitrification during overloaded clarifier conditions can lead to N_2 gas bubble induced rising sludge and be detrimental to the plant's efficiency (Henze et al., 1993). Detailed process understanding is thus needed to ensure safe and efficient system operation and control of denitrification in the settling tanks. Note that anaerobic conditions within the sludge blanket can lead to the release of phosphorus in secondary clarifiers as well but this is outside the scope of this work.

Within this PhD research project, an improved 1-D reactive settler model is pursued to increase the understanding of reactive settling processes and obtain a better prediction of the nitrogen mass balance in wastewater treatment systems. To achieve that, a good prediction of the hindered and compression behaviour at high sludge concentrations and a better prediction of sludge blanket height (SBH) and sludge concentration profile over the depth of the settler are needed. This allows determining the biological reaction rates (and in particular the denitrification rate) occurring inside the sludge blanket. The presented work demonstrates the relevance of considering reactive settling for a good nitrogen mass balance in a plant-wide model and highlights the importance of the clarifier geometry and the choice of settling functions in SST models. It is the first modelling work that combines the full set-of ASM1 biokinetics with the 1-D Bürger-Diehl (BD) model which includes compression and is supported by a full-scale measurement campaign. The developed model can be used for control and optimization of WRRFs.

4.1 Data Collection

A unique measurement campaign was carried out with different operational scenarios to quantify the denitrification in a secondary settling tank. The measurement campaign was carried out on the pilEAUte WRRF that is located at Université Laval (Chapter 3.1 for details). During this campaign, it was aimed to quantify the N-removal rates inside a SST and to obtain data for development and calibration of the reactive settler model. Measuring reactive settling requires the presence of a minimum sludge mass inside the SST. Therefore, the sludge blanket height (SBH) was raised by reducing the underflow rate. During this experimental work, different operational scenarios were applied to create different SBH and different denitrifying activity levels.

The three different operational scenarios are presented in Table 4.1 and Figure 4.1. Each operational scenario was applied for a week till the system reached steady-state.

Table 4.1 Experimental Work Operational Scenarios

Scenario	Operational Change	NO_3-N load	SBH	Aim
1	-	Average (~10 mg/L)	-	Reference conditions
2	Reduced RAS	Average (~8 mg/L)	Increased	Effect of high SBH
3	Reduced RAS & IR	High (~14 mg/L)	Increased	Effect of high NO_3-N load and high SBH
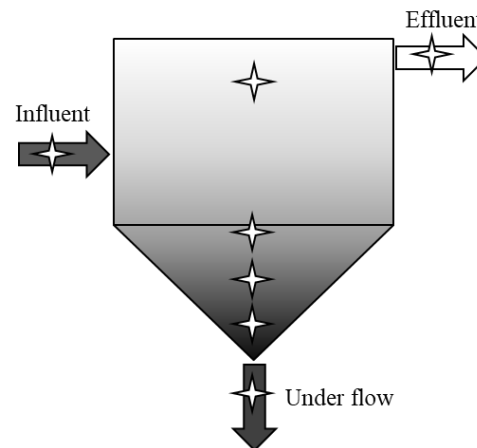
Figure 4.1 Sampling Points in the Studied SST

The reference scenario refers to normal operating conditions of the SST (no significant denitrification in the SST) with an average underflow rate (sludge recycle – RAS) (0.5 m³/h) and low SBH. The SBH was increased in Scenarios 2 and 3 by reducing the underflow rate (0.15 m³/h) to increase the reactive volume for substantial

denitrification in the SST. In order to determine at which point SST denitrification might lead to rising sludge, the nitrate loading to the settler was increased in Scenario 3 by reducing the internal recycle (IR) in the biological reactor leading to reduced denitrification in the pre-denitrification zone.

For each scenario, when the system reached steady-state, grab samples were taken with a ⅜" diameter tube brought down to different locations in the settler: from SST influent and effluent as well as at different depths of the SST, particularly in the sludge blanket (Figure 4.1). At least four measurements were collected throughout the depth of the sludge blanket and at least one measurement was collected in the clarification zone. The flow velocity in the sampling tube (0.13 m/s) was sufficiently high to prevent settling in the tube. Samples were analysed for the following parameters: NH_4-N, NO_3-N, NO_2-N, TN, COD_P, COD_S, TSS, pH, alkalinity and temperature (COD and pH measurements were not used for modelling particularly thus the results are not shown). Dissolved oxygen (DO) concentrations at each sampling point were also measured with a portable DO sensor. Moreover, for each scenario, the SBH was measured and a series of batch settling tests was performed to determine the hindered settling velocity. The batch tests were performed in a cylinder with a top diameter of 8 cm and a volume of 2 L.

Figure 4.2 shows the steady-state measurement results for the three different scenarios, for TSS and NO_3-N. SST influent (SST_{in}), effluent (SST_e) and underflow (SST_u) are shown in grey with concentration profiles along the height of the SST shown in black.

The TSS measurements for each scenario were validated by comparing the measured underflow TSS concentrations to the expected underflow concentration based on the steady-state mass balance over the SST (based on the influent and effluent concentrations and known flow rates in the system) (Table 4.2). Given typical measurement errors up to 15%, the mass balance is deemed acceptable.

Table 4.2 SST Mass Balance of TSS for Each Scenarios

	Scenario 1	Scenario 2	Scenario 3
SBH (m)	0.77	1.01	1.35
$Q_{influent}$ (m³/h)	1	0.65	0.65
$Q_{underflow}$ (m³/h)	0.5	0.15	0.15
$Q_{effluent}$ (m³/h)	0.5	0.5	0.5
$TSS_{influent}$ (mg/L)	2850	2473	3544
$TSS_{effluent}$ (mg/L)	15	8	9
$TSS_{underflow}$ calculated (mg/L) (based on mass balance)	5686	10692	15330
$TSS_{underflow}$ measured (mg/L)	5867	9234	15025
Mass balance error	-3%	14%	2%
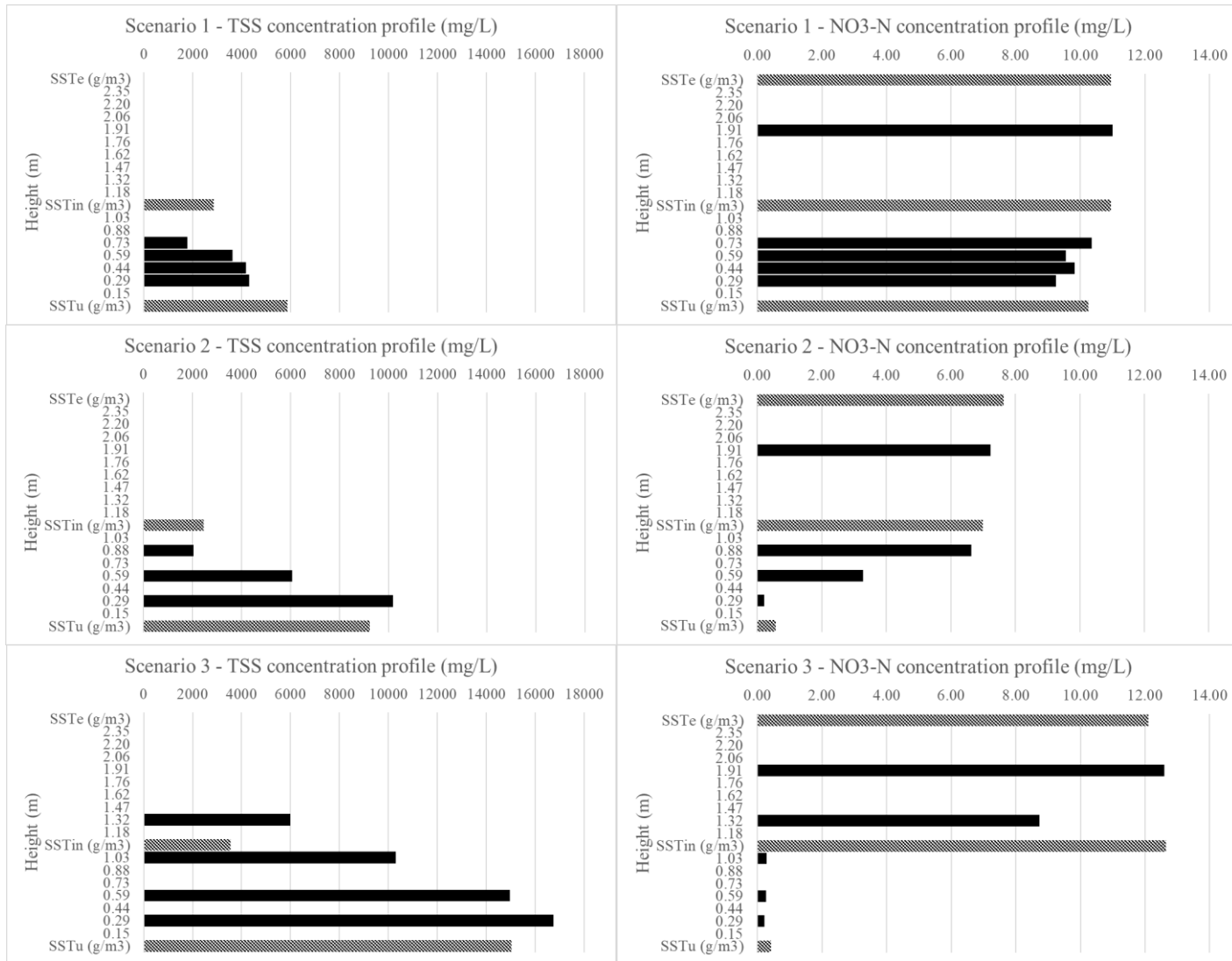
Figure 4.2 Measurement Results for TSS (left) and NO$_3$-N (right) for the Tested Operational Scenarios

The nitrate concentration profiles (Figure 4.2) show that no denitrification is occurring in the clarification zones for all scenarios. Only minor denitrification is occurring in the less concentrated sludge blanket of Scenario 1 and the top layers of the sludge blanket for Scenario 2. 90-95% nitrate removal is achieved in the more concentrated bottom layers of Scenario 2 and over most of the sludge blanket for Scenario 3 (even in face of the high nitrate loading in Scenario 3).

The DO concentration profiles reveal that DO consistently drops inside the sludge blanket layers and that this is accelerated when the sludge blanket is more concentrated. As expected, denitrification can only be observed in layers where DO has been entirely consumed. Alkalinity increment in the bottom layers in Scenario 2 and 3 also supports that denitrification occurs (Appendix I-Reactive settler measurement campaign results).

Given the very low soluble COD concentrations measured in the mixed liquor entering the SST, it can be concluded that all readily biodegradable COD was utilized in the biological reactors prior to the secondary settling process. As electron donor for the denitrification organic matter originating from biomass decay and hydrolysis of particulate degradable COD in biomass is utilized. Biomass decay is confirmed by the presence of increased NH_4-N concentration in the bottom layers under increased TSS concentrations. DO, NH_4-N and alkalinity measurement results for the campaign are presented in Appendix I - Reactive settler measurement campaign results.

Even though denitrification clearly occurred in the sludge blanket, no direct impact on the effluent NO_3-N was observed for any of the scenarios. Whereas this can be expected for Scenarios 1 and 2 where the sludge blanket is located below the feed point, this observation is surprising for Scenario 3 where the sludge blanket exceeds the inlet point (inlet hopper). It is highly probable that a short-circuiting effect in the inlet zone of the clarifier exists. DO was also measured in the effluent of Scenario 3 (above 3 mg/L) which was consumed in the sludge blanket above the feed layer (Appendix I-Reactive settler measurement campaign results) and supports the short-circuiting effect. This warrants a closer look at its design, but, a detailed study of the inlet structure and upflow pattern is out of the scope of this study which focuses on denitrification in the sludge blanket.

Inside the sludge blanket, high NO_3-N removal rates indicate that denitrification inside the SST can have a significant contribution to the overall denitrification capacity of the WRRF. Explicitly modelling this behaviour in SST models is therefore important to accurately describe the nitrate balance in the plant (NO_3-N recycling from the underflow to the biological reactors) and to capture the risk of nitrogen gas formation in SSTs.

4.2 Model Development

The 1-D BD settling model, which includes compression at high TSS concentrations, was used as a starting point for the development of the reactive settling model (Bürger et al., 2013). Based on the mass conservation law, the settling process can be described by a partial differential equation (PDE) (Equation 4.1).

$$\textbf{Equation 4.1:} \quad \frac{\partial C}{\partial t} + \frac{\partial}{\partial z} F(C, z, t) = \frac{\partial}{\partial z}\left(d_{comp}(C) \frac{\partial C}{\partial z} \right) + \frac{Q_f(t) C_f(t)}{A} \, \delta(z)$$

where C: =C(z,t) is the total solid concentration as function of depth z and time t, $F(C, z, t)$ is the flux function comprised of both the advective and hindered settling flux and d_{comp} is the compression function. The feed source term contains the feed flow (Q_f), the feed concentration (C_f) and the Dirac function ($\delta(z)$).

4.2.1 Implementation of Clarifier Geometry

The BD settling model only considers the vertical dimension along the SST and mass balance equations are formulated based on a constant surface area for each layer. However, the bottom of a real SST may be sloped and the surface area thus varies with depth (see examples in Figure 4.3). By not considering this typical geometry, the model may overpredict the SST volume by up to 30-50%. The pilEAUte SST that is modelled in this work, has an approximate 32% error when the bottom part is not considered conical for the total volume calculation (Chapter 3.1-Figure 3.4).
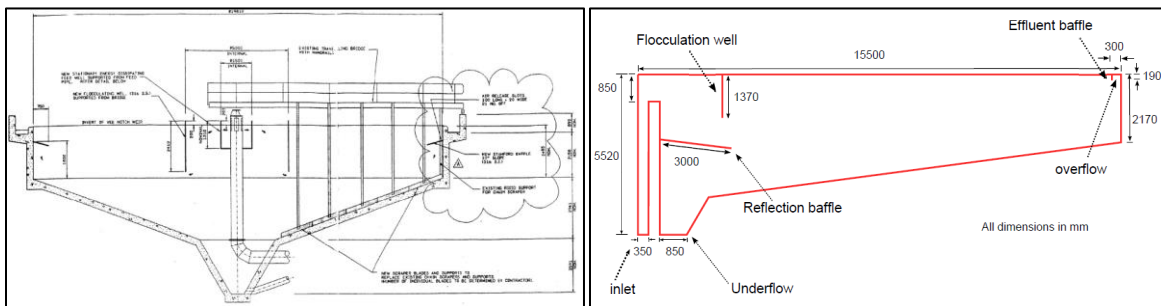
Figure 4.3 Cross-sections of the Oxley Creek and Roeselare circular SSTs respectively (De Clercq 2003; Torfs 2015)

This surface area variation along the depth of the SST affects the downward (advective) bulk velocity (present in the term *F(C,z,t)*. When assuming a flat-bottom geometry, the downward bulk velocity will be underpredicted in the bottom layers leading to a higher hydraulic retention time. In reality, the reduced surface area at the bottom of the SST causes the bottom velocity to increase and thus sludge to leave the layer faster. Hence, the assumption of constant surface area leads to a severe overprediction of the sludge residence time in the settler and to an unrealistic sludge mass accumulation. Also, the extent of biokinetic reactions (such as denitrification)

is overpredicted due to the too high hydraulic retention time in the sludge blanket for the constant area settler. For that reason, to improve the model predictions, the actual clarifier geometry was implemented in the reactive settler model in order to correct the model structural error originating from the constant area assumption. Some theoretical works on extension of 1-D settling models with varying surface area are available in literature, e.g. (Bürger et al., 2017; Bürger et al. 2021). The implementation of clarifier geometry within the scope of this modelling work is presented in Appendix I- Clarifier Geometry Implementation in detail.

4.2.2 Modelling Hindered Settling Behaviour

To describe hindered settling behaviour, the double exponential function by Takács et al. (1991) and the power-law function by Diehl (2015) were evaluated (Equation 4.2 & Equation 4.3). In these equations, X represents the TSS concentration and V_0, r_H, r_P, $\bar{X}$ and q are the model parameters to be calibrated. Since previous research indicated that power-law functions appear more suited to describe hindered settling behaviour at high sludge concentrations and high sludge blanket heights (Torfs et al. 2017), this work verified whether these previous observations could be confirmed by comparing the suitability of both settling functions to describe the concentration profiles in the SST.

$$\text{Equation 4.2: } v_s(X) = V_0 \left(e^{-r_H X} - e^{-r_P X} \right)$$

$$\text{Equation 4.3: } v_s(X) = \frac{V_0}{1 + \left(\frac{X}{\bar{X}} \right)^q}$$

4.2.3 Modelling Compression Settling Behaviour

Compression of the network of flocculated particles takes place when the TSS concentration in the sludge blanket exceeds a critical concentration (De Clercq et al. 2008). Many compression functions are available in literature (De Clercq et al. 2008; Bürger et al. 2011; Ramin et al. 2014a). In the current work, the compression function given in Equation 4.4 was used (Torfs et al. 2015) as it has only two parameters to estimate (γ – effective solids stress and X_{crit} – critical TSS concentration) thus simplifying implementation and calibration. Here, ρ_s and ρ_f are the densities of the solids and the fluid, respectively, and g is the constant of gravity.

$$\text{Equation 4.4: } d_{comp}(X) = \frac{\rho_s \, \gamma \, v_s(X)}{g(\rho_s - \rho_f)} \qquad X \geq X_{crit}$$

Implementation of the PDE (Equation 4.1) in a method of lines approach requires integration of the compression function d_{comp}. However, when using a power-law function for hindered settling, the integral of the resulting compression function does not have an analytical solution. Hence, a numeric approximation of the compression flux is implemented based on Algorithms 2&3 given by Bürger et al. (2013). As proposed by Bürger et al. (2013), the compression function was discretized over 400 points corresponding to the square of the number of layers.

A dispersion function is not included in the reactive settler model which is developed in the scope of this PhD research project, since dispersion around the inlet only influences concentrations locally and the effluent concentrations, so that the underflow concentration is not influenced (Bürger et al 2013). The main focus of this work is predicting the correct TSS concentrations within the sludge blanket and in the underflow.

4.2.4 Modelling Biokinetic Reactions

A continuous reactive settler model in which biological conversions and physical sedimentation occur simultaneously is developed by including the full set of Activated Sludge Model 1 (ASM1) biokinetic equations (Henze et al. 2006) into the BD 1-D settling model. The reactive settling process can be described by the extended PDE (Equation 4.5), where for each model component i, its concentration is represented by C_i: $= C_i$ (z,t) as a function of depth z and time t.

$$\text{Equation 4.5: } \frac{\partial C_i}{\partial t} + \frac{\partial}{\partial z} F(C, C_i, z, t) = \frac{\partial}{\partial z}\left(\frac{d_{comp}(C)}{C_i}\frac{\partial C}{\partial z}\right)C_i + \frac{Q_f(t)C_{i,f}(t)}{A}\delta(z) + r_i(z)$$

In this extended PDE, the flux function and compression behaviour are function of both the total solids concentration $C=\sum C_{p,i}(z,t)$ and the specific component concentration $C_{p,i}$. $C_{p,i}$ hereby represents the concentration of the ith particulate component. For soluble components, the hindered settling and compression terms vanish.

The last term represents the reactions (r_i) for each model component i (ASM1- Henze et al. 2006). The temperature dependence of the reaction rates is implemented in the biokinetic model with the Arrhenius equation using reference temperature 20ºC (Ruano et al. 2007).

The total flux $F(C, C_i, z, t)$ per particulate component can be written as follows (Equation 4.6).

$$\text{Equation 4.6: } F(C, C_i, z, t)_{above\ feed} = v_{hs}(C)C_i - \frac{Q_e(t)Ci}{A(z)}$$

$$F(C, C_i, z, t)_{feed} = v_{hs}(C)C_i + \frac{(-Q_u(t) - Q_e(t))Ci}{A(z)}$$

$$F(C, C_i, z, t)_{below\ feed} = v_{hs}(C)C_i + \frac{Q_u(t)Ci}{A(z)}$$

In Equation 4.6, note that the advective flux is surface area dependent and changes with depth. Q_e and Q_u represent the effluent and under flowrates respectively. Hindered (v_{hs}) and compression settling (d_{comp}) are only active for particulate components and zero for soluble components.

4.2.5 Numerical Solution

For numerical solution, the PDE describing the settling behaviour over the depth of the settler is discretized in layers. The overall mass balance in each layer accounts for the hindered settling flux, the upward or downward bulk advective flux, a flux due to sludge compression and biokinetic reactions based on ASM1. The reactive SST was modelled with 20 layers (16 layers along the height of the SST and 4 boundary layers) to have at least one measurement point in each layer so as to facilitate comparison of model predictions with measured concentrations. A discretization in 20 layers was found sufficiently accurate after comparison with a more detailed discretization (99 layers, results not shown). The mass balances for each of the 7 soluble and 6 particulate components are solved over the 16 layers of the SST model (Appendix I). No reaction takes place in the boundary layers.

The model was implemented in the WEST modelling and simulation software (Chapter 3.2.2). The input file was defined based on the measurement results in the influent of the SST using a constant outflow of a bioreactor with typical COD fractionation of mixed liquor concentrations (Henze et al. 2006) (Figure 4.4). Simulations were run for 5 days to ensure reaching a steady state SBH for each scenario.
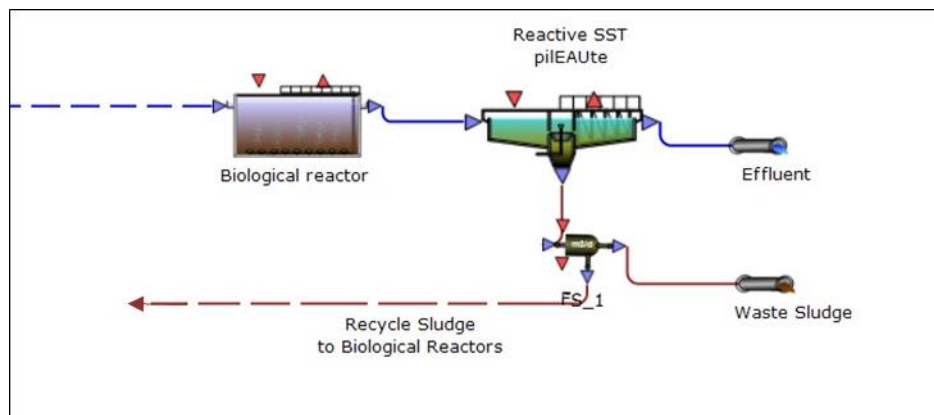
Figure 4.4 Reactive Settler Model Layout in WEST

4.3   Model Calibration and Testing

4.3.1 Calibration of Hindered Settling Behaviour

Data collected from the batch settling tests for different initial sludge concentrations (Figure 4.5) were used to estimate the hindered settling parameters. The hindered settling velocities were determined by calculating the maximum slopes of the batch curves and plot them as function of the initial solids concentration. The data points of hindered settling velocity as function of initial TSS concentrations were subsequently used to perform

parameter estimations for the settling functions of Takács et al. (1991) and Diehl (2015) by minimizing the Sum of Squared Errors between the model predictions and the experimental data.
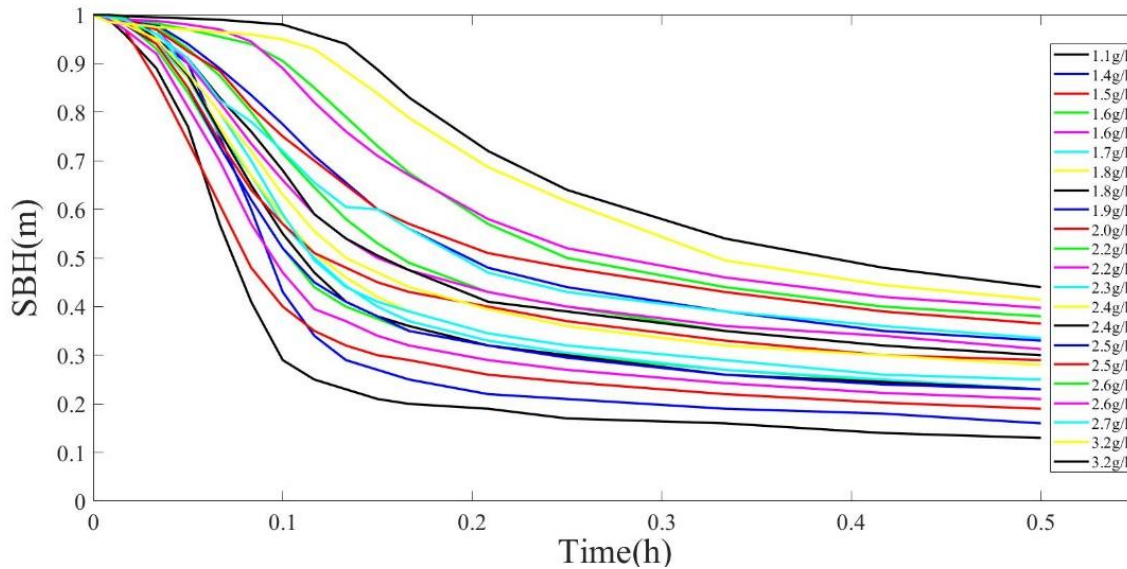
Figure 4.5 Settling Curves of Batch Settling Tests for Different Initial TSS Concentrations

Most of the (2 parameter) power-law hindered settling functions in literature (e.g. Cole 1968) have very high settling velocities at low sludge concentrations, leading to unrealistic effluent concentration predictions. The function of Diehl compensates for this effect by introducing a third parameter (similar as to the r_P parameter in the double exponential function of Takács et al. (1991) (Equation 4.2)). It is, however, not possible to identify this parameter on a series of batch settling curves collected at concentration above 1 g/L. $\bar{X}$ and r_P were therefore fixed at typical values and only respectively V_0 and q, and V_0 and r_H were estimated. As shown in the results, this gives sufficient degrees of freedom to capture the hindered settling behaviour. (Note that in dynamic modelling studies, $\bar{X}$ and r_P can be further calibrated based on the effluent TSS concentrations but this work does not focus on predicting effluent TSS precisely). Figure 4.6 shows the resulting model fit for both hindered settling functions.
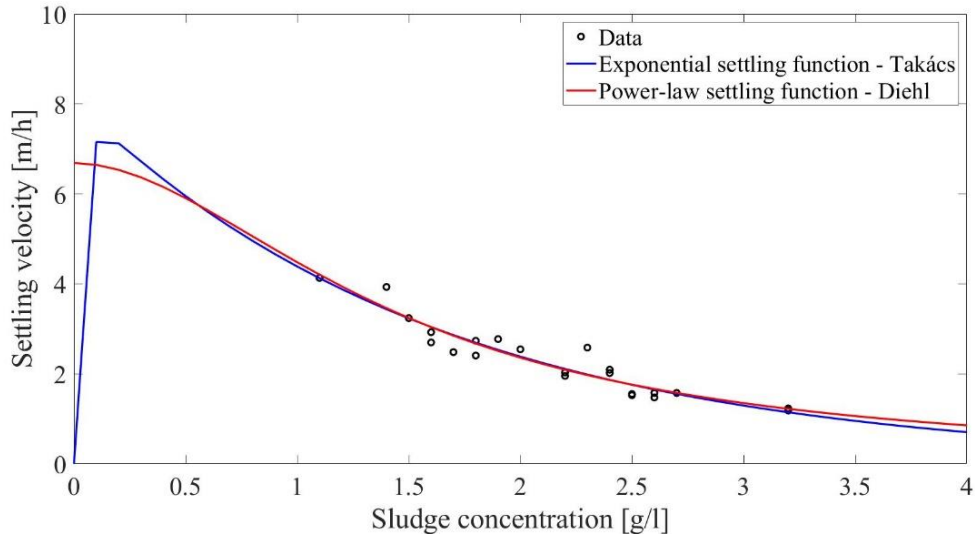
Figure 4.6 Exponential vs Power-Law Hindered Settling Functions Calibrated to the Batch Settling Test Results

Figure 4.6 shows that both settling functions agree well with the velocities in the TSS concentration range for which batch settling curves with a clear hindered settling region could be performed (1.1 g/L to 3.2 g/L). It is thus not possible to distinguish between the exponential and power-law model structure based on the batch settling data. The estimated settling function parameter values based on these batch settling tests are given in Table 4.3.

Table 4.3 Settling Functions Evaluated and Estimated Parameter Values

Settling function	Optimal Parameter Values
Takács: $v_s(X) = V_0 \left(e^{-r_H X} - e^{-r_P X} \right)$	V_0 (m/d) : 193.88
	r_H (m³/kg) : 0.00062
	r_P (m³/kg) : 28.99* (Takács et al. 1991)
Diehl: $v_s(X) = \dfrac{V_0}{1+\left(\frac{X}{\overline{X}}\right)^q}$	V_0 (m/d) : 223.23
	$\overline{X}$ (kg/m³) : 1.00* (assumed, see text)
	q (-) : 1.5826

*_Fixed parameter value_

4.3.2 Testing the Inclusion of Clarifier Geometry

4.3.2.1 Rectangular Geometry (Flat-Bottom)

In most modelling studies, the settling tank is considered rectangular (i.e. having a constant cross-sectional area over its entire depth) for simplicity reasons. Through calibration of the settling functions, underflow concentrations can be captured even if this assumption does not hold. In the current work too, the assumption of constant cross-sectional area was originally applied. However, accurate modelling of reactive settling requires a good description of the overall sludge mass and its distribution over the sludge blanket, putting more emphasis on proper settling model calibration. The measured hindered settling velocity parameter for different settling velocity functions are tested on the reactive settler model with constant cross-sectional area. However, it was impossible to capture the sludge concentration profiles of all three scenarios with a single parameter set for the settling velocity function. Figure 4.7 illustrates the simulated sludge concentration profiles for the SST under study with constant cross-sectional area for both settling functions tested: the Takács exponential hindered settling function and Diehl's power-law hindered settling function.

For both settling velocity functions, it was not possible to obtain a good fit with the rectangular geometry. Both functions result in high sludge settling velocities for Scenario 1 and underestimate the SBH which could be corrected by including the sludge compression behaviour. However, the Takács settling function is severely overestimating the SBH and the sludge mass prediction inside the sludge blanket for Scenarios 2 and 3. In this case, including the sludge compression would lead to much higher SBH predictions and sludge overflow. On the other hand, the Diehl's settling function gives high sludge settling velocities at high TSS concentrations as expected and result in very low SBH predictions in all scenarios. Before including the sludge compression, the actual clarifier geometry is included to the reactive settler model to see how it affects the TSS concentration profiles.
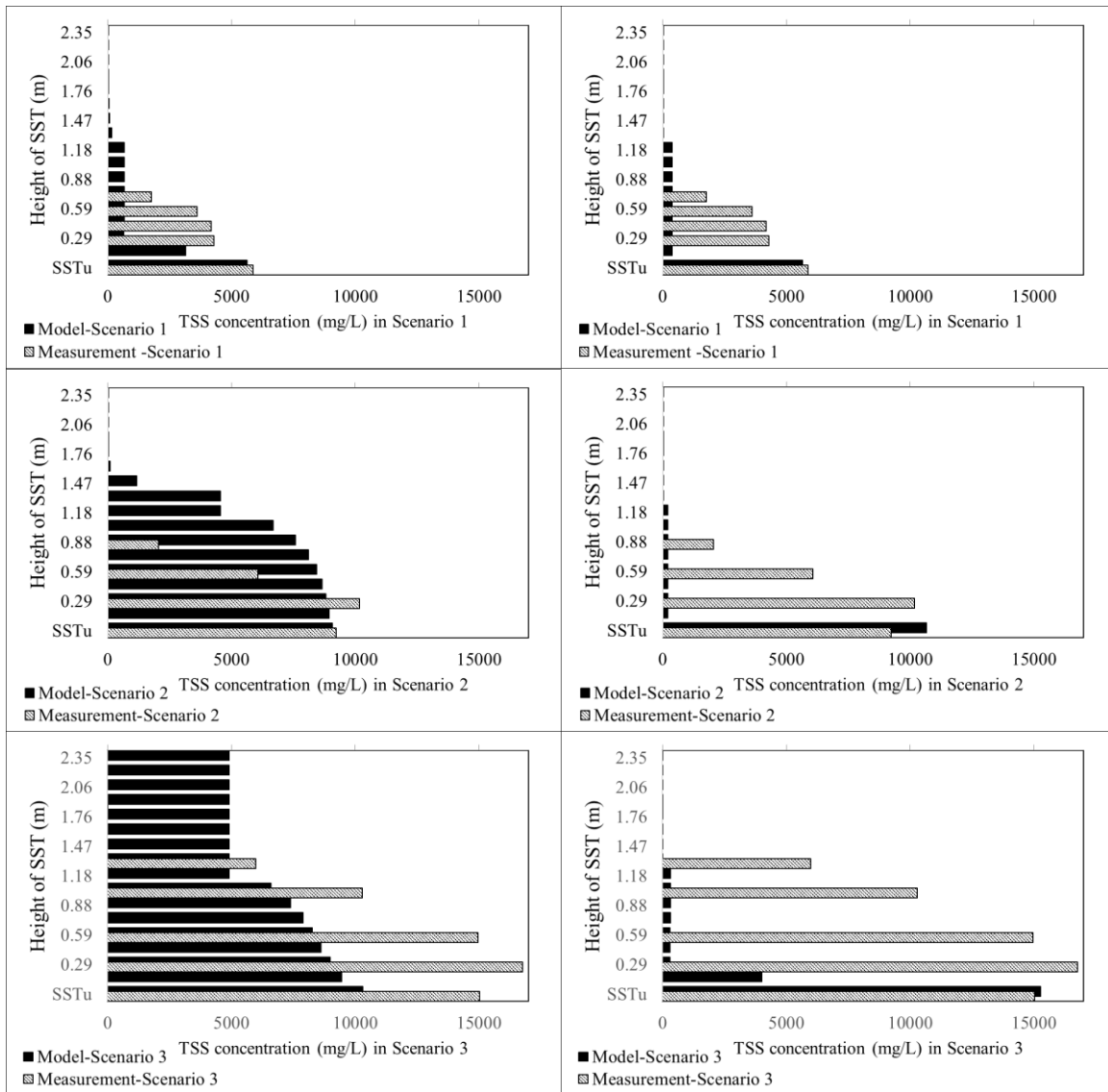
Figure 4.7 Best TSS Concentration Profiles Obtained with SST Models with Rectangular Geometry for Takács (left) and Diehl (right) Settling Velocity Functions with Parameters Obtained from the Batch Settling Curves

4.3.2.2 Actual Geometry (Conic-Bottom)

After this unsuccessful calibration attempt of the model with constant cross-sectional area, it was decided to implement the actual clarifier geometry according to the procedure explained in Chapter 4.2.1 and Appendix I-Clarifier Geometry Implementation. The calculated surface area and volume for each layer can then be applied directly to the mass balance equations.

In order to select the best hindered settling function to be used, the calibrated Takács and Diehl settling functions were implemented in the BD settling model with correct geometry of the clarifier and their performance in

predicting the TSS profiles of the measurement campaign was compared in Figure 4.8. Specific attention is given to high TSS concentrations as this is crucial for a reactive settler model (as explained above) and since information on high TSS concentrations is not present in the settling velocity data of Figure 4.6. Note that no additional calibration was performed at this point but simulations were performed with the parameter sets of Table 4.3. Compression settling was not considered in these first simulations.
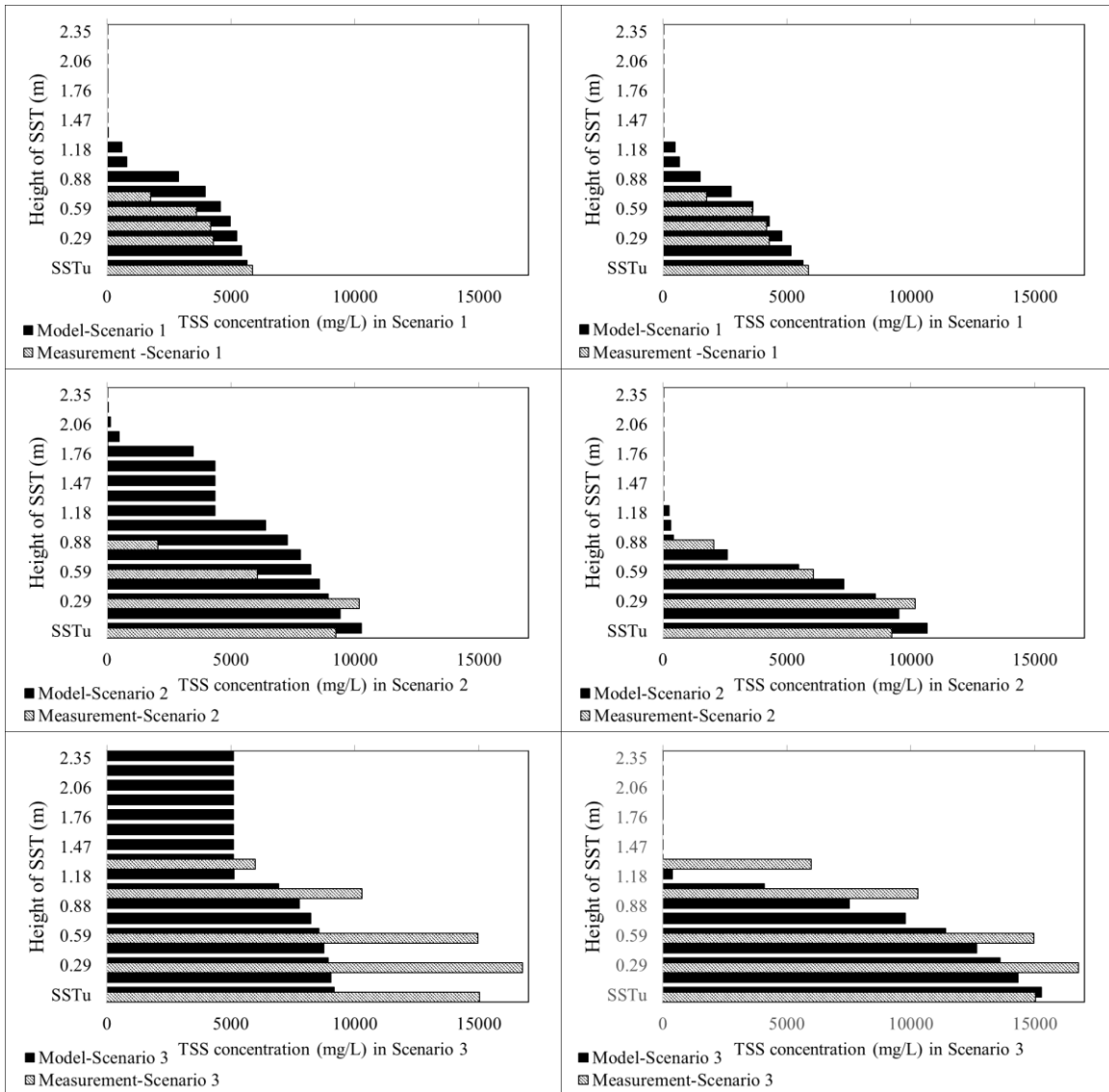
Figure 4.8 Comparison of Measured TSS Profiles of the Three Scenarios with BD Model Simulations with Takács (left) and Diehl (right) Hindered Settling Functions Calibrated Using Batch Settling Tests*

* No compression modelled.

As can be seen in Figure 4.8 when adopting the correct geometry, both settling functions give good predictions for both the TSS concentration profile and SBH prediction in Scenario 1 which represents the normal operating

conditions of a SST. However, in Scenarios 2 and 3 the Takács settling function is again severely overestimating the SBH and fails to capture the concentration profile and thus sludge mass prediction inside the sludge blanket. It even led to sludge overflow of the settler for simulations under the operating conditions of Scenario 3. With conical geometry implemented, it becomes apparent that the Takács settling function calibrated on batch settling data is thus underpredicting the settling velocities at high TSS concentrations whereas the Diehl power-law function clearly performs better at high TSS concentrations.

The difference between both settling functions at high TSS concentrations is illustrated in Figure 4.9. Note that adding compression, which will reduce settling velocities further at high TSS concentrations, would only exacerbate this poor performance of the Takács-based SST model. These observations confirm previous findings from literature (Torfs et al. 2017). Thus, based on these modelling results and the previous modelling efforts, the Diehl settling function was selected in the proposed 1-D reactive settler model.
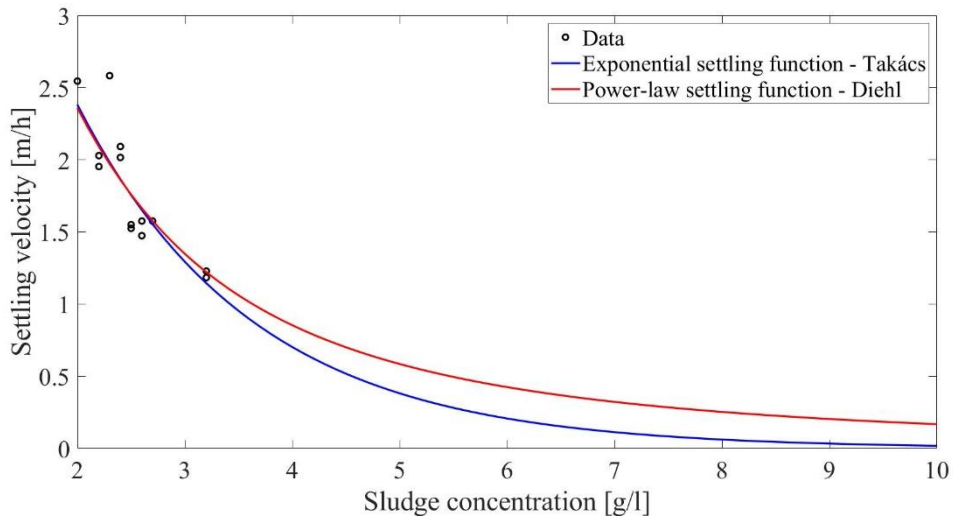
Figure 4.9 Exponential vs Power-Law Hindered Settling Functions Behaviour at High TSS Concentrations

4.3.3 Calibration of Sludge Compression Behaviour

Although the model results with only hindered settling according to Diehl's model already show quite a good fit for the concentration profiles in all three scenarios, a slight underestimation of the sludge concentrations and the sludge blanket height can be observed in Scenario 3. To further improve the model results and accurately capture the active biomass concentration, compression settling is included in the developed 1-D reactive settler model. The compression function adopted within this model includes 2 parameters to calibrate: γ – the effective solids stress and X_{crit} – the critical TSS concentration at which compression starts (Equation 4.4). The Monte

Carlo approach of Sin et al. (2007) was used for model calibration with Latin Hypercube Sampling (LHS) of the parameter values from the defined parameter space (Table 4.4).

Table 4.4 Properties of the LHS Sampling for the Monte Carlo Approach to Find Optimal Compression Parameter Values for Three Scenarios

Parameter	Parameter range sampled
γ , effective solids stress (m^2/s^2)	0.01 – 0.0001
X_{crit} , critical TSS concentration (mg/L)	3000 - 8000
Number of Monte Carlo Runs for each scenario	200

For each parameter set (θ), model predictions ($y_{m,i}$) and measured (y_i) TSS concentration profiles along the sludge blanket were used to calculate the Sum of Squared Errors (SSE) (**Equation 4.7**), for each scenario. The final objective function was calculated as the average SSE of the three scenarios. The parameter set that gives the minimum overall objective value is chosen as the optimal parameter set.

$$\text{Equation 4.7: } SSE = \sum_{i=1}^{N}(y_i - y_{m,i}(\theta))^2 \text{ ; } \textit{N: number of data points \& i:variable}$$

Based on the evaluation of the objective values (**Equation 4.7**) calculated for each Monte Carlo run, it was not possible to obtain a good model fit for each scenario with a unique parameter set. Since the compression function also includes the hindered settling velocity in its structure (see Equation 4.4) the parameter values of the hindered settling function might have a significant effect on the compression behaviour. As these parameters were estimated based on batch settling data within the concentration range of hindered settling behaviour (1.1-3.2g/l) and the transferability of the parameter values from batch settling conditions to continuous flow conditions might not be perfect, it was decided to evaluate whether further fine-tuning of the hindered settling parameters could allow achieving a good model fit for the three full concentration profiles.

To avoid overfitting the model, a local sensitivity analysis (LSA) was carried out for the parameters of the Diehl hindered settling velocity function in order to assess which parameter has the highest influence at high TSS concentrations and thus may be the most appropriate for further fine-tuning. The sensitivity analysis was performed based on the central relative sensitivity (CRS) of the settling velocity on each model parameter (V_0, $\bar{X}$ and q) (Claeys 2008). The LSA results confirm that parameter q is the most influential model parameter in the Diehl hindered settling velocity function at high TSS concentrations (>3 mg/L) (Equation 4.7).
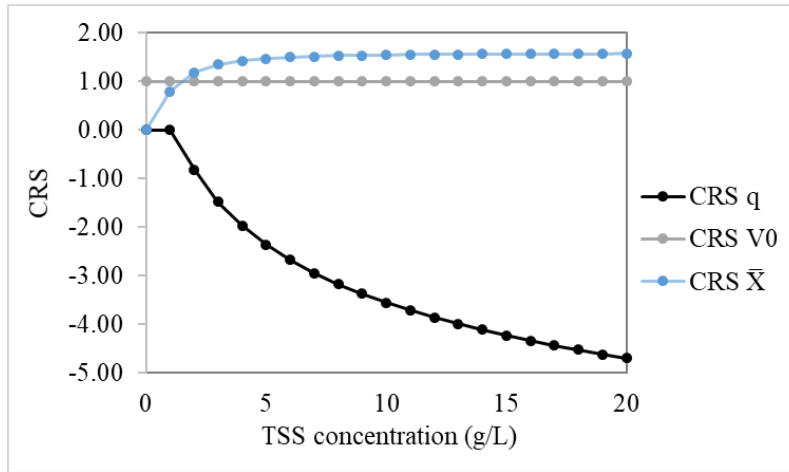
Figure 4.10 Central Relative Sensitivities (CRS) of Diehl Settling Function Model Parameters Based on Local Sensitivity Analysis

Figure 4.11 shows the Diehl settling velocity function versus experimental data with the q value calibrated on the batch settling test results (Table 4.3) and with slightly different values for q to see how the values of q influence the curve. It can be concluded that the upper and lower values of q still show a good fit with the batch settling data within the hindered settling zone, but those have a significant influence on the settling velocity at high TSS concentrations.
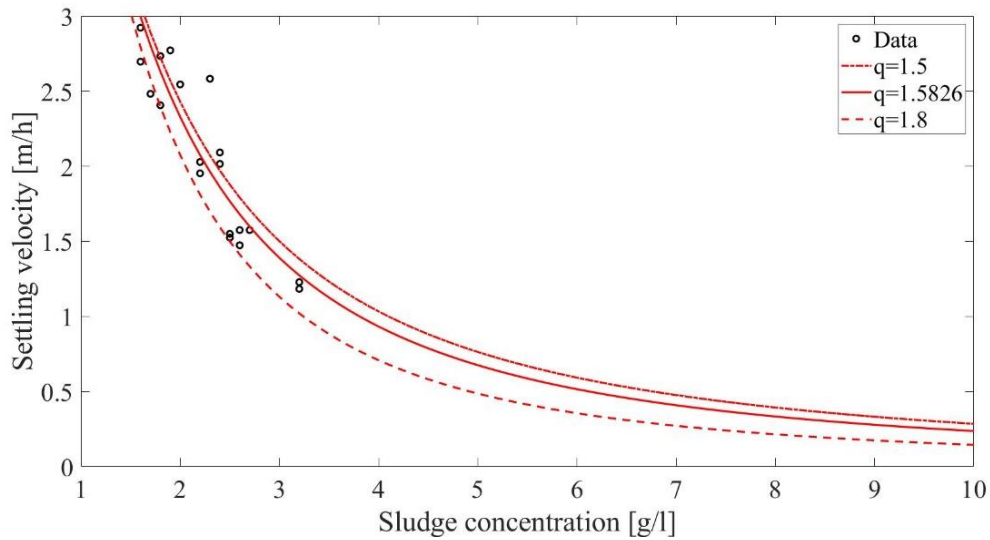
Figure 4.11 Diehl Settling Functions Calibrated to Batch Settling Curves (*q:1.5826)* and Different *q* Values

Motivated by the significant influence of the parameter q at high solids concentrations, another set of Monte Carlo simulations was carried out including the parameter q values within the range given in Table 4.5.

Table 4.5 Properties of the LHS Sampling for the Monte Carlo Approach to Find Optimal Compression and *q* Parameter Values for Three Scenarios

Parameter	Parameter range sampled
γ , effective solids stress (m²/s²)	0.01 – 0.0001
X_{crit} , critical TSS concentration (mg/L)	3000 - 8000
q , Diehl settling function parameter (-)	1.5 – 1.8
Number of Monte Carlo Runs for each scenario	500

This additional analysis made it possible to find a unique parameter set for all three scenarios with a good fit to each of the TSS concentration profiles. The optimal parameter set also gives good predictions for both total sludge mass and SBH. The final set of calibrated model parameters is presented in Table 4.6 and the TSS concentration profiles for all scenarios are given in Figure 4.12.

Table 4.6 Optimal Parameter Set for Settling Model Calibration

q – Diehl settling function parameter (-)	1.69
V_0 – Diehl settling function parameter (m/d)	223.23*
$\bar{X}$ (kg/m³)	1.00**
γ – effective solids stress (m²/s²)	3.21×10^{-4}
X_{crit} – critical TSS concentration (mg/L)	5550

*See details in Chapter 4.3.1 for: * Fixed parameter value on batch settling curves, ** Fixed parameter value*
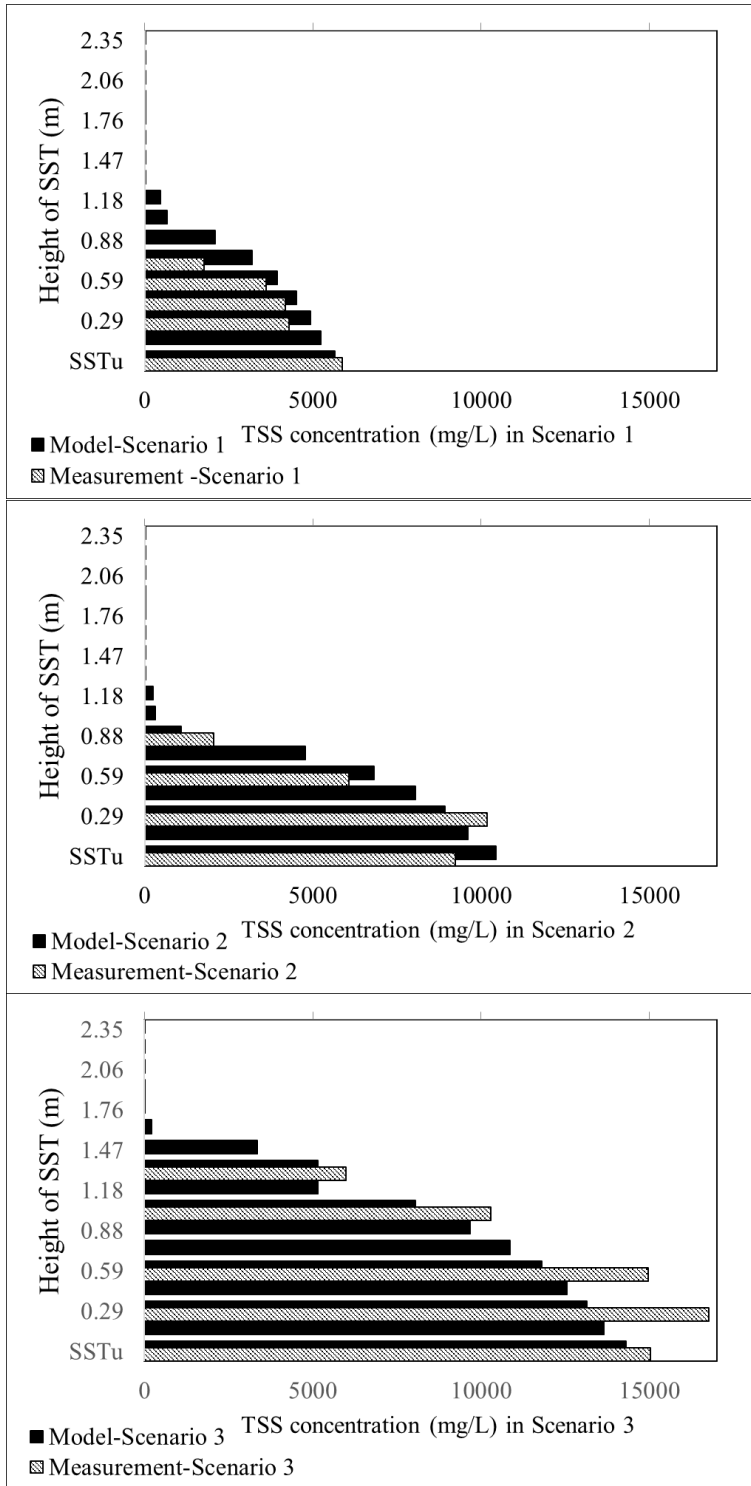
Figure 4.12 Comparison of Model Results with Final Set of Calibrated Parameters Measurement Results for TSS for the Three Tested Operational Scenarios

To be fair, the reactive settler model with Takács settling velocity function was also attempted to be calibrated by changing the settling velocity parameters and including the sludge compression behaviour. However, Takács function required significant changes on the settling velocity parameters in order to accelerate the hindered settling velocities at high TSS concentrations and to give a good estimation of the SBH and TSS concentration profiles. The estimated parameter values were much different than the measured values from the batch settling tests, thus requiring to make unrealistic changes on the model parameter values. However, the final version of the reactive settler model with Diehl's settling function only required to do a fine-tuning on one of the settling velocity parameters to obtain a good fit for the three operational scenarios.

4.3.4 Calibration of ASM1 biological reactions in BD settler model

Figure 4.13 shows the model results for NO_3-N and DO along the 16 layers in the SST for all scenarios with the calibrated settling parameters and the default ASM1 model parameter values for biokinetic reactions with temperature correction (temperature in all scenarios was $26°C$) (Henze et al. 2006). It is remarkable that without calibration of the kinetic parameters, the model is able to capture the general trends of the biokinetic reactions quite well.

The NO_3-N concentration decreases in the bottom layers of the SST (where the TSS concentration is substantial) due to denitrification after DO is consumed completely in the sludge blanket. Scenario 1, which has the lowest sludge mass in the clarifier, does not have significant denitrification in the sludge blanket, which is well predicted by the model. In Scenario 2 and 3, the model predicts high denitrification rates in the concentrated bottom layers of the sludge blanket as was observed in the measurement campaign.

The main discrepancy between the model and measurements can be found in the clarification zone for Scenario 3. In this scenario, the sludge blanket extends above the feed layer of the SST (observed and simulated). Hence, the model predicts significant denitrification in these upper layers of the sludge blanket, thus predicting reduced effluent NO_3-N and DO concentrations. However, the measured NO_3-N and DO concentrations in the effluent were close to the SST influent concentrations. As explained in Chapter 4.1, it is hypothesized that this is due to short circuiting in the inlet zone of the clarifier which is not reflected in the 1-D model. Further analysis of the hydraulics would be needed to confirm this hypothesis, but this is beyond the scope of this study. The effect of observed short-circuiting in full-scale could in theory be compensated in the model by calibrating the biokinetic model and reducing the denitrification efficiency in the clarifier. However, the developed reactive settler model is further to be used as part of the plant-wide pilEAUte model and the biokinetic model parameters are to be the same for the biological reactor and the reactive SST.
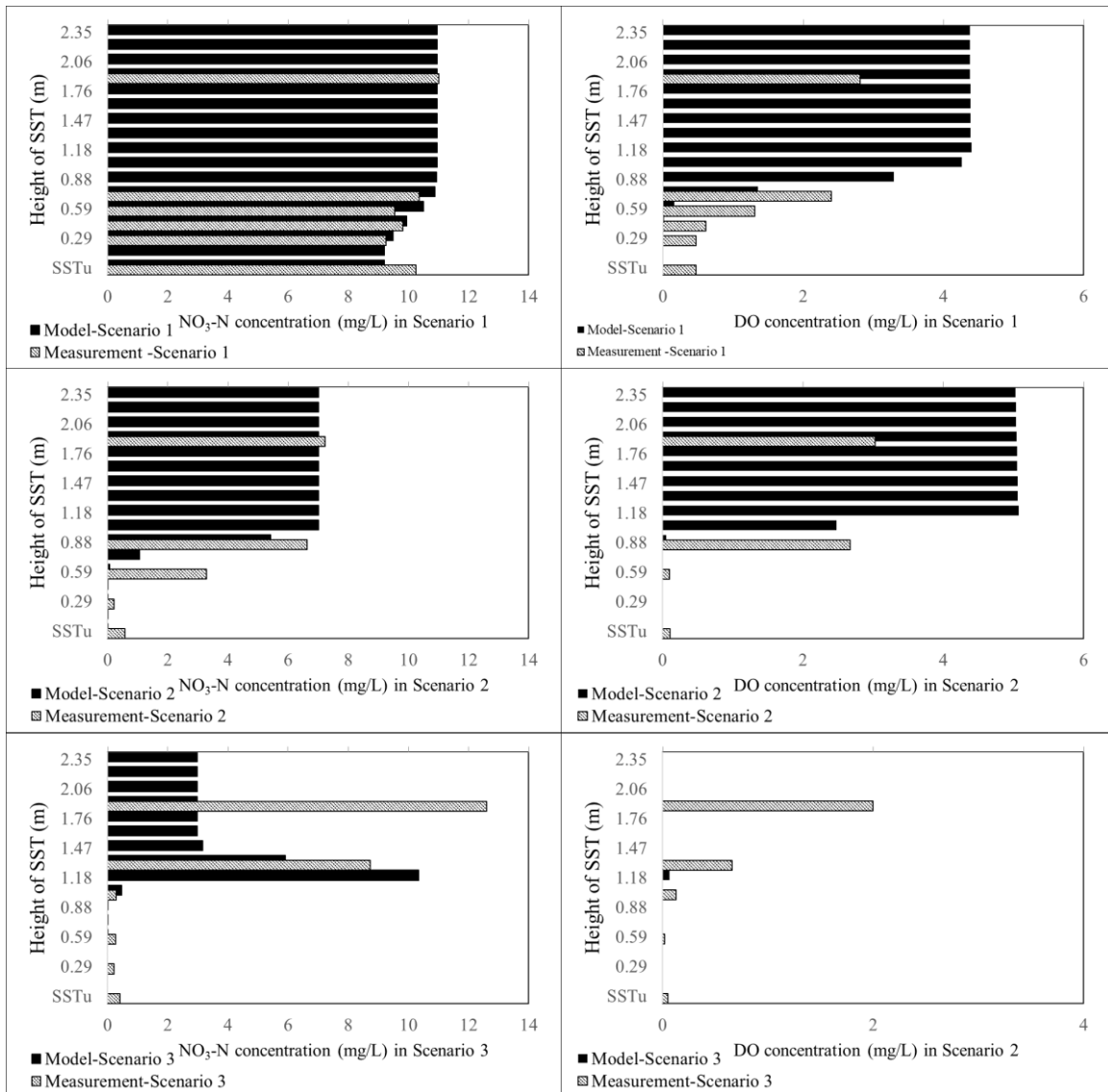
Figure 4.13 Model Predictions of NO₃-N (left) and DO (right) using the Calibrated Settling Model and ASM1 Default Parameter Values Corrected for Temperature (Henze et al. 2006) (Temperature in all scenarios 26ºC) for the Three Scenarios

The calibrated model is thus giving promising results for biokinetic reactions and the resulting concentration profile of the soluble components. The small differences between the model predictions with default ASM1 parameters and the measurement results – except for the short-circuiting effect – are found acceptable. Therefore, there is no need for further calibration of the biokinetic model parameters in the developed and calibrated 1-D reactive settler model. The default biokinetic parameter values of ASM1 were not changed (Henze et al. 2006). In addition, note that the pilEAUte plant is receiving municipal wastewater originated from the university campus (Chapter 3.1), and ASM1 default model parameters are proposed for treatment of wastewater with municipal characteristics (Henze et al. 2006). If needed, it would be appropriate to calibrate the biokinetic

model parameters in a plant-wide model and the same parameter values would be applied in both the biological reactor and the reactive SST. The plant-wide pilEAUte model including the developed reactive settler model is presented in Chapter 5.

An interesting feature of a reactive settler model like the one proposed would be to estimate the risk of N_2 production (indicating a risk of rising sludge). However, specific modelling of the liquid-gas mass transfer for prediction of N_2 production and especially bubble formation would unnecessarily increase model complexity. On the other hand, it has been suggested that denitrification may lead to bubble formation when more than 6-8 mg/L NO_3-N is denitrified in the sludge blanket (Henze et al. 1993). N_2 gas bubble induced sludge rising problem is also observed in the measurement camping of this study as well while high nitrate and readily biodegradable COD is loaded to the clarifier (results not presented). Hence, the reliable prediction of SST denitrification in the developed model allows to evaluate the risk of N_2 gas formation by setting up a warning signal once a threshold NO_3-N removal is exceeded.

In addition to that, theoretically, enhanced denitrification in the SST can -for the same overall N-removal- allow for reducing internal recycle pumping and thus result in energy and carbon source savings. Based on calibrated model results, it was found that up to 160 g/d NO_3-N can be removed through reactive settling provided the sludge blanket height is controlled at approximately 50% of the total SST height in the pilEAUte WRRF.

Within the scope of this PhD research project, the developed reactive settler model which is only calibrated for the settling model parameter at this stage, is further used to model the plant-wide pilEAUte WRRF.

4.4   Conclusions

The key findings of the reactive settler model development is presented here. Within this study, a reactive settler model was developed, calibrated and tested on a unique dataset in order to better incorporate the potential importance of reactions in the sludge blanket of secondary settling tanks.

- A detailed measurement campaign was performed on a pilot-scale settler under different sludge blanket and NO_3 loading conditions. It was confirmed that significant denitrification in the SST can occur depending on the biomass concentration and the hydraulic retention time in the sludge blanket.

- The 1-D settler model was developed based on the Bürger-Diehl framework including hindered settling and compression processes, a full set of ASM1 biokinetic equation and proper attention for the actual (conical) clarifier geometry. It was found that accurate description of biokinetic reactions in the SST puts high calibration demands on the settling model as it should capture the full concentration profiles of active biomass in the sludge blanket.

- An extensive calibration and model selection effort was performed. The Diehl hindered settling function (a 3 parameter power-law function) was found to be the most adequate to describe the hindered settling process over the entire TSS concentration range and particularly at high TSS concentrations. The developed reactive settler model was able to predict concentration profiles and sludge blanket height for three different operational scenarios with a unique parameter set for hindered and compression parameters. Approximate hindered settling parameters could be obtained from batch settling experiments with only minor fine-tuning required for one of the hindered settling parameters in the full-scale model. This one parameter was the one to which high TSS concentrations were most sensitive.

- The calibrated model was subsequently able to accurately predict the TSS, NO_3-N and DO concentration profiles, sludge mass in the SST and sludge blanket height without the need to calibrate the biokinetic model parameters at this stage. They could be maintained at typical values for municipal wastewater treatment which agrees with the pilot's behaviour.

The developed reactive settler model can be used for better predictions of effluent and underflow concentrations of a SST together with the concentration profile of the sludge blanket. It can be integrated in a plant-wide model and used for scenario analysis to properly calculate the nitrogen mass balance of a WRRF. Moreover, it can also be used to demonstrate the denitrification potential of the secondary settling process in a plant-wide model or to avoid the N_2 gas bubble induced rising sludge problem.

5. MODELLING of BIOLOGICAL N-REMOVAL PROCESSES

5.1 pilEAUte Model – Conventional Nitrogen Removal

The objective of this PhD research project was to improve the understanding of N-removal mechanisms in the biological treatment of wastewater through modelling and optimizing the existing WRRFs to reduce energy and resource consumption. For this purpose, the pilEAUte WRRF (only the pilot lane) was modelled and scenario analyses were applied. The model layout of the pilEAUte WRRF which consists of 5 biological tanks and a secondary clarifier is presented in Figure 5.1.

- The process units' volumes and flowrates (internal & sludge recycle, waste sludge) were selected based on the plant's design and operational values as explained in Chapter 3.1.

- The data used for the model input (influent, operational and effluent data) is described in Chapter 5.2.

- The BIOMATH calibration protocol was applied for the model calibration and for the biokinetic model calibration, the calibration methodology of Mannina et al. (2011) was modified and applied (Chapter 3.2.1).

- The additional backflows in between the basins on the model layout were added based on the hydraulic model results presented in Chapter 5.3.

- The developed 1-D reactive settler model was used for the secondary settling process in the pilEAUte plant-wide model (Chapters 4 & 5.5).

- The ASM1_AN biokinetic model which is an extension of ASM1 was used as the biokinetic model. The model calibration details are presented in Chapter 5.6.
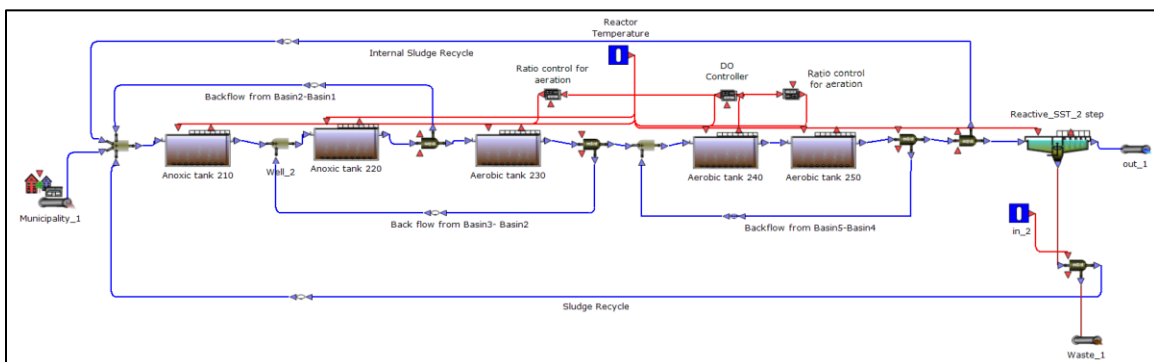
Figure 5.1 pilEAUte WRRF Model Layout

5.2   Model Input Data

The pilEAUte WRRF operational data for the time period February 1st − March 31st 2018 were used for the model. The time period was chosen to reflect the normal operational conditions (the whole system is operated under dry weather conditions) and was selected in view of the sensors' reliability. The raw monitoring data was treated with the univariate data validation method of Alferes and Vanrolleghem (2016) and the outlier detection and data smoothing filters were applied prior to modelling (Alferes and Vanrolleghem 2016; Philippe 2018). The time periods used for the different modelling purposes are presented in Table 5.1.

Table 5.1 Model Input Data Time Periods

Modelling purpose	Period	Days	Number of days
Model initialization	01 - 23 February	0-23	23
Model calibration	24 February - 17 March	24-47	23
Model validation	18 March - 31 March	48-59	11

5.1.1   Influent Data

The influent flowrate used for the model is shown in Figure 5.2. As can be seen, the influent flowrate is most of the time 12 m^3/d with, sometimes, an influent pump stop. The stop is mostly temporarily (for a couple hours max.) and it does not affect the biological processes. From day 49 to 51, the influent pump completely stopped working, thus there was no influent to the system. This period is included as part of the model validation time period to see if the calibrated model is able to predict the plant performance and the effluent concentrations under these conditions.
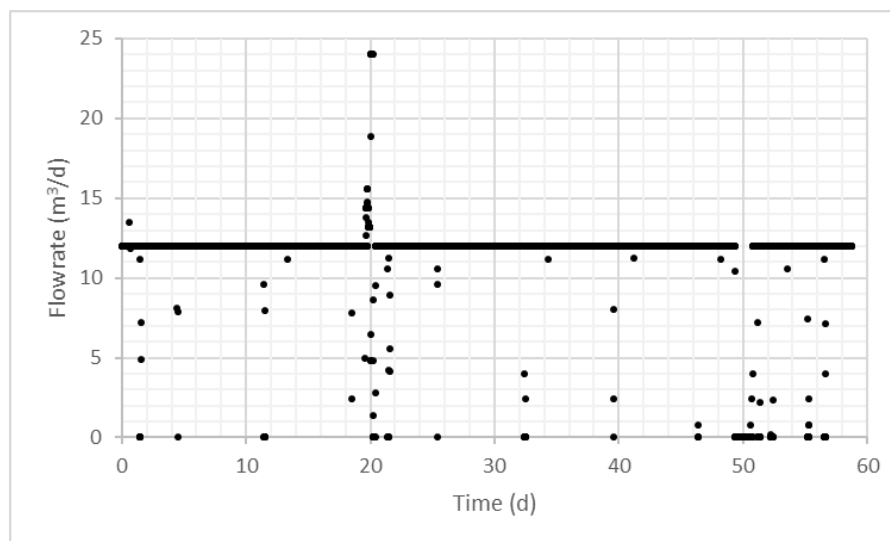
Figure 5.2 Influent Flowrate
(In day 20, due to an operational mistake on the SCADA, the influent flowrate was doubled to 24 m^3/d for 15 minutes which would not impact the biological process significantly.)

The influent total COD vs soluble COD is shown in Figure 5.3. Note that the pilEAUte is known to behave very similar to a traditional predenitrifying municipal WRRF, with classic municipal wastewater composition (Li et al., 2019). The total COD varies between 250 and 400 mg/L while the soluble COD is around 100-150 mg/L. The ratio of soluble COD to total COD is around 40%.
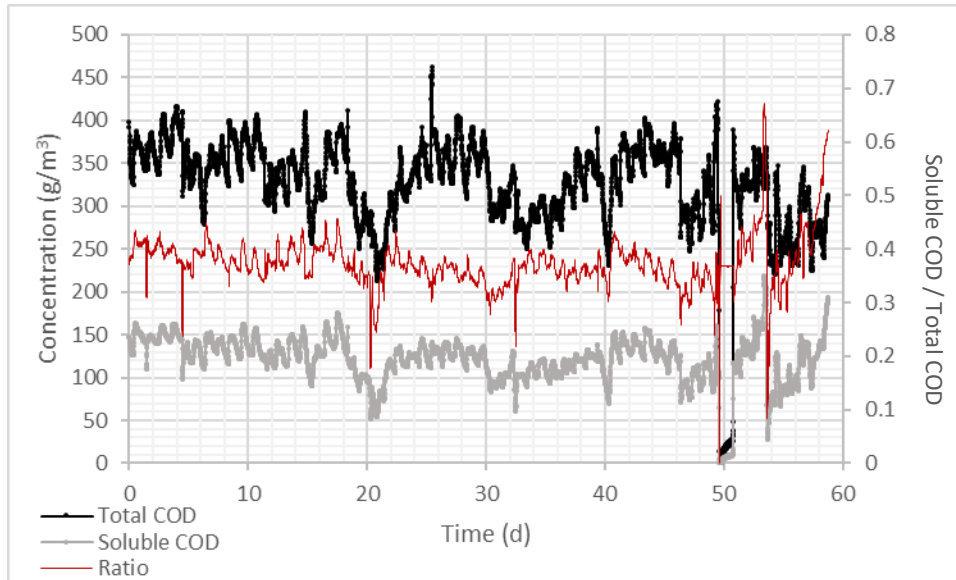
Figure 5.3 Primary Effluent Total COD vs Soluble COD Measured with Spectro::lyser

The influent COD fractionation study for the pilEAUte by Li et al. (2019) was used for the fractionation of COD. However, this influent characterization study was performed for the influent of the primary clarifier. However, the COD data that is used for this model is taken at the outlet of the primary clarifier where the sensors are located (influent of biological reactors). Thus, a backward calculation had to be done by considering the average concentrations of total and soluble COD at the outlet of primary clarification. The particulate material removal efficiency of the primary clarifier was measured as 50% (Ponzelli et al. 2019) and the average particulate COD was calculated at the inlet of the clarifier (for which the backward calculation takes place). Then the COD fractionation by Li et al. (2019) can be applied and the final COD fractionation for the outlet of the primary clarifier is calculated (by considering the 50% removal efficiency in the primary clarification again) and used as model input (Table 5.2).

Table 5.2 COD Fractionation of Primary Effluent (based on Li et al. (2019))

COD Component	Ratio over Total COD	
Inert particulate COD (X_I)	15.9%	63%
Biodegradable particulate COD (X_S)	47.4%	
Inert soluble COD (S_I)	8.6%	37%
Readily biodegradable COD (S_S)	28.2%	

The influent ammonium (NH_4-N), soluble organic nitrogen and particulate organic nitrogen concentrations are presented in Figure 5.4. NH_4-N is the only parameter that is measured at the primary effluent, but organic nitrogen is also present in the influent in soluble and particulate forms. To determine the organic nitrogen concentrations, an influent total nitrogen fractionation was performed (based on the monitoring data presented in Chapter 6) and based on the ratios in Table 5.3, the soluble and particulate organic nitrogen concentrations are calculated from the ammonium data. Note that the soluble organic nitrogen is not a model variable in the used biokinetic model (ASM1_AN), thus the calculated soluble organic nitrogen concentration is included in the influent ammonium concentration.
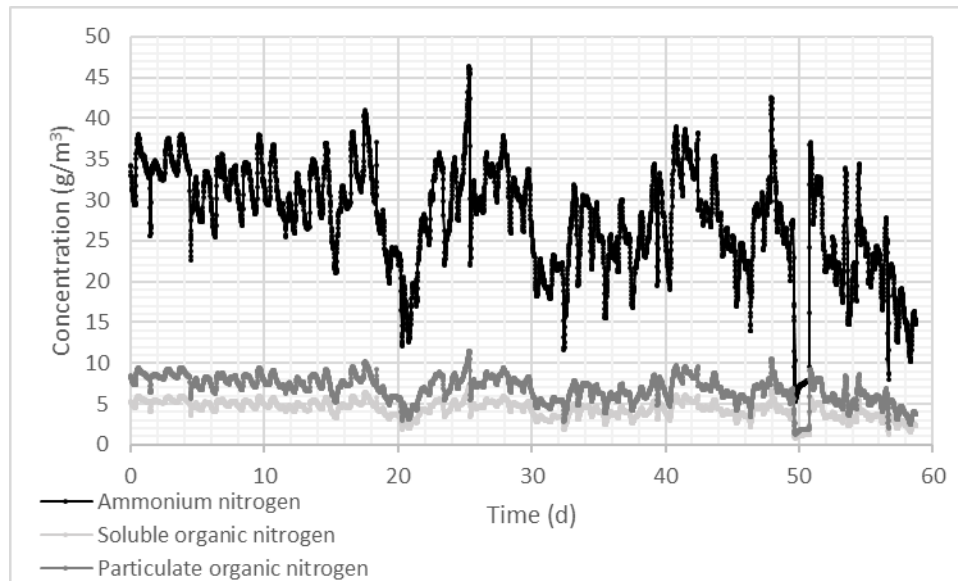
Figure 5.4 Primary Effluent Nitrogen Concentrations

Table 5.3 Primary Effluent Total Nitrogen Fractionation

Nitrogen Component	Fraction of Total Nitrogen
Ammonium nitrogen (S_{NH})	71%
Soluble organic nitrogen (S_{ND})	11%
Particulate organic nitrogen (X_{ND})	18%

Influent alkalinity is another parameter that needs to be considered for the model. However, no continuous alkalinity measurement is available for the pilEAUte. For that reason, influent alkalinity data was produced prior to modelling. For their study of fermentation in the primary clarifier, Ponzelli et al. (2019) monitored and evaluated the daily variation of alkalinity for the pilEAUte influent wastewater, both primary influent and effluent. In addition, Tohidi (2019) demonstrated the relation between the influent ammonium concentration and alkalinity. By considering this daily pattern and the influent ammonium sensor data, an influent alkalinity time series was created (Figure 5.5).
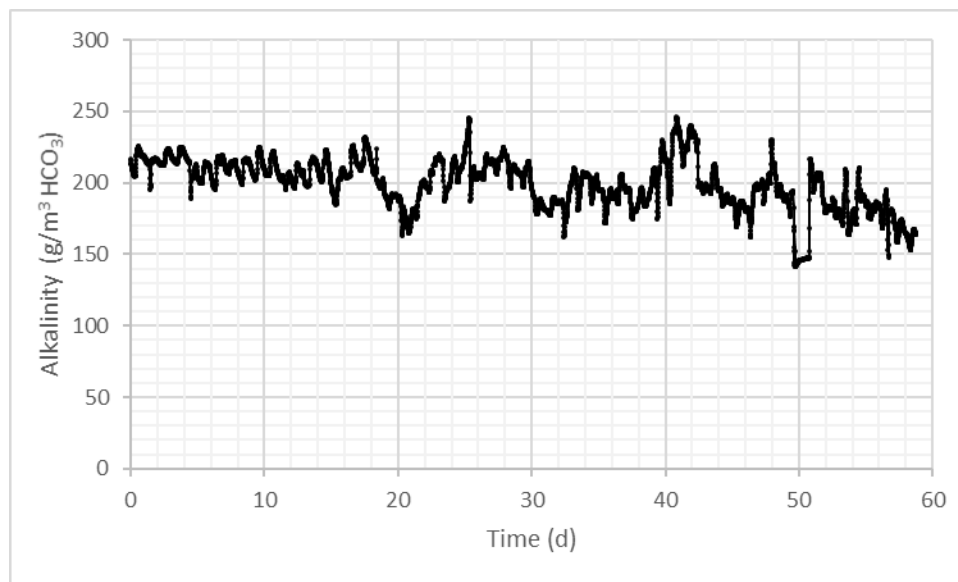
Figure 5.5 Primary Effluent Alkalinity Concentration

The pH of the influent wastewater is also considered for the model. The pH is quite stable, located between 6.5-8.5 and suitable for the growth of both heterotrophs and nitrifiers. The average value of the influent pH given in Figure 5.6 is used in the model (on average 7.5).
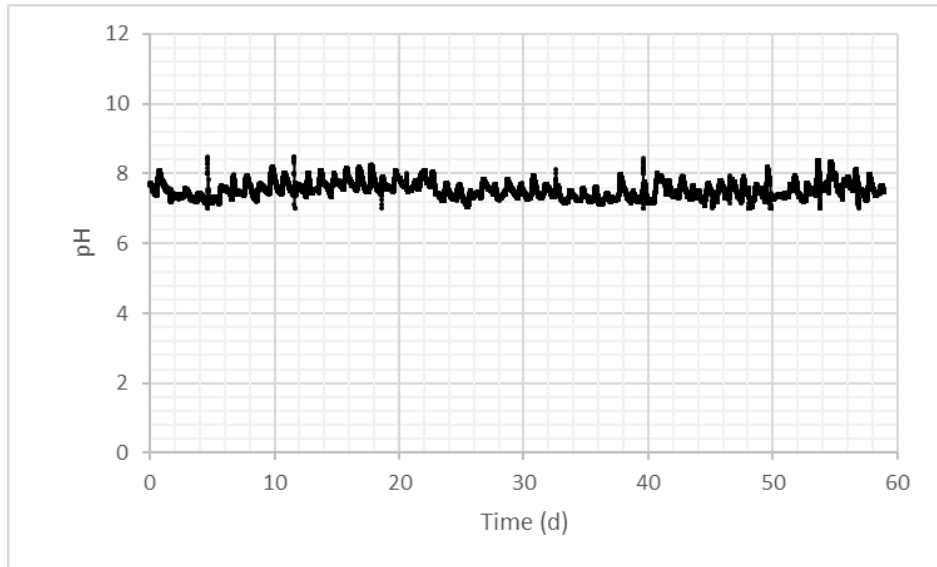
Figure 5.6 Primary Effluent pH

5.1.2 System Operational Data

The TSS concentrations measured in the biological reactors (anoxic basin 2) are compared to the sludge recycle TSS concentrations in Figure 5.7. The MLSS concentration in the biological reactors varies between 2500-4000 g/m^3. The sludge recycle TSS concentration data were corrected by considering the TSS mass balance around the secondary clarifier. The orange line in Figure 5.7 represents the data calculated based on the mass balance. The grey line in Figure 5.7 represents the data that was actually used for modelling. It uses the sensor measurement data if it is 20% below or above the value calculated with the mass balance. If not, the mass balance calculated value is assumed as the recycle TSS. Note that around day 20 and 50, the sludge recycle TSS concentration becomes equal to the one in the biological reactors because there was no influent fed to the plant.
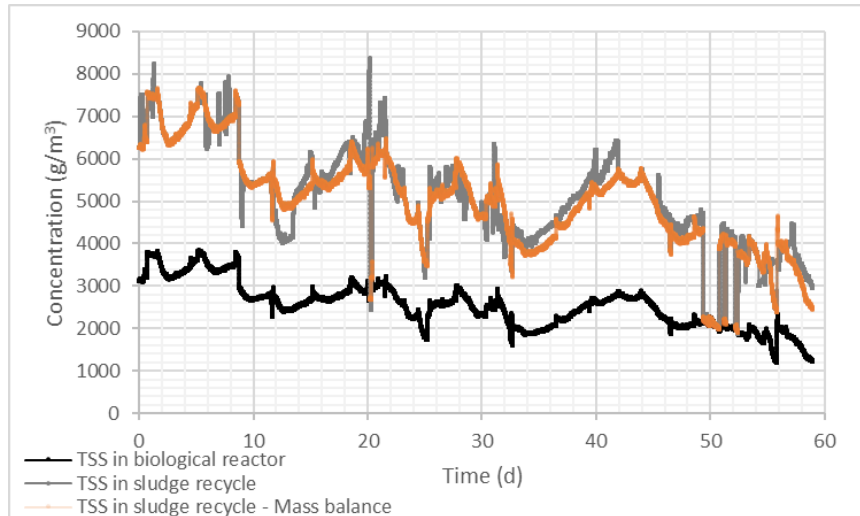
Figure 5.7 TSS Concentration in Biological Reactors vs Sludge Recycle

The dissolved oxygen concentration in the biological reactors is controlled (with a set-point of 3 mg/L) and measured only in Basin 4. Figure 5.8 compares the measured DO concentration with the air consumed in Basin 4. Note that the same air flowrate is applied to Basin 3 and Basin 5, thus the overall air consumption of the pilEAUte is three times the air flow time series of Figure 5.8.
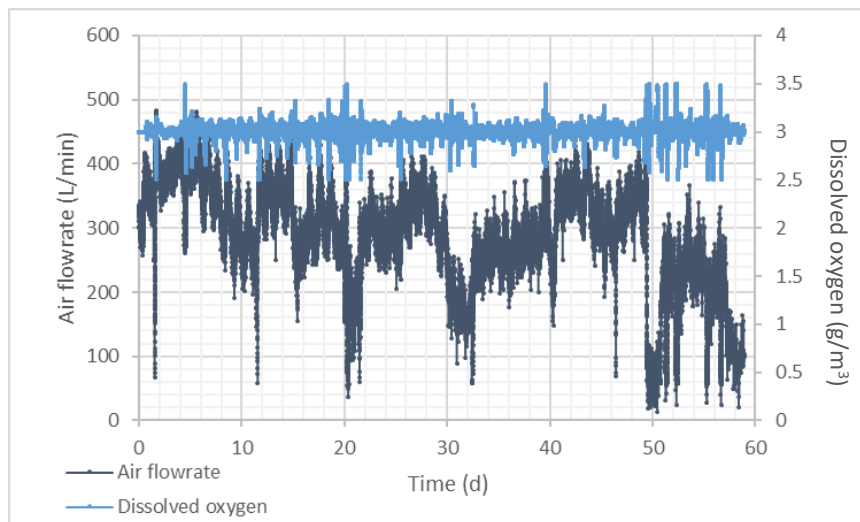
Figure 5.8 Dissolved Oxygen Concentration in Biological Reactor vs Air Flowrate Utilized

The temperature measured in the biological reactors (Basin 4) and used for the model is given in Figure 5.9. The reactor temperature is implemented as a model input and used in the Arrhenius temperature dependency of the biokinetic model. On average, the temperature was around 20ºC, thus prior to model calibration the ASM1 default biokinetic model parameters for 20ºC are used.
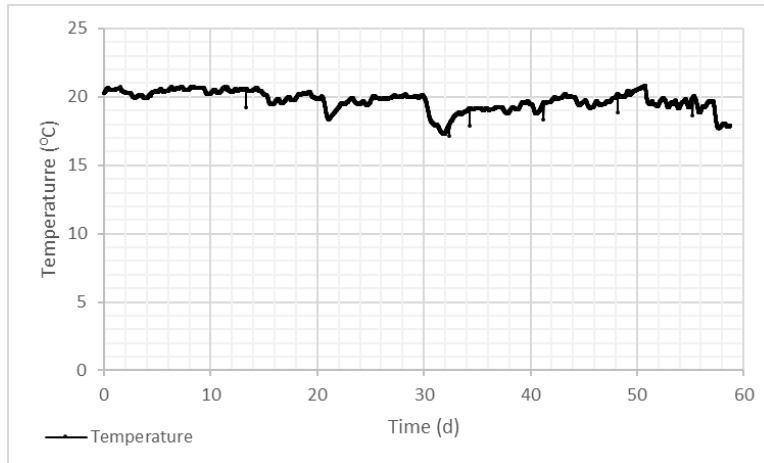
Figure 5.9 Temperature in Biological Reactors

5.1.3 Effluent Data

The effluent concentrations that were used for model calibration are presented in Figure 5.10 and Figure 5.11. Based on Figure 5.10, the ammonium in the effluent is quite low, so the nitrification works well for the selected time period. The effluent nitrate nitrogen varies between 4 to 14 mg/L probably reflecting the influent N load.
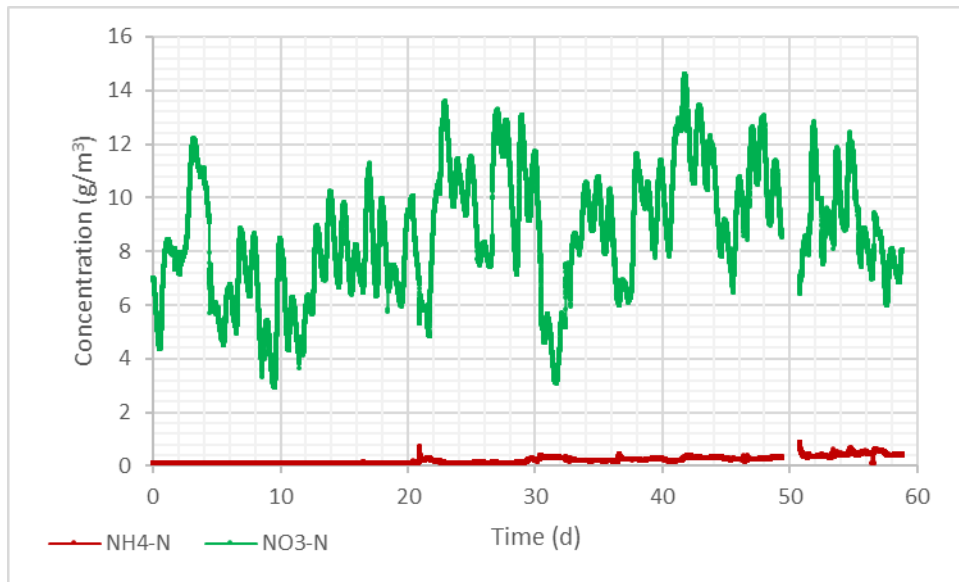
Figure 5.10 Effluent Ammonium and Nitrate Nitrogen Concentrations

The effluent turbidity data in Figure 5.11 shows that the sludge settles well in the secondary clarifier for the given time period.
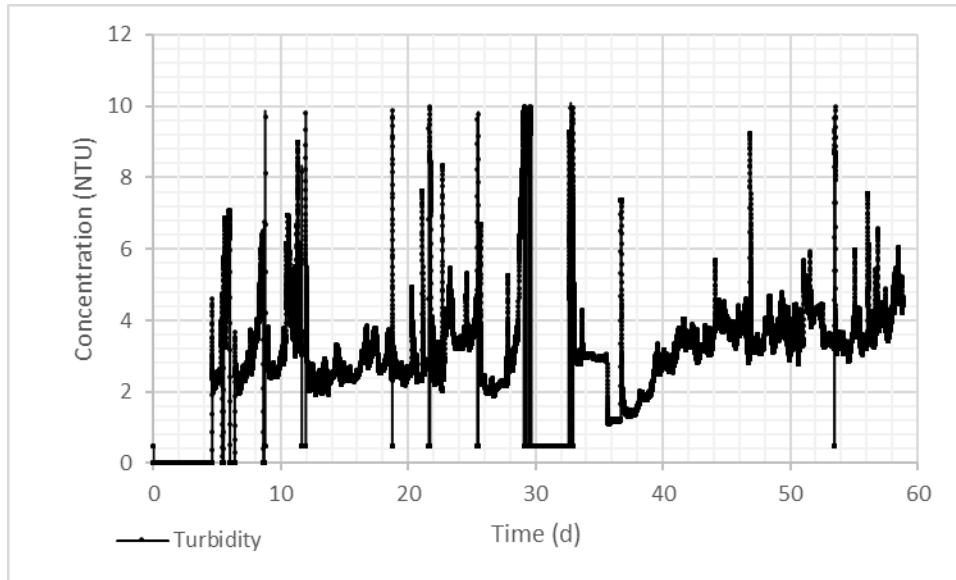
Figure 5.11 Effluent Turbidity

5.3   Hydraulic Model

The first step of the model calibration consists of the hydraulic characterization of the plant and to calibrate the hydraulic model. This evaluation is quite important for the pilEAUte WRRF since important backflows were observed between the different basins of the biological reactors. As previously mentioned (Chapter 3.1), the wastewater flows through basin 1 to basin 5 in the plant (Figure 3.3). However, the baffles between basins 4&5 and also basins 2&3 were found insufficient to divide the reactors when aeration is on in the reactors, leading to important, undesired backflows. A tracer test and a hydraulic model (Zhao and Vanrolleghem 2015) had already been developed for the pil*EAU*te WRRF. It was concluded that the baffles in between the basins cannot prevent backflow and the backflows between basins 4&5 are such that these basins have to be considered as one completely mixed reactor. There is also an important backflow from basin 3 to basin 2 which is increasing with the air flowrate in basin 3 (Figure 5.12). Note that the tracer test data was obtained for the normal operational conditions of pilEAUte where the average air flowrate applied in each aerated basin is 200 L/min. Rhodamine was used as the tracer in the experiments from Zhao and Vanrolleghem (2015) and analyzed in the laboratory.

In addition to that, another tracer test was designed and applied to confirm and determine the backflows between the different basins of the biological reactors (Souidi et al. 2018). For this tracer test, ammonium and nitrate were used as the tracer and the measurements were done with the ion-selective sensors that measure the ammonium and nitrate concentrations continuously. Within this study, two tracer tests were conducted, one for reference operational conditions and one for step-feed conditions to the 3rd basin.

Figure 5.12 Backflow between Basins 3 and 2 due to Aeration

Within this PhD research project, the data obtained from the different tracer tests were used to determine the backflow flowrates and calibrate the hydraulic model. The tracer applied to the measurement campaigns is defined in the model as inert soluble COD (S_I). By applying different backflow flowrates in between the basins, the S_I concentrations in different basins were compared with the tracer concentration data (model versus measurement results).

5.3.1 Reference Case

The reference case represents the normal operational conditions of the pilEAUte WRRF. Zhao & Vanrolleghem (2015) had already demonstrated backflows from basin 5 to 4 and from basin 3 to 2. This model layout (Figure 5.13) was used as the starting point and tested with the data from the measurement campaign of Souidi et al. (2018). The secondary clarifier model was replaced with the reactive settler model developed within the scope of this PhD research project (Chapter 4).
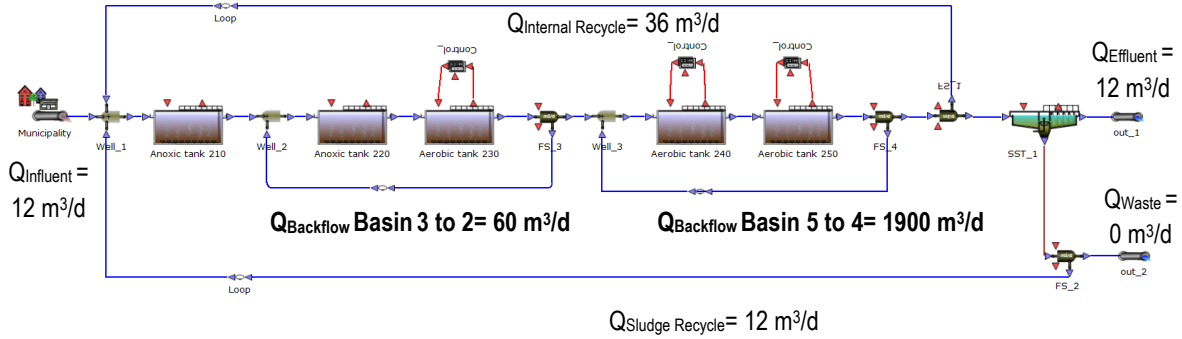
Figure 5.13 Hydraulic Model Layout (Zhao & Vanrolleghem, 2015)

In order to simplify the model, the backflow from basin 5 to 4 is tested for 1800 m³/d instead of the 1900 m³/d proposed by Zhao & Vanrolleghem (2015). Thus, the backflow becomes 150 times the influent flowrate of the plant. The model was tested with the 2018 measurement data and presented for each basin in Figure 5.14. Note that no data was available for Basin 5 from the 2018 measurement campaign.
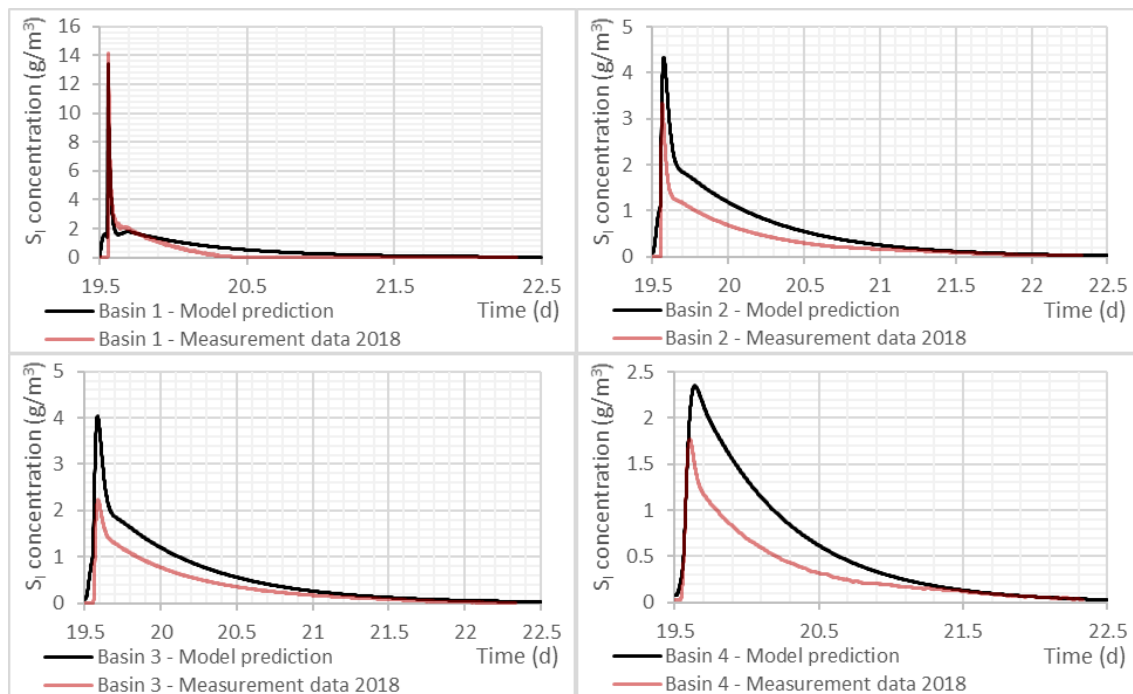
Figure 5.14 Hydraulic Model Results for Reference Case Tracer Experiment

Based on the model predictions versus the measurement data (2018) of Figure 5.14, the applied backflowrates (Figure 5.13 by Zhao and Vanrolleghem (2015)) are considered valid. The model predictions in the first three basins correspond well with the added tracer amount. The time of the peaks in each of the basins and the curves' shapes correspond with the measurement data of the 2018 campaign. However, a difference is observed

between the simulated and the measurement data curves in Basin 4 which might be due to a loss of tracer or a measurement error of the sensor installed in this basin.

5.3.2 Step-Feed Case

The step-feed case refers here to another operational case applied in the measurement campaign of 2018 which feeds the influent and the internal sludge recycle to Basin 3 (instead of Basin 1). This operational scenario is carried out to verify whether the backflows applied in the reference case (Chapter 5.3.1) are still valid in different operational cases. The 2018 measurement campaign data showed an additional backflow from Basin 2 to Basin 1. Thus, this backflow was added to the model layout in Figure 5.15 and its value was determined to be 25 m³/d by fitting the model to the measurement results given in Figure 5.16. Model results without the backflow from Basin 2 to 1 are also shown in Figure 5.16 to see the improvement in model predictions.
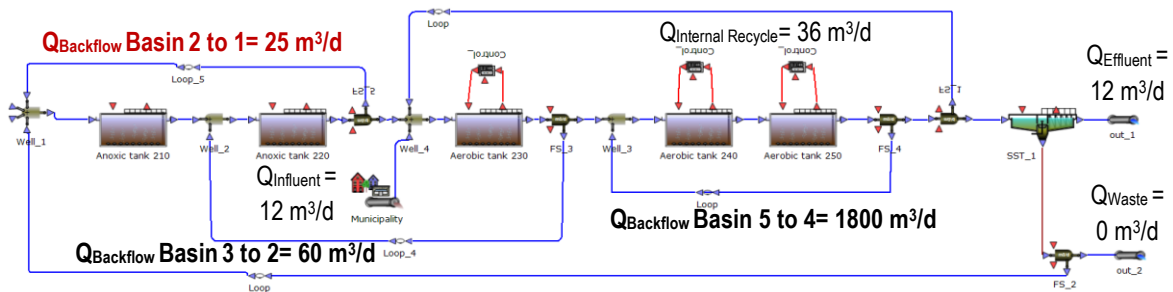
Figure 5.15 Hydraulic Model Layout for Step-Feed Case
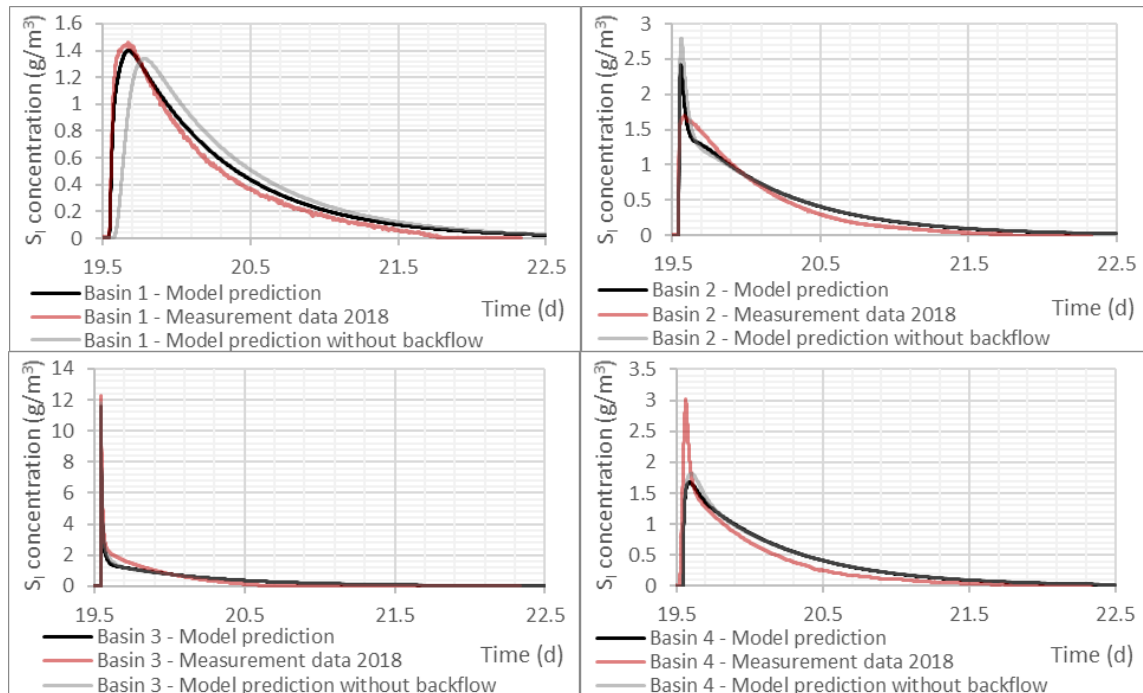
Figure 5.16 Hydraulic Model Results for Step-Feed Case

5.3.3 Final Hydraulic Model

The updated model layout (Figure 5.17) with the backflows in between the different basins were tested for the reference case to determine whether the predictions fit the reference case measurement data of 2018.

$Q_{Backflow}$ **Basin 2 to 1**= 25 m³/d $\quad Q_{Internal\ Recycle}$= 36 m³/d $\quad Q_{Effluent}$ = 12 m³/d

$Q_{Influent}$ = 12 m³/d

$Q_{Backflow}$ **Basin 3 to 2**= 60 m³/d $\quad Q_{Backflow}$ **Basin 5 to 4**= 1800 m³/d $\quad Q_{Waste}$ = 0 m³/d

$Q_{Sludge\ Recycle}$= 12 m³/d
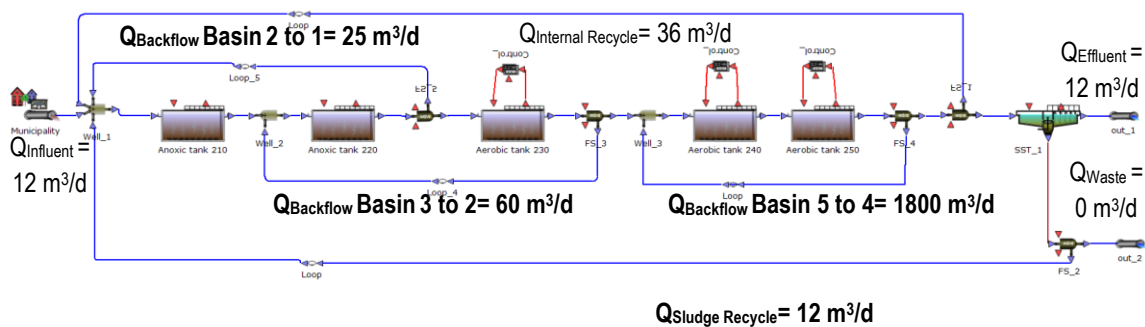
Figure 5.17 Final Hydraulic Model Layout for Reference Case

The final hydraulic model predictions versus the 2018 measurement data are shown in Figure 5.19. The time of the peaks in each of the basins and the curves' shapes correspond with the measurement data and, thus, this configuration is accepted as the final model layout for the pilEAUte WRRF. The curves are slightly different in basin 4, a finding also mentioned in Chapter 5.3.1. The difference is probably due to measurement errors in the sensor installed in basin 4.
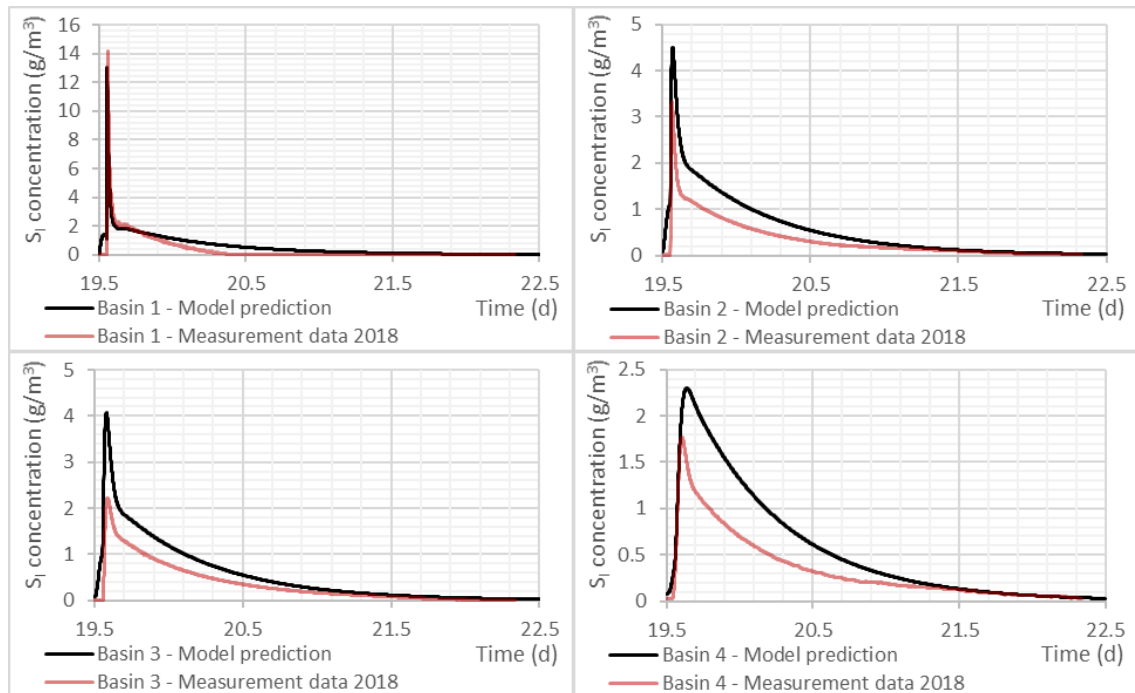
Figure 5.18 Updated (Final) Hydraulic Model Results for Reference Case

5.4   Aeration Model

Aeration model calibration and oxygen transfer characterization make up the second step of the BIOMATH model calibration. Since one of the aims of the PhD project is energy optimization through aeration control, determination of the parameters related to aeration and predicting the air flowrate is important. The pilEAUte model implemented in WEST describes each basin as an ideally mixed, activated sludge tank with constant volume and the oxygen transfer coefficient (k_{La}) is the most important parameter to characterize the aeration and the gas-liquid mass transfer. The model is able to predict the k_{La} for each time step by considering the reactor temperature, and the aeration energy consumption is calculated based on the k_{La} as follows:

$$\text{Equation 5.1: } P_{Aer} = \frac{S_{O,sat} * k_{La} * V}{24 * OTR}$$

where the saturation oxygen concentration ($S_{O,sat}$), tank volume (V), and standard oxygen transfer rate (OTR) are also considered. However, the air flowrate is the only measured parameter that allows to quantify the aeration in the real system. Thus, the air flowrate must be used for the aeration model calibration. It is also well-known that the value of k_{La} is a function of the air flowrate applied (Equation 5.2) and the correlation between these two parameters is adopted to predict the aeration in WRRF models and scenario analysis (Boyle et al. 1989; Rosso et al. 2005).

$$\text{Equation 5.2: } k_{La} = \frac{\rho * Q_{Air} * OTE}{(\beta * S_{O,sat} - S_O) * V} \quad \rightarrow \quad \frac{k_{La}}{\frac{\rho * OTE}{(\beta * S_{O,sat} - S_O) * V}} = k_{La} * Ɏ = Q_{Air}$$

where ρ is the density of air, β denotes a correction factor for the oxygen saturation, $S_{O,sat}$ and S_O are the standard oxygen saturation and the dissolved oxygen concentration in the aerated tank and V is the volume of the tank. This relation can be simplified as in the right side of the Equation 5.2 and the air flowrate becomes at dependent on k_{La} based on an "Ɏ" conversion factor.

By considering the relationship between air flowrate and k_{La}, the air flowrate consumption in Basin 4 (where the DO is controlled) is added to the model as a WEST calculator variable. The "Ɏ" conversion factor is determined to be 1.9 by comparing the calculated air flowrate with the measured values (Figure 5.19) and Equation 5.3 is adopted. As can be seen in Figure 5.19, the predicted air flowrate dynamics in Basin 4 correspond well with the measured air flowrate calculated from the k_{La} predictions.

$$\text{Equation 5.3 : } Q_{Air\,Basin4} = 1.9\,k_{La\,Basin4}$$
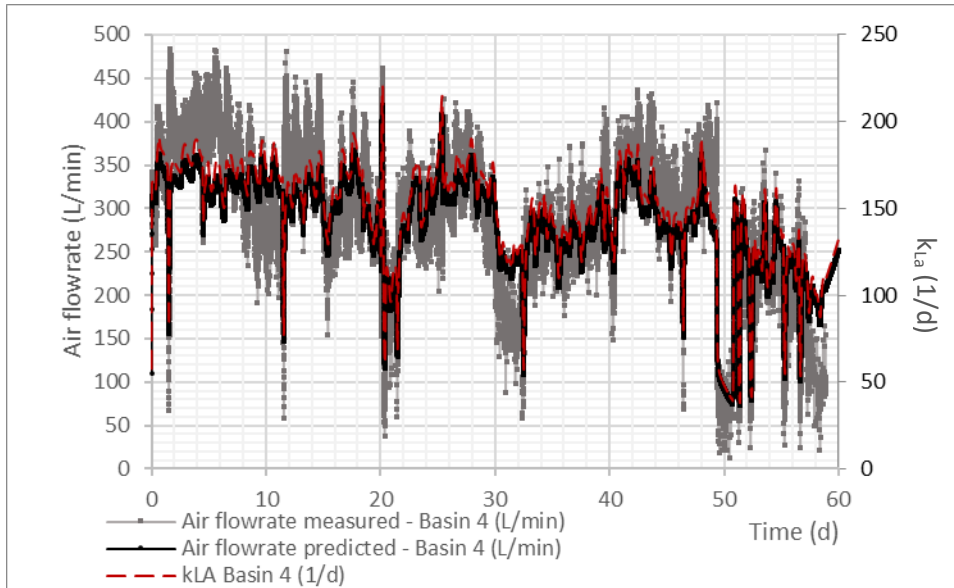
Figure 5.19 Measured vs Predicted Air Flowrate and k_{La} in Basin 4

As stated before (Chapters 3.1 & 5.1.2), the DO is controlled in Basin 4 and the same air flowrate is applied to all basins. To be able to include this in the model, the inverse relation between the reactor volume and the k_{La} (Equation 5.2) is used. Ratio controllers are used to manipulate the aeration in Basin 3 and 5, based on the k_{La} in Basin 4 (Figure 5.20). The volume of Basin 3 is equal to Basin 4, thus the same k_{La} is applied in both basins. The volume of Basin 5 (1.94 m³) is larger than that of Basin 4 (1.08 m³), thus the k_{La} is applied using the ratio of their volumes (0.56). The k_{La} values applied to the different basins in the model are shown in Figure 5.21.
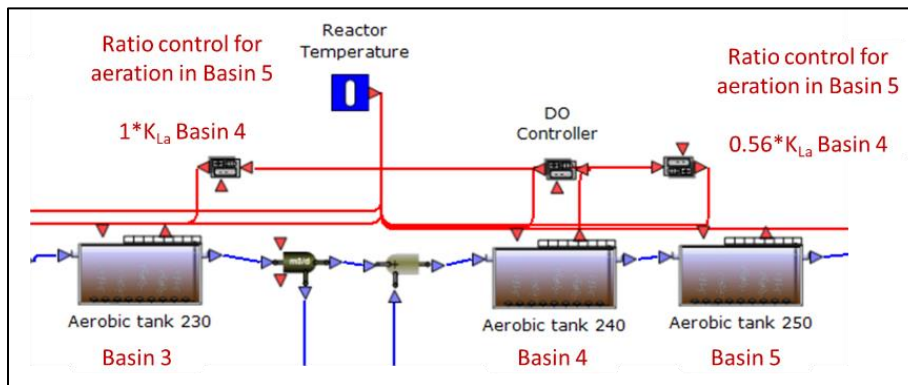
Figure 5.20 pilEAUte WRRF Aeration Model Layout and k_{LA} Manipulation
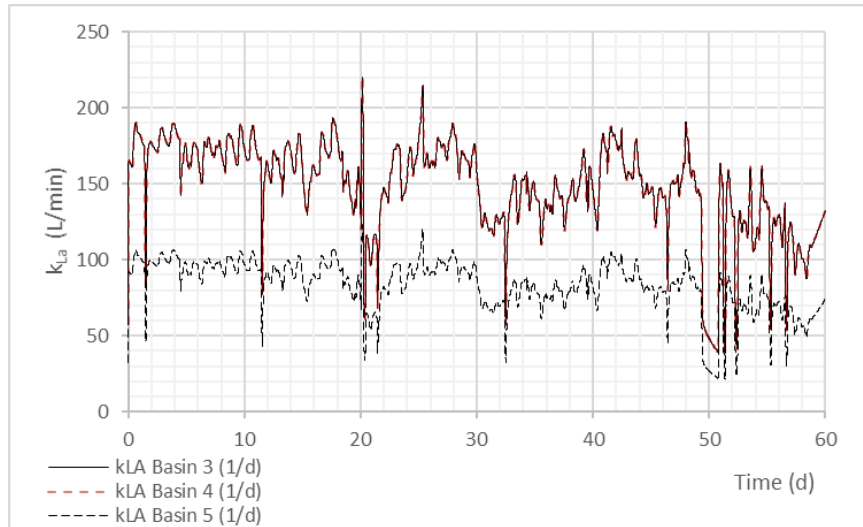
Figure 5.21 k$_{LA}$ Values Applied to the Three Aerated Basins

Based on the k$_{La}$ applied to each basin, the DO concentrations predicted by the model with the default biokinetic model parameters (before calibration of the biokinetic model) is presented in Figure 5.22. Note that the DO measurement is only available in Basin 4. As expected, the DO concentration predicted in Basin 3 is low since it is the first aerated tank which is fed with the highest pollutant loads. In Basin 4, the DO is always around 3 mg/L since the controller is installed there. Finally, the DO concentration in Basin 5 is also around 3 mg/L even if the applied k$_{La}$ is low because it is the last aerated tank and little pollution is left there. Also, Basin 4 and 5 are known to be in fact a single completely mixed bioreactor based on the hydraulic characterization of the plant (Chapter 5.3), thus the same DO concentration is expected to occur.
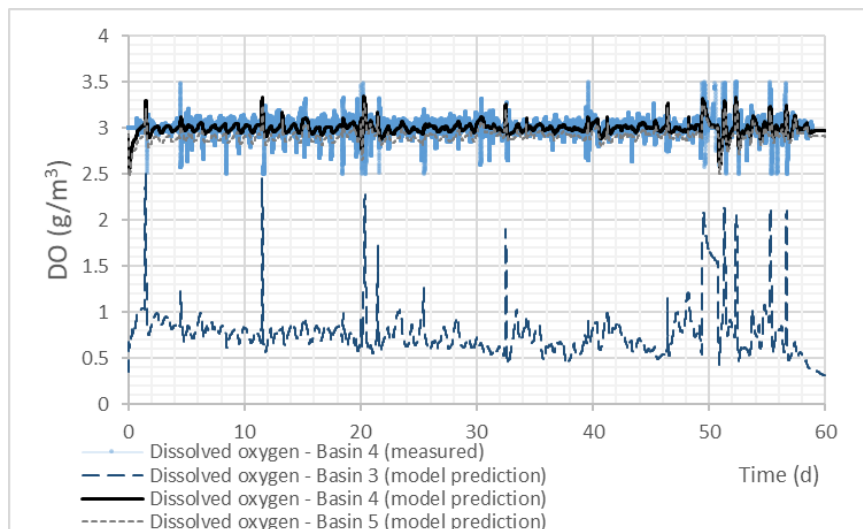
Figure 5.22 DO Concentration Predictions in Aerated Basins with the Applied k$_{LA}$ Values

5.5   SST Model Calibration

The developed reactive settler model (Chapter 4) which was so far only calibrated for the settling model parameters (Chapter 4) is used for the plant-wide pilEAUte model. The ASM1 biokinetic model within the reactive settler model was thus replaced with the ASM1_AN model that is one of the models available in the model library of the WEST simulation platform. Calibration of the biokinetic model is done for the plant-wide model by considering the biological reactors and the reactive settler at the same time. Thus, the same parameter values are applied in both the biological reactor and the reactive SST for the biokinetic model (Chapter 5.6).

5.6   Calibration of Biokinetic Model

The ASM1_AN biokinetic model is used to model the pilEAUte WRRF which is an extension of ASM1 with Anammox and two-step nitrification and denitrification processes. Thus, the model considers NO_2-N as an intermediate model variable and distinguishes the growth of ammonium oxidizers (AOB) and nitrite oxidizers (NOB). Because this model will further be used to investigate process optimization scenarios and applicability of short-cut N removal processes, it is important to consider the different microorganism species involved in nitrification and also NO_2-N as a denitrification intermediate (Kirim et al. 2022).

A step-wise Monte Carlo-based calibration methodology inspired by Mannina et al. (2011) was adopted as explained in Chapter 3 Step 4. The pilEAUte operational data (TSS concentrations in biological reactors and underflow, air flowrate-Q_{air}) and effluent data (NH_4-N and NO_3-N) were considered for the calibration of the biokinetic model and chosen as representative model outputs/variables.

5.6.1   Pre-selection of the Model Parameters

The biokinetic model used includes 51 model parameters in total. Before starting the model calibration, model parameters were pre-selected based on engineering expertise and the available data. Measured parameters (pH, temperature), conversion factors (fractions BOD/COD, TSS/COD), yield coefficients and temperature correction factors were excluded from the model calibration and kept at their default values. Twenty-seven model parameters including all the kinetics remained to be calibrated after this pre-selection (Appendix II-Table 1).

5.6.2   Pre-screening of Model Parameters

A preliminary sensitivity analysis was carried out to determine the influential model parameters and reduce the number of parameters that need to be calibrated reliably. Local sensitivity analysis (LSA) was applied in this step in order to quantify the influence of model parameters on the relevant model outputs. The central relative sensitivity (CRS) of each model parameter was calculated for each model output. To do that, the finite difference approach already implemented in the WEST simulator was used (Claeys 2008). Based on the LSA results presented in Appendix II, the parameters which have CRS values equal or higher than 0.05 on any model

output/variable are chosen as influential. Thus, 17 model parameters were selected for calibration (Appendix II-Table 2) (Table 5.4).

5.6.3 Parameter Subsets Selection

Prior to calibration, different parameter subsets were selected, each focusing on a different group of output variables (Mannina et al. 2011). Global sensitivity analysis (GSA) was applied in this step to determine the parameter subsets based on the standardized regression coefficients (SRC) for each model output. To obtain the SRCs, Monte Carlo simulations were performed and the multivariate linear regression between each of the model parameters and the variable of interest was calculated. The variation range of the model parameters for the GSA was determined by considering the relevant literature and engineering expertise (Appendix II-Table 2). Parameter sampling was done with Latin Hypercube Sampling (LHS).

The model output variable groups were formed by putting together all variables related to TSS and N. Parameters which have SRCs equal or higher than 0.1 were chosen for the subsets. Based on the GSA results and calculated SRC values presented in Appendix II, 3 parameter subsets were selected for the groups of output variables (Table 5.4).

Table 5.4 Parameter Subsets and Output Variable Groups

		Parameter	Variables
Subset 1 (TSS variables)	b_H	Decay Coefficient for Heterotrophic Biomass	TSS in biological reactor TSS underflow
	f_XI	Fraction of Biomass Converted to Particulate Inert Matter	
	k_h	Maximum Specific Hydrolysis Rate	
Subset 2 (N variables)	b_NH	Decay Coefficient for NH4 Oxidizing Autotrophic Biomass	Effluent NH$_4$-N Effluent NO$_3$-N Qair
	b_NO	Decay Coefficient for NO Oxidizing Autotrophic Biomass	
	K_HNO2_NO	Nitrous Acid Half-Saturation Coefficient for NO Oxidizing Autotrophic Biomass	
	K_NH3_NH	Ammonia Half-Saturation Coefficient for NH4 Oxidizing Autotrophic Biomass	
	K_SH	Substrate Half-Saturation Coefficient for Heterotrophic Biomass	
	mu_H	Maximum Specific Growth Rate for Heterotrophic Biomass	
	mu_NH	Maximum Specific Growth Rate for NH4 Oxidizing Autotrophic Biomass	
	mu_NO	Maximum Specific Growth Rate for NO Oxidizing Autotrophic Biomass	
Subset 3 (All parameters)	K_NO2_H	Nitrite Half-Saturation Coefficient for Denitrifying Heterotrophic Biomass	TSS in biological reactor TSS underflow Effluent NH$_4$-N Effluent NO$_3$-N Qair
	K_O_NH	Oxygen Half-Saturation Coefficient for NH4 Oxidizing Autotrophic Biomass	
	K_O_NO	Oxygen Half-Saturation Coefficient for NO Oxidizing Autotrophic Biomass	
	K_OH	Oxygen Half-Saturation Coefficient for Heterotrophic Biomass	
	n_NO2	Correction Factor for Anoxic Growth of Heterotrophs on Nitrite	
	n_NO3	Correction Factor for Anoxic Growth of Heterotrophs on Nitrate	

TSS in the biological reactor and underflow are the variables to be considered for the calibration of parameter subset 1. Effluent NH_4-N and NO_3-N concentrations and the air flowrate in Basin 4 are the variables to be used for the calibration of parameter subset 2. Finally, the parameters which have influence on all variables (and the parameters which were not yet grouped in subset 1 or 2) are selected as parameter subset 3. These parameters are present because they influence more than one process (Mannina et al. 2011). Also, note that parameter b_H which is chosen for subset 1, is also highly influential for Qair and effluent NO_3-N. This parameter is therefore also included in subset 3 and recalibrated within the subset 3 based on all output variables.

5.6.4 Calibration of Parameter Subsets

Following the global sensitivity analysis, the set of model parameters to be calibrated is organized into the sets of influential ones grouped according to a number of related model variables. The next step is the group calibration of the model parameters given in Table 5.4. Each model parameter subset is calibrated according to the model outputs and the objective function by carrying out Monte Carlo simulations. The same variation range of the model parameters is used as in Chapter 5.6.3 (Appendix II-Table 2) and parameter sampling is done with LHS.

For each Monte Carlo run, the sum of squared errors (SSE) between the model predictions and the measurements is calculated for each model variable. A weighted average of the square root of the SSEs is used as the overall objective function for each parameter set (for details see Appendix II - Calibration of parameter subsets (6.6.4)). Then, the parameter set (or the Monte Carlo run) that gives the minimum overall objective value is chosen as the optimal parameter set. Details of the objective function and model calibration is given in Appendix II.

The calibration order of the parameter subsets is given in Figure 5.23. Calibration of parameter subsets 1 and 2 could be done simultaneously because their evaluation criteria (influenced model variables) are independent of each other. Then, the calibrated parameter values for subset 1 and 2 are fixed and used in the Monte Carlo simulation to calibrate the parameters of subset 3 which covers all the model variables considered for the biokinetic model calibration. Note that parameter b_H is recalibrated within subset 3.

	Parameter	Variables
Subset 1	b_H f_XI k_h	TSS in biological reactor TSS underflow

Number of Monte Carlo runs: 80

	Parameter	Variables
Subset 2	b_NH b_NO K_HNO2_NO K_NH3_NH K_SH mu_H mu_NH mu_NO	Effluent NH$_4$-N Effluent NO$_3$-N Qair

Number of Monte Carlo runs: 120

	Parameter	Variables
Subset 3	K_NO2_H K_O_NH K_O_NO K_OH n_NO2 n_NO3 b_H	TSS in biological reactor TSS underflow Effluent NH$_4$-N Effluent NO$_3$-N Qair

Number of Monte Carlo runs: 200

Simultaneous Monte Carlo Runs and Calibration of Parameter Subsets

Monte Carlo Run for Subset 3 by applying the calibrated parameter values for Subset 1&2

Final set of Calibrated Model parameters

Figure 5.23 Calibration Order of Parameter Subsets

The 17 calibrated model parameter values are presented in Table 5.5. As can be seen, they are mostly in the range given in the literature and similar to default values. Only the model parameters *K_HNO2_NO* and *K_NH3_NH* related to the biokinetics of the 2-step nitrification process are calibrated to much lower values than their default values. These model parameter values in the literature are mostly calibrated for side-stream applications which are operated at much higher substrate concentrations leading to higher half-saturation concentration of the substrates for the growth of AOBs and NOBs. The same situation holds for the oxygen half-saturation concentrations (*K_O_NH & K_O_NO*). The calibrated values of these parameters are mostly case-specific and not transferable to other models (Kirim et al. 2022). Also note that the effluent NH$_4$-N data which was used for the model calibration were at low values continuously and no dynamics were observed (Figure 5.10). All these estimated parameter values related to nitrification kinetics might have also been affected due this stable data set and might be unidentifiable. It would have been more appropriate to use NH$_4$-N concentrations along the different basins of the biological reactor to calibrate these parameters. However, such data set was not available for this project.

Figure 5.24 shows the calibrated model predictions and the measurement results for each model variable for the calibration time period (days 24-47). For TSS, the model predictions mostly meet with the measurements and the trends of change are the same. There are small deviations in the underflow TSS concentration on days 24-30 and 36-42 which can be attributed to measurement errors. The air flowrate model predictions and measurements are meeting quite well. The measurement data varies a lot at each time step, while the model predictions are more stable and in parallel to the trends of the measurement data. Finally, model predictions for the effluent ammonia are low in accordance with the measurement data, i.e. the model describes the observed full nitrification of the influent nitrogen. Effluent nitrate predictions are meeting the measurement data on average

but there are occasional deviations (e.g. day 25 or 37). Possible reasons are the assumptions related to influent nitrogen fractionation or measurement errors of the effluent nitrate (e.g. a sudden change in the influent ammonia on day 25 results in high effluent nitrate prediction in the model, but not in the measurement – see Figure 5.4).

Table 5.5 Calibrated Biokinetic Model Parameter Values

		Parameter	Default Value	Calibrated Value	Unit
Subset 1	b_H	Decay Coefficient for Heterotrophic Biomass	0.62	0.70	1/d
	f_XI	Fraction of Biomass Converted to Particulate Inert Matter	0.1	0.13	-
	k_h	Maximum Specific Hydrolysis Rate	3	3.20	gCOD/(gCOD*d)
Subset 2	b_NH	Decay Coefficient for NH4 Oxidizing Autotrophic Biomass	0.05	0.06	1/d
	b_NO	Decay Coefficient for NO Oxidizing Autotrophic Biomass	0.033	0.04	1/d
	K_HNO2_NO	Nitrous Acid Half-Saturation Coefficient for NO Oxidizing Autotrophic Biomass	0.000872	0.000061	$gCOD/m^3$
	K_NH3_NH	Ammonia Half-Saturation Coefficient for NH4 Oxidizing Autotrophic Biomass	0.75	0.0057	gNH_3-N/m^3
	K_SH	Substrate Half-Saturation Coefficient for Heterotrophic Biomass	20	8.74	$gCOD/m^3$
	mu_H	Maximum Specific Growth Rate for Heterotrophic Biomass	6	4.77	1/d
	mu_NH	Maximum Specific Growth Rate for NH4 Oxidizing Autotrophic Biomass	0.8	0.71	1/d
	mu_NO	Maximum Specific Growth Rate for NO Oxidizing Autotrophic Biomass	0.79	0.95	1/d
Subset 3	K_NO2_H	Nitrite Half-Saturation Coefficient for Denitrifying Heterotrophic Biomass	1	3.31	$gCOD/m^3$
	K_O_NH	Oxygen Half-Saturation Coefficient for NH4 Oxidizing Autotrophic Biomass	0.6	0.25	gO_2/m^3
	K_O_NO	Oxygen Half-Saturation Coefficient for NO Oxidizing Autotrophic Biomass	1.5	0.27	gO_2/m^3
	K_OH	Oxygen Half-Saturation Coefficient for Heterotrophic Biomass	0.2	0.10	gO_2/m^3
	n_NO2	Correction Factor for Anoxic Growth of Heterotrophs on Nitrite	0.6	0.92	-
	n_NO3	Correction Factor for Anoxic Growth of Heterotrophs on Nitrate	0.6	0.49	-
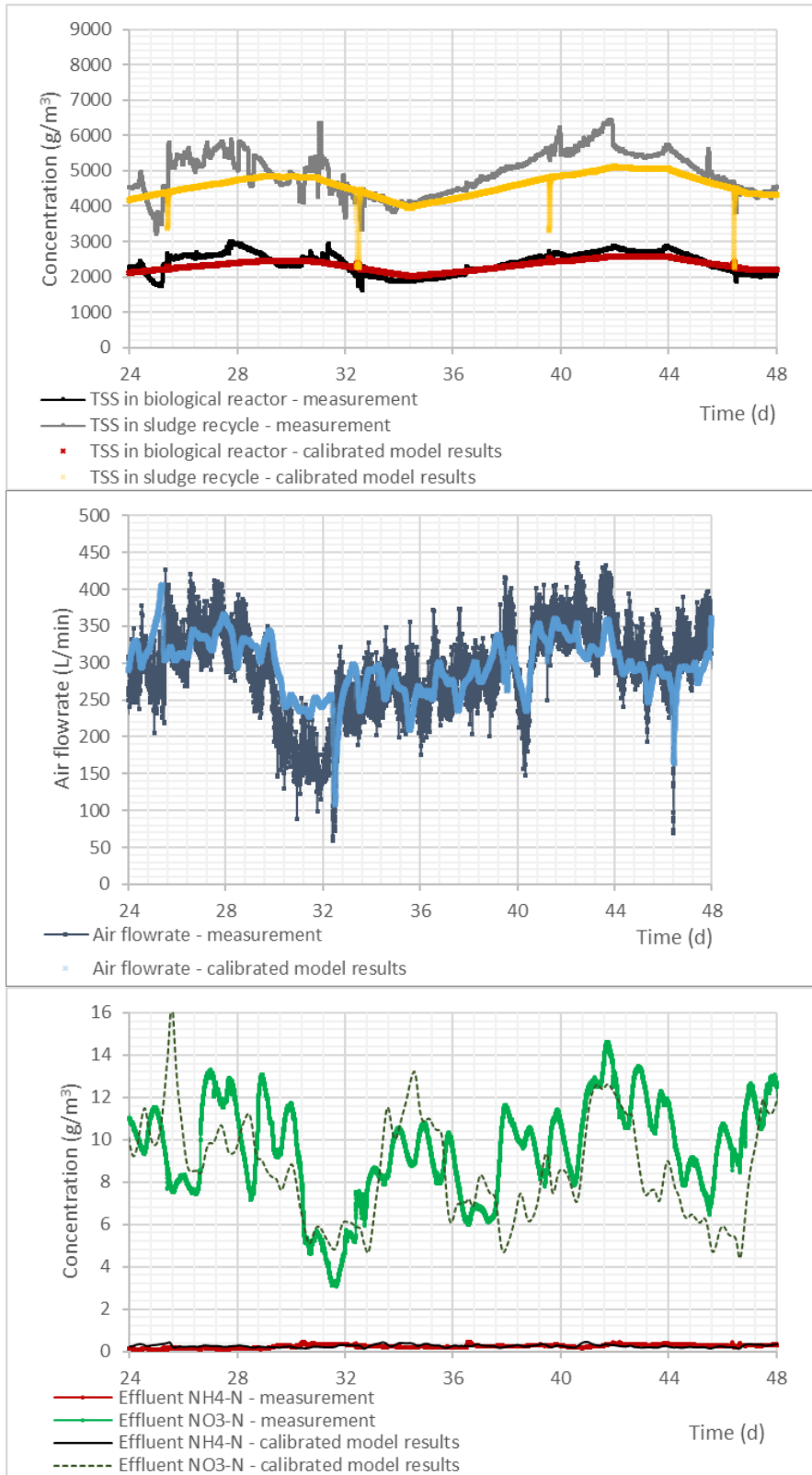
Figure 5.24 Calibrated Model Results vs Measurements

5.7　Validation

For validation, the calibrated model is run with the influent data for the validation time period (from Day 48 to 59). Figure 5.25 shows the model predictions for TSS concentrations, air flowrate and effluent N components. As can be noticed from the graphs, the plant did not receive influent wastewater between the days 49-51 (see Figure 5.2). This of course affects the system and sudden drops are observed both in measurement and model prediction data.

The TSS concentration predictions for the biological reactor and the sludge recycle agree with the measurement data for the validation time period. For the time that there was no influent, the TSS concentration in the SST underflow (thus the sludge recycle) becomes equal to the TSS in the biological reactors. In the subsequent days, similar behaviour is seen as well for shorter time periods (e.g. days 51.5, 52.2, 55). After day 55, the model predictions are no longer overlapping with the measurement data, however they still have the same order of magnitude. The difference might be due to sensor drift (lack of calibration) or an error in the amount of sludge wasting within that time period. Unfortunately, no laboratory measurements are available to confirm the sensor reliability issues.

For the air flowrate, model predictions and measured values are agreeing well during the whole validation time period. It is also known that the oxygen transfer coefficient (k_{La}), thus the air flowrate, is heavily dependent on the gas-liquid mass transfer and not directly to the biokinetic processes. Thus, the model is able to predict the air flowrate in accordance with the DO set-point of the controller and the influent flowrate. The model predictions in the validation time period also confirm that the assumptions for the aeration model are valid and working well in a different time period than the calibration period (Chapter 5.4).

Finally, the model predictions and the measurements of the effluent ammonium concentration correspond well at very low values. The model confirms that the pilEAUte is fully nitrifying the influent nitrogen during the validation time period. However, the effluent nitrate is not agreeing as well with the measurements. The order of magnitude is the same for most of the validation time period, but there are significant differences for days 48-53. It is also the time period for which there was no influent (the measurement NO_3-N data are removed from the dataset when there is no influent). The reason of the sudden peak at the effluent nitrate predictions for the days 51-53 might be due to the high ammonium load to the plant just after the no influent time period. On the other hand, it is known that the sensors measuring the effluent nitrate may be problematic and the measured values may not be reliable. This problem could not be confirmed though since no laboratory measurements were conducted during this time period.
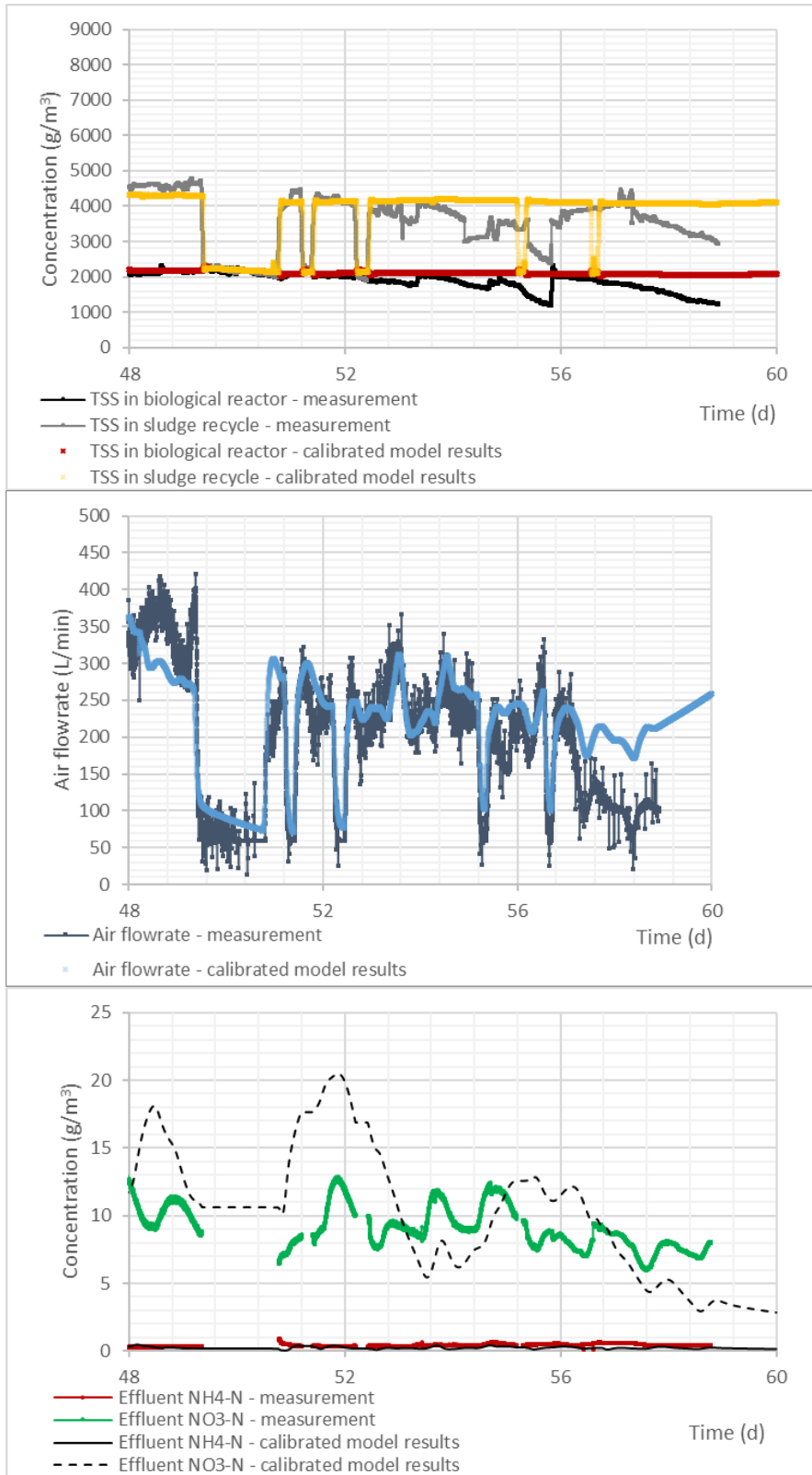
Figure 5.25 Calibrated Model Results vs Measurements for the Validation Time Period

5.8   Conclusions

The pilEAUte WRRF was modelled to improve the understanding of N-removal mechanisms in the biological treatment of wastewater through modelling and optimizing the existing WRRF. The pilEAUte WRRF operational data for the time period February 1st − March 31st 2018 were used. The influent flowrate, total and soluble COD, ammonium, alkalinity and pH were evaluated in detail for the selected time period and the model input file was created based on that. For the fractionation of COD, a backward calculation was done between the effluent and influent of the primary clarifier to be able to apply the influent COD fractionation study for the pilEAUte by Li et al. (2019). Since NH_4-N is the only parameter that is measured at the primary effluent, an influent total nitrogen fractionation was performed based on the monitoring data which was collected during another measurement campaign in the scope of this PhD (presented in Chapter 6). Air flowrate, dissolved oxygen (DO) and TSS concentrations measured in the biological reactors and the sludge recycle TSS concentrations were used as the system operational data for the model calibration. The sludge recycle TSS concentration data were corrected by considering the TSS mass balance around the secondary clarifier. Effluent ammonium and nitrate nitrogen were also used for the model calibration.

To constitute and calibrate the hydraulic model of the plant, two tracer test data sets were used. Important backflows were observed despite the baffles between basins 4&5, basins 2&3 and also basins 1&2 were found insufficient to divide the reactors. The backflows between basins 4&5 are such that these basins have to be considered as one completely mixed reactor. Standard (reference) and step-feed (which feeds the influent and the internal sludge recycle to Basin 3) operational conditions were tested. By considering the tracer tests data, different backflow flowrates in between the basins were determined and included to the final model layout.

Aeration model calibration and oxygen transfer characterization were also performed. The developed model is able to predict the oxygen transfer coefficient (k_{La}) for each time step from the air flowrate by considering the reactor temperature, and the aeration energy consumption is calculated based on the k_{La}. The air flowrate is the only measured parameter at the pilEAUte's biological reactors that allows quantifying the aeration in the real system. Thus, the air flowrate is used for the aeration model calibration. To do that, the correlation between the k_{La} and the air flowrate was adopted to predict the aeration in the pilEAUte model and during subsequent scenario analysis. In the pilEAUte, the DO is controlled in Basin 4 and the same air flowrate is applied to all basins. To include this in the model, the inverse relation between the reactor volume and the k_{La} is used and ratio controllers are used to adjust the aeration in Basins 3 and 5, based on the k_{La} in Basin 4. The calibrated aeration model gave promising results to predict the DO concentrations in the biological reactors and the air consumption.

The ASM1_AN biokinetic model which is an extension of ASM1 was used as the biokinetic model. The developed reactive settler model which was so far only calibrated for the settling model parameters was used for the plant-wide pilEAUte model and the biokinetic model within the reactive settler model was replaced with the ASM1_AN model. Calibration of biokinetic model parameters were done at the same time for the biological reactors and the reactive SST. A step-wise Monte Carlo-based calibration methodology inspired by Mannina et al. (2011) was adopted for the calibration of the biokinetic model. The biokinetic model used includes 51 model parameters in total and these model parameters were pre-selected based on engineering expertise and the available data. Twenty-seven model parameters including all the kinetics remained to be calibrated after this pre-selection. Next, a preliminary sensitivity analysis was carried out to determine the influential model parameters and reduce the number of parameters that need to be calibrated. For that, local sensitivity analysis (LSA) was applied and the central relative sensitivity (CRS) of each model output was calculated for each model parameter. Seventeen model parameters were selected for calibration in this step. Then, different parameter subsets were selected, each focusing on a different group of output variables. Global sensitivity analysis (GSA) was applied in this step to determine the parameter subsets based on the standardized regression coefficients (SRC) for each model output. The model output variable groups were formed by putting together all variables related to TSS (TSS in the biological reactor and underflow) and N (effluent NH_4-N and NO_3-N concentrations and the air flowrate). Three parameter subsets were selected for the groups of output variables. Then, the group calibration of the model parameters was executed according to the model outputs and the objective function (the sum of squared errors - SSE) by carrying out Monte Carlo simulations. The 17 model parameters' calibrated values are presented in Table 5.5. The calibrated parameter values are mostly in the range given in the literature and remain quite similar to the model's default values. Only the model parameters K_HNO2_NO and K_NH3_NH related to the biokinetics of the 2-step nitrification process are calibrated to much lower values than their default values.

Finally, the calibrated model predictions were compared with the measurements of the chosen variables. For the TSS in the biological reactor and the underflow, the air flowrate and the effluent ammonium, the predictions and measurements are found to be meeting quite well. Effluent nitrate predictions are meeting the measurement data on average but there are occasional deviations which might be due to the assumptions related to influent nitrogen fractionation or measurement errors. Similar conclusions were drawn for the model validation results. The model confirms that the pilEAUte is fully nitrifying the influent nitrogen during the validation time period. However, the effluent nitrate is not agreeing as well with the measurements. The order of magnitude is the same for most of the validation time period, but significant differences were observed for a few days. The reason of this might be that the validation time period includes a few days during which no influent was available or that the sensors measuring the effluent nitrate may have been problematic and the measured values may not be reliable.

6. APPLICATION of CONTINUOUS & INTERMITTENT AVN CONTROL STRATEGIES FOR ENERGY & RESOURCE CONSUMPTION

This chapter of this PhD dissertation provides a summary of the activities performed in the scope of the industrial collaboration between Université Laval, DC Water and Hampton Roads Sanitation District. It discusses the results obtained and provides perspectives for the application of both continuous and intermittent Ammonia vs. NO_x-N (AvN) control strategies in view of mainstream anammox treatment (see Chapter 1.5.3.3 for details).

The duration of this project was anticipated to be 1 year, including the time for implementing modifications to the pilEAUte WRRF needed to test the AvN control strategies in both manual and automatic operation. The main objective was to quantify the improvements that can be obtained by application of continuous and intermittent AvN control strategies on a pilot-scale WRRF which is designed for carbon and nitrogen removal. Performance comparison of these two control strategies was made possible by making used of the 2 identical treatment lanes of the pilEAUte WRRF.

The objective of AvN controllers is to maintain an equal concentration of NH_4-N and NO_3-N (NO_x-N preferably) in the effluent by manipulating the extent of aeration in the aerobic reactors. By maintaining this ratio, the effluent is optimized for a downstream deammonification process (anammox treatment), and as such the overall energy budget for aeration, required to remove COD and N, can be reduced. Of course, the deammonification process requires equal amounts of NH_4-N and NO_2-N and this can be achieved through partial nitrification and out-selection of NOB. However, it would also be possible to convert an excess amount of NO_3-N into NO_2-N through partial denitrification (by adding external COD) and then achieve the short-cut N removal with the anammox process (details related to application of the deammonification processes were already presented in Chapter 1.5.1). The partial denitrification anammox process consumes more resources; aeration and organic matter, than the partial nitrification anammox route, but this nitrite generating pathway is found more stable (Ma et al. 2017; Kirim et al., 2022). Through AvN control, nitrogen removal in the aerated biological reactors is also expected to occur through simultaneous nitrification and denitrification (SND) under low DO operation (see Chapter 1.5.2 for SND process details).

AvN is a cascade control where the AvN controller uses measurements both NH_4-N and NO_3-N and cascades the DO controller to manipulate the DO concentration in the aerated tank (details presented in Chapter 1.5.3.3). Two different AvN control strategies were applied to manipulate aeration for N removing systems. Continuous AvN, which provides a low but continuous DO set-point and intermittent AvN, which provides a modulated

ON/OFF aeration pattern that results in the reactor switching between aerobic and anoxic phases. Both AvN control strategies rely on a PID controller to maintain the measured AvN ratio close to its desired value.

Within this PhD research project, it is aimed to identify the minimum applicable sludge retention time (SRT) for both AvN control strategies while optimizing N removal in the aerated reactors. In addition to that, this research aims at finding out if SND and low effluent concentrations can be sustained to the same extent for both AvN control strategies.

6.1   Application of AvN at pilEAUte WRRF

Several modifications were made on the pilEAUte WRRF to be able to apply the AvN control strategies (the normal operational conditions of the pilEAUte WRRF were presented in Chapter 3.1). For this purpose, the active bioreactor volume of the two biological reactors (pilot and co-pilot) were reduced by installing a by-pass of the two first basins. The 3rd basin was converted into an anoxic basin and the 4th and 5th basins remained aerobic basins (Figure 6.1). As such, the influent wastewater is by-passed directly to the 3rd basin and is fed to the system with an hourly varying or a constant flowrate. Also, the internal recycling from basin 5 to 1 was stopped, thus NO$_3$-N was not recycled for denitrification. The 3rd basin was anoxic and the 4th and 5th basins were aerobic during the AvN Project. Thus, in continuous AvN, it is expected to remove the NO$_3$-N only in basin 3 through denitrification, but SND is also expected in the aerated basins (basins 4 & 5) under low DO operation. For the intermittent aeration AvN, denitrification can occur during the non-aerated periods. The fraction of aerated basins to the overall reactor volume is 74% which is used to determine the aerobic sludge retention time.
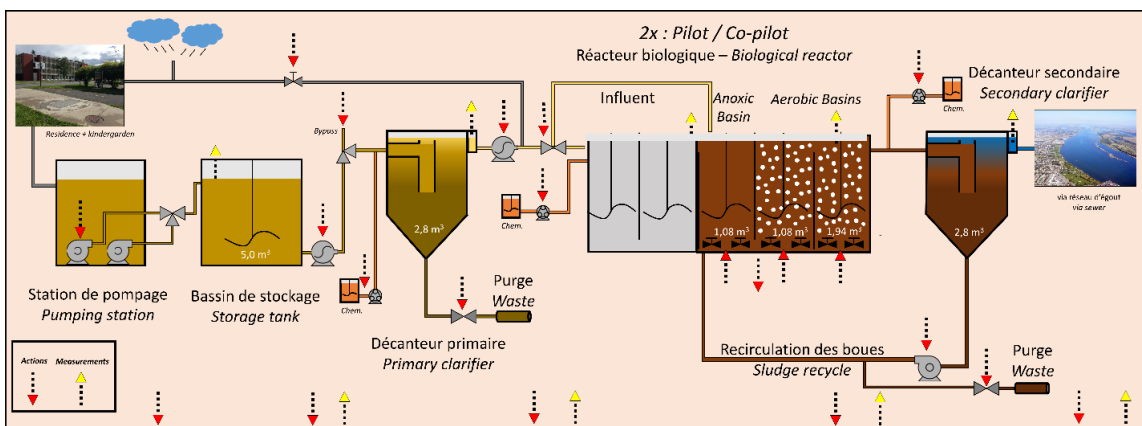
Figure 6.1 pilEAUte WRRF AvN Project Configuration

To achieve the objectives of this project, new piping was installed for the sludge recycle. The new pipe is an addition to the existing recycle line that transfers the sludge to the 3rd basin. It is activated by regulating the valve

manually (Figure 6.2). In addition to that, the baffle height between the 4th and 5th basins was increased to prevent any possible backflow due to changes in air flowrate in the aerobic basins (Figure 6.3).
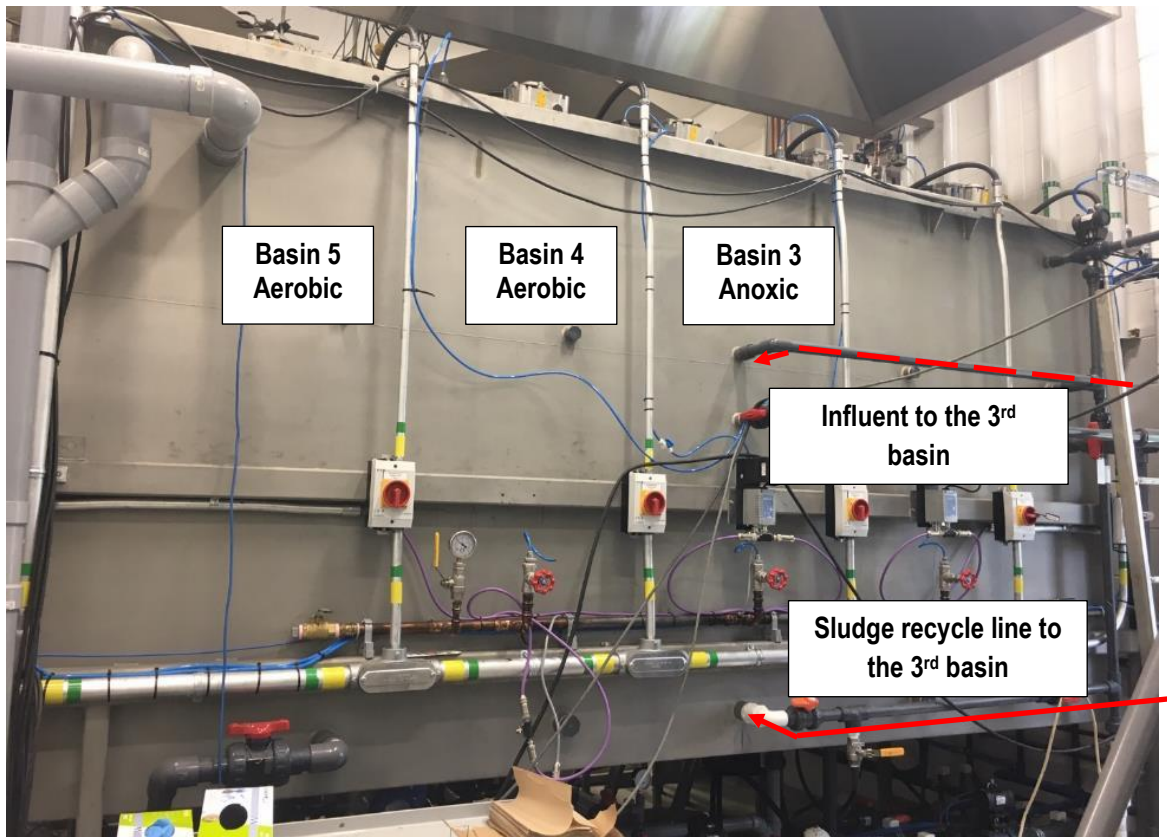
Figure 6.2 The Influent Feeding and the Installed Sludge Recycle Line

Figure 6.3 The Increased Baffle Height and Flow from 4th to 5th Basin

6.2 Implementation of the AvN Controllers and Experimental Work

The project started with the implementation of the necessary modifications to the pil*EAU*te WRRF as well as the operational changes required to operate under AvN conditions. The experimental work and controller activation started in April 2019. The project time line can be seen in Figure 6.4.
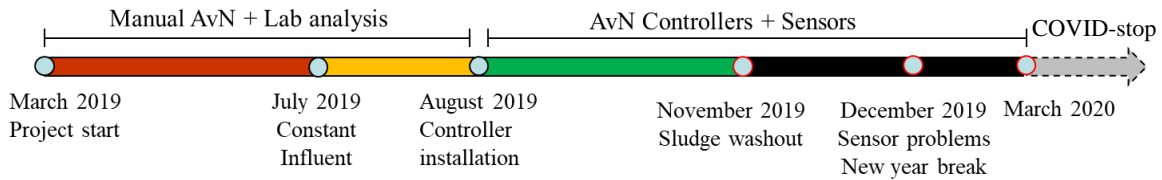
Figure 6.4 AvN Project Timeline

During the first phase of the project, AvN control was imposed manually (until August 2019). For continuous AvN, different low DO set-points were adjusted manually; for intermittent AvN, different cycle times and aerobic fractions were applied manually. Initially, both systems were fed with hourly dynamic influent based on the detailed influent monitoring study of pilEAUte (Li et al. 2019) (Figure 6.5). However, due to the challenges this dynamic operation causes to interpret the results, the system was fed with constant influent flowrate with 0.5 m^3/h (12 m^3/d) starting July 2019.
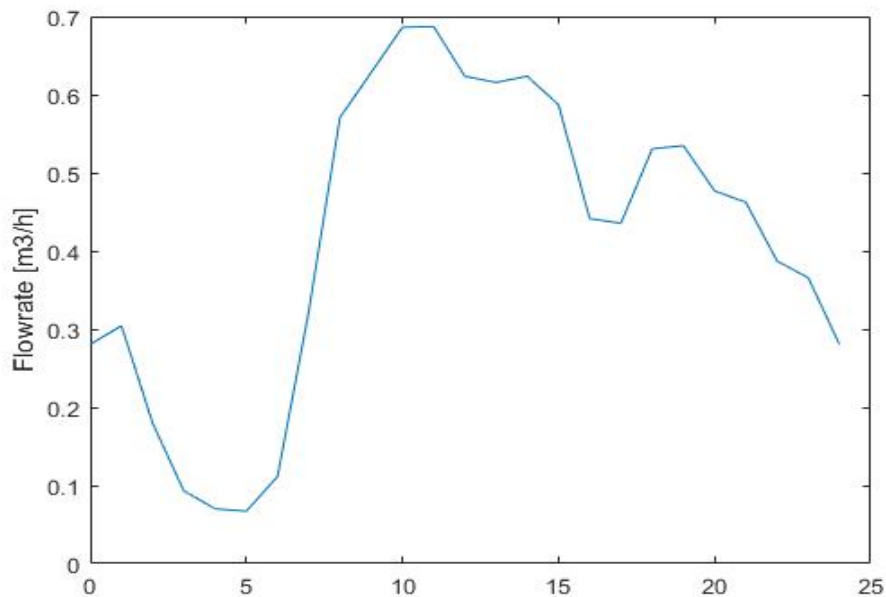
Figure 6.5 Hourly Dynamic Influent Flowrate Applied

A measurement campaign was carried out during the time of manual AvN operation based on composite samples. Table 6.1 shows the locations and parameters that were analysed in the lab.

Table 6.1 Lab Analyses Locations and Measured Parameters during Manual AvN Control

Influent	Effluent
Total suspended solids (TSS)	Total suspended solids (TSS)
Total chemical oxygen demand (COD)	Total chemical oxygen demand (COD)
Soluble chemical oxygen demand (CODsol)	Soluble chemical oxygen demand (CODsol)
Total nitrogen (TN)	Total nitrogen (TN)
Soluble total nitrogen (TNsol)	Soluble total nitrogen (TNsol)
Ammonium nitrogen (NH$_4$-N)	Ammonium nitrogen (NH$_4$-N)
	Nitrate nitrogen (NO$_3$-N)
	Nitrite nitrogen (NO$_2$-N)

Given the large array of sensors installed on the pilEAUte WRRF, continuous monitoring of the plant is also possible, using the various online sensors given in Table 6.2. During the second phase of the project, the automatic AvN controllers were implemented in the pilEAUte WRRF SCADA system. Implementation of the continuous AvN controller was achieved in August 2019 whereas the intermittent AvN controller was implemented in September 2019. From that point onwards, both AvN control strategies could be applied as long as the online effluent sensors provided reliable measurements needed to calculate the AvN ratio.

Table 6.2 Online Monitoring Locations and Measured Parameters during Automatic AvN Control
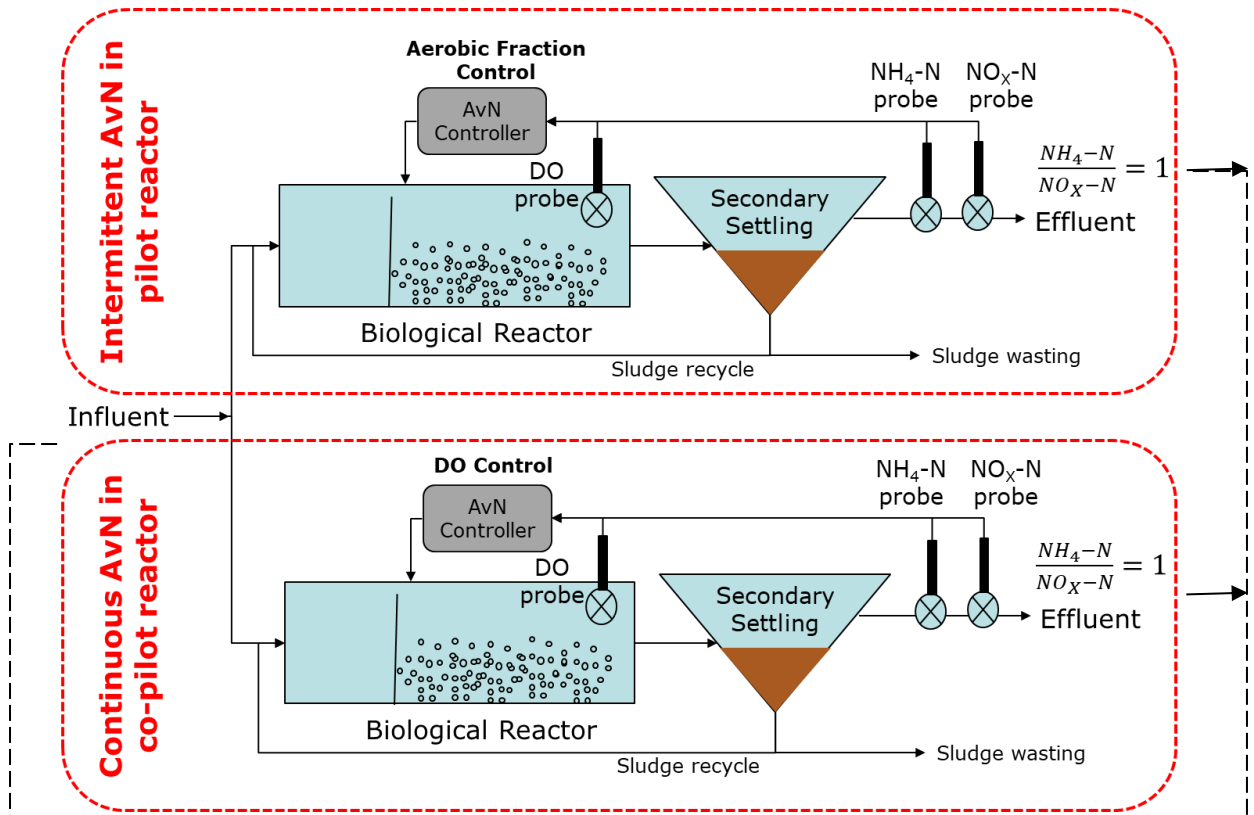
Influent	Biological Reactors	Effluent
Total suspended solids (spectro::lyser)	Total suspended solids (Solitax)	Ammonium nitrogen (Varion)
Total chemical oxygen demand (spectro::lyser)	Dissolved Oxygen (LDO)	Nitrate nitrogen (Varion)
Soluble chemical oxygen demand (spectro::lyser)	Ammonium nitrogen (TresCon)	Turbidity (Turbidity meter)
Ammonium nitrogen (ammo::lyser)	Nitrate + Nitrite (NOx-N) (TresCon)	pH (Varion)
Nitrate nitrogen (spectro::lyser)	Nitrite nitrogen (TresCon)	Temperature (Varion)
pH (ammo::lyser)		
Potassium (ammo::lyser)		

In November 2019, for both systems, the effluent NH$_4$-N concentration were observed to be too high for an extended period of time (concentrations nearly equal to the influent NH$_4$-N concentrations, ~30 mg/L). Based on multiple lab measurements performed at different times of the day, it was concluded that the nitrifiers were not working properly and might have been washed out of the system. The reason for this washout might be related to a brief change of operations because of a tracer test conducted on the primary clarifier by the pil*EAU*te team.

When the test finished, the sludge wasting of the primary clarifier was not returned to its ON position. Hence, the sludge blanket level and suspended solids concentrations increased in the primary clarifier which might have led to septic conditions with the production of sulfide which is known to inhibit nitrification. Sludge wasting from the primary clarifier was re-started immediately after realizing this (approximately 5 days later). To recover the nitrifiers, secondary sludge wasting was paused to increase sludge retention time. AvN controllers were stopped and the aeration in both reactors was switched to continuous aeration at a high DO of 2.0 mg/L. The system was kept at these operational conditions during December 2019 and January 2020 new-year's break.

Note that the system continued to be operated with manual AvN control due to effluent sensor problems (Varion) used to calculate the AvN ratio. After many calibration attempts and regular maintenance of the sensor, it was concluded that it was not possible to accurately monitor the effluent NH_4-N and NO_3-N concentration.

Finally, in March 2020 the pil*EAU*te WRRF had to be shut down due to a lack of influent wastewater produced at the university campus due to the application of COVID-19 confinement measures.

6.3   Manual AvN Control

This section includes the general outcomes when AvN control was applied manually to both treatment trains. Note that continuous and intermittent DO control is performed in the last aerobic basin (basin 5) of each system. Based on the DO control in basin 5, the same air flowrate was applied in basin 4 as in 5 $\left({k_{La}basin\,5}/{k_{La}\,basin\,4} \right.$=1 and this ratio is adjustable). However, in some periods of the manual AvN control, the air flowrate capacity in basin 4 was not sufficient to reach the desired DO concentration.

Figure 6.6 shows the concentration dynamics for NH_4-N, COD_{total} and $COD_{soluble}$ respectively and Figure 6.7 shows the load ratio for NH_4-N to COD_{total} and $COD_{soluble}$. It can be seen that the concentrations are relatively stable whereas the dynamic influent flowrate applied leads to dynamic influent loads applied to the system.
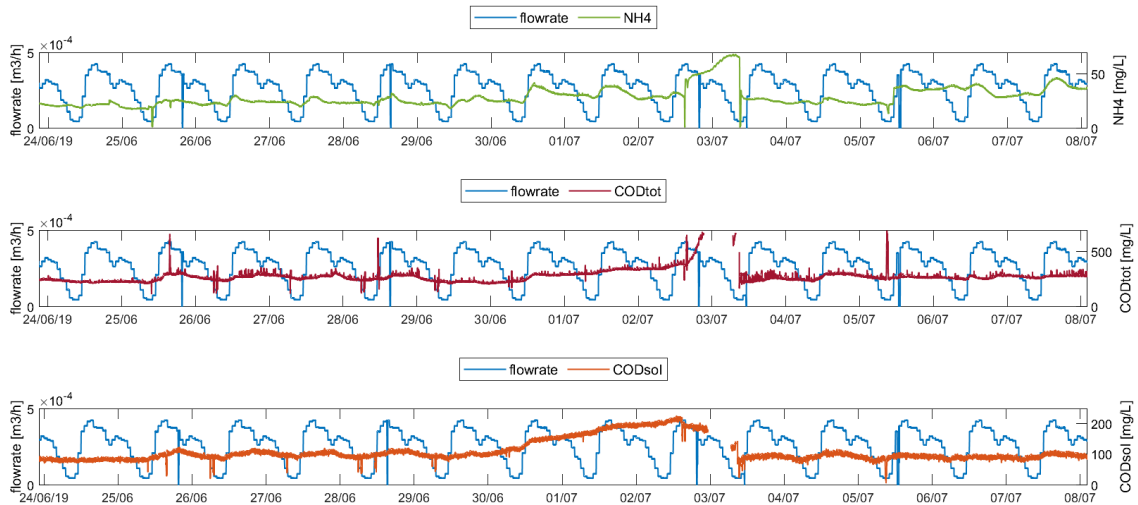
Figure 6.6 Influent Flowrate together with Concentrations of NH₄-N (top), COD_total (middle) and COD_soluble (bottom)
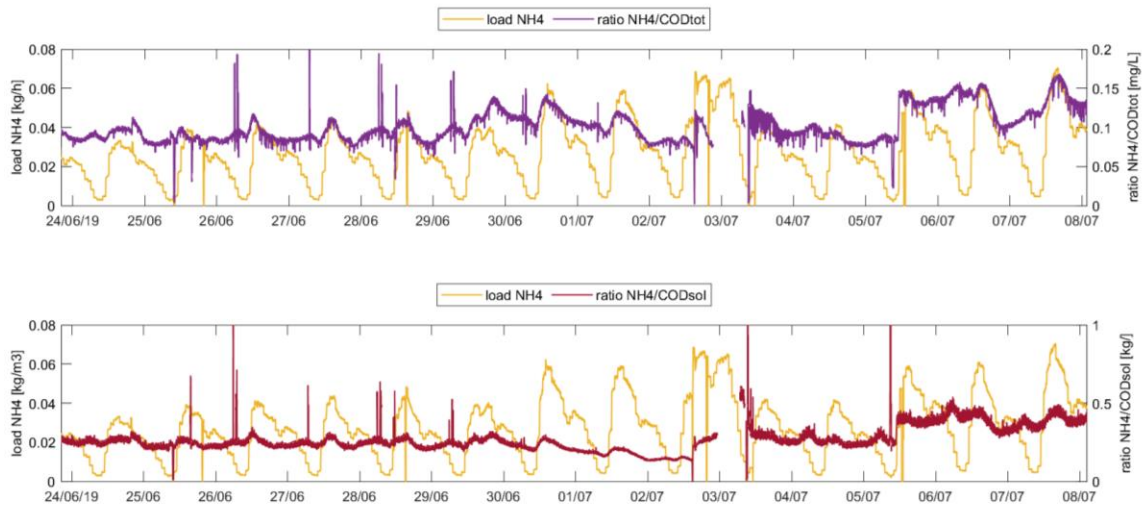
Figure 6.7 NH₄-N load and the Load Ratio for NH₄-N to COD_total (top) and COD_soluble (bottom)

The influent NH$_4$-N/COD$_{total}$ ratio is changing between 0.10 and 0.15 (Figure 6.7) which allows nitrifier growth in the system (COD$_{total}$/ NH$_4$-N ~ 10-15). Also, the temperature in the biological reactors is changing between 18 and 25°C which should not impact nitrifiers negatively (Figure 6.8).
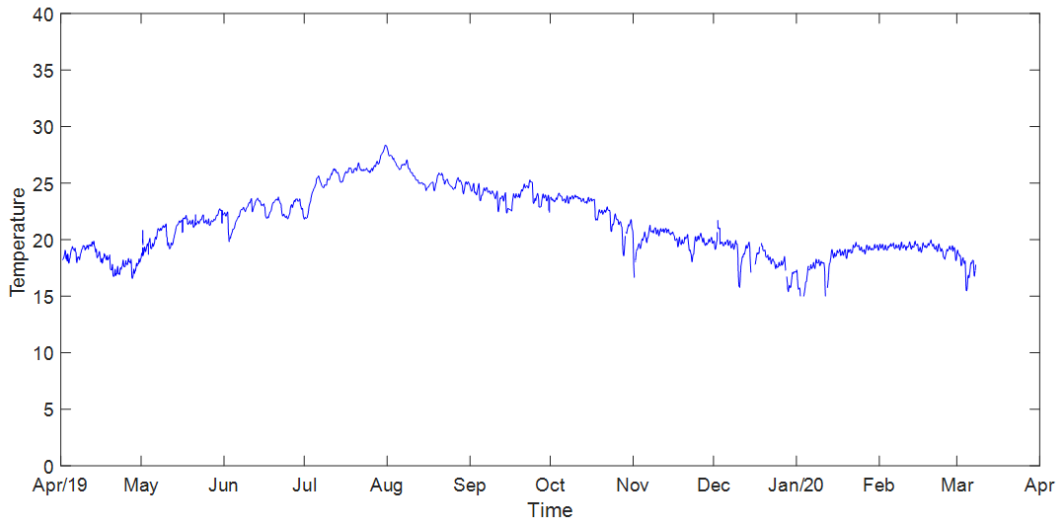
Figure 6.8 Temperature in Biological Reactors (°C) (March 2019-March 2020)

6.3.1 Application of Continuous AvN

6.3.1.1 Sludge Retention Time

The SRT in the continuous AvN system can be seen in Figure 6.9. The SRT calculation is performed based on the daily average TSS in the biological reactors, the recycle stream and the effluent. Between 18-28 June the SRT is around 5-6 days which is a result of higher sludge wasting in the system (0.35 m³/d). However, this led to a sharp decrease in the reactor TSS concentration and in the recycle stream. In order not to lose the sludge, the sludge wasting was reduced (0.25 m³/d) and the SRT was kept around 8-10 days (aerobic SRT 6-7.5 d). This was the optimum achievable SRT for this system during most of the project.
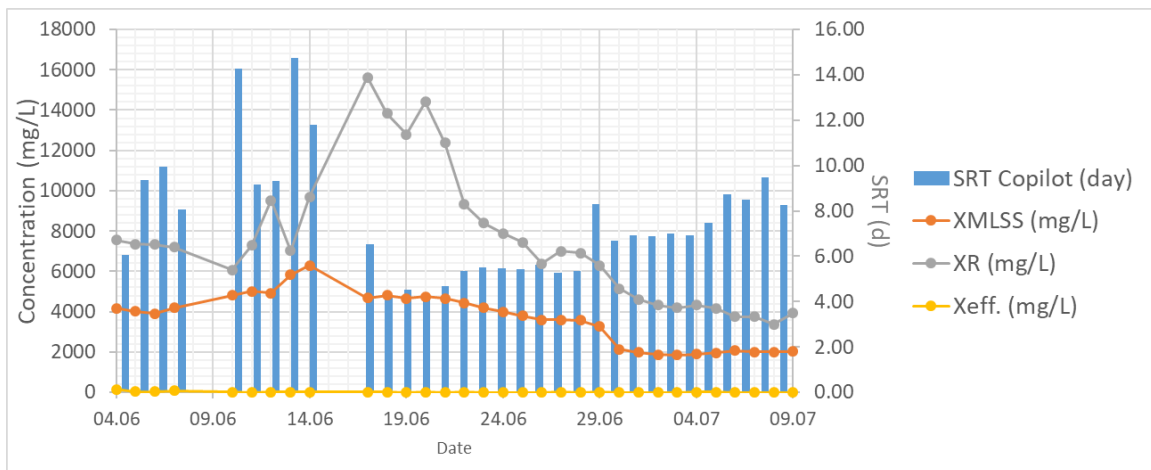
Figure 6.9 SRT in Continuous AvN System w/Manual AvN Control

6.3.1.2 Sludge Volume Index

A bulking sludge problem existed in the continuous AvN system, probably due to the operation of the system at low DO concentrations (Rossetti et al. 2005; Van den Akker et al. 2010; Nittami et al. 2019). The SSVI (stirred sludge volume index) measurements of the sludge are varying between 150-180 ml/g for the period shown in Figure 6.9. Figure 6.10 shows all SSVI measurement results during the manual AvN control of the continuous AvN system.

Figure 6.10 SSVI in Continuous AvN System with Manual AvN Control

6.3.1.3 Biological Reactor and Secondary Clarifier TSS Balance

It was observed that the dynamic influent led to the movement of sludge from the biological reactors to the secondary clarifier during daytime while the influent load is high (Figure 6.11). At night, the sludge came back to the biological reactors from the secondary clarifier as the influent loads were reduced due to the lower influent flowrates.
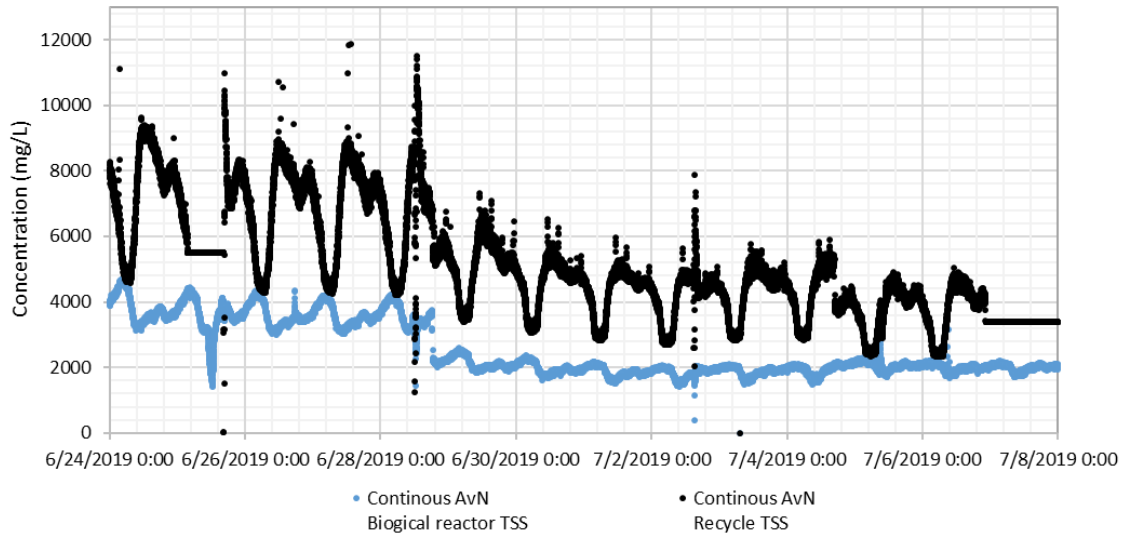
Figure 6.11. TSS Balance in the Continuous AVN Application

6.3.1.4 Application Results

Figure 6.12 shows the observed DO concentration in the aerated basins during the same period with manual AvN control and dynamic influent load. On June 29th, the DO set-point was reduced from 0.5 mg/L to 0.25 mg/L. As can been on Figure 6.12, the DO concentration in Basin 5 is maintained close to the set-point for most of the time. Even though the same air flowrate was applied to basin 4 as to basin 5, the DO concentration changes in Basin 4 depending on the influent load during the day and the DO set-point could not be achieved there. Note that the DO was controlled only in Basin 5 during this time period.

On June 30th and July 1st, unexpected peaks above the set-point were observed in the DO concentration and the air flowrate in both basins became minimum. This could be explained by the fact that there was no influent fed to the system during these periods due to an influent pump problem.

Starting from July 3rd, the ratio of the applied air flowrate between basins 5 and 4 was increased from 1 to 1.2 (thus decreased air flowrate in basin 4). In this way, it was expected to decrease the nitrification rate in basin 4 and improve AvN ratio at the effluent (Figure 6.13). This led a more stable DO concentration in basin 4, but it was still higher than the DO control set-point of 0.25.
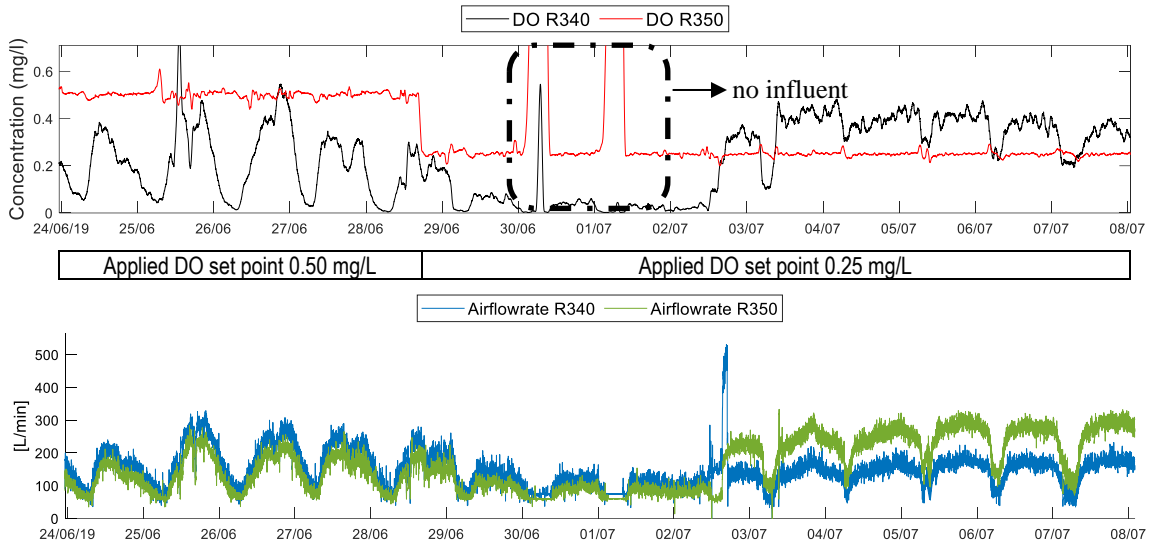
Figure 6.12 DO Concentration and Air Consumption in Aerated Basins (R350 is where DO Control Applied) – Dynamic Influent Load

Figure 6.13 shows the observed effluent NH₄-N and NO₃-N concentrations based on the lab analysis of composite samples collected during manual AvN application and dynamic influent load. It can be seen that NH₄-N could only be observed with the reduced DO set-point and increased $k_{La}basin\ 5/k_{La}\ basin\ 4$ ratio. Since the NH₄-N sensor in the effluent was not working properly in this period, it is not possible to see the dynamics of AvN ratio.
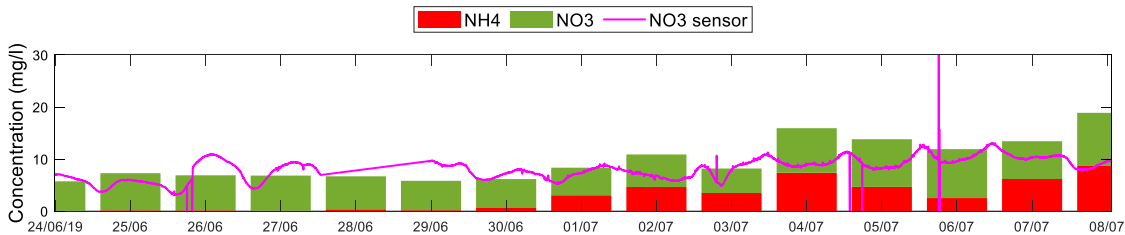
Figure 6.13 Lab Measurement Results at the Effluent (composite samples) and Available Sensor Measurements – Dynamic Influent Load

Changing the influent flowrate from time-varying to constant made the AvN control more stable and more reliable and easier to interpret. Figure 6.14 shows the observed DO concentration in the aerated basins during the manual AvN application and constant influent load. The $k_{La}basin\ 5/k_{La}\ basin\ 4$ ratio was applied as 1.5 in this period. As can be seen, the DO concentration in the aerated basins is much more stable and could be maintained

around the applied set-point, especially in Basin 4 where the DO is not controlled and only manipulated through the applied air flowrate.
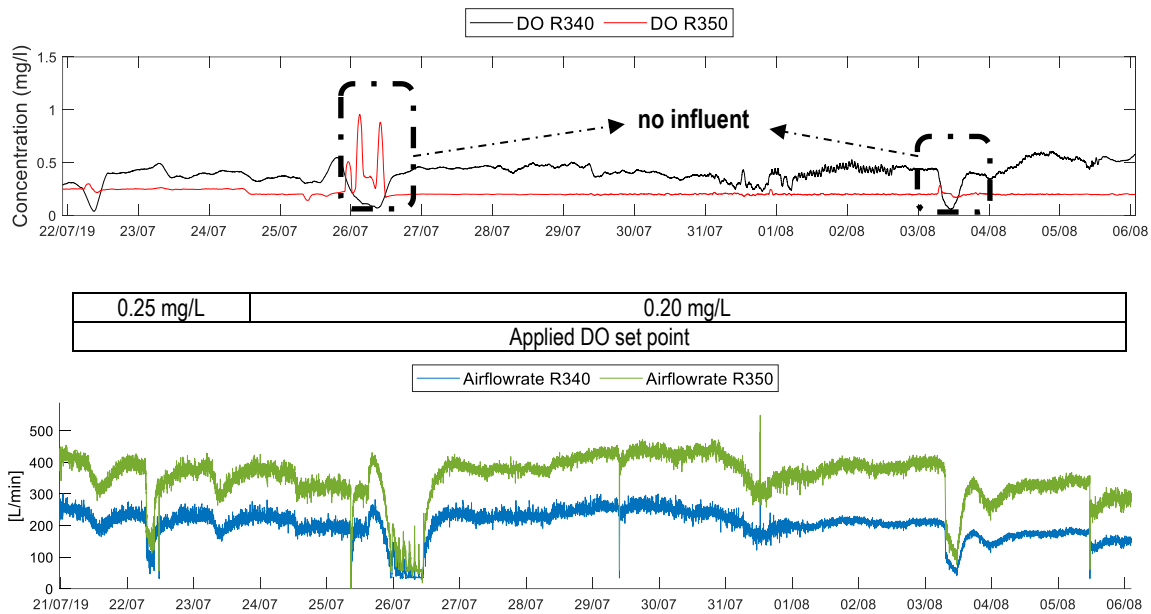
Figure 6.14 DO Concentration in Aerated Basins (R350 is where DO Control Applied) – Constant Influent Load

Figure 6.15 shows the observed effluent NH$_4$-N and NO$_3$-N concentrations based on the lab analysis of composite samples collected under manual AvN control and constant influent load. It can be seen that the AvN ratio calculated based on the sensor data is more stable than before (dynamic influent load). Still, because the system is operated with manual AvN control, a completely stable AvN ratio could not be achieved as desired.

Figure 6.15 Lab Measurement Results at the Effluent (Composite Samples) and Available Sensor Measurements and AvN ratio – Constant Influent Load

NH4 val and NO3 val correspond to the sensor validation data based on lab measurement.

6.3.2 Application of Intermittent AvN

6.3.2.1 Sludge Retention Time

The SRT in the intermittent AvN system is shown in Figure 6.16. Between June 18 and 28, the SRT is around 5-6 days which is the result of higher sludge wasting in the system (0.35 m^3/d). However, this led to a sharp decrease in the reactor TSS concentration and in the recycle stream. In order not to lose the sludge, the sludge wasting was reduced (0.25 m^3/d) and the SRT was kept around 8-10 days (aerobic SRT 6-7.5 d). This was the optimum achievable SRT of the system during the Project.
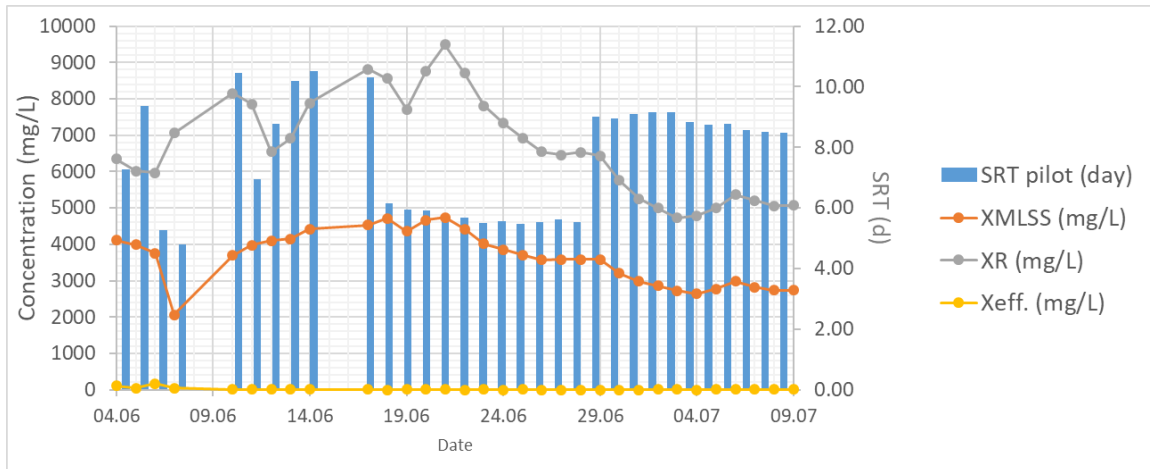
**Figure 6.16 SRT in Intermittent AvN System with Manual AvN Control**

6.3.2.2 Sludge Volume Index

As in the continuous system, bulking sludge was observed in the intermittent AvN system as well, probably due to the operation of the system with low DO concentrations. The SSVI measurements of the sludge are varying between 180-200 ml/g for the period shown in Figure 6.16. See Figure 6.17 for all the SSVI measurement results during the manual AvN control in the continuous AvN system.
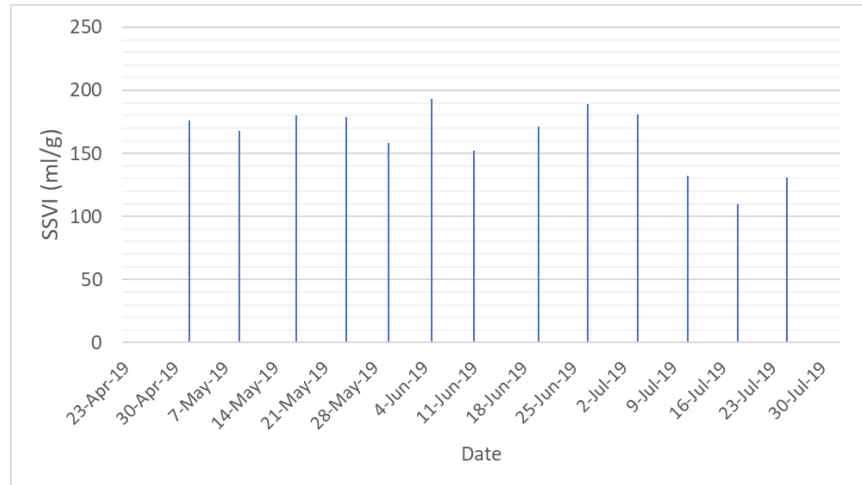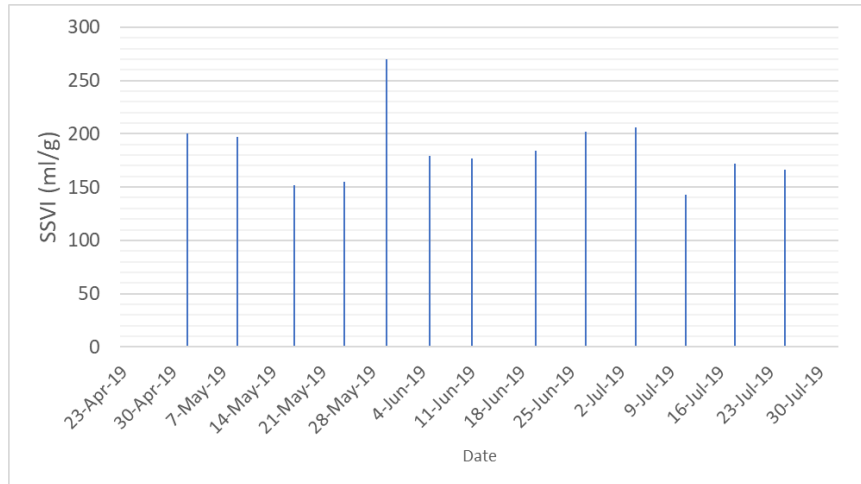
Figure 6.17 SSVI in Intermittent AvN System with Manual AvN Control

6.3.2.3 Biological Reactor and Secondary Clarifier TSS Balance

It should be noted that the dynamic influent led to the movement of sludge from the biological reactors to the secondary clarifier during daytime while the influent load is high (Figure 6.18) similar to the continuous AvN application (Figure 6.11).
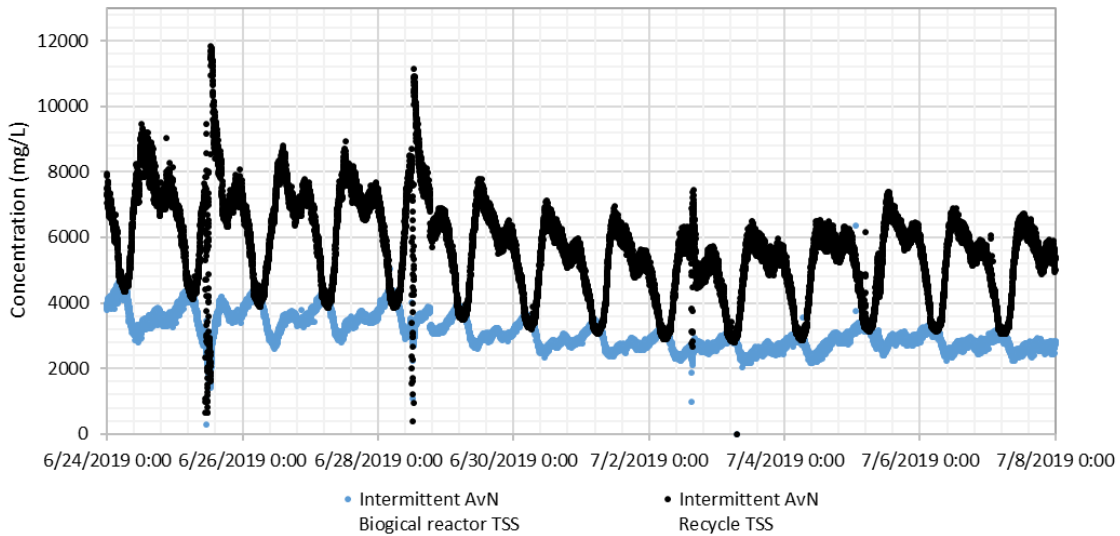
Figure 6.18 TSS Balance in the Intermittent AVN System

6.3.2.4 Application Results

Figure 6.19 shows the DO concentration in the aerated basins averaged over each cycle's aerobic fraction (AF) with the manual AvN application and dynamic influent load. The $k_{La}b\ asin\ 5/k_{La}\ basin\ 4$ ratio applied was 1 and DO control was done in basin 5. Different AF's were applied (with the same DO set-point in the aerated periods)

113

to see its effect on the observed average DO concentrations. As can be deduced from Figure 6.19, the average DO concentration that could be achieved in the aerated phases was similar and independent of the applied AF and cycle time. The desired 2.0 mg/L DO set-point for the aerated periods was however not achieved for the whole aerated period, hence the average value of DO concentration of only 1.2 mg/L. In the last 2 days of this period, there was a SCADA issue causing that the intermittent AvN not to be applied properly. The average of the air flowrate applied in each cycle is also given in Figure 6.19. In the first phase, when the AF was low, the applied air flowrate was not stable for both aerated basins. However, the overall applied average air flowrate looks the same for both basins.
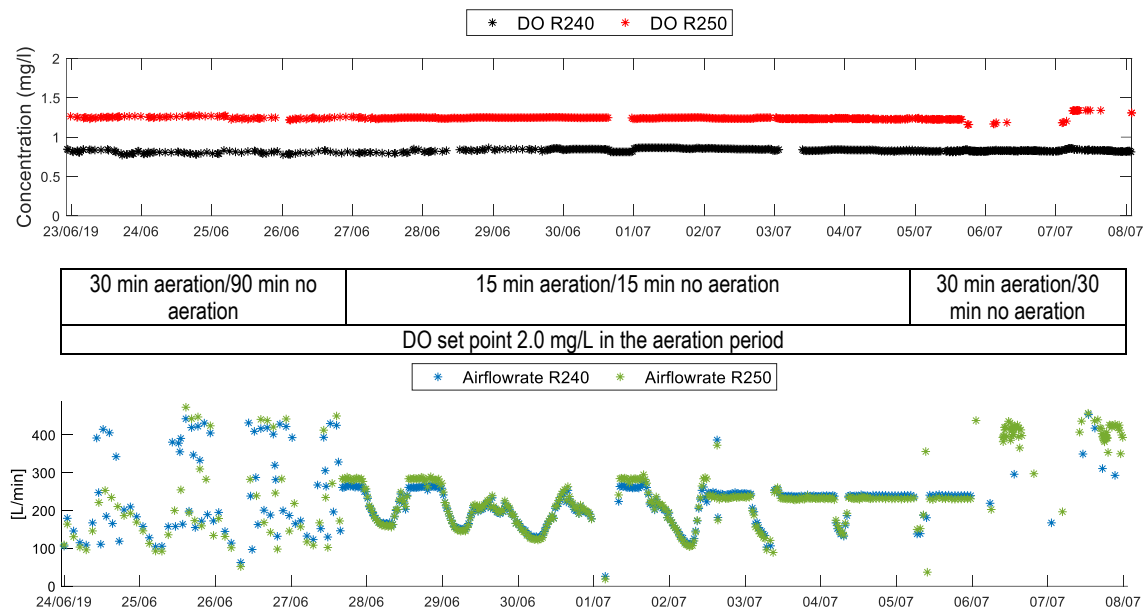
Figure 6.19 AF Averaged DO Concentration and Air Flowrate Applied in the Aerated Basins (R250 is where DO Control is Applied) – Dynamic Influent Load

Figure 6.20 shows the observed effluent NH_4-N and NO_3-N concentrations based on lab analysis of composite samples. In the beginning with 25% AF, NH_4-N is too low and the system is completely nitrifying, most probably due to the low influent loads. Later, 50% AF was applied in the system together with a reduced cycle time. There is no significant difference in the effluent concentration until the 2nd of July when the effluent NH_4-N starts to increase. The AvN ratio is calculated based on the available online monitoring data and varies between 0.1-1.5 during the day.

30 min aeration/90 min no aeration	15 min aeration/15 min no aeration	30 min aeration/30 min no aeration
DO set point 2.0 mg/L in the aeration period		
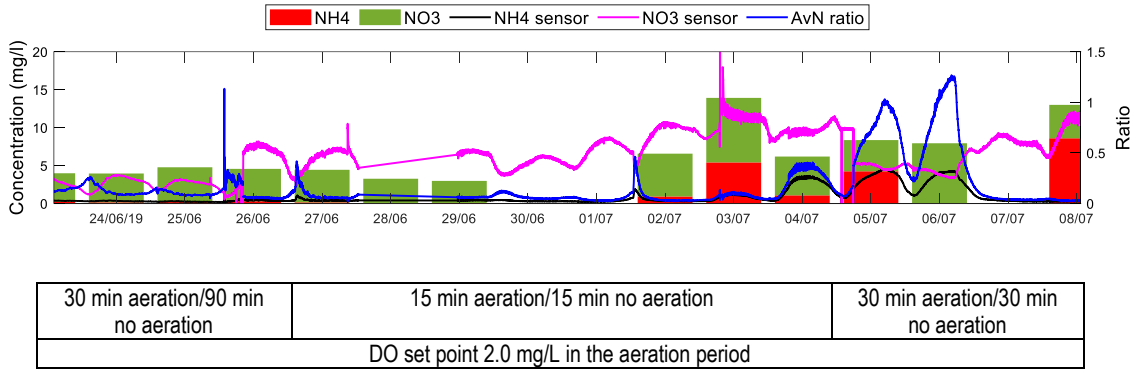
Figure 6.20. Lab Measurement Results at the Effluent (Composite Samples) and Available Sensor Measurements and AvN ratio

Figure 6.21 shows the observed average DO concentration and averaged air flowrate (for the aerated periods) during the manual AvN application but this time constant influent load for each cycle time. The $k_{La}b\ asin\ 5 / k_{La}\ basin\ 4$ ratio applied was 1.5 and DO control was done in basin 5. The constant influent did affect the DO concentrations. Again, it was not possible to achieve the desired DO setpoint of 2 mg/L in the aerated periods.

35 min aeration/25 min no aeration	40 min aeration/20 min no aeration	30 min aeration/30 min no aeration	32 min aeration/28 min no aeration
DO set point 2.0 mg/L in the aeration period			
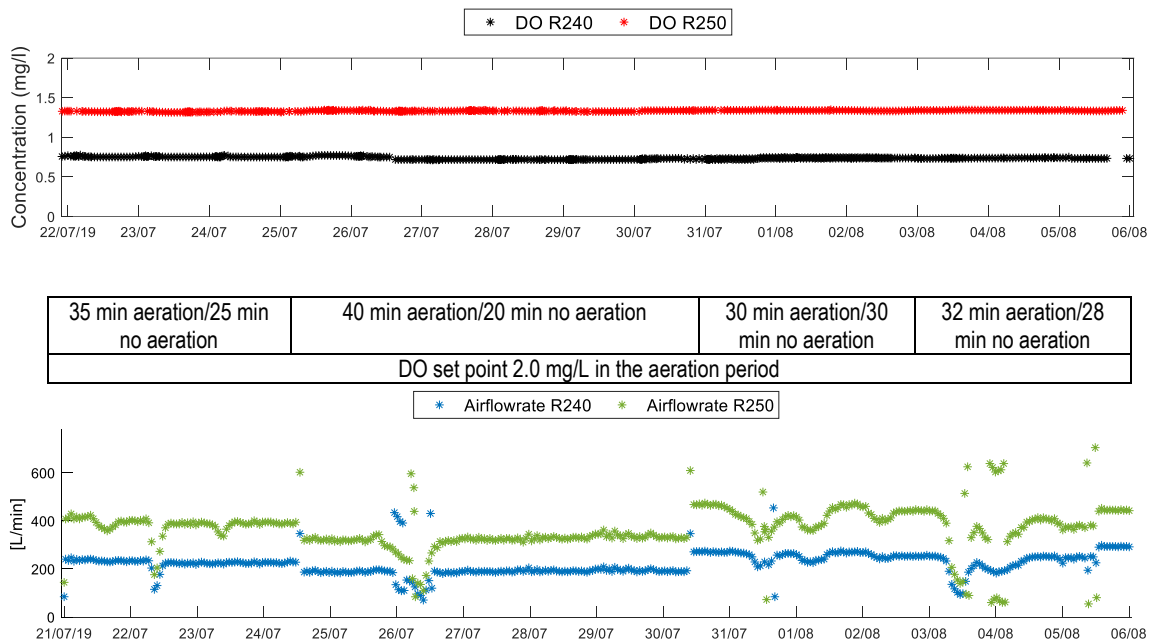
Figure 6.21 Average DO Concentration in Aerated Basins (R350 is where DO control is Applied) – Constant Influent Load

115

By changing the influent flowrate from time-varying to constant flow, the AvN control was made more stable and easier for intermittent AvN as can be seen in Figure 6.22. In the beginning of the period, the NH_4-N concentration is higher than the NO_3-N concentration, which leads to an AvN ratio > 1. To decrease the NH_4-N and increase the NO_3-N concentration, the AF was extended starting from 25th July. However, NH_4-N was still too high, probably because of the high influent loads. The NH_4-N concentration decreased around the 31st of July then the AF was reduced to bring the AvN ratio closer to 1.

Based on these observations, it can be stated that the system is responding according to expectations when changing the AF (i.e. higher AF results in more nitrification and reduced NH_4-N, while increasing NO_3-N). However, it is still not possible to achieve a stable AvN ratio of 1 in the effluent. This might be due to the imperfect tuning of the DO controller or due to the frequent problems with the sensors. Also, the system is operating with a manual AvN controller here, which definitely affects the stability of the N removal performance and effluent AvN ratio.
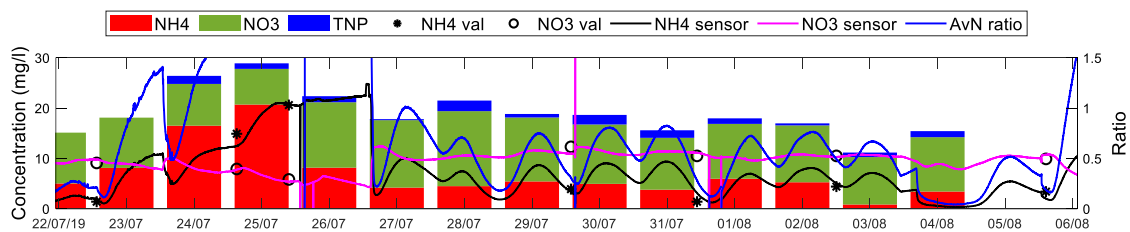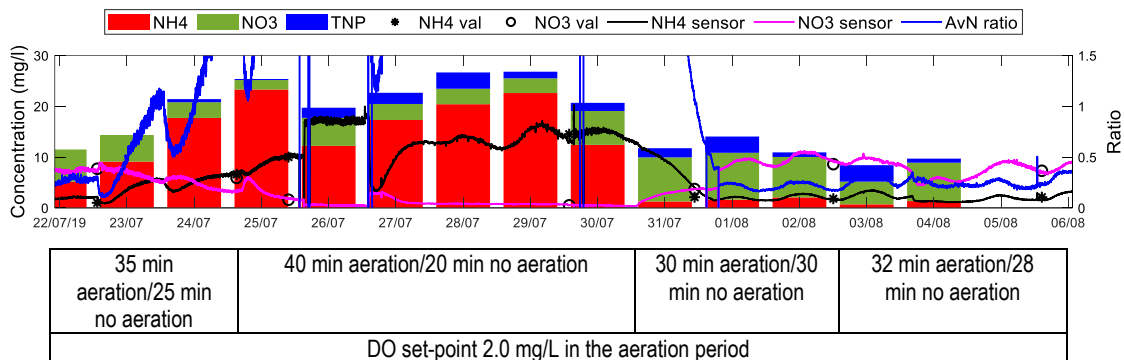

Figure 6.22 Lab Measurement Results at the Effluent (Composite Samples) and Available Sensor Measurements – Constant Influent Load

NH4 val and NO3 val correspond to the sensor validation data based on lab measurement.

6.3.3 Comparison of Continuous & Intermittent AvN Systems under Manual Control

6.3.3.1 Sludge Activity Comparison for AvN Control Strategies

A sludge activity test for both control strategies was performed while the system was operated with manual AvN. It aimed to determine the activity of ammonia-oxidizing bacteria (AOB) and nitrite-oxidizing bacteria (NOB) under non-limiting substrate conditions. As stated before, the objective of AvN controllers is to maintain an equal concentration of NH_4-N and NO_3-N (NO_x-N preferably) in the effluent for a downstream deammonification processes and this deammonification process requires equal amounts of NH_4-N and NO_2-N through partial nitrification and out-selection of NOB. The sludge activity test was used to determine whether the NOB out-selection could be achieved or not with the application of manual AvN control.

For the test, sludge samples were taken from continuous and intermittent AvN applied bioreactors and they were aerated until all the ammonia and nitrite were removed. Then, samples were taken to evaluate the initial conditions and measure ammonia and nitrite levels. Following that, a spiking solution was added (including a certain amount of ammonia, nitrite and bicarbonate) and samples were taken to measure the NH_4-N, NO_2-N and NO_3-N evolution with time and to calculate the maximum rate of AOB and NOB conversions. The trend of nitrite concentrations during the test (accumulation or decrement) is an indicator of the ratio of the AOB over NOB conversion rates. The test procedure was provided by DC Water and it was applied by using the RODTOX sensor (Kelma, Niel, Belgium).

Results for the sludge activity test are given for both the continuous and intermittent AvN system (Figure 6.23). According to the results, the activity of AOB and NOB are close to each other for both systems. This shows that, at this stage of the project, it was not possible to suppress the NOBs and increase the rate of AOBs above the one of NOBs through manual AvN, which would be desirable for a downstream anammox process.
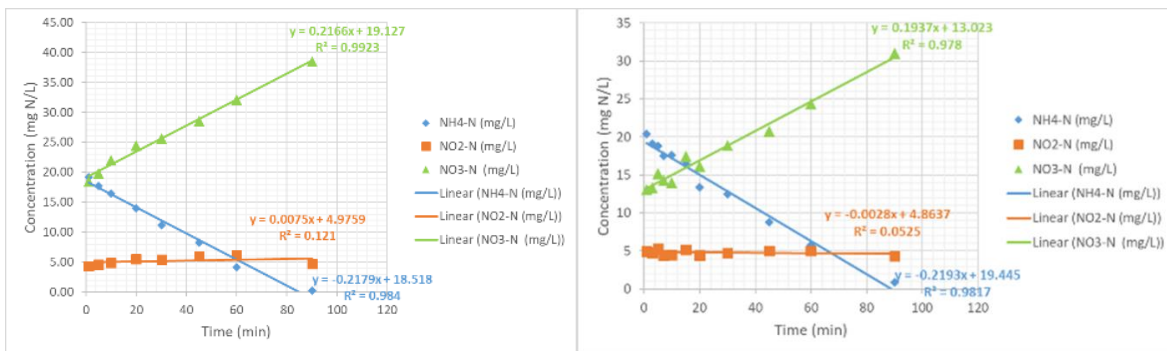
	Continuous AvN	Intermittent AvN
NOB rate	0.22 mg N/L/min	0.18 mg N/L/min
	169 mg N/g VSS/d	150 mg N/g VSS/d
AOB rate	0.25 mg N/L/min	0.24 mg N/L/min
	191 mg N/g VSS/d	200 mg N/g VSS/d

Figure 6.23 Comparison of AOB and NOB Conversion Rates for both AvN Control Strategies with Manual AvN Control

6.3.3.2 Performance Comparison of AvN Control Strategies

Manual AvN control was applied for both strategies while adapting the system into operation at low DO concentrations and to understand the system behaviour. It was possible to compare the N removal performance of both control strategies based on the influent and effluent N components. It is also important to consider the air consumption for both control strategies to interpret the results correctly. To do that and evaluate the TN removal and air flowrate consumption, the performance of both control strategies was evaluated in this section.

The evaluation was done separately for the time period with dynamic and constant influent loads and for different SRTs.

Figure 6.24 shows the TN removal comparison of continuous and intermittent AvN systems with the average DO concentrations achieved and average airflow rate consumptions in the system for lower SRTs. The evaluation is done for the SRT of 5-6 days in the time period 19-28 June 2019 (see the SRTs in Figure 6.9 & Figure 6.16). Based on that, intermittent AvN was shown to have a greater N removal performance than continuous AvN. However, on average, it also has a higher air flowrate applied.

	Influent TNT	Influent NH4-N	Effluent NO3-N	Effluent NO2-N	Effluent NH4-N	Effluent TN
Continuous AvN SRT 5-6 Days	29.92	21.25	6.66	0.02	0.15	12.71
Intermittent AvN SRT 5-6 Days	29.92	21.25	4.08	0.02	0.30	8.36
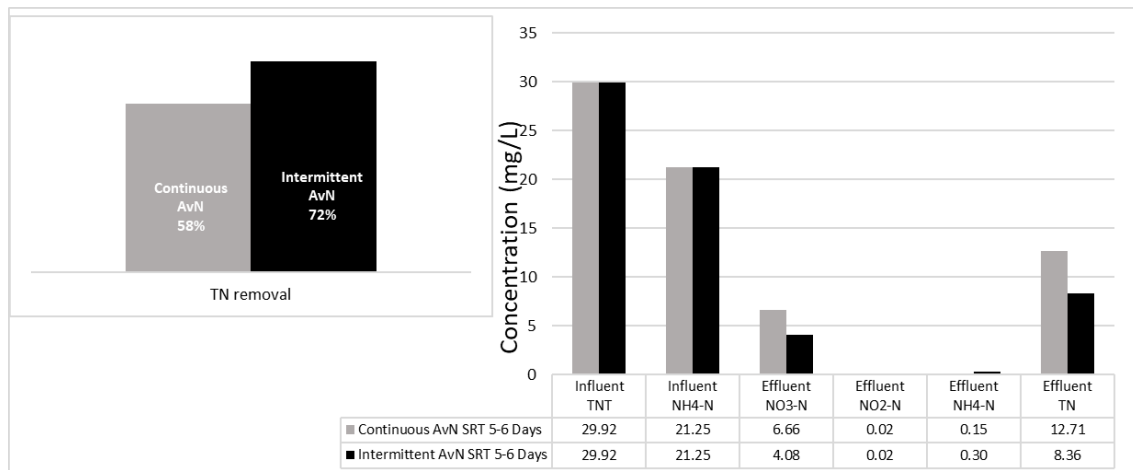
	Continuous AvN	Intermittent AvN
Average DO (mg/L)	0.5 (Figure 6.12)	1.25* (Figure 6.19)
Average airflow rate (L/min)	180	250**

*In aerated periods, **Average for each cycle - not only aerated periods*

Figure 6.24 N Removal Performance Comparison of both AvN Control Stratgeies with Lower SRT (Dynamic Influent)

Figure 6.25 shows the TN removal comparison of continuous and intermittent AvN systems with the average DO concentrations and air consumptions in the system at higher SRTs. The evaluation is done for the SRT of 8-10 days in the time period 29 June-9 July 2019 (see the SRTs on Figure 6.9 & Figure 6.16) with dynamic influent loads. Similar to the lower SRT period, intermittent AvN has a greater N removal performance than continuous AvN, however on average, it also has a higher air flowrate applied. Of course, higher SRTs mean lower sludge wasting which also affects the overall N removal and increases air consumption. For that reason, this project aimed to achieve N removal with as low as possible SRTs to maximize energy savings per gram of N removed.
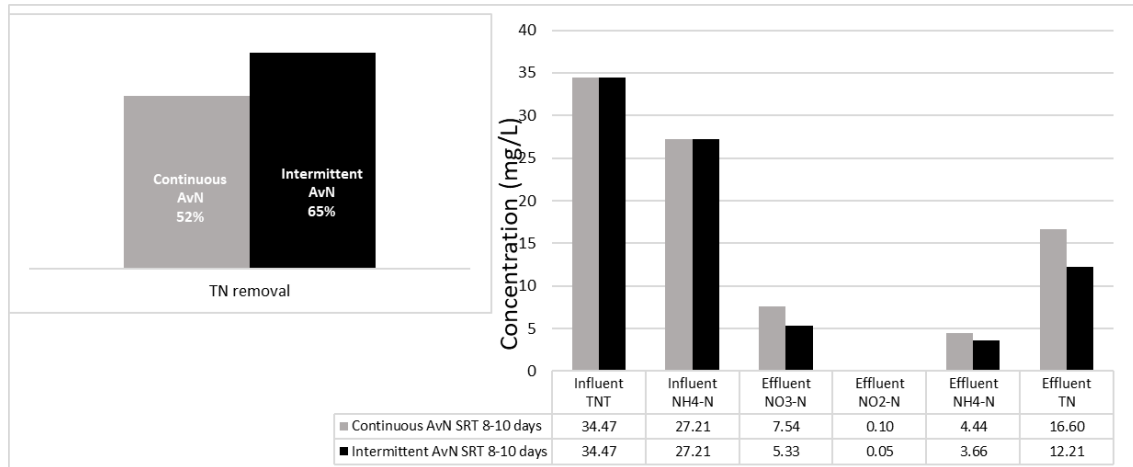
	Continuous AvN	Intermittent AvN
Average DO (mg/L)	0.25 (Figure 6.12)	1.25 mg/L* (Figure 6.19)
Average airflow rate (L/min)	210	250**

*In aerated periods, **Average for each cycle - not only aerated periods*

Figure 6.25 N Removal Performance Comparison of both AvN Control Strategies with Higher SRT (Dynamic Influent)

Figure 6.26 shows the comparison of both AvN systems with the average DO concentrations and average air consumptions in the system for higher SRTs (8-10 days for the time period 21 July-4 August 2019) but this time with constant influent loads. Interestingly, the removal performance of both systems is close to each other albeit with different averaged observed DO concentrations. However, in the same way, the applied air flowrates are relatively close for both systems.
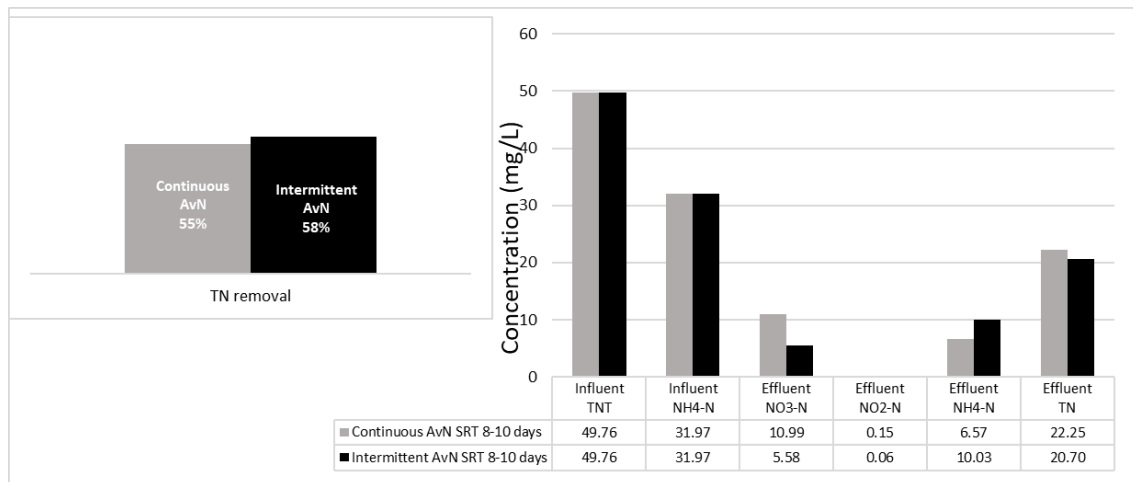
	Continuous AvN	Intermittent AvN
Average DO (mg/L)	0.20-0.25 mg/L (Figure 6.14)	1.3 mg/L* (Figure 6.21)
Average airflow rate (L/min)	370	400**

*In aerated periods,**Average for each cycle - not only aerated periods*

Figure 6.26 N Removal Performance Comparison of both AvN Control Strategies with Higher SRT (Constant Influent)

It can also be seen that the averaged effluent NH_4-N of the continuous AvN system is lower than that for intermittent one. This could be due to the better adaptation of the continuous system's biomass to operation at lower DO values than the intermittent system, thus allowing to maintain a better nitrification performance. The difference can also be due to the loss of nitrogen through floating sludge in the continuous system. When the continuous AvN (Figure 6.15) and the intermittent AvN (Figure 6.22) effluent concentrations are compared, it can be seen that the intermittent system effluent NH_4-N concentration was high even with increased AF. So, it could also simply be a lab measurement error in the intermittent system (however, the lab NH_4-N measurements and the sensor measurements are parallel to each other in Figure 6.22).

To compare the performance of both control strategies under dynamic and constant influent load, we evaluated the July 2019 data collected when the influent flowrate changed to constant was evaluated. Figure 6.27 shows the DO concentrations and the effluent N concentrations of the continuous AvN. At the beginning of the period, the system was operated with dynamic influent. In this period, the DO concentration in the aerobic basins is more unstable which affects the nitrification performance in the system and results in quite unstable AvN ratios during the day. When the influent loads become constant, the DO concentration in the aerated basins becomes more stable and the effluent AvN ratio gets closer to 1 and varies only in a narrow range.
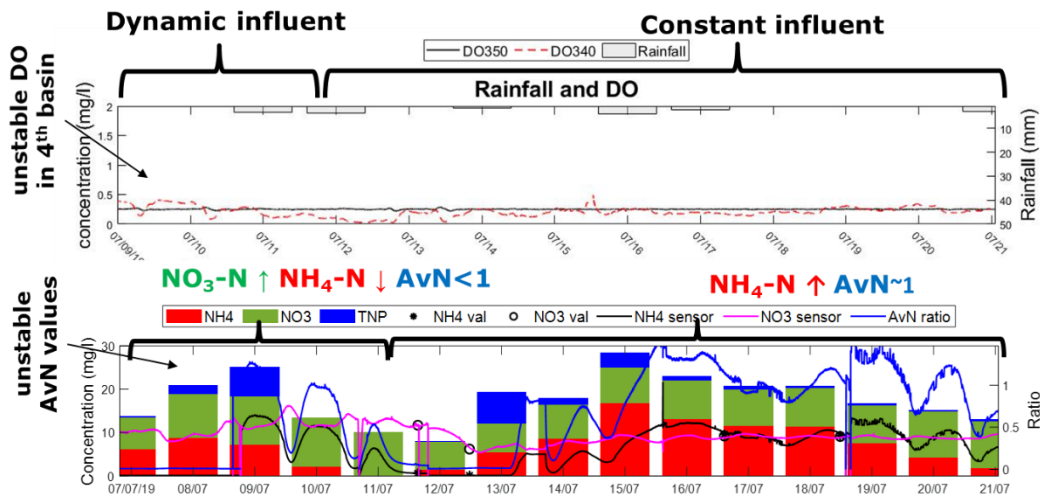
Figure 6.27 Continuous AvN Performance with Dynamic and Constant Influent Loads

A similar effect is found for the intermittent AvN (Figure 6.28). It is clear that the AvN ratio becomes much more stable with constant influent loads.
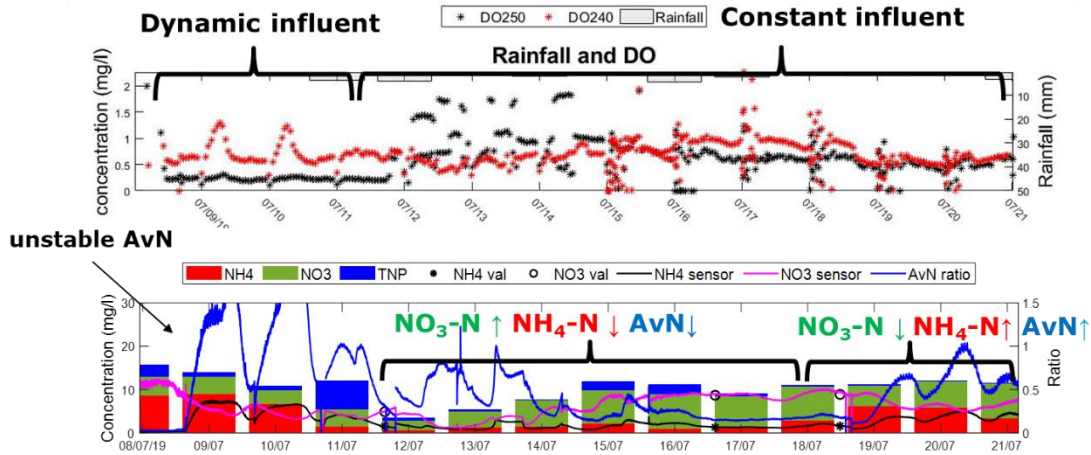
Figure 6.28 Intermittent AvN Performance with Dynamic and Constant Influent Loads

However, for both control strategies, the AvN ratio is varying during the day independent of the influent loads being dynamic or constant. The reason for this is of course the application of both control strategies through manual manipulation of the DO controller. As stated before, manual AvN control for both strategies was performed as works were underway to modify the SCADA system for automatic control. It allowed studying operation at low DO concentrations and understand the system behaviour under AvN control, but it is not effective in tackling dynamic changes.

6.4   Automatic AvN Control

This section includes the general outcomes of the project while the AvN controllers were applied automatically for both systems. Note that DO control is done in the last aerobic basin of each system (continuous and intermittent).

6.4.1 AvN Controller Algorithm and Implementation in pilEAUte WRRF

Both AvN control strategies rely on PID control. For continuous AvN the low DO set-point is the manipulated variable, whereas for intermittent AvN control the aeration fraction (AF) width is modulated (i.e. considering a fixed cycle time, the relative duration of the aerobic and anoxic periods is changed). The controlled variable in both cases is the difference between the NH_4-N and NO_3-N concentration, with a set-point value of 0 (i.e. AvN=1).

It should be noted that the controlled variable could also be defined as the ratio NH_4-N/NO_3-N, and a set-point value of 1. However, this option is not chosen as it leads to non-linear behaviour when calculating the control error. This is easily verified by considering a fixed value for the NH_4-N concentration and letting the NO_3-N concentration change. In case the difference is chosen as controlled variable, a positive and negative change of the same magnitude in the NO_3-N concentration will result in a similar change of the error. However, when

121

considering the ratio as the control variable, a positive and negative change of the same magnitude in the NO_3-N concentration will result in very different changes of the error. Hence, simple linear behaviour is therefore not guaranteed in the latter case. Controlling the ratio of NH_4-N/NO_3-N is, therefore, more complex as compared to controlling the difference between NH_4-N and NO_3-N. The control error is thus calculated as in Equation 6.1.

$$\text{Equation 6.1: } e = y_{sp} - y_m = 0 - ([NH_4] - [NO_3]) = [NO_3] - [NH_4]$$

Note that **Equation 6.1** will result in a reverse acting control law:

If $[NO_3$-N$] > [NH_4$-N$]$ then $e > 0$ then   decrease aeration

If $[NO_3$-N$] < [NH_4$-N$]$ then $e < 0$ then   increase aeration

Meaning that depending on the sign of the error the aeration needs to respond inversely. One way of taking this into account is by providing a negative sign to the control parameters. Often this leads to confusion. Therefore, the definition of the error is slightly modified to end up with a direct-acting control law as in Equation 6.2.

$$\text{Equation 6.2: } e = [NH_4] - [NO_3]$$

which has the property that the sign of the error is the same as that of the control action, and therefore it is easier to interpret.

The implementation of both AvN controllers in the SCADA system is visualized in Figure 6.29. The effluent data (for NH_4-N and NO_3-N) is stored in the datEAUbase which is the database of the pilEAUte WRRF. The script of AvN controllers queries the datEAUbase for the latest values of the measurements of interest (effluent NH_4-N and NO_3-N). Then, it filters the data using a rolling average and calculates the control action to be applied in the SCADA system.
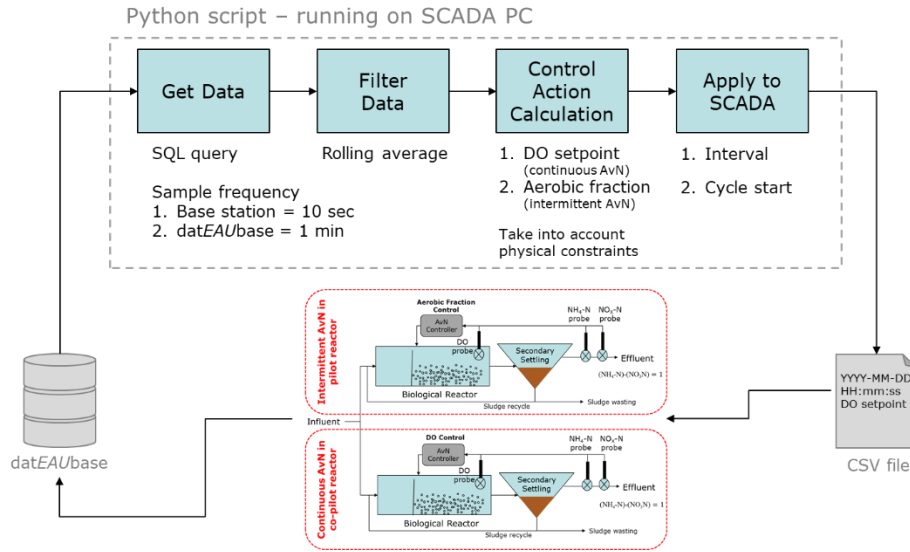
Figure 6.29 AvN Controller Algorithms in pilEAUte WRRF

Figure 6.30 provides a schematic of the software architecture used for supervisory control of the pilEAUte. The AvN control algorithm which is running on the SCADA computer outputs a CSV file containing the set-point for one of the low-level controllers of the pilEAUte. This set-point file is subsequently read by the SCADA software (i.e. FactoryTalk) which transfers the set-point to the PLC. The latter is in charge of the low-level process automation and ensures that the set-point value is achieved.
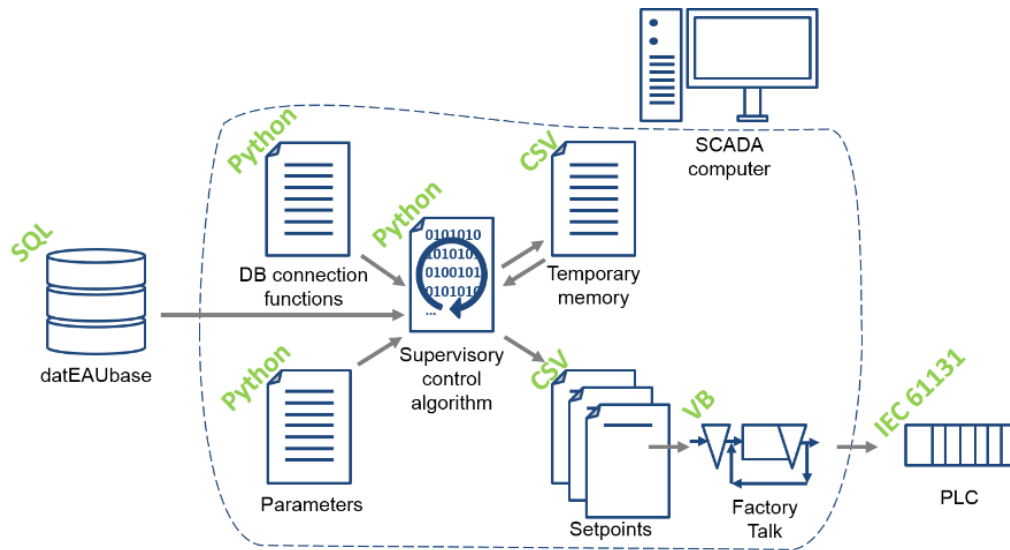
Figure 6.30. Schematic Overview of the Software Architecture behind the Supervisory Control of the pilEAUte WRRF with AvN Algorithms

6.4.2 Application of Automatic Continuous AvN

6.4.2.1 Sludge Retention Time

The SRT in the continuous AvN system is shown in Figure 6.31. The overall SRT was kept between 7-9 days generally (stated with the grey area). The sludge lost through floating (effluent TSS) was also considered in the SRT calculation. The temperature effect was considered to calculate the minimum SRT needed to prevent the washout of autotrophs (then the safety factor could be calculated based on the minimum SRT needed and the SRT calculated based on the sludge mass in the system). However, reactor temperature was not significantly affecting the minimum SRT as it was not changing a lot (See Figure 6.8 for the reactor temperature). Since the aerobic volume of the biological reactor is 74% of the overall volume, the aerobic SRT of the system was around 5-7 days.
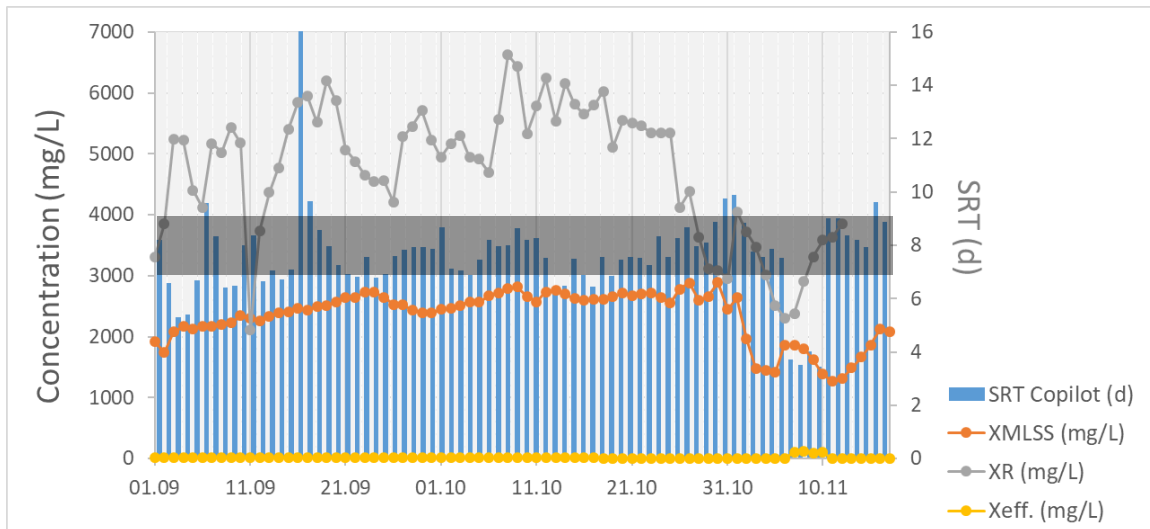
Figure 6.31. SRT in Continuous AvN System with Automatic AvN Control

SRT 7-9 days is stated with the grey area.

6.4.2.2 Sludge Volume Index

The SSVI (stirred sludge volume index) of the sludge is varying between 100-160 ml/g for the period that the continuous AvN control was running successfully (Figure 6.32).
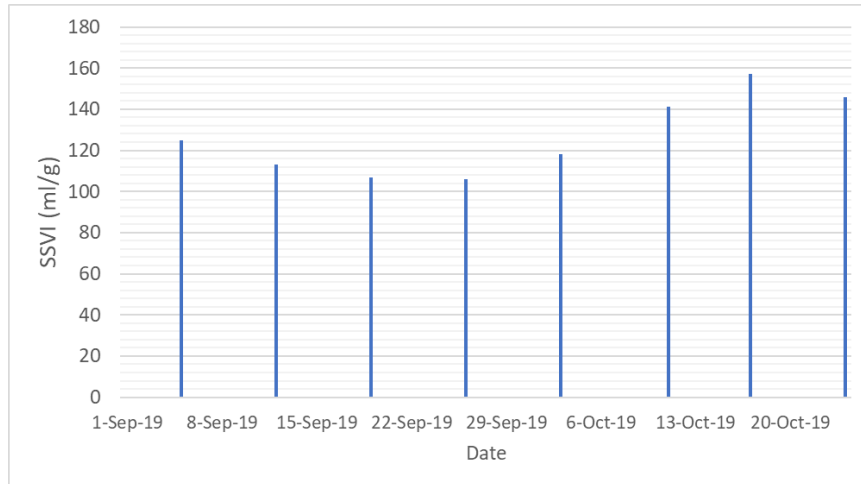
Figure 6.32. SSVI in Continuous AvN System with Automatic AvN Control

6.4.2.3 Application Results

Figure 6.33 shows an example of a 3 days period of continuous AvN application. It can be seen that the AvN controller is changing the DO set-point – and thus also the aeration intensity – to keep the AvN ratio around 1. It can be seen that when the influent NH_4-N concentration increased, the effluent NH_4-N concentration was increasing as well. As a response to that, the AvN controller is increasing the DO set-point and thus the aeration to increase NH_4-N oxidation and achieve the NH_4-N equals NO_3-N objective in the effluent. This demonstrates that the controller is correctly working, albeit a bit slow.

The results of the continuous AvN application are presented in more detail in Appendix- III.
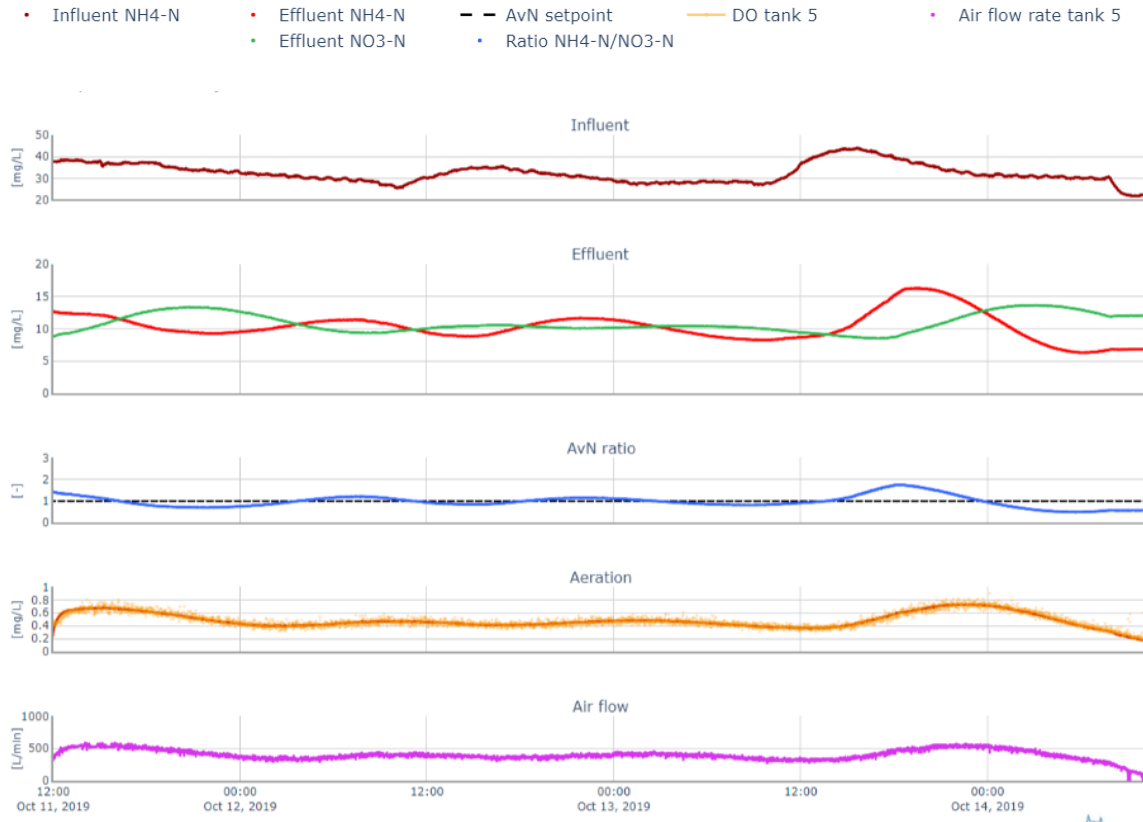
Figure 6.33. Continuous AvN Application Results over a 3 Day Time Period

6.4.3 Application of Intermittent AvN

6.4.3.1 Sludge Retention Time

The SRT in the intermittent AvN system can be seen in Figure 6.34. The overall SRT was kept between 9-11 days (stated with the grey area). The sludge lost through floating (effluent TSS) was also considered in the SRT calculation. Similar to the period with application of automatic continuous AvN, the reactor temperature was not significantly impacting the minimum SRT since it was not changing a lot. The aerobic SRT of the system was around 6.5-8 days.
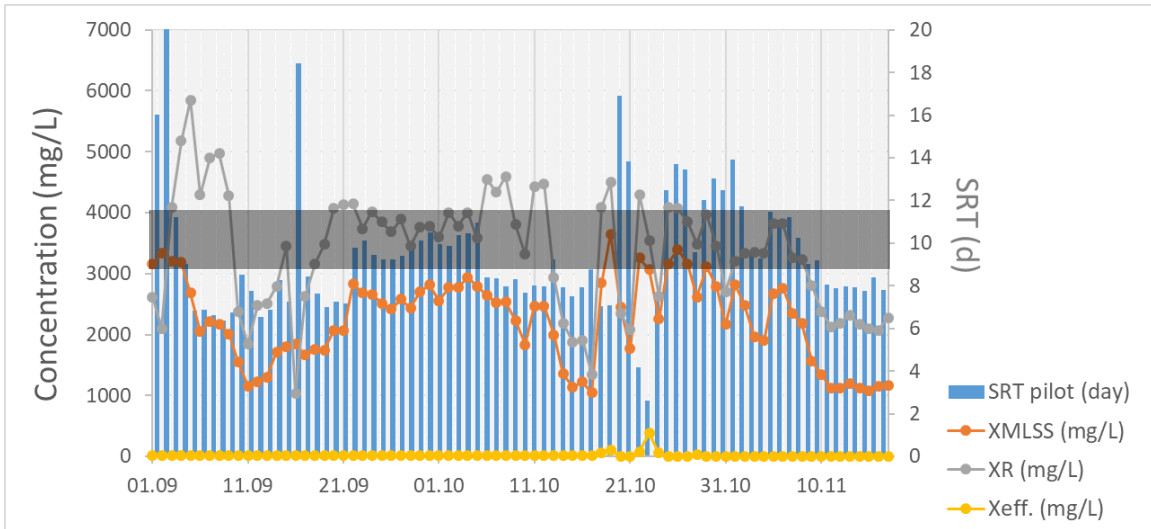
Figure 6.34. SRT in Intermittent AvN System with Automatic AvN Control

*SRT 9-11 days is stated with the grey area.

6.4.3.2 Sludge Volume Index

The SSVI (stirred sludge volume index) of the sludge is changing between 60-110 ml/g for the period that the intermittent AvN control was done successfully (Figure 6.35).
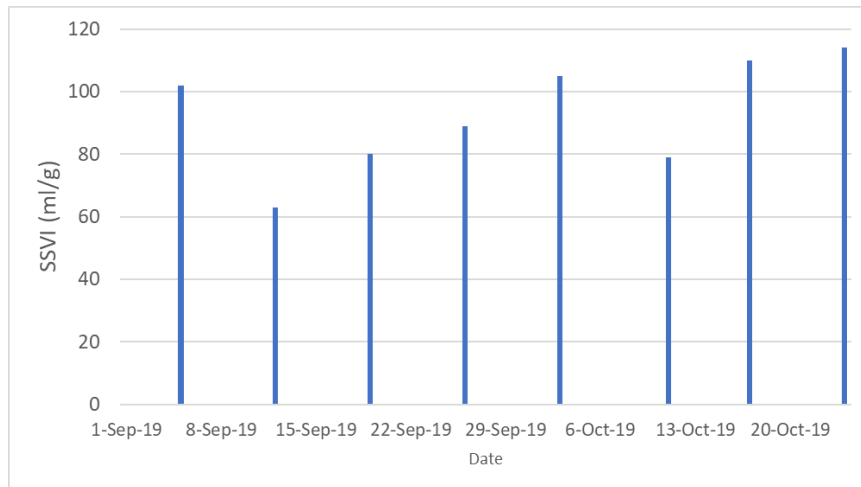
Figure 6.35. SSVI in Intermittent AvN System w/Automatic AvN Control

6.4.3.3 Application Results

Figure 6.36 shows an example of a 3-day time period of intermittent AvN application. It can be seen that the AvN controller is changing the AF applied in a cycle time – so the aeration amount – to keep the AvN ratio around 1. It can be seen that when the effluent NH_4-N concentration increased the AvN controller increased the AF

applied in a cycle time and thus the aeration to achieve the NH_4-N equal to NO_3-N objective in the effluent. The results of the intermittent AvN application are presented in more detail in Appendix- III.
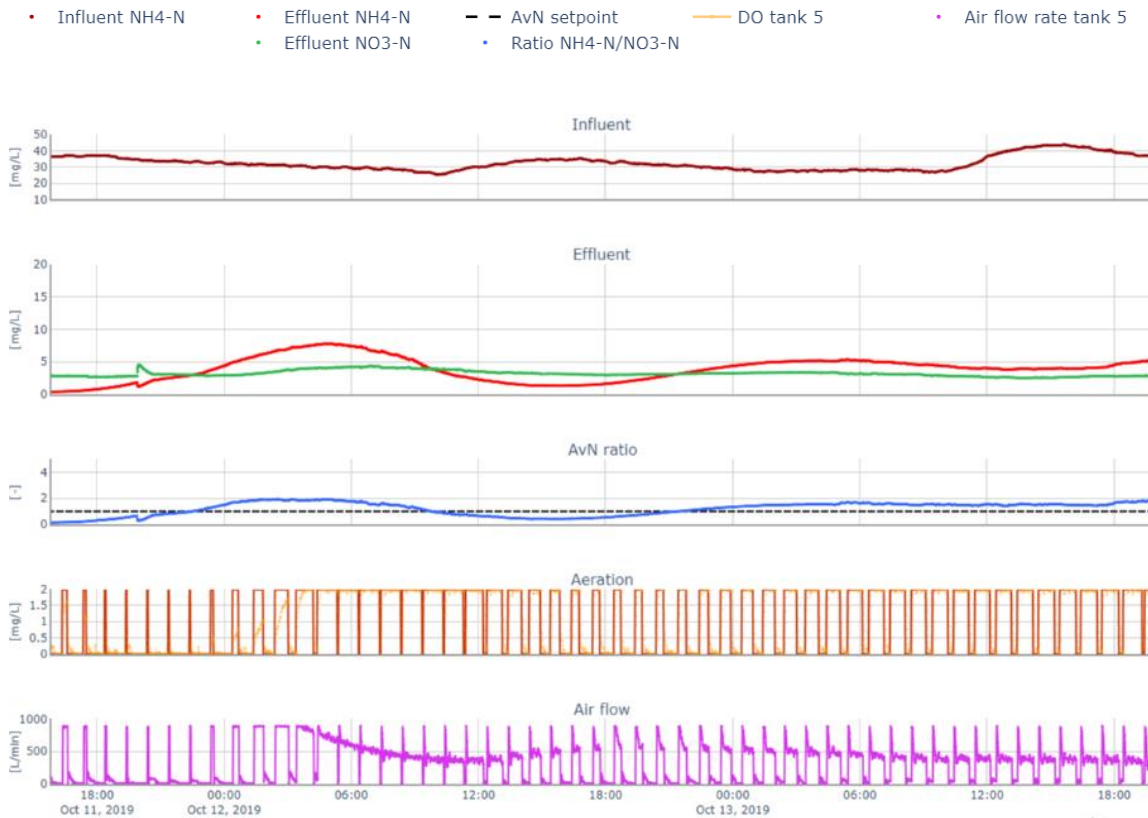
Figure 6.36. Intermittent AvN Application Results over a 3 Day Time Period

6.4.4 Comparison of Continuous & Intermittent AvN Control Strategies with Automatic Control

Continuous and intermittent AvN control were applied successfully in the pilEAUte WRRF starting from September 2019 until February 2020, as long as the sensors that measure the effluent nitrogen concentrations worked without any failure. In this section, both control strategies are compared based on a detailed measurement campaign for 24 hours (for the date October 30th 2019). The objective was to calculate the overall N removal performance in both systems and also the N removal in the aerated basins thanks to SND. The sampling points and measured parameters for both systems can be seen in Figure 6.37. It is assumed that the effluent concentrations are equal to those in the outlet of the aerobic basins. Based on the results of the 24-hour measurement campaign, a nitrogen mass balance of the system could be established based on daily average data.
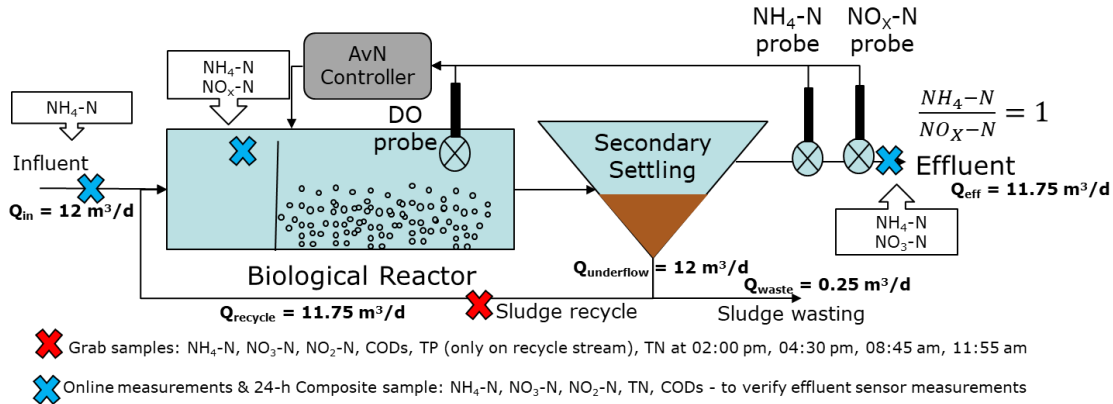
Figure 6.37. Measurement Campaign Sampling Points

- Overall TN removal in both control systems is calculated based on the influent and effluent TN concentrations and flowrates.

$$TN_{removal\_overall} = (Q_{influent} * TN_{influent}) - (Q_{effluent} * TN_{effluent})$$

- SND removals are calculated based on the total inorganic nitrogen (TIN) load difference at the outlet of the anoxic basin and the outlet of the aerobic basin.

$$N_{removal\_SND} = (Q_{influent} + Q_{sludge\_recycle}) * (TIN_{Basin3\_Outlet} - TIN_{Basin5\_Outlet})$$

- Removal in the secondary clarifiers (through denitrification) is calculated based on the TIN load difference between the outlet of the aerobic basin, effluent and, the sludge recycle stream.

$$N_{removal\_SST} = (Q_{influent} + Q_{sludge\_recycle}) * TIN_{Basin5\_Outlet} - (Q_{effluent} * TN_{effluent}) - (Q_{sludge\_recycle} * TN_{effluent})$$

- Removal in the anoxic basins through denitrification is calculated based on the TIN load difference by considering the influent and underflow loads together and subtracting the outlet of the anoxic basin load.

$$N_{removal\_anoxic} = Q_{sludge\_recycle} * (NO_3\text{-}N_{sludge\_recycle} + NO_2\text{-}N_{sludge\_recycle}) - (Q_{influent} + Q_{sludge\_recycle}) * (NO_3\text{-}N_{Basin3\_Outlet} + NO_2\text{-}N_{Basin3\_Outlet})$$

- Finally, the difference between overall TN removal with the sum of TIN removal with SND, secondary clarifier and anoxic basin denitrification is assigned as the N removal through sludge wasting.

$$TN_{removal\_sludge\_wasting} = TN_{removal\_overall} - N_{removal\_SND} - N_{removal\_SST} - N_{removal\_anoxic}$$

Based on these mass balance calculations, N removal for both control strategies is given in Table 6.3.

Table 6.3. N Mass Balance Calculation Results (g/d)

	Continuous AvN	Intermittent AvN
TN load	**454.3**	**454.3**
Removal in the aerated basin through SND	**121.1**	**227.5**
Removal in the anoxic basin through denitrification	9.9	17.2
Removal in secondary clarifier through denitrification	20.6	13.8
Removal with sludge wasting	81.1	54.8
Overall N removal	**234.6**	**314.5**

Results shown in Table 6.3 are converted into percentages to interpret the removal efficiencies easier in Figure 6.38. In this figure, the overall N removal in both systems is shown in the top charts and, the details of the N removal processes are given in the bottom charts. Note that, SRTs for this measurement date were calculated as 9 and 12 days for the continuous and intermittent AvN systems respectively.
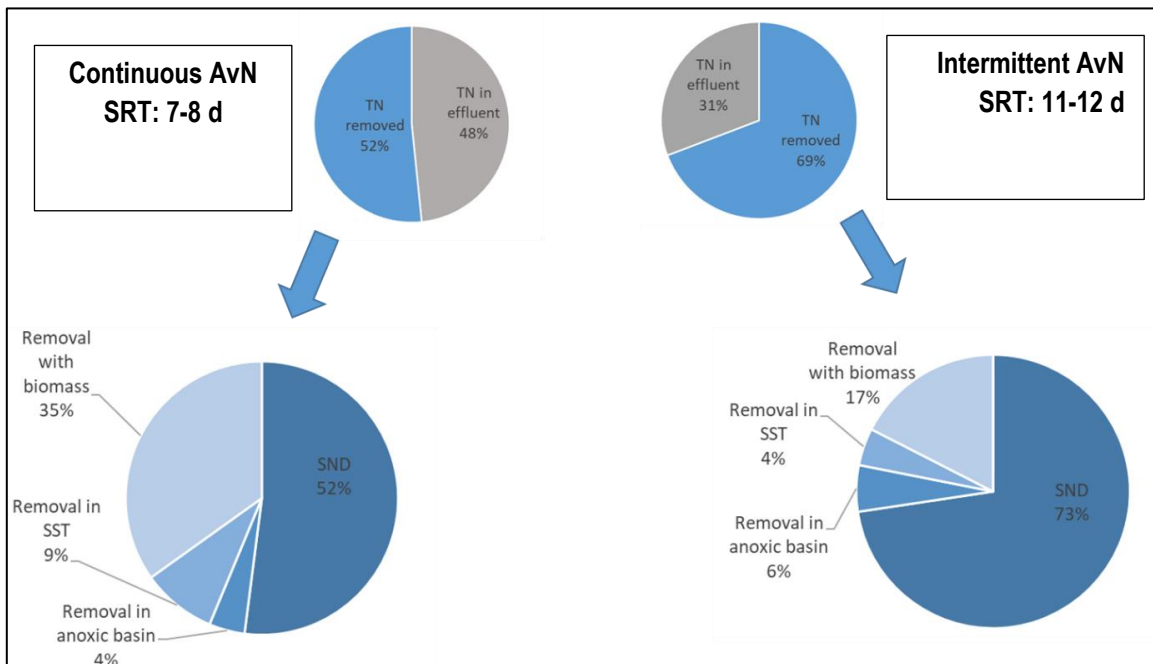
Figure 6.38. N Mass Balance Results for both Control Strategies

Based on the results in Table 6.3 and Figure 6.38, the overall N removal efficiency is found to be higher in the intermittent AvN system. With continuous AvN 52% of the TN in the influent is removed. Of this removed percentage, 52% could be achieved through SND in the aerated basins. With intermittent AvN 69% of the TN in the influent is removed. Of this removed percentage, 73% is achieved through SND in the aerated basins. So, overall, the SND performance is also higher in the intermittent AvN system. The removal in the SST and the anoxic basin are quite low for both systems, as expected (TIN concentrations in the sludge recycle system for

both systems were too low, around 2-3 mg/L). N removal due to sludge wasting (N incorporated in biomass) is higher in the continuous system, but this also expected since the calculated SRT of the continuous system is lower which indicates higher sludge production and thus more N incorporated in waste sludge.

On the other hand, the average airflow consumption is also evaluated (Table 6.4). Based on this evaluation, actually, the airflow consumption per gram of N removed in both systems is not significantly different, so the energy consumption for aeration is similar.

Table 6.4. Air consumption & N Removal Comparison for both Control Strategies

	Unit	**Continuous AvN**	**Intermittent AvN**
Volume	m^3	4.1	4.1
SRT	d	7-8	8-9
Average MLSS	g/m^3	2200	1750
TN removal	g/d	234.6	314.5
Air flow	m^3/d	311	405
Air consumption/g N removed	**m^3/g**	**1.33**	**1.29**

6.5   Conclusions & Perspectives

Based on the project results, it is found possible to achieve successfully AvN control for both continuous and intermittent control strategies. However, keeping the AvN ratio in the effluent at the desired value (1) highly depends on the operational conditions such as influent variations, SRT and sensors' measurement reliability. The general outcomes of the project in parallel to the project goals are given below.

6.5.1 Influent Characteristics

It was found that the dynamic influent flow leads to dynamic influent loads which make it harder to achieve AvN control. On the other hand, dynamic influent load could only be tested during the manual AvN application period which might be deceptive. Automatic AvN control could be achieved with stable influent loads, but could not be tested with dynamic influent load during the project time period. It is also known that influent NH_4-N/$COD_{soluble}$ is important for AvN systems. In this project, the influent NH_4-N/$COD_{soluble}$ was around 0.4 while the NH_4-N/COD_{total} ratio was varying between 0.10 to 0.15. Both were quite stable.

6.5.2 Sensor Reliability

The successful application of automatic AvN control heavily depends on sensor reliability. During this project, it was possible to achieve the AvN control successfully for both control strategies but it was only temporary because of the operational problems with the sensors. In case of drifts in the sensor signal or when a failure

occurs, the control action is not correct which affects the performance of both control strategies. The experience in this project is that ion-selective NH_4-N and NO_3-N sensors need a lot of maintenance and suffer from faults during operation. The reason could be that the ion-selective sensors operation heavily depends on the water matrix and they are recommended to be used at higher N concentrations. On the other hand, wet chemistry analysers (such as the TresCon system installed at the pilEAUte) are more reliable measurements for AvN systems. However, use of those sensors at the outlet of the pilot scale system could not be achieved during the project.

6.5.3 Sludge Retention Time

A successful AvN ratio of 1 at the effluent could be achieved for an aerobic SRT of 5-7 days for the continuous AvN and 6.5-8 days for the intermittent AvN. Higher sludge wasting to reduce the SRT in the pilEAUte WRRF resulted in a sharp decrease in the reactor TSS concentration and in the recycle stream, thus leading to unstable effluent nitrogen concentrations. Lower SRT values could not be applied in the AvN system during the project time. Also, the SRT of the continuous AvN system was always lower than the intermittent one.

6.5.4 Temperature

During the project, the operational temperature of the system was around 20ºC in the pilEAUte WRRF which was enough to successfully achieve AvN control around 1. However, full-scale WRRFs in the Quebec region would have a 10-15ºC operational temperature. Since the pilot plant is in a closed space with higher room temperatures, the impact of lower temperatures on the system performance could not be investigated.

6.5.5 Feedforward Control Necessity

In this study, the principle of a cascade feedback aeration control strategy was applied in the AvN controller. Another approach to maintain the desired AvN ratio would be through the use of what is called a feedforward control or a combination of feedback and feedforward control strategies. Instead of solely monitoring the ammonia concentration in the effluent, feedforward control relies directly on ammonia measurements in the influent. This way, sudden changes in influent load can be anticipated by the controller and thereby prevent the propagation of ammonia peaks to the effluent. Such an approach has been shown to be beneficial for plants that encounter unusually high influent disturbances (Rieger et al. 2014). The latter observation also holds for the pilEAUte treatment plant during the operation with dynamic influent flowrate. Since it depends entirely on the wastewater generated by a small university community, the ammonia load fluctuations arrive undamped in the pilEAUte system. Hence, large variations in ammonia loads are observed which could make a combination of feedforward and feedback AvN control more appropriate. Also, the influent COD needs to be considered for the feedforward control since the NH_4-N/COD ratio is important for system operation to oxidize only the amount of ammonia that can be denitrified by utilizing the carbon available to the system. On the downside, feedforward

control requires a mathematical understanding of how load disturbances influence aeration demands. In practice it might be hard to establish such relation due to unknown or complex process behaviours.

6.5.6 Energy Consumption

Based on the results of a short-term detailed measurement campaign during the project, the overall N removal efficiency and SND performance was higher in the intermittent AvN system than the continuous one. However, the average airflow consumption per removed gram of N in both systems were not significantly different, and were thus the energy consumption due to aeration. Still, application of the AvN controller to the pilEAUte WRRF resulted in a 36% total volume reduction and also a 50% SRT reduction which makes a significant gain in comparison to the conventional operation of the plant. If the airflow consumption of the AvN operation (with an average air flow consumption 400 m^3/d) and the conventional operation of the pilEAUte plant are compared, then more than 60% reduction is observed.

7. SCENARIO ANALYSES for ENERGY & RESOURCE OPTIMIZATION of N-REMOVING WRRF

This chapter of the PhD dissertation presents the results of scenario analyses on the pilEAUte model presented in Chapter 5 to optimize energy and resource consumption by aeration and pumping of sludge. For that purpose, grid scenario analyses were performed to determine the optimal operational conditions for the pilEAUte WRRF while ensuring effluent water quality.

7.1   pilEAUte Model – Conventional Nitrogen Removal

Scenario analyses were conducted on the calibrated pilEAUte model of Chapter 5. Three scenarios were investigated. As evaluation criteria total air consumption, aeration and pumping energy consumption, overall nitrogen removal efficiency and effluent quality (in terms of nitrogen components) were used. The model results for these criteria during the calibration and validation periods were taken as the reference case to compare the scenario analysis results with and to determine optimal operational conditions. Note that many N-removing WRRFs are not operated optimally due to the large safety margins applied during plant design, lack of process control or ensuring the effluent criteria under dynamic loading conditions (Fiter et al. 2004; Vanrolleghem and Vaneeckhaute 2014; Sweetapple et al. 2014). The results of these scenario analyses were evaluated/investigated as proof of a concept for energy and resource optimization for conventional nitrogen removal processes.

7.1.1 Evaluation Criteria for the Scenario Analyses Outputs

Key variables (which are calculated by the model as an output of each simulation) and the criteria to evaluate the scenario analyses are stated below. Average air flowrate consumption, aeration and pumping energy, TN load removed in the overall plant, including the reactive settler, and effluent nitrogen concentrations were calculated for the time period between day 24 and 59 for the reference case and each scenario analysis. Also, the average total sludge mass in the WRRF for the given time period was calculated and the sludge accumulation in the system is evaluated by considering the wasted sludge.

Operational Energy:

n: *Number of time steps*; t_i: *Start time of calibration-validation time period (Day 24)*; t_l: *End time of calibration-validation time period (Day 59); V: volume*

- Total average air consumption (m³/d):

$$Q_{air\ total} = \frac{\sum_{t_i}^{t_l}(Q_{air\ Basin\ 3_t} + Q_{air\ Basin\ 4_t} + Q_{air\ Basin\ 5_t})}{n_{t_l} - n_{t_i}}$$

- Aeration energy (kWh/m³):

$$AE_{total} = \frac{\sum_{t_i}^{t_l}(AE_{Basin\ 3_t} + AE_{Basin\ 4_t} + AE_{Basin\ 5_t})}{\frac{\sum_{t_i}^{t_l} Q_{influent_t}}{n_{t_l} - n_{t_i}} * (t_l - t_i)}$$

AE is the aeration energy calculated by the model, given in Equation 5.1.

- Pumping energy (kWh/m³):

$$PE_{total} = \frac{\sum_{t_i}^{t_l}(PE_{\text{Internal Recycle}_t} + PE_{\text{Sludge Recycle}_t} + PE_{\text{Sludge Waste}_t})}{\frac{\sum_{t_i}^{t_l} Q_{influent_t}}{n_{t_l} - n_{t_i}} * (t_l - t_i)}$$

Nitrogen Removal Efficiency

- Total nitrogen removal in the overall WRRF (g/m³):

$$TN = NH_4^+ - N + NO_3^- - N + NO_3^- - N$$

Soluble and particulate organic nitrogen is considered to be part of the influent NH$_4$-N since it is not a model variable in the ASM1_AN biokinetic model used.

$$TN_{removal\ overall} = \sum_{t_i}^{t_l} \frac{TN_{influent_t} * Q_{influent_t} - TN_{effluent_t} * Q_{effluent_t}}{Q_{influent_t}}$$

- Total nitrogen removal in the reactive secondary settling tank (g/m³):

$$TN_{removal\ overall\ SST} = \sum_{t_i}^{t_l} \frac{TN_{Basin\ 5_t} * (Q_{influent\ t} + Q_{underflow\ t}) - TN_{effluent_t} * Q_{effluent_t}}{Q_{influent_t}}$$

Effluent Quality

- Average effluent total inorganic nitrogen over the evaluation time period (g/m³/d):

$$TIN_{effluent} = \frac{\sum_{t_i}^{t_l} TIN_{effluent_t} * Q_{effluent_t}}{(n_{t_l} - n_{t_i}) * Q_{effluent_t}}$$

- Average effluent ammonium nitrogen over the evaluation time period (g/m³/d):

$$NH_{4_{effluent}} = \frac{\sum_{t_i}^{t_l} NH_{4_{effluent_t}} * Q_{effluent_t}}{(n_{t_l} - n_{t_i}) * Q_{effluent_t}}$$

Sludge Mass Accumulation

- Average sludge mass in the system over the evaluation time period (g/d):

$$\frac{\sum_{ti}^{tl} TSS_{Basin\,1_t} * V_{Basin\,1} + TSS_{Basin\,2_t} * V_{Basin\,2} + TSS_{Basin\,3_t} * V_{Basin\,3} + TSS_{Basin\,4_t} * V_{Basin\,4} + TSS_{Basin\,5_t} * V_{Basin\,5} + Sludge\,mass_{SST_t}}{n_{t_l} - n_{t_i}}$$

- Sludge mass difference over the evaluation time period (g): $Sludge\,mass_{t_l} - Sludge\,mass_{t_i}$

- Sludge mass accumulation in the overall WRRF over the evaluation time period (g/d):

$$Sludge\,Mass_{accumulation}$$
$$= \frac{[Sludge\,Mass_{difference} + \sum_{t_i}^{t_l} TSS_{underflow} * Q_{waste} * (n_{t_l} - n_{t_i})]}{(n_{t_l} - n_{t_i})}$$

7.1.2 Scenario Analysis I - Optimization of DO Set-Point and Internal Recycle Flowrate

The goal of this scenario is to determine whether the pilEAUte WRRF can be operated at lower dissolved oxygen (DO) concentrations in the aerated basins and whether the internal nitrate recycle (IR) flowrate can be reduced without influencing the overall nitrogen removal performance. In this way, the reduced aeration and IR flowrate would lead to lower energy consumption for the same N removal performance in the plant. To do that, the set-point of the DO controller (which is installed in Basin 4) and the internal sludge recycle from Basin 5 to Basin 1 were selected as the operational parameters to be optimized. The aeration strategy of the plant which is described in Chapter 5.4, was not changed. Simulations for a WEST "grid scenario analysis" were run with the properties given in Table 7.1. The evaluation criteria given in Chapter 7.1.1 were calculated for each run.

Table 7.1 Scenario Analyses I – WEST Grid Scenario Analysis Properties

Number of simulation runs	55
Parameter ranges	DO set-point in Basin 4 : 0.5 – 3 mg/L → 11 values
	Internal recycle flowrate : 12 – 36 m^3/d → 5 values
Parameter sampling	Uniform within the given range

Based on the simulation results, the dependency of the average concentration of effluent N components (NH_4-N, NO_2-N, NO_3-N and TIN) on the operational conditions is shown in Figure 7.1. It shows that effluent ammonium is quite low for all simulations (max value around 1 mg/L) and the plant can achieve full nitrification even if the DO concentration is lowered to 0.5 mg/L. On the other hand, effluent nitrate decreases, as the DO concentration and the internal recycle flowrate are lowered, probably thanks to simultaneous nitrification and denitrification (SND) occurring in the aerated basins. The results generally show that the pilEAUte plant is being operated with a higher DO set-point and internal recycle than needed. This might be due to the fact that the plant was designed using standard design guidelines and standard operating conditions (DO set-point 2 mg/L, IR=$3Q_{influent}$).

The continuous low DO operation results in the scope of the AvN control application in the pilEAUte WRRF (Chapter 6) support the outcomes of this scenario analysis. It had already been demonstrated when the biological reactors are operated continuously at 0.5 mg/L DO, all the influent ammonia is removed and up to 10 mg/L nitrate is found in the effluent (Figure 6.12 & Figure 6.13). There was also no internal recycling in the AvN control operation which proves that simultaneous nitrification denitrification can take place in the aerated basins at low DO and contribute to overall nitrogen removal. Note that, within this scenario analysis reducing the DO set-point down to 0.5 mg/L and reducing the internal recycle flowrate down to 18 m^3/d improves total nitrogen removal in the plant. However, this adjustment is also increasing the nitrite concentration in comparison to normal operating conditions which might lead to N_2O emissions. The risk of greenhouse gas emissions is of course not desired, but still, the results are in favour of reducing the DO set-point and internal recycling which would lead to significant reduction and optimization in energy consumption and operational cost.
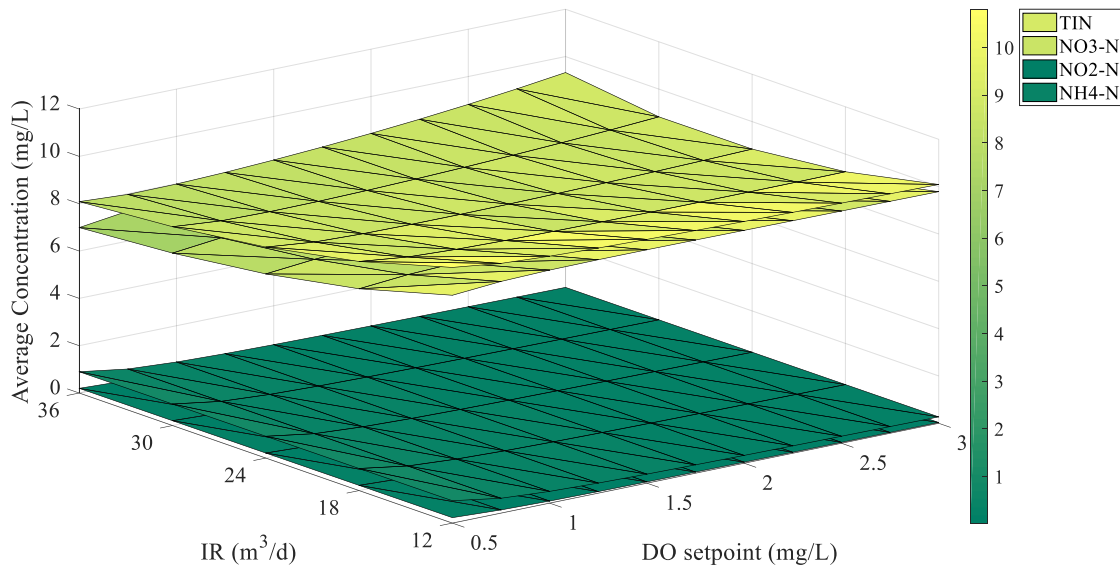
Figure 7.1 Average Effluent Concentrations for N Components for Scenario Analysis I

The aeration and pumping energy consumption and the overall energy consumption are shown in Figure 7.2. In this figure, the average energy consumption for the scenario analysis time period (day 24-59) is given for each simulation. The gain in energy consumption in corporation to standard operational conditions is much more visible with the adjusted operational conditions. As expected, lowering the DO set-point in the aerated basins reduces the aeration energy by up to 20% in comparison to normal (reference) operational conditions. In addition, pumping energy significantly reduces with the reduced internal nitrate recycle flowrate. Up to 50% of total pumping energy can be gained when the internal recycle flowrate is reduced from 36 to 12 m³/d. In accordance with the aeration and pumping energy, the overall energy consumption is also decreased thanks to reduced aeration and internal recycling.

In order to determine the optimized operational conditions to reduce energy consumption while ensuring effluent water quality, an effluent TIN limit of 10 mg/L on average over the day was chosen as limit. Based on the evaluation of each simulation result within the scenario analysis, operating the pilEAUte WRRF with a DO set-point of 0.5 mg/L and 18 m³/d internal sludge recycle flowrate can reduce the energy consumption significantly without hampering the overall nitrogen removal performance.

A detailed comparison of the reference versus the optimized operational conditions is presented in Table 7.2 based on the different evaluation criteria. Note that the presented values in Table 7.2 are the averages of the scenario analysis time period (day 24-59) next to the maximum concentrations reached for effluent N components. Based on the results, average effluent ammonium and total inorganic nitrogen concentrations

increase slightly due to reduced aeration. However, aeration and pumping energy are reduced by 21% and 37% respectively in comparison to normal operational conditions with optimized DO set-point and internal sludge recycle flowrate. Following that, the total energy consumption can be decreased by up to 26% which would lead to a significant reduction in operational costs.
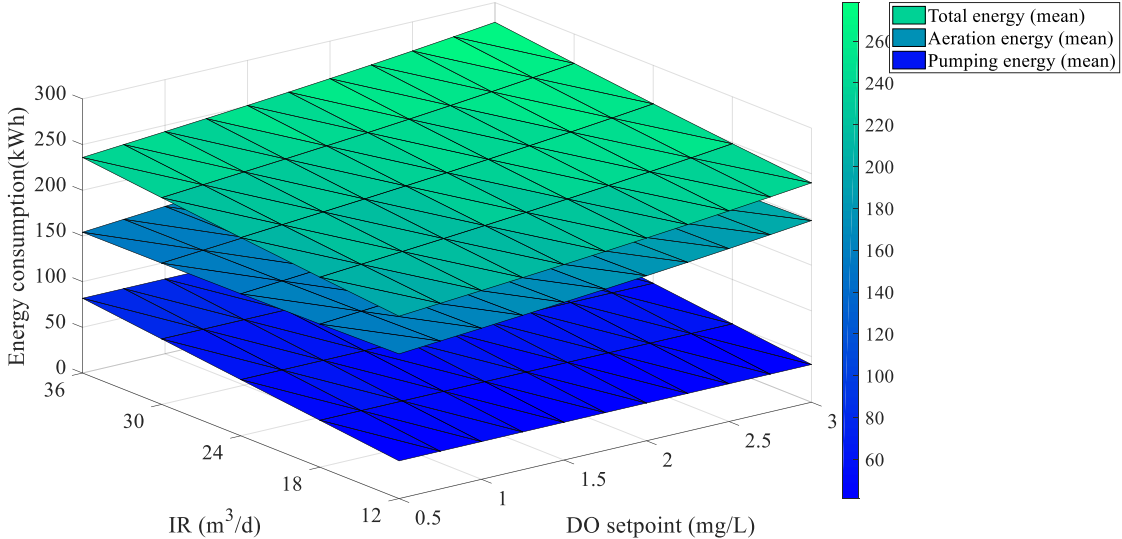
Figure 7.2 Average Energy Consumption for Scenario Analysis I

Table 7.2 Comparison of Energy and Effluent Quality Criteria for Reference vs Optimized Operational Conditions for Scenario Analysis I

	Reference Operational Conditions	Optimized Operational Conditions
Operational Conditions		
$Q_{internal\ recycle}$ (m^3/d)	36	18
DO set-point (Basin 4)	3.0	0.5
Energy Consumption		
Q_{air} (m^3/d)	1165	916
Aeration Energy (kWh) (total)	147.37	115.81
Pumping Energy (kWh) (total)	67.02	42.38
Aeration Energy (kWh/m^3)	0.38	0.30
Pumping Energy (kWh/m^3)	0.17	0.11
Total energy consumption (kWh/m^3)	0.55	0.40
Effluent Quality		
Effluent NH$_4$-N (g/m^3) (average)	0.20	0.93
Effluent NO$_3$-N (g/m^3) (average)	8.71	8.53
Effluent TIN (g/m^3) (average)	8.93	9.68
Effluent TN (g/m^3) (average)	10.70	11.19
Effluent NH$_4$-N (g/m^3) (max.)	0.44	4.53
Effluent NO$_3$-N (g/m^3) (max.)	19.74	14.66
Effluent TIN (g/m^3) (max.)	20.05	16.67
Effluent TN (g/m^3) (max.)	21.76	18.27
Sludge Mass Accumulation		
Sludge mass in the system (g/d) (average)	18089	18089
Sludge waste (g/d) (average)	721	722
Sludge mass accumulation (g)	769	770

To compare the dynamic behaviour of the reference and optimized operational conditions, times series of effluent N components are presented in Figure 7.3. It can be observed that, on the one hand, the average and maximum observed NH$_4$-N concentrations increase with reduced aeration, but that, on the other hand, NO$_3$-N concentrations decrease. The low DO concentration in the biological reactors leads to lower nitrate concentrations in the effluent on average. This might also be due to reduced aeration creating anoxic conditions in Basin 3 and promoting denitrification there (Figure 7.4). As stated before, the effluent TIN concentration increases on average, but its maximum value during the simulation time period is reduced which may indicate a safer operation in terms of the TIN discharge criterion.

Noteworthy, the optimized operational conditions do not influence the growth of biomass, thus there is no significant change in overall the sludge mass in the system.
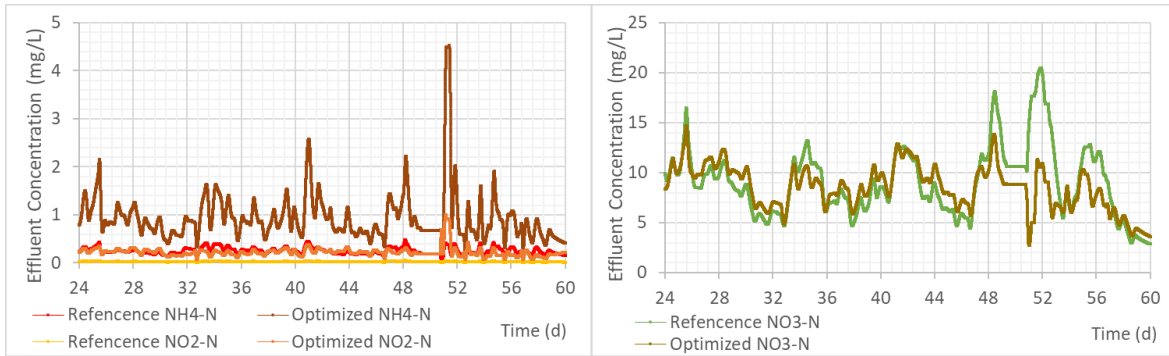
Figure 7.3 Comparison of Effluent N Components Concentrations for Reference vs Optimized Operational Conditions for Scenario Analysis I
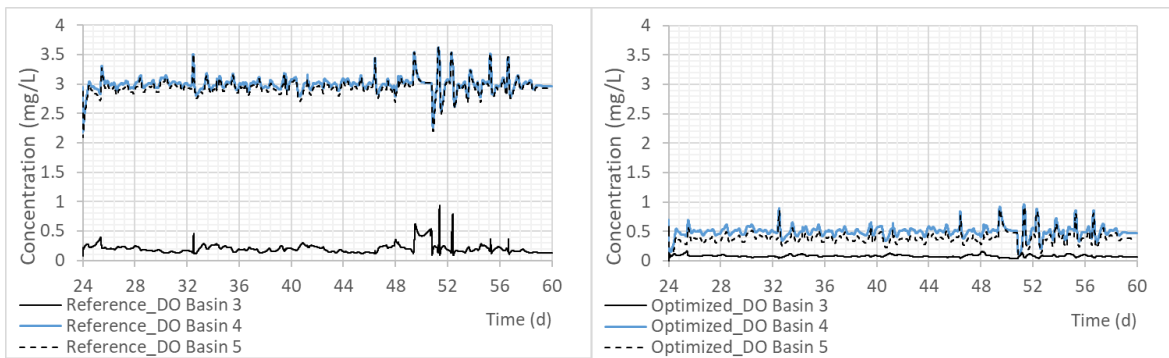
Figure 7.4 Comparison of DO Concentrations for Reference vs Optimized Operational Conditions for Scenario Analysis I

7.1.3 Scenario Analysis II - Implementation of Individual DO Controllers

The evaluation of the DO and air consumption in the first aerated basin (Basin 3) of the biological reactors shows that the aeration intensity is much lower than in the following basins (Figure 5.21, Figure 5.22, Figure 7.4) for the reference operational conditions. Inspired by Vanrolleghem and Gillot (2002), the aeration strategy of the pilEAUte WRRF model was changed and individual DO controllers were applied in each aerated basin. The second scenario analysis presented here aims at finding out whether the overall aeration energy consumption can be reduced with separate DO control in each aerated basin and also at determining how it affects the nitrogen removal performance of the plant. To do that, the model layout was updated with 3 DO controllers for the aerated basins. The same controller properties as in the original model for basin 4 were used for basin 3 and 5 (Figure 7.5).

The set-points of the 3 DO controllers are the operational parameters to be optimized. Another scenario analysis was run with the properties given in Table 7.3 and the evaluation criteria given in Chapter 7.1.1 were calculated for each run.
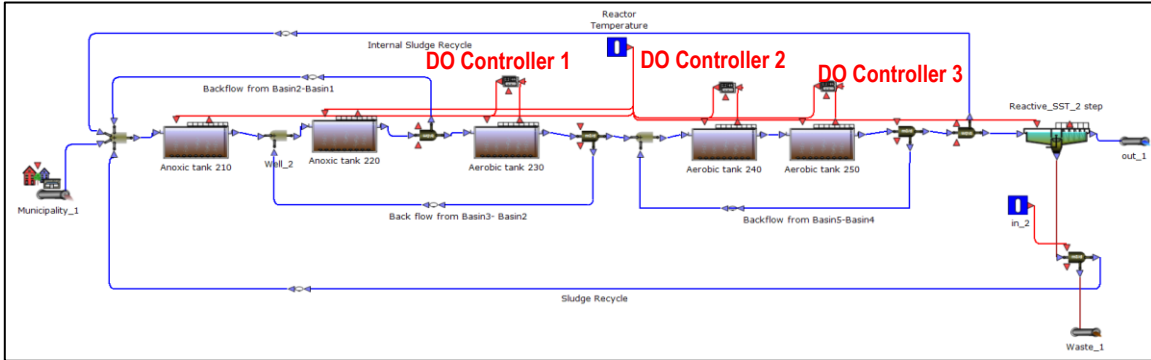
Figure 7.5 Model Layout with Individual DO Controllers in each Aerated Basin for Scenario Analysis II

Table 7.3 Scenario Analysis II – WEST Grid Scenario Analysis Properties

Number of simulation runs	216
Parameter ranges	DO set-point in Basin 3: 0.5 – 3 mg/L $\rightarrow$ 6 values
	DO set-point in Basin 4: 0.5 – 3 mg/L $\rightarrow$ 6 values
	DO set-point in Basin 5: 0.5 – 3 mg/L $\rightarrow$ 6 values
Parameter sampling	Uniform within the given range

For each simulation, the average of the effluent N components was calculated and presented in Figure 7.6 as function of the DO set-point in each basin. Similar to the results of the previous scenario analysis, the effluent ammonium is quite low for all simulations (max value around 0.4 mg/L) and the plant can achieve full nitrification even if the DO concentration is lowered to 0.5 mg/L in each aerated basin. The effluent TIN and nitrate concentrations increase as the applied DO set-point is increased. It can be seen that the effluent TIN is mostly composed of nitrate and the decrease in the DO set-point can lead to up to a 5 mg/L reduction in the effluent TIN and NO_3-N concentrations. On the other hand, nitrite concentration is at its highest value when the DO set-point is 0.5 mg/L in each basin which indicates the potential for N_2O emission in full-scale application.

The aeration and the overall energy consumption (including the pumping energy which is not shown since it does not change) for each run are shown in Figure 7.7. It is clear that the aeration energy needs can be reduced by lowering the DO set-point in the aerated basins by up to 30% when the simulation results are compared to each other for scenario analysis II. However, in none of these simulations, the aeration energy is getting lower than the reference operational case. Note that, with the applied aeration strategy in normal operational

conditions, the plant is operated with a 3 mg/L DO concentration in basins 4 and 5 and a lower than 0.5 mg/L DO concentration in basin 3 (Figure 7.4). Thus, the proposed aeration strategy with scenario analysis II does not improve either the energy consumption or the overall nitrogen removal efficiency compared to the reference situation. Still, operating the aerated basins with individual DO controllers might be important in long-term operation to ensure nitrogen removal efficiency in case of peak nitrogen loads to the WRRF.
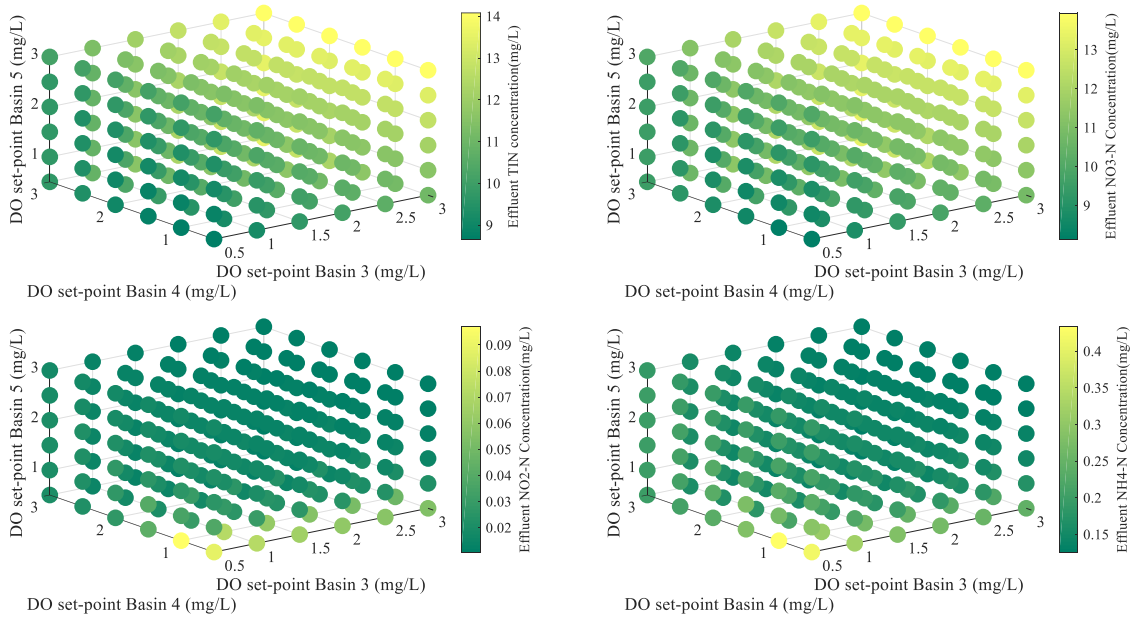
Figure 7.6 Average Effluent Concentrations for the Different N Components* for Scenario Analysis II (TIN top-left, NO$_3$-N top-right, NO$_2$-N bottom-left, NH$_4$-N bottom-right)
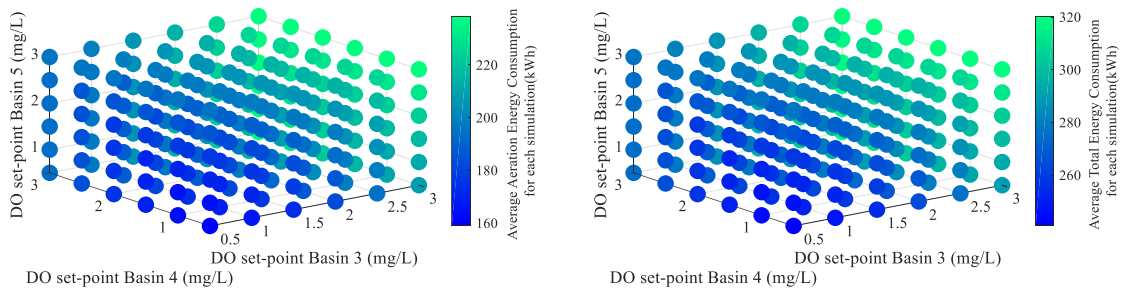
Figure 7.7 Average Aeration (left) and Total Energy Consumption (right) for Scenario Analysis II

7.1.4 Scenario Analysis III – Taking Advantage of Reactive Settling

Within this scenario analysis, it is aimed to investigate whether:

- reactive settling can be used to contribute to the overall nitrogen removal in the plant through denitrification

- the internal sludge recycle flowrate can be reduced.

The developed and calibrated reactive settler model presented in Chapter 4 is used and the operational conditions to achieve reactive settling tested in Chapter 4 are adopted in the plant-wide pilEAUte model. Herein, the model is run with 2 different operational conditions and compared with the reference case.

1. The sludge recycle flow is reduced from 12 m³/d to 3.6 m³/d to accumulate sludge in the settler, and enhance biological reactions in the SST. Also, the internal nitrate recycle flowrate is reduced to 18 m³/d to increase the nitrate loading to the clarifier.

2. In addition to the conditions above, the feed layer of the SST is changed from Layer 11 to Layer 16, thus the SST is fed from its bottom. In this way, the hydraulic retention time of the mixed liquor within the sludge blanket is increased to be able to see the influence of reactive settling on effluent concentrations.

The TSS concentrations in the biological reactor and the sludge recycle with the adjusted operational conditions are given in Figure 7.8. As compared to normal operational conditions (reference case), the SST underflow TSS concentration significantly increases with the reduced underflow rate. Sludge blanket concentration profiles and the SST feeding points for the reference and reactive settler operational cases are shown in Figure 7.9.
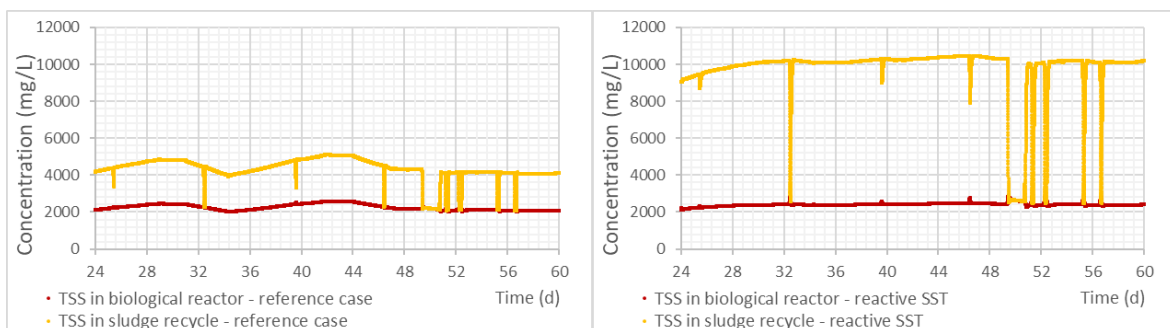
Figure 7.8 TSS Concentrations in Reference Case (left) vs Reactive SST Operational Cases (right) for Scenario Analysis II
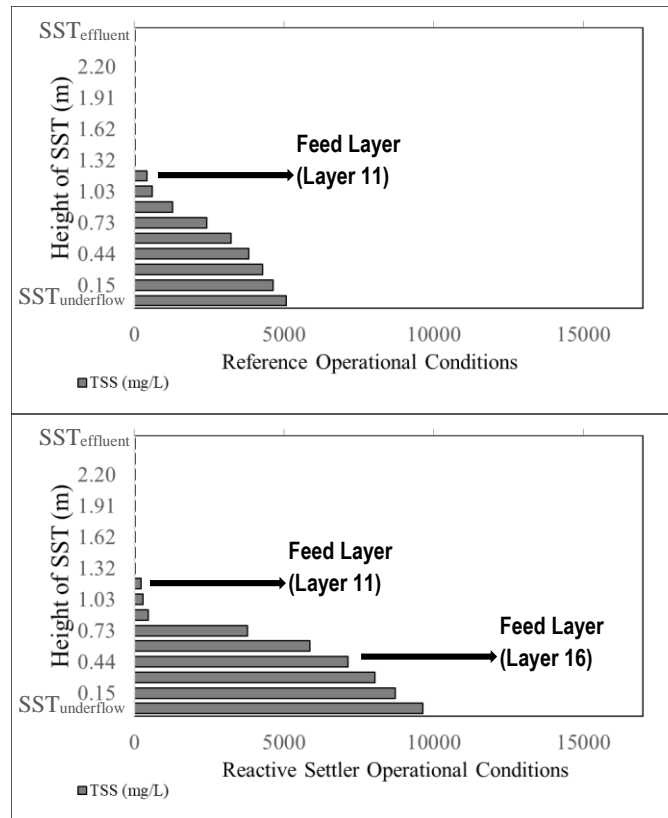
Figure 7.9 TSS Concentrations Profiles in Reference Case (top) vs Reactive SST Operational Cases (bottom) for Scenario Analysis II with the Locations of Feed Layers

Based on the simulation results for the different operational cases applied for scenario analysis III, the TIN removal for the overall pilEAUte WRRF and the secondary clarifier are calculated and compared in Table 7.4. The reactive settler operational cases significantly reduce the pumping energy consumption, thus optimising the overall energy consumption of the plant (up to 20% gain) thanks to the reduced internal sludge recycle. There is no significant difference in the air flowrate and aeration energy consumption since the DO set-point and aeration strategy are not changed in the different operational cases. Aeration is directly related to the nitrification process, and in this scenario analysis denitrification process efficiency is being investigated.

The goal of the scenario analysis is not only energy optimization, but also to take advantage of the denitrification in the SST to improve nitrate removal and effluent quality. When the SST is fed from its existing feed point (Layer 11 which is at the height of 1.1 m. from the bottom of the tank), there is no direct impact on the effluent nitrate even though denitrification clearly occurred in the sludge blanket based on the underflow concentrations. In this case, only the water going to the underflow passes through the sludge blanket, thus the nitrate in the effluent remains. On the other hand, when the feed layer is lowered and the SST is fed from closer to its bottom (in this case Layer 16 which is at the height of 0.4 m. from the bottom of the tank), the mixed liquor passes through the sludge blanket with a higher retention time and the effluent nitrate concentration significantly reduces. The high

nitrate removal rate in the SST leads to a significant contribution to the overall denitrification capacity of the WRRF.

In reactive settler operation with bottom-feeding and a large sludge blanket, effluent ammonia seems to increase, probably due to the decay of biomass or hydrolysis of slowly biodegradable particulate matter, and it affects the effluent concentration due to the upward bulk flux. The effluent nitrate concentration decreases below 1 mg/L on average, but the nitrite concentration in the effluent increases up to 1.2 mg/L. This might indicate incomplete denitrification in the sludge blanket and trigger N_2O emission through heterotrophic denitrification. Figure 7.10 shows the N component (NH_4-N, NO_2-N, NO_3-N) time series for the normal operational conditions (reference case) versus the reactive settler operation with bottom-feeding. As can be seen, the nitrate concentration significantly decreases in the reactive settler operational case (up to 90% lower NO_3-N in the effluent in comparison to the reference case). However, the nitrite concentration is much higher and changes in parallel to the nitrate concentration. Also, the ammonium concentration significantly increases.
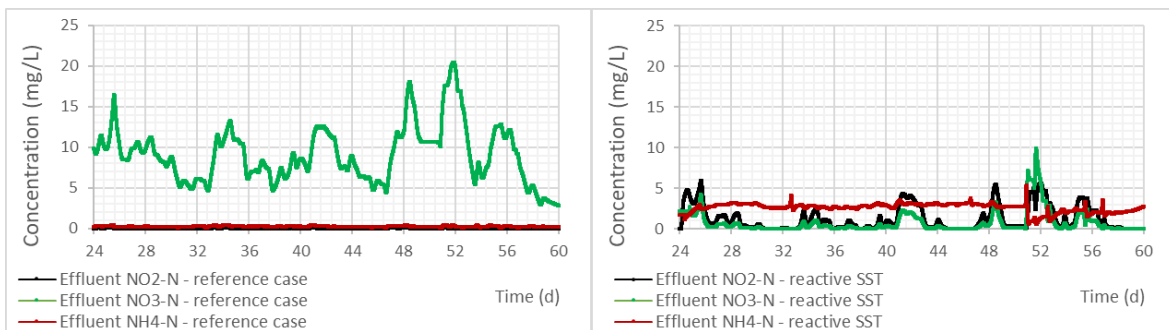
Figure 7.10 Effluent N Components Concentrations in Reference Case (left) vs Reactive SST with Bottom Feeding Operational Case (right) for Scenario Analysis II

On the other hand, the effluent TIN concentration is reduced thanks to the significant removal of nitrate in the reactive settling process (Figure 7.10). The nitrogen mass balance of the SST and the overall pilEAUte WRRF shows that up to 18% of the TIN can be removed in the SST when the reactive settler is fed from the bottom (layer 16). Thus, this type of operational strategy can both improve the nitrogen removal and effluent TIN concentration, but can also reduce the operational costs thanks to the reduced internal sludge recycle rates.

Finally, reactive settler operation requires increasing the sludge blanket in the clarifier and also feeding the SST from the bottom of the tank (thus through the sludge blanket). Operation of the SST under these conditions, in reality, might be challenging due to the upward bulk flux being continuously passed through the sludge blanket which may disturb the sludge blanket concentration profile and may even lead to an overflow. This effect can be seen by comparing the effluent TIN and TN concentrations in the effluent (Table 7.4). The effluent TN is higher

than the TIN which indicates more organic nitrogen is present in the effluent in particulate form. The increased effluent TSS concentration confirms this. Thus, reactive settler operation requires monitoring the effluent quality carefully and adjusting the operational parameters (such as underflow rate, sludge blanket height, feed layer) if needed. There are commercially available technologies to adjust the SST feed point and install a height-variable inlet structure (e.g. hydrograv 2020) (Figure 7.11). This type of inlet structure is mostly oriented to eliminate sludge overflow and keep the sludge blanket at low levels, but it could also be adopted to operate the SST as a reactive settler to optimize nitrogen removal. Also, the effluent of the SST can be treated with downstream filtration to comply with effluent TN and TSS discharge criteria. In addition, with the reactive settler conditions applied in this simulation, more than 8 mg/L nitrate is being removed through settler denitrification which may cause N_2 gas bubble induced rising sludge in the SST in full-scale application (Henze et al. 1993). Note that this simulation was done to demonstrate the highest possible denitrification potential in the SST to determine how a reactive settler process can contribute to the overall N removal in a WRRF and can be used for energy optimization through reduced need for internal sludge recycle flows.
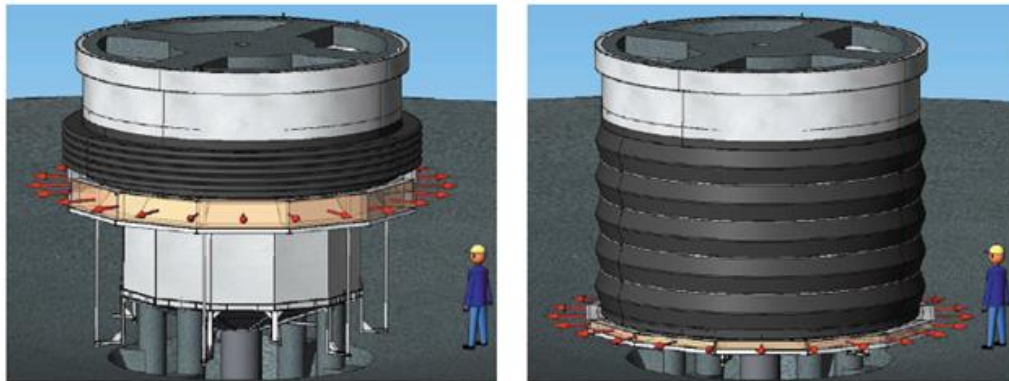
Figure 7.11 An Example of a Height-Varible Inlet Structure (hydrograv 2020)

When the sludge mass accumulations are compared, reactive settler operational cases have higher sludge accumulation than the reference case. While the sludge wasting flowrate was not changed in these simulations, a higher amount of sludge was wasted due to the higher concentrations in the bottom of the SST. When the reactive settler operational cases are compared to each other, the bottom-feeding case accumulates less sludge because a higher TSS concentration is observed in the effluent. Thus, sludge is lost through the effluent as well.

Table 7.4 Comparison of Reference vs Reactive Settler Operational Conditions for Scenario Analysis III

	Reference Operational Conditions	Reactive Settler Operational Conditions	
Operational Conditions			
$Q_{sludge\ recycle}$ ($Q_{underflow\ rate}$) (m^3/d)	**12**	**3.6**	**3.6**
$Q_{internal\ recycle}$ (m^3/d)	**36**	**18**	**18**
SST feed layer	**Layer 11***	**Layer 11***	**Layer 16****
DO set-point (Basin 4)	3.0	3.0	3.0
Energy Consumption			
Q_{air} (m^3/d)	1165	1179	1065
Aeration Energy (kWh) (total)	147.37	148.59	138.49
Pumping Energy (kWh) (total)	**67.02**	**30.24**	**30.24**
Aeration Energy (kWh/m^3)	0.38	0.38	0.35
Pumping Energy (kWh/m^3)	0.17	0.08	0.08
Total energy consumption (kWh/m^3)	**0.55**	**0.46**	**0.43**
Effluent Quality			
Effluent NH$_4$-N (g/m^3) (average)	**0.20**	**0.26**	**2.56**
Effluent NO$_3$-N (g/m^3) (average)	**8.71**	**10.24**	**0.83**
Effluent NO$_2$-N (g/m^3) (average	**0.02**	**0.03**	**1.20**
Effluent TIN (g/m^3) (average)	**8.93**	**10.54**	**4.59**
Effluent TN (g/m^3) (average)	10.70	12.21	14.18
Effluent TSS (g/m^3) (average)	9.63	9.29	53.68
Underflow Concentrations			
Underflow NH$_4$-N (g/m^3) (average)	0.32	1.85	0.56
Underflow NO$_3$-N (g/m^3) (average)	6.36	1.20	8.51
Underflow NO$_2$-N (g/m^3) (average)	2.11	1.35	2.21
TIN Removal			
TIN removal of overall WRRF (g/d)	**384.94**	**358.73**	**425.35**
TIN removal in the reactive SST (g/d)	**6.01**	**21.06**	**76.78**
% $\dfrac{TIN\ removal\ in\ the\ reactive\ SST}{TIN\ removal\ of\ overall\ WRRF}$	**1.56%**	**5.87%**	**18.05%**
Sludge Mass Accumulation			
Sludge mass in the system (g/d) (average)	18089	17546	19418
Sludge waste (g/d) (average)	721	1575	1067
Sludge mass accumulation (g)	769	1635	1186

*Layer 11 is at 1.1 m. height from the bottom of the SST. ** Layer 16 is at 0.4 m. height from the bottom of the SST.*

7.1.5 Conclusions

Scenario analyses were performed with the pilEAUte model to optimize energy and resource consumption by aeration and pumping of sludge. Grid scenario analyses were conducted to determine the optimal operational conditions for the pilEAUte WRRF while ensuring effluent water quality for scenarios I and II. In Scenario III, the model was simply run with operational conditions that take full advantage of denitrification in the SST so as to determine the maximum settler denitrification potential in the pilEAUte WRRF.

The first scenario analysis to optimize the DO set-point in the biological reactors and the internal nitrate recycle flowrate showed that the pilEAUte plant is being operated with a higher DO set-point and internal nitrate recycle than needed. This might be due to the fact that it was designed using standard design guidelines and for standard operational conditions. Reducing the DO set-point to 0.5 mg/L and the internal nitrate recycle flowrate to 18 m^3/d could improve total nitrogen removal in the plant, because the effluent ammonium was quite low ($\sim$1 mg/L) while the effluent nitrate concentration could be decreased in comparison the one obtained under to normal operational conditions. Thus, the overall TIN removal of the conventional N removal plant can be improved by adjusting the operational conditions to lower values and aeration and pumping energy could be reduced by 21% and 37% respectively in comparison to normal operational conditions.

Implementation of individual DO controllers in each aerated basin in the second scenario analysis gave similar results as the scenario analysis I, i.e. the plant can achieve full nitrification even if the DO concentration is lowered to 0.5 mg/L in each aerated basin. Effluent TIN and nitrate concentrations increase as the DO set-point is increased. However, the aeration energy consumed was not lower than the normal operational case. Note that for both scenario analyses (I & II), the reduced DO set-point in the aerated basins also led to higher NO_2-N concentrations in the effluent which indicates the potential for N_2O emission in the full-scale application.

In the last scenario analysis (III), reactive settler operation was investigated in the plant-wide model to determine its potential to contribute to the overall nitrogen removal in the plant through settler denitrification and energy reduction through a reduced internal sludge recycle flowrate. This could only be achieved when the feed layer of the SST was lowered and the SST was fed closer to its bottom. In this case, the mixed liquor passes through the sludge blanket with a higher retention time and the effluent nitrate concentrations significantly reduce. This high nitrate removal in the SST was a significant contribution to the overall denitrification capacity of the WRRF. The nitrogen mass balance of the SST and the overall pilEAUte WRRF showed that up to 18% of the TIN can be removed in the SST under these operational conditions. Thus, this type of operational condition could both improve the nitrogen removal and effluent TIN concentration, but it can also reduce the operational costs thanks to reduced internal sludge recycle flowrates. On the other hand, reactive settler operation requires increasing the sludge blanket in the clarifier and also feeding the SST from the bottom of the tank. The simulation results

indicated that effluent TSS may significantly increase due to the upward bulk flux passing continuously through the sludge blanket. Also, with the reactive settler conditions applied, even more than 8 mg/L nitrate could be removed through settler denitrification and this has been shown to potentially cause N_2 gas bubble induced rising sludge in the SST in full-scale application. Operation of the SST under these conditions, in reality, might be challenging. Reactive settler operation in full-scale application requires monitoring the overall system and the effluent quality very carefully and adjusting the operational parameters (such as underflow rate, sludge blanket height, feed layer) if needed. The sludge blanket height level should be selected carefully to allow a substantial sludge concentration profile in the settler without leading to any sludge overflow or increased effluent turbidity. Thus, frequent or continuous monitoring of the concentration and flux of sludge removed from the SST and the SBH level are needed. Also the solids loading rate and the surface loading rate of the clarifier must be monitored.

CONCLUSIONS & PERSPECTIVES

Conclusions

The aim of this thesis was to investigate energy and resource-efficient processes and operational conditions for nitrogen removal systems through pilot-scale experimentation, modelling and model-based optimization. This was accomplished though different studies including dedicated experimentation and model development for reactive settling processes; experimentation and modelling for conventional N removal; and implementation of AvN control strategies for short-cut N removal processes. The research conducted was closely linked to the pilEAUte WRRF which is a pilot-scale plant located at Université Laval with 12 m³/d treatment capacity. Even though the research was driven by the case studies applied in this pilot-scale WRRF, the developed methodologies to demonstrate and model the energy and resource-efficient processes and operational conditions are applicable and transferable to other full-scale systems.

First, to better understand the reactive settling process and its potential for denitrification, a 1-D reactive settler model was developed which is the first modelling work that combines the full set of ASM1 biokinetics with the 1-D Bürger-Diehl settler model with compression. The unique measurement campaign carried out allowed to confirm that significant denitrification in the SST can occur depending on the biomass concentration profile and the hydraulic retention time in the sludge blanket. Thus, the simultaneous occurrence of biokinetic processes and physical settling phenomena in the secondary settling tanks must be considered and modelled to correctly determine the effluent and underflow characteristics, and also analyse the contribution of SST denitrification to the overall N removal in a WRRF. During model development, two types of hindered settling velocity functions were tested to properly model the hindered settling behaviour: the double exponential function by Takács et al. (1991) and the power-law function by Diehl (2015). The extensive calibration and model selection effort demonstrated that the power-law function is more suited to describe hindered settling behaviour at high sludge concentrations and high sludge blanket heights. The modelling also demonstrated the importance of including actual clarifier geometry, especially for properly quantifying the biological conversions at the bottom of a SST. Initial estimates of the hindered settling parameters could be obtained from standard batch settling experiments. Fine-tuning was required for one of the hindered settling parameters in the overall SST model which was found to be especially influential at high TSS concentrations. The calibrated model was subsequently able to accurately predict the TSS, NO_3-N and DO concentration profiles and no further calibration of the biokinetic model was needed and the default values of the ASM1 biokinetic model could be used to predict the DO and NO_3-N concentrations adequately. There are the typical values for municipal wastewater treatment and this agrees with the pilEAUte's behaviour. The developed 1-D reactive settler model allowed illustrating the denitrification potential of a secondary settler and can be applied to other case studies to properly calculate the nitrogen mass

balance of WRRFs and improve the overall total inorganic nitrogen removal in the plant. On the other hand, it can also be used to warn whether a N_2 gas bubble induced rising sludge problem may occur since this problem is closely linked to the amount of nitrate removed in the secondary clarifiers.

Second, the pilEAUte WRRF, designed and operated as a conventional pre-denitrification N removal WRRF, was modelled. An extensive model calibration methodology was adopted by merging the Good Modelling Practice (GMP) Unified Protocol, the BIOMATH calibration protocol and the step-wise Monte Carlo-based calibration protocol by Mannina et al. (2011). The tracer test results and the hydraulic model calibration demonstrated the importance of hydraulic characterization of a WRRF prior to biokinetic model calibration. For the pilEAUte WRRF case, significant backflows in between the basins were observed and included in the final model layout by considering different potential operational conditions (e.g. feeding the influent to basin 3 rather than basin 1). For the aeration model, a simplified relation between the oxygen transfer coefficient (k_{La}) and the air flowrate could be adopted where the model predictions corresponded quite well to the measured air flowrates, both for calibration and validation periods. The adopted case-specific k_{La} and air flowrate correlation could reduce the model calibration effort significantly. Finally, the biokinetic model (both for biological reactors and the reactive settler) was calibrated using a modified version of the calibration protocol of Mannina et al. (2011). A pre-selection of model parameters based on available data and engineering expertise, and a pre-screening of model parameters through local sensitivity analysis were performed prior to the parameter subset grouping according to the model output variables which was performed using a protocol modified from the original methodology of Mannina et al. (2011). Overall, the pilEAUte model was calibrated and validated to simulate the selected model variables (N and TSS variables) successfully and to be ready for further scenario analysis for energy and resource optimization. While developing the model of the pilEAUte case study, the adopted overall (merged) calibration methodology is applicable to other case studies to ensure a reliable model calibration and reduce calibration efforts.

Third, the applicability of continuous and intermittent Ammonia vs. NO_X-N (AvN) control strategies was investigated on the pilEAUte WRRF. Based on the application results, it was possible to achieve successful AvN control for both continuous and intermittent control strategies. However, keeping the AvN ratio at the effluent on the desired value (1) highly depends on operational conditions such as influent variations and SRT. For both strategies, automatic AvN control heavily depended on the sensor's reliability. The desired AvN ratio could be achieved for an aerobic SRT of 5-7 days for the continuous AvN and 6.5-8 days for the intermittent AvN. Higher sludge wasting to reduce the SRT further in the pilEAUte WRRF resulted in sharp losses in TSS, and unstable effluent nitrogen concentrations. Based on the results of a short-term detailed measurement campaign, the overall N removal efficiency and simultaneous nitrification and denitrification (SND) performance was found higher in the intermittent AvN system than in the continuous one. However, the average air consumption per

removed gram of N in both systems was not significantly different and so was the energy consumption due to aeration.

Finally, the pilEAUte model for conventional pre-denitrification N removal was used in scenario analysis to optimize energy consumption for aeration and pumping of sludge. Scenario analysis related to optimizing the air consumption in the biological reactors and the internal recycle (IR) flowrate showed that the plant is operated at a higher DO set-point and IR than needed. This might be due to the fact that the plant was designed and operated with traditional design and operation guidelines. Reducing both operational parameters improved the overall nitrogen removal in the plant, probably thanks to SND occurring in the aerated basins. The overall TIN removal of the conventional N removal plant could be improved by adjusting the operational conditions to lower values (i.e. 0.5 mg/L DO set-point and 18 m^3/d IR), thus significantly reducing aeration and pumping energy. Implementation of individual DO controllers in each aerated basin gave similar results to the previous scenario analysis, i.e. the plant can achieve full nitrification even if the DO concentration is lowered to 0.5 mg/L in each aerated basin. Effluent TIN and nitrate concentrations increased proportionally to the increment in the applied DO set-point. However, it was remarkable that the aeration energy was not lower than the reference operational case. Importantly, for both scenarios the reduced DO set-point in the aerated basins led to higher NO_2-N concentrations in the effluent which creates the potential for N_2O emission in full-scale application. In addition, reactive settler operation was investigated in the plant-wide model to determine whether it has potential to contribute to the overall nitrogen removal in the plant through settler denitrification. Significant effluent NO_3-N reduction, however, could only be achieved when the feed layer of the SST was lowered in the sludge blanket and the SST was fed from closer to its bottom. In this case, the mixed liquor could pass through the sludge blanket at a higher retention time and the effluent nitrate concentration could be significantly reduced. The high nitrate removal in the SST led to a significant contribution to the overall denitrification capacity of the WRRF. The nitrogen mass balance of the SST and overall pilEAUte WRRF showed that up to 18% of the TIN can be removed in the SST under these operational conditions. On the other hand, in reality, operation of the SST with reactive settler conditions might be challenging. The results showed that effluent TSS can significantly increase and N_2 gas bubble induced rising sludge might occur due to the high nitrate removal rates. Thus, reactive settler operation requires monitoring the effluent quality carefully and adjusting the operational parameters if needed. This type of operational conditions could both improve the overall nitrogen removal and the effluent TIN concentration, but also could reduce the operational costs thanks to the reduced internal sludge recycle rates needed for equivalent NO_3-N removal. After all, with the way the system is set up, a post-denitrification stage is created in the available settler volume.

Perspectives

The developed models for the pilEAUte WRRF allow investigating operational conditions to optimize energy and resource consumption in N-removal processes. Nevertheless, the models can be further upgraded and future studies can be performed to better understand the removal mechanisms taking place and implement the optimization scenarios in full-scale.

Based on the results of the reactive settling measurement campaign, even though denitrification clearly occurred in the sludge blanket, no direct impact on the effluent NO_3-N could be observed which is surprising since the sludge blanket reached above the feed point. A short-circuiting effect in the inlet zone of the pilEAUte's clarifier was confirmed by the DO measured in the effluent of the reactive settler. This warrants a closer look at the design of the SST, and a detailed study of the inlet structure and upflow pattern may be needed. To include the short-circuiting effect in the reactive settler model was not possible with the 1-D model, but CFD modelling could be adopted to model the internal flow pattern and transport phenomena of solids and solubles. In addition, effective reactive settler operation requires increasing the sludge blanket height in the clarifier and also feeding the SST from the bottom of the tank to take advantage of SST denitrification. This might be challenging in full-scale applications. The available height-variable inlet structure for SSTs available on the market could be applied in the pilEAUte plant's SST to verify the model results and this would help to confirm potential application challenges in full-scale systems.

The plant-wide pilEAUte model results showed that the biological reactors can be operated at lower DO concentrations down to 0.5 mg/L and reduced IR flowrates. Even though the continuous low DO operation was already applied in the pilEAUte for the AvN operation and supported this model outcome, it would be useful to test the low DO operation in the system to ensure that the plant is capable of full-nitrification on the long-term.

The application of both continuous and intermittent AvN control strategies could be achieved successfully in the pilEAUte plant. With the available data provided from the AvN application monitoring, it should be possible to model both control strategies for the pilot-plant and use it for further scenario analysis. Through the AvN models, it would be useful to investigate the system operation with dynamic influent flowrate and reduced temperature and see if the AvN ratio of 1 is still achievable. Also, including feedforward control to anticipate the impact of influent ammonia load variations and applying a combination of feedforward and feedback AvN control should be tested through model simulations. Its expected performance improvement under influent ammonia load fluctuations could be evaluated. With the experience that successful application of automatic AvN control heavily depends on sensor reliability, the use of more robust wet chemistry analysers for AvN control, the application of fault detection on time series data and reconfiguration of controllers under sensor failure could be tested on the pilEAUte WRRF and eventually at full-scale.

REFERENCES

Agrawal, S., Seuntjens, D., De Cocker, P., Lackner, S., & Siegfried E. Vlaeminck. 2018. Success of mainstream partial nitritation/anammox demands integration of engineering, microbiome and modeling insights. *Current Opinion in Biotechnology, 50,* 214-221.

Alex, J., Rönner-Holm, S. G. E., Hunze, M., & N. C. Holm. 2011. A combined hydraulic and biological SBR model. *Water Science and Technology, 64,* 1025–1031.

Alferes, J., & Vanrolleghem, P. A. 2016. Efficient automated quality assessment: Dealing with faulty on-line water quality sensors. *AI Communications, 29 (6),* 701-709.

Al-Omari, A., Wett, B., Nopens, I., De Clippeleir, H., Han, M., Regmi, P., Bott, C., & Murthy, S. 2015. Model-based evaluation of mechanisms and benefits of mainstream shortcut nitrogen removal processes. *Water Science and Technology, 71 (6),* 840-847.

Al-Omari, A., De Clippeleir, H., Ladipo-Obasa, M., Klaus, S., Bott, C. B., McCullough, K., Fofana, R., Wadhawan, T., Murthy, S., Fevig, S., Jimenez, J., Wett, B., & Nopens, I. 2021. Modelling partial heterotrophic denitrification in mainstream nitrogen removal processes - model development and evaluation. *Proceedings of 7th IWA Water Resource Recovery Modelling Seminar,* 67-69, International Water Association.

Åmand, L., Olsson, G., & Carlsson, B. 2013. Aeration control – a review. *Water Science and Technology, 67 (11),* 2374-2398.

Amaral, A., Schraa, O., Rieger, L., Gillot, S., Fayolle, Y., Bellandi, G., Amerlinck, Y., Mortier, S. T. F. C., Gori, R., Neves, R., & Nopens, I. 2017. Towards advanced aeration modelling: from blower to bubbles to bulk. *Water Science and Technology, 75 (3),* 507–517.

Amaral, A., Gillot, S., Garrido-Baserba, M., Filali, A., Karpinska, A. M., Plósz, B. G., De Groot, C., Bellandi, G., Nopens, I., Takács, I., Lizarralde, I., Jimenez, J. A., Fiat, J., Rieger, L., Arnell, M., Andersen, M., Jeppsson, U., Rehman, U., Fayolle, Y., Amerlinck, Y., & Rosso R. 2019. Modelling gas-liquid mass transfer in wastewater treatment: When current knowledge needs to encounter engineering practice and vice versa. *Water Science and Technology, 80 (4),* 607-619.

Anthonisen, A. C., Loehr, R. C., Prakasam, T. B. S., & Srinath, E. G. 1976. Inhibition of nitrification by ammonia and nitrous acid. *Water Pollution Control Federation, 48 (5),* 835-852.

Asprey, S. P., & Macchietto, S. 2000. Statistical tools for optimal dynamic model building. *Computers & Chemical Engineering, 24 (2-7),* 1261-1267.

Baeten, J. E., Batstone, D. J., Schraa, O., van Loosdrecht, M. C. M., & Volcke, E. I. P. 2019. Modelling anaerobic, aerobic and partial nitritation-anammox granular sludge reactors - A review. *Water Research, 149,* 322-341.

Bagchi, S., Biswas, R., & Nandy, T. 2010. Alkalinity and dissolved oxygen as controlling parameters for ammonia removal through partial nitration and ANAMMOX in a single-stage bioreactor. *Journal of Industrial Microbiology and Biotechnology, 37 (8),* 871-876.

Barker, P. S., & Dold, P. L. 1997. General model for biological nutrient removal activated-sludge systems: Model presentation. *Water Environment Research, 69,* 969-984.

Benninger, R. W., & Sherrard, J. H. 1978. Nitrification and alkalinity relationships in activated sludge. *Journal of Water Pollution Control Federation, 50 (9),* 2132-2142.

Bertanza, G. 1997. Simultaneous nitrification-denitrification process in extended aeration plants: Pilot and real scale experiences. *Water Science and Technology, 35 (6),* 53-61.

Blackburne, R., Yuan, Z., & Keller, J. 2008. Demonstration of nitrogen removal via nitrite in a sequencing batch reactor treating domestic wastewater. *Water Research, 42 (8-9),* 2166-2176.

Boyle, W. C., Craven, A., Danley, W., & Rieth, M. 1989. *Oxygen Transfer Studies at the Madison Metropolitan Sewerage District Facilities, EPA/600/R-94/096.* Washington, D.C., USA: U.S. Environmental Protection Agency.

Bürger, R., Careaga, J., & Diehl, S. 2021. A method-of-lines formulation for a model of reactive settling in tanks with varying cross-sectional area. *IMA Journal of Applied Mathematics, 86 (3),* 514–546.

Bürger, R., Careaga, J., & Diehl, S. 2017. A simulation model for settling tanks with varying cross-sectional area. *Chemical Engineering Communications, 204 (11),* 1270-1281.

Bürger, R., Diehl, S., & I. Nopens. 2011. A consistent modelling methodology for secondary settling tanks in wastewater. *Water Research, 45(6),* 2247–2260.

Bürger, R., Diehl, S., Faras, S., Nopens, I., & Torfs, E. 2013. A consistent modelling methodology for secondary settling tanks: A reliable numerical method. *Water Science and Technology, 68 (1),* 192-208.

Bürger, R., Careagaa, J., Diehl, S., Mejías, C., Nopens, I., Torfs, E., & Vanrolleghem, P. A. 2016. Simulations of reactive settling of activated sludge with a reduced biokinetic model. *Computers and Chemical Engineering, 92,* 216-229.

Bürger, R., Diehl, D., & Mejías, C. 2018. A difference scheme for a degenerating convection-diffusion-reaction system modelling continuous sedimentation. *ESAIM: Mathematical Modelling and Numerical Analysis, 52 (2),* 365-392.

Cao, Y., van Loosdrecht, M., & Daigger, G. T. 2017. Mainstream partial nitritation-anammox in municipal wastewater treatment: Status, bottlenecks, and further studies. *Applied Microbiology and Biotechnology, 101 (4),* 1365-1383.

Capodaglio, A. G., & Olsson, G. 2020. Energy issues in sustainable urban wastewater management: Use, demand reduction and recovery in the urban water cycle. *Sustainability, 12 (1),* 1-17.

Castro-Barros, C. M., Rodríguez-Caballero, A., Volcke, E. I. P., & Pijuan, M. 2016. Effect of nitrite on the N2O and NO production on the nitrification of low-strength ammonium wastewater. *Chemical Engineering Journal, 287,* 269-276.

CCME. 2009. *Stratégie pancanadienne pour la gestion des effluents d'eaux usées municipales.* Whitehorse, YK, Canada.

Chavan, P. V., Batista, J. R., & Shepherd, W. 2007. Application of sludge blanket height and flux theory as a tool to control denitrification in the secondary clarifier. *Journal of Environmental Research and Development, 2 (2),* 111-118.

Chen, Q., Ni, J., Ma, T., Liu, T., & Zheng, M. 2015. Bioaugmentation treatment of municipal wastewater with heterotrophic-aerobic nitrogen removal bacteria in a pilot-scale SBR. *Bioresource Technology, 183,* 25-32.

Chen, S., & Chen, B. 2013. Net energy production and emissions mitigation of domestic wastewater treatment system: A comparison of different biogas–sludge use alternatives. *Bioresource Technology (144)* 296-303.

Cheremisinoff, N. P. 1997. Nitrification and denitrification in the activated sludge process. *Biotechnology for Waste and Wastewater Treatment*, 151-188. Norwich, NY, USA: William Andrew.

Cho, S. H., Colin, F., Sardin, M., & Prost, C. 1993. Settling velocity model of activated sludge. *Water Research, 27 (7),* 1237-1242.

Ciudad, G., Rubilar, O., Muñoz, P., Chamy, R., Vergara, C., & Jeison, D. 2005. Partial nitrification of high ammonia concentration wastewater as a part of a shortcut biological nitrogen removal process. *Process Biochemistry, 40 (5),* 1715-1719.

Claeys, F. H. A. 2008. *A Generic Software Framework for Modelling and Virtual Experimentation with Complex Biological Systems.* Ghent, Belgium: PhD Thesis, Ghent University.

Cole, R. 1968. *Experimental evaluation of the Kynch theory.* Chapel Hill, USA: PhD Thesis, University of North Carolina.

Cui, F., Park, S., Mo, K., Lee, W., Lee, H., & Kim, M. 2017. Experimentation and mathematical models for partial nitrification in aerobic granular sludge process. *KSCE Journal of Civil Engineering, 21,* 127-133.

Daigger, G. T., Adams, C. D., & Steller, H. K. 2007. Diffusion of oxygen through activated sludge flocs: Experimental measurement, modeling, and implications for simultaneous nitrification and denitrification. *Water Environment Research, 79 (4),* 375-387.

Daw, J., Hallett, K., DeWolfe, J., & Venner, I. 2012. *Energy Efficiency Strategies for Municipal Wastewater Treatment Facilities.* NREL/TP-7A30-53341.

De Clercq, J., Nopens, I., Defrancq, J., & Vanrolleghem, P. A. 2008. Extending and calibrating a mechanistic hindered and compression settling model for activated sludge using in-depth batch experiments. *Water Research, 42 (3),* 781-791.

De Clercq, B. 2003. *Computational Fluid Dynamics of Settling Tanks: Development of Experiments and Rheological, Settling, and Scrapper Submodels.* PhD Thesis, Ghent University, Belgium.

De Clippeleir, H., Vlaeminck, S. E., De Wilde, F., Daeninck, K., Mosquera, M., Boeckx, P., Verstraete, W., & Boon, N. 2013. One-stage partial nitritation/anammox at 15°C on pretreated sewage: Feasibility demonstration at lab-scale. *Applied Microbiology and Biotechnology, 97 (23),* 10199–10210.

Deng, L., Peng, Y., Li, J., Gao, R., Li, W., & Du, R. 2021. Enhanced simultaneous nitrogen and phosphorus removal from low COD/TIN domestic wastewater through nitritation-denitritation coupling improved anammox process with an optimal Anaerobic/Oxic/Anoxic strategy. *Bioresource Technology, 322,* 124526.

DHI. 2017. *MIKE Powered by DHI.* https://www.mikepoweredbydhi.com/products/west.

Diehl, S. 2015. Numerical identification of constitutive functions in scalar nonlinear convection-diffusion equations with application to batch sedimentation. *Applied Numerical Mathematics, 95,* 154-172.

Dochain, D., & Vanrolleghem, P. A. 2001. *Dynamical Modelling and Estimation in Wastewater Treatment Processes.* IWA Publishing.

Domingo-Félez, C., & Smets, B. F. 2020. Modeling denitrification as an electric circuit accurately captures electron competition between individual reductive steps: The activated sludge model−electron competition model. *Environmental Science & Technology, 54* 7330-7338.

Dosta, J., Vila, J., Sancho, I., Basset, N., Grifoll, M., & Mata-Álvarez, J. 2015. Two-step partial nitritation/Anammox process in granulation reactors: Start-up operation and microbial characterization. *Journal of Environmental Management, 164,* 196-205.

Du, R., Cao, S., Li, B., Niu, M., Wang, S., & Peng, Y. 2017. Performance and microbial community analysis of a novel DEAMOX based on partial-denitrification and anammox treating ammonia and nitrate wastewaters. *Water Research, 108,* 46-56.

Du, R., Peng, Y., Cao, S., Li, B., Wang, S., & Niu, M. 2016. Mechanisms and microbial structure of partial denitrification with high nitrite accumulation. *Applied Microbiology and Biotechnology, 100 (4),* 2011-2021.

Duan, H., Ye, L., Lu,X., & Yuan, Z. 2019. Overcoming nitrite oxidizing bacteria adaptation through alternating sludge treatment with free nitrous acid and free ammonia. *Environmental Science and Technology, 53 (4),* 1937-1946.

Ekama, G. A. 2010. The role and control of sludge age in biological nutrient removal activated sludge systems. *Water Science and Technology, 61 (7),* 1645-1652.

EPA. 1972. Clean Water Act. U.S. Environmental Protection Agency.

EPA. 2013. *Energy Efficiency in Water and Wastewater Facilities: A Guide to Developing and Implementing Greenhouse Gas Reduction Programs.* U.S. Environmental Protection Agency.

EPA. 2010. *Evaluation of energy conservation measures for wastewater treatment facilities. EPA-832-R-10-005.* Pennsylvania, Washington: U.S. Environmental Protection Agency.

EPA. 2002. *Office of Ground Water and Drinking Water Distribution System Issue Paper: Nitrification.* Washington DC, USA: U.S. Environmental Protection Agency.

EPA. 2021. *Basic Information about Water Reuse*. U. S. Environmental Protection Agency. 03 August 2021. https://www.epa.gov/waterreuse/basic-information-about-water-reuse.

EU. 2000. Directive 2000/60/EC of the European Parliament and of the Council establishing a framework for the Community action in the field of water policy.

Evans, M., & Sober, G. 2015. How alkalinity affects nitrification. *Florida Water Resources Journal,* 50-51.

Farina, T. 2012. An Overview of Sidestream Treatment Alternatives Used to Increase Nutrient Removal. *Ohio Water Environment Association Annual Conference.* Aurora, OH, USA.

Fiter, M., Colprim, J., Poch, M., & Rodríguez-Roda, I. 2004. Enhancing biological nitrogen removal in a small wastewater treatment plant by regulating the air supply. *Water Science and Technology, 48 (11-12),* 445-452.

Fitzsimons, L., Clifford, E., McNamara, G., Doherty, E., Phelan, T., Horrigan, M., Delauré, Y., & Corcoran, B. 2012. *EPA Research Report: Increasing Resource Efficiency in Wastewater Treatment Plants (2012-W-MS-10).* Wexford, USA: U.S. Environmental Protection Agency.

Flores-Alsina, X., Gernaey, K. V., & Jeppsson, U. 2012. Benchmarking biological nutrient removal in wastewater treatment plants: Influence of mathematical model assumptions. *Water Science and Technology 65 (8),* 1496-1505.

Gao, D., & Xiang, T. 2021. Deammonification process in municipal wastewater treatment: Challenges and perspectives. *Bioresource Technology, 320,* 124420.

Gernaey, K. V., van Loosdrecht, M. C. M., Lind, M., & Jørgensen, S. B. 2004. Activated sludge wastewater treatment plant modelling and simulation: State of the art. *Environmental Modelling & Software, 19 (9),* 763-783.

Gernaey, K. V., Jeppsson, U., Batstone,D. J., & Ingildsen, P. 2006. Impact of reactive settler models on simulated WWTP performance. *Water Science and Technology, 53 (1)* 159-167.

Gibbs, B., Third, K. A., Newland, M., & Ruwisch, R. 2005. Long-term aeration management for improved N-removal via SND in a sequencing batch reactor. *Water Research, 39,* 3523-3530.

Giberti, M., Dereli, R. K., Flynn, D., & Casey, E. 2020. Predicting wastewater treatment plant performance during aeration demand shifting with a dual-layer reaction settling model. *Water Science and Technology, 81 (7),* 1365–1374.

Gikas, P. 2017. Towards energy positive wastewater treatment plants. *Journal of Environmental Management, 203, Part 2,* 621-629.

Gilbert, E. M., Agrawal, S., Brunner, F., Schwartz, T., Horn, H., & Lackner, S. 2014. Response of different Nitrospira species to anoxic periods. *Environmental Science and Technology, 48 (5),* 2934-2941.

Gilbert, E. M., Agrawal, S., Schwartz, T., Horn, H., & Lackner, S. 2015. Comparing different reactor configurations for Partial Nitritation/Anammox at low temperatures. *Water Research, 81,* 92-100.

Griborio, A., Rohrbacher, J., McGehee, M., Pitt, P., Latimer, R., & Gellner, J. 2010. Combining Stress Testing and Dynamic Linking of Whole Plant Simulators and CFD for the Evaluation of WWTP Wet Weather Capacity. *Proceeding of 83th Annual Water Environment Federation Technical Exhibition and Conference (WEFTEC).* New Orlans, Louisiana, USA.

Guerrero, J., Flores-Alsina, X., Guisasola, A., Baeza, J. A. & Gernaey, K. V. 2013. Effect of nitrite,limited reactive settler and plant design configuration on the predicted performance of simultaneous C/N/P removal WWTPs. *Bioresource Technology, 136,* 680-688.

Gujer, W. 2008. *Systems Analysis for Water Technology.* Springer-Verlag Berlin Heidelberg.

Gujer, W., & Jenkins, D. 1975. A nitrification model for the contact stabilization activated sludge process. *Water Research, 9,* 561-566.

Gujer, W., Henze, M., Mino, T., & van Loosdrecht, M. 1999. Activated Sludge Model No. 3. *Water Science Technology,39 (1),* 183-193.

Gupta, R. K., Poddar, B. J., Nakhate, S. P., Chavan, A. R., Singh, A. K., Purohit, H. J., & Khardenavis, A. A. 2022. Role of heterotrophic nitrifiers and aerobic denitrifiers in simultaneous nitrification and denitrification process: A non-conventional nitrogen removal pathway in wastewater treatment. *Letters in Applied Microbiology, 74 (2),* 159-184.

Gustavsson, D. J., Suarez, C., Wilén, B. M., Hermansson, M., & Persson, F. 2020. Long-term stability of partial nitritation-anammox for treatment of municipal wastewater in a moving bed biofilm reactor pilot system. *Science of the Total Environment, 714,* 136342.

Gut, L., Plaza, E., & Hultman, B. 2007. Assessment of a two-step partial nitrition /Anammox system with implementation of multivariate data analysis. *Chemometrics and Intelligent Laboratory System, 86 (1),* 26-34.

Hackworth, D. 2013. *Process Optimization of Wastewater Treatment Plants.*
http://www.ohiowea.org/docs/Optimization_Wastewater_Utilities_Hackworth.pdf.

Han, M., De Clippeleir, H., Al-Omari, A., Wett, B., Vlaeminck, S. E., Bott, C., & Murthy, S. 2016. Impact of carbon to nitrogen ratio and aeration regime on mainstream deammonification. *Water Science and Technology, 74 (2),* 375-384.

Hao, X., Heijnen, J. J., & van Loosdrecht, M. C. M. (2002). Sensitivity analysis of a biofilm model describing a one-stage completely autotrophic nitrogen removal (CANON) process. *Biotechnology and Bioengineering, 77 (3)*, 266-277.

Hauduc, H., Rieger, L., Oehmen, A., van Loosdrecht, M. C. M., Comeau, Y., Héduit, A., Vanrolleghem, P. A., & Gillot, S. 2013. Critical review of activated sludge modeling: State of process knowledge, modeling concepts, and limitations. *Biotechnology and Bioengineering, 110 (1),* 24-46.

Hauduc, H., Rieger, L., Takács, I., Héduit, A., Vanrolleghem, P. A., & Gillot, S. 2010. A systematic approach for model verification: Application on seven published activated sludge models. *Water Science and Technology, 61 (4),* 825-839.

Hellinga, C., Schellen, A. A. J. C., Mulder, J. W., van Loosdrecht, M. C. M., & Heijnen, J. J. 1998. The SHARON process: An innovative method for nitrogen removal from ammonium-rich waste water. *Water Science and Technology, 37 (9),* 135-142.

Hellinga, C., van Loosdrecht, M. C. M., & Heijnen, J. J. 1999. Model based design of a novel process for nitrogen removal from concentrated flows. *Mathematical and Computer Modelling of Dynamical Systems, 5 (4),* 351-371.

Henze, M., Dupont, R., Grau, P., & De La Sota, A. 1993. Rising sludge in secondary settlers due to denitrification. *Water Research, 27 (2),* 231-236.

Henze, M., Gujer, W., Mino, T., & van Loosdrecht. M. 2006. *Activated sludge models ASM1, ASM2, ASM2d and ASM3.* Cornwall, UK: IWA Publishing.

Hiatt, W. C., & Grady, C. P. L. 2008. An updated process model for carbon oxidation, nitrification, and denitrification. *Water Environment Resource, 80,* 2145-2156.

Hirata, A., Terada, A., Hibiya, K., & Tsuneda, S. 2003. Simultaneous nitrification and denitrification by controlling vertical and horizontal microenvironment in a membrane aerated biofilm reactor. *Journal of Biotechnology, 100,* 23-32.

Hoekstra, M., Geilvoet, S. P., Hendrickx, T. L. G., van Erp Taalman Kip, C. S., Kleerebezem, R., & van Loosdrecht, M. C. M. 2018. Towards mainstream anammox: Lessons learned from pilot-scale research at WWTP Dokhaven. *Environmental Technology, 40 (13),* 1721-1733.

Holenda, B., Domokos, E., Rédey, Á., & Fazakas, J. 2008. Dissolved oxygen control of the activated sludge wastewater treatment process using model predictive control. *Computers & Chemical Engineering, 32 (6),* 1270-1278.

Huang, X., Mi, W., Hong, N., Ito, H., & Kawagoshi, Y. 2020. Efficient transition from partial nitritation to partial nitritation/Anammox in a membrane bioreactor with activated sludge as the sole seed source. *Chemosphere, 253,* 126719.

Hubaux, N., G. Wells, & Morgenroth, E. 2015. Impact of coexistence of flocs and biofilm on performance of combined nitritation-anammox granular sludge reactors. *Water Research, 68,* 127-139.

Hulsbeek, J. J. W., Kruit, J., Roeleveld, P. J., & van Loosdrecht, M. C. M. 2002. A practical protocol for dynamic modelling of activated sludge systems. *Water Science Technology, 45 (6),* 127-136.

Husin, M., Rahmat, M., Wahab, N. A., & Sabri, M. F. M. 2019. Neural Network Ammonia-based aeration control for activated sludge process wastewater treatment plant. *Proceedings of the 11th National Technical Seminar on Unmanned System Technology.* 471-487.

hydrograv. 2020. *hydrograv adapt at a glance: The main advantages of the height-variable inlet structure.* https://www.hydrograv.com/en/hydrograv-adapt/#benefits-and-details.

International Energy Agency. 2016. *World Energy Outlook 2016.* Paris, France: International Energy Agency.

IPCC. 2019. 2019 Refinement to the 2006 IPCC Guidelines for National Greenhouse Gas Inventories, Chapter 6: Wastewater Treatment and Discharge.

Jeppsson, U. 1996. A General Description of the Activated Sludge Model No. 1 (ASM1). *Modelling aspects of wastewater treatment processes.* PhD Thesis: Lund University, Sweden.

Jimenez, J., Dursun, D., Dold, P., Bratby, J., Keller, J., & Parker, D. 2010. Simultaneous nitrification-denitrification to meet low effluent nitrogen limits: Modeling, performance and reliability. *Proceedings of the Water Environment Federation, 15.* 2404-2421.

Jimenez, J., Wise, G., Regmi, P., Burger, G., Conidi, D., Weiwei, D., & Dold, P. 2020. Nitrite-shunt and biological phosphorus removal at low dissolved oxygen in a full-scale high-rate system at warm temperatures. *Water Environment Research, 92 (8),* 1111-1122.

Jimenez, J., Regmi, P., & Wise, G. 2015. Mainstream nitrite-shunt with biological phosphorus removal using a low dissolved oxygen aeration control. *Proceedings of the Water Environment Federation* 1-6.

Jones, R. M., Bye, C. M., & Dold, P. L. 2005. Nitrification parameter measurement for plant design: Experience and experimental issues with new methods. *Water Science and Technology, 52 (10-11),* 461-468.

Kaelin, D., Manser, R., Rieger, L., Eugster, J., Rottermann, K., & Siegrist, H. 2009. Extension of ASM3 for two-step nitrification and denitrification and its calibration and validation with batch tests and pilot scale data. *Water Research, 43 (6),* 1680-1692.

Kampschreur, M. J., Picioreanu, C., Tan, N., Kleerebezem, R., Jetten, M. S. M., & van Loosdrecht, M. C. M. 2007. Unraveling the source of nitric oxide emission during nitrification. *Water Environment Research, 79 (13),* 2499-2509.

Katebi, R., Johnson, M. A., & Wilkie, J. 1999. *Control and Instrumentation for Wastewater Treatment Plants.* London, UK: Springer London.

Kato, H., Fujimoto, H., & Yamashina, K. 2019 . Operational improvement of main pumps for energy-saving in wastewater treatment plants. *Water, 11 (12),* 2438.

Kazmi, A. A., Fujita, M., & Furumai, H. 2001. Modeling effect of remaining nitrate on phosphorus removal in SBR. *Water Science and Technology, 43 (3),* 175-182.

Keene, N. A., Reusser, S. R., Scarborough, M. J., Grooms, A. L., Seib, M., Domingo, J. S. & Noguera, D. R. 2017. Pilot plant demonstration of stable and efficient high rate biological nutrient removal with low dissolved oxygen conditions. *Water Research, 121,* 72-85.

Kehrein, P., van Loosdrecht, M. C. M., Osseweijer, P., Garfí, M., Dewulf, J., & Posada, J. 2020. A critical review of resource recovery from municipal wastewater treatment plants – market supply potentials, technologies and bottlenecks. *Environmental Science: Water Research & Technology, 6 (4),* 877-910.

Kim, D., Bowen, J. D., & Ozelkan, E. 2015. Optimization of wastewater treatment plant operation for greenhouse gas mitigation. *Journal of Environmental Management, 163,* 39-48.

Kirim, G., McCullough, K., Bressani-Ribeiro, T., Domingo-Félez, C., Duan, H., Al-Omari, A., De Clippeleir, H., Jimenez, J., Klaus, S., Ladipo-Obasa, M., Mehrani, J., Regmi, P., Torfs, E., Volcke, E. I. P., & Vanrolleghem, P. A. 2022. Mainstream short-cut N removal modelling: Current status and perspectives. *Water Science and Technology, 85 (9),* 2539–2564.

Klaus, S., Parsons, M., & Bott, C. 2020a. Mainstream Partial Denitrification/Anammox: Results from Operation in a Full-Scale Deep-Bed Filter. *Proceedings of IWA Nutrient Removal and Recovery Conference 2020,* Helsinki, Finland.

Klaus, S., Sadowski, M. S., Kinyua, M. N., Miller, M. W., Regmi, P., Wett, B., De Clippeleir, H., Chandran, K, & Bott, C. 2020b. Effect of influent carbon fractionation and reactor configuration on mainstream nitrogen removal and NOB out-selection. *Environmental Science: Water Research & Technology, 6, 691-701.*

Klaus, S. 2019. *Intensification of Biological Nutrient Removal Processes.* Virginia, USA: PhD Dissertation, Virginia Polytechnic Institute and State.

Klaus, S., & Bott, C. 2020c. Comparison of sensor driven aeration control strategies for improved understanding of simultaneous nitrification/denitrification. *Water Environment Research, 92 (11),* 1999-2014.

Koch, G., Pianta, R., Krebs, P., & Siegrist, H. 1999. Potential of denitrification and solids removal in the rectangular clarifier. *Water Resource, 33 (2),* 309-318.

Kolisch, G., Osthoff, T., Hobus, I., & Hansen, J. 2008. Increasing the Energy Efficiency of Sewage Plants – Experiences of Energy Analyses carried out in Germany. *IWA Conference 'Water and Energy 2009'*, Copenhagen, Denmark.

Kumar, S. S., & Latha, K. 2021. A supervisory fuzzy logic control scheme to improve effluent quality of a wastewater treatment plant. *Water Science and Technology, 84 (10-11),* 3415-3424.

Kynch, G. 1952. A theory of sedimentation. *Transaction of the Faraday Society, 48,* 166–176.

Lackner, S., & Agrawal, S. 2015. Process fundamentals-microbiology, stoichiometry, kinetics and inhibition. In *Shortcut Nitrogen Removal - Nitrite Shunt and Deammonification*. Water Environment Federation.

Lackner, S., Gilbert, E. M., Vlaeminck, S., Joss, A., Horn, H., & van Loosdrecht, M. C. M. 2014. Full-scale partial nitritation/anammox experiences – An application survey. *Water Research, 55,* 292-303.

Langergraber, G., Rieger, L., Winkler, S., Alex, J., Wiese, J., Owerdieck, C., Ahnert, M., Simon, J., & Maurer, M. 2004. A guideline for simulation studies of wastewater treatment plants. *Water Science and Technology, 50 (7),* 131-138.

Laureni, M., Weissbrodt, D. G., Szivak, I., Robin, O., Nielsen, J. L., Morgenroth, E., & Joss, A. 2015. Activity and growth of anammox biomass on aerobically pre-treated municipal wastewater. *Water Research, 80,* 325-366.

Layer, M., Villodres, M. C., Hernandez, A., Reynaert, E., Morgenroth, E., & Derlon, N. 2020. Limited simultaneous nitrification-denitrification (SND) in aerobic granular sludge systems treating municipal wastewater: Mechanisms and practical implications. *Water Research X, 7,* 100048.

Le, T., Peng, B., Su, C., Massoudieh, A., Torrents, A., Al-Omari, A., Murthy, S., Wett, B., Chandran, K., deBarbadillo, C., Bott, C., & De Clippeleir, H. 2019. Nitrate residual as a key parameter to efficiently control partial denitrification coupling with anammox. *Water Environment Research, 91,* 1455-1465.

Le, T., Peng, B., Su, C., Massoudieh, A., Torrents, A., Al-Omari, A., Murthy, S., Wett, B., Chandran, K., deBarbadillo, C., Bott, C., & De Clippeleir, H. 2018. Impact of carbon source and COD/N on the concurrent operation of partial denitrification and anammox. *Water Environment Research, 91,* 185-197.

Leix, C., Drewes, J. E., Ye, L., & Koch, K. 2017. Strategies for enhanced deammonification performance and reduced nitrous oxide emissions. *Bioresource Technology, 236,* 174-185.

LégisQuébec. 2017. Règlement sur les ouvrages municipaux d'assainissement des eaux usées. *Q-2, r. 34.1 - Règlement sur les ouvrages municipaux d'assainissement des eaux usées*. Québec, Canada. http://legisquebec.gouv.qc.ca/fr/ShowDoc/cr/Q-2,%20r.%2034.1.

Li, B., & Stenstrom, M. K. 2016. A sensitivity and model reduction analysis of one-dimensional secondary settling tank models under wet-weather flow and sludge bulking conditions. *Water Research, 288,* 813-823.

Li, B., & Stenstrom, M. K. 2014. Dynamic one-dimensional modeling of secondary settling tanks and design impacts of sizing decisions. *Water Research, 50,* 160-170.

Li, F., Kirim, G., & Vanrolleghem, P. A. 2019. Characterizing the dynamics of pollutant concentration and biodegradability in raw domestic wastewaters. *Poster presented at the 2e Journée québécoise des étudiants CentrEau.* Québec, QC, Canada.

Li, L., Ling, Y., Wang, H., Chu, Z., Yan, G., Li, Z., & Wu, T. 2020. N2O emission in partial nitritation-anammox process. *Chinese Chemical Letters, 31 (1),* 28-38.

Li, X., Klaus, S., Bott, C., & He, Z. 2018. Status, challenges, and perspectives of mainstream nitritation-anammox for wastewater treatment. *Water Environment Research, 90 (7),* 634-649.

Li, Y., Xu, Y., Fu, Z., Zheng, L., & Li, M. 2021. Assessment of energy use and environmental impacts of wastewater treatment plants in the entire life cycle: A system meta-analysis. *Environmental Research, 198,* 1-13.

Lim, J., Kim, H., Park, S. Y., & Kim, J. H.. 2019. Simultaneous nitrification and denitrification by using ejector type microbubble generator in a single reactor. *Environmental Engineering Research, 25 (2),* 251-257.

Liu, T., Quan, X., & D. Li. 2017. Evaluations of biofilm thickness and dissolved oxygen on single stage anammox process in an up-flow biological aerated filter. *Biochemical Engineering Journal, 119,* 20-26.

Liu, X., Kim, M., Nakhla, G., Andalib, M., & Fang, Y. 2020. Partial nitrification-reactor configurations, and operational conditions: Performance analysis. *Journal of Environmental Chemical Engineering, 8 (4),* 103984.

Lotti, T., Kleerebezem, R., Abelleira-Pereira, J. M., Abbas, B., & van Loosdrecht, M. C. M. 2015. Faster through training: The anammox case. *Water Research, 81,* 261-268.

Lu, W., Zhang, Y., Wang, Q., Wei, Y., Bu, Y., & Ma, B. 2021a. Achieving advanced nitrogen removal in a novel partial denitrification/anammox-nitrifying (PDA-N) biofilter process treating low C/N ratio municipal wastewater. *Bioresource Technology, 340,* 125661.

Lu, W., Ma, B., Wang, Q., Wei, Y., & Zengjian, S. 2021b. Feasibility of achieving advanced nitrogen removal via endogenous denitratation/anammox. *Bioresource Technology, 325,* 124666.

Ma, B., Zhang, S., Zhang, L., Yi, P., Wang, J., Wang, S., & Peng., Y. 2011. The feasibility of using a two-stage autotrophic nitrogen removal process to treat sewage. *Bioresource Technology, 102 (17),* 8331-8334.

Ma, B., Qian, W., Yuan, C., Yuan, Z., & Peng, Y. 2017. Achieving mainstream nitrogen removal through coupling anammox with denitratation. *Environmental Science and Technology, 51 (15),* 8405-8413.

Ma, W. J., Li, G. F., Huang, B. C. & Jin, R. C. 2020. Advances and challenges of mainstream nitrogen removal from municipal wastewater with anammox-based processes. *Water Environment Research, 92,* 1899-1909.

Mannina, G., Ekama, G., Ødegaard, H., & Olsson, G. 2019. *Advances in Wastewater Treatment, ISBN: 9781780409719.* London, UK: IWA Publishing.

Mannina, G., Cosenza, A., Vanrolleghem, P.A. & Viviani, G. 2011. A practical protocol for calibration of nutrient removal wastewater treatment models. *Journal of Hydroinformatics, 13 (4),* 575-595.

McCormick, E. H., & Chakrabarti, A. R. 2013. *The energy roadmap: A water and wastewater utility guide to more sustainable energy management (No. ISBN: 978-1-57278-273-0).* Alexandria, USA: Water Environment Federation.

Medinilla, V. R., Sprague, T., Marseilles, J., Burke, J., Deshmukh, S., Delagah, S., & Sharbatmaleki, M. 2020. Impact of ammonia-based aeration control (ABAC) on energy consumption. *Applied Science, 10 (15),* 5227.

Melcer, H., Dold, P., Jones, R. M., Bye, C. M., Takács, I., Stensel, H. D., Wilson, A. W., Sun, P., & Bury, S. 2004. *Methods for wastewater characterization in activated sludge modelling.* WERF Report 99-WWF-3, Alexandria, VA, USA: Water Environment Research Foundation (WERF).

Metcalf&Eddy. 2014. *Wastewater engineering treatment and resource recovery (fifth edition).* New York, NY: Mc Graw Hill.

Miao, Y., Zhang, L., Yang, Y., Peng, Y., Li, B., Wang, S., & Zhang, Q. 2016. Start-up of single-stage partial nitrification-anammox process treating low-strength swage and its restoration from nitrate accumulation. *Bioresource Technology, 218,* 771-779.

Morales, N., Val del Río, Á., Vázquez-Padín, J. R., Méndez, R., Mosquera-Corral, A., & Campos, J. L. 2015. Integration of the Anammox process to the rejection water and main stream lines of WWTPs. *Chemosphere, 140,* 99-105.

Moussa, M. S., Rojas, A. R., Hooijmans, C. M., Gijzen, H. J., & van Loosdrecht, M. C. M. 2004. Model-based evaluation of nitrogen removal in a tannery wastewater treatment plant. *Water Science and Technology, 50 (6),* 251-260.

Nifong, A., Nelson, A., Johnson, C & Bott, C.. 2013. Performance of a Full-Scale Sidestream DEMON® Deammonification Installation. *Proceedings of the Water Environment Federation 2013 (13).* Water Environment Federation.

Nittami, T., Shoji, T., Koshiba, Y., Noguchi, M., Oshiki, M., Kuroda, M., Kindaichi, T., Fukuda, J., & Kurisu, F. 2019. Investigation of prospective factors that control Kouleothrix (Type 1851) filamentous bacterial abundance and their correlation with sludge settleability in full-scale wastewater treatment plants. *Process Safety and Environmental Protection, 124,* 137-142.

Nourmohammadi, D., Esmaeeli, M. B., Akbarian, H., & Ghasemian, M. 2013. Nitrogen removal in a full-scale domestic wastewater treatment plant with activated sludge and trickling filter. *Journal of Environmental and Public Health,* 504705.

NSF, DOE & EPA. 2015. *Energy-Positive Water Resource Recovery Workshop Report.* Arlington, Virginia: National Science Foundation, U.S. Department of Energy and U.S. Environmental Protection Agency.

Ohandja, D. G., Li, J. F., Ji, J., He, Y. L., Li, Y. Z., & Zhou, T. 2008. Simultaneous nitrification–denitrification achieved by an innovative internal-loop airlift MBR: Comparative study. *Bioresource Technology, 99,* 5867-5872.

Olsson, G. 2012. *Water and energy – Threats and opportunities.* London, UK: IWA Publishing.

Orhon, D., & Artan, N. 1994. *Modelling of Activated Sludge Systems.* Lancaster, Basel: Technomic Publishing Co. Inc.

Ortiz-Martínez, V.M., Martínez-Frutos, J., Hontoria, E., & Egea, J. A. 2021. Multiplicity of solutions in model-based multiobjective optimization of wastewater treatment plants. *Optimization and Engineering, 22,* 1-16.

O'Shaughnessy, M. 2016. *Mainstream Deammonification.* IWA Publishing.

Ostace, S. G., Cristea, V. M., & Agachi, P. S. 2012. Evaluation of different control strategies of the wastewater treatment plant based on a modified Activated Sludge Model No. 3. *Environmental Engineering and Management Journal, 11 (1),* 147-164.

Ostace, S. G., Mircea Cristea, V., & Agachi, P. Ş. 2011. Extension of activated sludge model no 1 with two-step nitrification and denitrification processes for operation improvement. *Environmental Engineering and Management Journal, 10 (10),* 1529-1544.

Palatsi, J., Ripoll, F., Benzal, A., Pijuan, M., & Romero-Güiza, M. S. 2021. Enhancement of biological nutrient removal process with advanced process control tools in full-scale wastewater treatment plant. *Water Research, 200,* 117212.

Pan, Y., Ni, B. J., & Yuan, Z. 2013. Modeling electron competition among nitrogen oxides reduction and N2O accumulation in denitrification. *Environmental Science & Technology, 47,* 11083-11091.

Parker, D. S., Merlo, R. P., Jimenez, J. A. & Wahlberg, E. J. 2008. Analyzing wet weather flow management using state of the art tools. *Water Science and Technology, 57 (8),* 1247-1251.

Peng, L., Xie, Y., Van Beeck, W., Weiqiang, Z., Van Tendeloo, M., Tytgat, T., Lebeer, S., & Vlaeminck, S. E. 2020. Return-sludge treatment with endogenous free nitrous acid limits nitrate production and N2O emission for mainstream partial nitritation/anammox. *Environmental Science and Technology, 54 (9),* 5822-5831.

Pérez, J., Isanta, E. & Carrera, J. 2015. Would a two-stage N-removal be a suitable technology to implement at full scale the use of anammox for sewage treatment? *Water Science and Technology, 72 (6),* 858-865.

Pérez, J., Lotti, T., Kleerebezem, R., Picioreanu, C., & van Loosdrecht, M. C. M. 2014. Outcompeting nitrite-oxidizing bacteria in single-stage nitrogen removal in sewage treatment plants: A model-based study. *Water Research, 66,* 208-218.

Philippe, R. 2018. *Automatic Data Quality Assessment Tools For Continuous Monitoring of Wastewater Quality.* Master Thesis, Université Laval, Québec, QC, Canada.

Plósz, B., Weiss, M., Printemps, C., Essemiani, K., & Meinhold, J. 2007. One-dimensional modelling of the secondary clarifier-factors affecting simulation in the clarification zone and the assessment of the thickening flow dependence. *Water Research, 41 (15),* 3359-3371.

Plosz, B., De Clercq, J., Nopens, I., Benedetti, L. & Vanrolleghem, P. A. 2011. Shall we upgrade one-dimensional secondary settler models used in WWTP simulators? – An assessment of model structure uncertainty and its propagation. *Water Science and Technology, 63 (8)* 1726-1738.

Ponzelli, M., Boisvert, C., Tohidi, M., Walton, J., Santoro, D., Elbeshbishy, E., & Vanrolleghem, P. A. 2019. Carbon and volatile fatty acids recovery in reactive primary clarifier: A pilot case study. *Proceedings of 54th CAWQ Central Canadian Symposium on Water Quality Research.* Toronto, ON, Canada.

Qasim, S. R., & Zhu, G. 2018. *Wastewater Treatment and Reuse, Theory and Design Examples, Volume 1.* Boca Raton, Florida, USA.: CRC Press.

Qi, W., He, C., Zhang, Y., Xu, J., Yang, X. J., & Li, Y. 2016. Optimisation for enriching ammonium oxidizing bacteria in membrane partial nitrification reactor: Mathematical simulation. *Journal of Water Sustainability, 6 (4),* 125-137.

Queralt, P., Alferes, J., Fuks, K., Kraft, T., Maruéjouls, T., Torfs, E., Vanrolleghem, P. A. 2017. datEAUbase: Water Quality Database for Raw and Validated Data with Emphasis on Structured Metadata. *Proceeding of 12th IWA Specialized Conference on Instrumentation, Control and Automation.* Québec, QC, Canada.

Ramin, E., Wágner, D. S., Yde, L., Binning, P. J., Rasmussen, M. R., Mikkelsen, P. S., & Plósz, B. G. 2014a. A new settling velocity model to describe secondary sedimentation. *Water Research, 66,* 447-458.

Ramin, E., Sin, G., Mikkelsen, P. S., & Plósz, B. G. 2014b. Significance of settling model structures and parameter subsets in modelling WWTPs under wet-weather flow and filamentous bulking conditions. *Water Research, 63,* 205-214.

Ramin, E. 2014. *Modelling of secondary sedimentation under wet weather and filamentous bulking conditions.* Lyngby: DTU Environment, PhD Thesis: Technical University of Denmark.

Ramirez, M. 2015. Report from the field: Nutrient and energy recovery at DC Water. *Technological State of the Art Panel at the Hydrogen, Hydrocarbons, and Bioproduct Precursors from Wastewaters Workshop.* Washington DC, USA.

Regmi, P., Holgate, B., Fredericks, D., Miller, M. W., Wett, B., Murthy, S., & Bott, C. 2014a. A pilot-scale mainstream nitritation-denitritation process followed by an anammox MBBR operated within wide range of operating conditions. *Proceedings of IWA World Water Congress, 21-26 September,* Lisbon, Portugal.

Regmi, P., Miller, M. W., Holgate, B., Bunce, R., Park, H., Chandran, K., Wett, B., Murthy, S. & Bott, C. 2014b. Control of aeration, aerobic SRT and COD input for mainstream nitritation/denitritation. *Water Research, 57 (15),* 162-171.

Regmi, P., Holgate, B., Fredericks, D., Miller, M. W., Wett, B., Murthy, S., & Bott, C. 2015. Optimization of a mainstream nitritation-denitritation process and anammox polishing. *Water Science and Technology, 72 (4),* 632-642.

Regmi, P., & Jimenez, J. 2018. A model based study: Revisiting conventional BNR configurations with advanced aeration control. *Proceedings of WEFTEC 2018,* 2531-2533, Water Environment Federation, New Orleans, LA, USA.

Revollar, S., Vilanova, R., Vega, P., Francisco, M., & Meneses, M. 2020. Wastewater treatment plant operation: simple control schemes with a holistic perspective. *Sustainability, 12 (3),* 768-796.

Revollar, S., Vilanova, R., Francisco, M., & Vega, P. 2018. PI dissolved oxygen control in wastewater treatment plants for plantwide nitrogen removal efficiency. *IFAX Papers OnLine, 51 (4),* 450-455.

Richardson, D., Felgate, H., Watmough, N., Thomson, A., & Baggs, E. 2009. Mitigating release of the potent greenhouse gas N2O from the nitrogen cycle - Could enzymic regulation hold the key? *Trends Biotechnology, 27 (7),* 388-397.

Rieger, L., Takács, I., Villez, K., Siegrist, H., Lessard, P., Vanrolleghem, P. A., & Comeau, Y. 2010. Data reconciliation for wastewater treatment plant simulation studies - Planning for high-quality data and typical sources of errors. *Water Environment Research, 82 (5),* 426-433.

Rieger, L., Jones, R. M., Dold, P., & Bott, C. 2014. Ammonia-based feedforward and feedback aeration control in activated sludge processes. *Water Environment Research, 86 (1),* 63-73.

Rieger, L., Gillot, S., Langergraber, G., Ohtsuki, T., Shaw, A., Takács, I., & Winkler, S. 2012. *Guidelines for Using Activated Sludge Models.* London, UK: IWA.

Rivas, A., Irizar, I., & Ayesa, E. 2008. Model-based optimisation of Wastewater Treatment Plants design. *Environmental Modelling & Software, 23 (4),* 434-450.

Rossetti, S., Tomei, M. C., Nielsen, P. H., & Tandoi, V. 2005. "Microthrix parvicella", a filamentous bacterium causing bulking and foaming in activated sludge systems: A review of current knowledge. *FEMS Microbiology Reviews, 29,* 49-64.

Rosso, D., Iranpour, R., & Stenstrom, M. K. 2005. Fifteen years of offgas transfer efficiency measurements on fine-pore aerators: Key role of sludge age and normalized air flux. *Water Environment Research, 77 (3),* 266-273.

Rosso, D., Larson, L. E., & Stenstrom, M. K. 2008. Aeration of large-scale municipal wastewater treatment plants: State of the art. *Water Science and Technology, 57 (7),* 973-978.

Rosso, D., Lothman, S. E., Jeung, M. K., Pitt, P., James Gellner, W., Stone, A. L., & Howard, D. 2011. Oxygen transfer and uptake, nutrient removal, and energy footprint of parallel full-scale IFAS and activated sludge processes. *Water Research 45 (18),* 5987-5996.

Ruano, V., Ribes, J., De Pauw, D. J. W., & Sin, G. 2007. Parameter subset selection for the dynamic calibration of activated sludge models (ASMs): Experience versus systems analysis. *Water Science and Technology, 56 (8),* 107-115.

Sadowski, M. S. 2015. Comparison of Aeration Strategies for Optimization of Nitrogen Removal in an Adsorption/Bio-oxidation Process with an Emphasis on Ammonia vs. NOx Control. MSc Thesis: Virginia Polytechnic Institute and State University, Virginia, VA, USA.

Salem, S., Berends, D., Heijnen, J. J., & van Loosdrecht, M. C. M. 2002. Model-based evaluation of a new upgrading concept for N-removal. *Water Science and Technology, 45 (6),* 169-176.

Salmistraro, M., Fernández, I., Dosta, J., Plaza, E., & Mata, J. 2017. Mainstream deammonification: Preliminary experience employing granular AOB-enriched biomass at low DO values. *Water, Air & Soil Pollution, 228 (5),* 178.

Saltelli, A., Ratto, M., Andres, T., Campolongo, F., Cariboni, J., Gatelli, D., Saisana, M., & Tarantola, S. 2008. *Global Sensitivity Analysis. The Primer, ISBN: 9780470059975.* Chichester, UK: John Wiley & Sons, Ltd.

Sawyer, C. N., & McCarty, P. L. 1978. *Chemistry for Environmental Engineering.* Newyork, USA: McGraw-Hill Inc.

Schlegel, S. 1992. Operational results of waste water treatment plants with biological N and N elimination. *Water Science and Technology, 25 (4-5),* 241-247.

Schraa, O., Rieger, L., Alex, J., & Miletić, I. 2019. Ammonia-based aeration control with optimal SRT control: improved performance and lower energy consumption. *Water Science and Technology, 79 (1),* 63-72.

Seifi, M., & Fazaelipoor, M. H. 2012. Modeling simultaneous nitrification and denitrification (SND) in a fluidized bed biofilm reactor. *Applied Mathematical Modelling, 36 (11),* 5603-5613.

Seyfried, C. F., Hippen, A., Helmer, C., Kunst, S. & Rosenwinkel, K. 2011. One-stage deammonification: nitrogen elimination at low costs. *Water Science and Technology: Water Supply, 1 (1),* 71-80.

Shourjeh, M. S., Kowal, P., Lu, X., Xie, L., & Drewnowski, J. 2021. Development of strategies for AOB and NOB competition supported by mathematical modeling in terms of successful deammonification implementation for energy-efficient WWTPs. *Processes, 9 (3),* 562-587.

Siegrist, H., Krebs, P., Bühler, R., Purtschert, I., Röck, C., & Rufer, R. 1995. Denitrification in secondary clarifiers. *Water Science and Technology, 31 (2),* 205-214.

Sin, G., Van Hulle, S. W. H., De Pauw, D. J. W., van Griensven, A., & Vanrolleghem, P. A. 2005. A critical comparison of systematic calibration protocols for activated sludge models: A SWOT analysis. *Water Research, 39,* 2459-2474.

Sin, G., & Vanrolleghem, P. A. 2006. Evolution of an ASM2d-like model structure due to operational changes of an SBR process. *Water Science and Technology, 53 (12),* 237-245.

Sin, G., Kaelin, D., Kampschreur, M. J., Takács, I., Wett, B., Gernaey, K. V., Rieger, L., Siegrist, H., & van Loosdrecht, M. C. M. 2008a. Modelling nitrite in wastewater treatment systems: A discussion of different modelling concepts. *Water Science and Technology, 58 (6)* 1155-1171.

Sin, G., Weijma, J., Spanjers, H., & Nopens, I. 2008b. Dynamic model development and validation for a nitrifying moving bed biofilter: Effect of temperature and influent load on the performance. *Process Biochemistry, 43 (4),* 384-397.

Sin, G., Gernaey, K. V., Neumann, M. B., van Loosdrecht, M. C. M., & Gujer, W. 2009. Uncertainty analysis in WWTP model applications: A critical discussion using an example from design. *Water Research, 43 (11),* 2894-2906.

SOR/2012-139. 2012. Wastewater Systems Effluent Regulations. http://laws-lois.justice.gc.ca/eng/regulations/SOR-2012-139/FullText.html.

Souidi, R., Kirim, G., & Vanrolleghem, P. A. 2018. *Caractérisations hydrauliques d'une station d'épuration pilote par boue activée : Back mixing.* Québec, QC, Canada: Internship Report, Université Laval.

Stewart, H. A., Al-Omari, A., Bott, C., De Clippeleir, H., Su, T., Takács, I., Wett, B., Massoudieh, A., & Murthy, S. 2017. Dual substrate limitation modeling and implications for mainstream deammonification. *Water Research, 116,* 95-105.

Sweetapple, C., Fu, G., & Butler, D. 2014. Multi-objective optimisation of wastewater treatment plant control to reduce greenhouse gas emissions. *Water Research, 55,* 52-62.

Takács, I., Patry, G., & Nolasco, D. 1991. A dynamic model for the clarification-thickening process. *Water Research, 25 (10),* 1263-1271.

Tao, X., & Chengwen, W. 2012. Energy Consumption in Wastewater Treatment Plants in China. *World Congress on Water, Climate and Energy.* Dublin, Ireland.

Tohidi, M. 2019. *Titrimetric monitoring of chemical equilibrium and pH dynamics in the pilot scale treatment plant: Using PHREEQC and buffer capacity methodology.* Québec, QC: Master Thesis, Université Laval.

Tomaszewski, M., Cema, G., & Ziembinska-Buczynska, A. 2017. Influence of temperature and pH on the anammox process: A review and meta-analysis. *Chemosphere, 182,* 203-214.

Torfs, E., Balemans, S., Locatelli, F., Diehl, S., Bürger, R., Laurent, J, Francois, P., & Nopens, I. 2017. On constitutive functions for hindered settling velocity in 1-D settler models: Selection of appropriate model structure. *Water Research, 110,* 38-47.

Torfs, E., Maere, T., Bürger, R., Diehl, S., & Nopens, I. 2015. Impact on sludge inventory and control strategies using the benchmark simulation model no. 1 with the Bürger-Diehl settler model. *Water Science and Technology, 71 (10),* 1524-1535.

Torfs, E. 2015. *Different settling regimes in secondary settling tanks: experimental process analysis, model development and calibration.* PhD Thesis, Ghent University, Ghent, Belgium.

Trapote, A., Albaladejo, A., & Simon, P. 2014. Energy consumption in an urban wastewater treatment plant: the case of Murcia Region (Spain). *Civil Engineering and Environmental Systems, 4,* 304-310.

Trojanowicz, K., Plaza, E., & Trela, J. 2017. Model extension, calibration and validation of partial nitrition–anammox process in moving bed biofilm reactor (MBBR) for reject and mainstream wastewater. *Environmental Technology, 40 (9),* 1079-1100.

U.S. Department of Energy. 2017. *Energy Data Management Manual for Wastewater Treatment Sector DOE/EE-1700.* United States Government.

UNEP. 2001. *Lakes and Reservoirs vol. 3 Water Quality: The Impact of Eutrophication.*

Unicef. 2021. *Water, Sanitation and Hygiene (WASH).* https://www.unicef.org/wash.

Valverde Pérez, B., Mauricio-Iglesias, M., & Sin, G. 2016. Systematic design of an optimal control system for the SHARON-Anammox process. *Journal of Process Control, 39,* 1-10.

Van Dongen, L., Jetten, M. S. M. & van Loosdrecht, M. C. M. 2001. *The combined SHARON/Anammox process.* London: IWA Publishing, UK.

Van den Akker, B., Beard, H., Kaeding, U., Giglio, S., & Short, M. D. 2010. Exploring the relationship between viscous bulking and ammonia-oxidiser abundance in activated sludge: A comparison on conventional and IFAS systems. *Water Research, 44 (9),* 2919-2929.

Van Hulle, S. (2005). *Modelling, Simulation and Optimization of Autotrophic Nitrogen Removal Processes.* Ghent, Belgium: PhD Thesis, Ghent University.

Van Hulle, S. W. H., Volcke, E. I. P., López Teruel, J., Donckels, B., van Loosdrecht, M. C. M., & Vanrolleghem, P. A. 2007. Influence of temperature and pH on the kinetics of the Sharon nitrition process. *Journal of Chemical Technology and Biotechnology, 82 (5),* 471-480.

Vaneeckhaute, C., Lebuf, V., Michels, E., Belia, E., Vanrolleghem, P. A., Tack, F. M. G., & Meers, E. 2017. Nutrient recovery from digestate: Systematic technology review and product classification. *Waste Biomass Valorization, 8,* 21-40.

Vanhooren, H., Meirlaen, J., Amerlinck, Y., Claeys, F., Vangheluwe, H., & Vanrolleghem, P. A. 2003. WEST: modelling biological wastewater treatment. *Journal of Hydroinformatics, 5(1),* 27-50.

Vanrolleghem, P., Van Daele, M. & Dochain, D. (1995). Practical identifiability of a biokinetic model of activated sludge respiration. *Water Research, 29*, 2561-2570.

Vanrolleghem, P. A., & Vaneeckhaute, C. 2014. Resource Recovery from Wastewater and Sludge: Modelling and Control Challenges. Proceeding of *Global Challenges: Sustainable Wastewater Treatment and Resource Recovery, IWA Specialist Conference.* Kathmandu, Nepal.

Vanrolleghem, P. A., & Gillot, S. 2002. Robustness and economic measures as control benchmark performance criteria. *Water Science and Technology, 45 (4-5),* 117-126.

Vanrolleghem, P. A., Insel, G., Petersen, B., Sin, G., De Pauw, D., Nopens, I., Weijers, S., & Gernaey, K. V. 2003. A Comprehensive Model Calibration Procedure for Activated Sludge Models. *Proceedings WEFTEC 2003, 76th Annual Exhibition and Conference.* Los Angeles, CA, USA.

Veuillet, F., Zozor, P., Stefansdottir, D., Christensson, M., Skonieczny, T., Ochoa, J., & Lemaire, R. 2015. Mainstream deammonification using ANITA™Mox Process. *Proceedings of IWA Specialist Conference Nutrient Removal and Recovery: Moving innovation into practice.* Gdańsk, Poland.

Volcke, E. I. P., Picioreanu, C., De Baets, B., & van Loosdrecht, M. C. M. 2012. The granule size distribution in an anammox-based granular sludge reactor affects the conversion - Implications for modeling. *Biotechnology and Bioengineering, 109 (7),* 1629-1636.

Volcke, E. I. P., Gernaey, K. V., Vrecko, D., Jeppsson, U., van Loosdrecht, M.C.M., & Vanrolleghem, P. A. 2006. Plant-wide (BSM2) evaluation of reject water treatment with a SHARON-Anammox process. *Water Science and Technology, 54 (8),* 93-100.

Volcke, E. I. P., Sbarciog, M., Loccufier, M., Vanrolleghem, P. A., & Noldus, E. J. L. 2007. Influence of microbial growth kinetics on steady state multiplicity and stability of a two-step nitrification (SHARON) model. *Biotechnology and Bioengineering, 98 (4),* 882-893.

Volcke, E. I. P., Van Hulle, S., Donckels, B. M. R., & Vanrolleghem, P. A. 2005. Coupling the SHARON process with anammox: Model-based scenario analysis with focus on operating costs. *Water Science and Technology, 52 (4),* 107–115.

Volcke, E. I. P., Hellinga, C., Van Den Broeck, S., van Loosdrecht, M. C. M., & Vanrolleghem, P. A. 2002. Modelling the Sharon process in the view of coupling with anommox. *Proceedings of 1st IFAC International Scientific and Technical Conference on Technology, Automation and Control of Wastewater and Drinking Water Systems (TiASWiK'02)*, 19-21, Gdańsk, Poland.

Wałęga, A., Chmielowski, K., & Młyński, D. 2019. Nitrogen and phosphorus removal from sewage in biofilter – activated sludge combined systems. *Polish Journal of Environmental Studies, 28 (3),* 1939-1947.

Wang, D., Wang, Q., Laloo, A., Xu, Y., Bond, P. L., & Yuan, Z. 2016. Achieving stable nitration for mainstream deammonification by combining free nitrous acid-based sludge treatment and oxygen limitation. *Scientific Reports, 6, 25547.*

Wang, J., Gong, B., Wang, Y., Wen, Y., Zhou, J., & He, Q. 2017. The potential multiple mechanisms and microbial communities in simultaneous nitrification and denitrification process treating high carbon and nitrogen concentration saline wastewater. *Bioresource Technology, 243,* 708-715.

Wang, L., Shammas, N., & Hung, Y. T. 2009. *Advanced Biological Treatment Processes.* New York, NY, USA: Humana Press.

Wang, Q., Duan, H., Wei, W., Ni, B. J., Laloo, A., & Yuan, Z. 2017. Achieving stable mainstream nitrogen removal via the nitrite pathway by sludge treatment using free ammonia. *Environmental Science and Technology, 51 (17),* 9800-9807.

Wang, X., Zhao, J., Yu, D., Du, S., Yuan, M., & Zhen, J. 2019. Evaluating the potential for sustaining mainstream anammox by endogenous partial denitrification and phosphorus removal for energy-efficient wastewater treatment. *Bioresource Technology, 284,* 302-314.

WEF. 2010. *Energy Conservation in Water and Wastewater Facilities, MOP-32.* Alexandria, VA.: WEF Press.

WEF. 2009. *Energy conservation in water and wastewater facilities. Prepared by the Energy Conservation in Water and Wastewater Treatment Facilities Task Force of the Water Environment Federation.* New York: McGraw Hill.

WEF. 2013. *The Energy Roadmap: A Water and Wastewater Utility Guide to More Sustainable Energy Management.* VA, USA: The Water Environment Federation.

WEF. 2015. *The Nutrient Road Map.* VA, USA: Water Environment Federation.

WEF. 2020. *Wastewater Treatment And Water Resource Recovery Facilities (WRRFs).* 09 October. https://www.wbdg.org/resources/wastewater-treatment-and-water-resource-recovery-facilities-wrrfs.

Weijers, S.R., & Vanrolleghem, P. A. 1997. A procedure for selecting best identifiable parameters in calibrating activated sludge model no.1 to full-scale plant data. *Water Science and Technology, 36 (5),* 69-79.

WERF & NYSERDA. 2015. *Guide to Net Zero Energy Solutions for Water Resource Recovery Facilities, Executive Summary.* Water Environment Research Foundation and New York State Energy Research & Development Authority.

WERF. 2010. *Overview of state of the energy reduction programs and guidelines for the wastewater sector.* Alexandria, VA, USA: Water Environment Research Foundation.

Wett, B., Al-Omari, A., Podmirseg, S. M., Akintayo, O., Gomez Brandon, M., Murthy, S., Bott, C., Hell, M., Takács, I., Nyhuis, G., & O'Shaughnessy, M. 2013. Going for mainstream deammonification from bench to full scale for maximized resource efficiency. *Water Science and Technology, 68 (2),* 283-289.

Wett, B., Nyhuis, G., Takács, I., & Murthy, S. 2010. Development of enhanced deammonification selector. *Proceedings of the Water Environment Federation, 2010 (10).* Water Environment Federation. 5917 - 5926.

Wicklein, E., & Samstag, R. 2009. Comparing Commercial and Transport CFD Models for Secondary Sedimentation. *Proceedings of 82th Annual Water Environment Federation Technical Exhibition and Conference (WEFTEC).* Chicago, Illinois, USA.

World Bank. 2019. *From Waste to Resource.* Washington: International Bank for Reconstruction and Development/The World Bank.

World Bank. 2020. *Wastewater a Resource that Can Pay Dividends for People, the Environment, and Economies, Says World Bank.* 19 March. https://www.worldbank.org/en/news/press-release/2020/03/19/wastewater-a-resource-that-can-pay-dividends-for-people-the-environment-and-economies-says-world-bank.

Wu, J., He, C., van Loosdrecht, M. C. M., & Pérez, J. 2016. Selection of ammonium oxidizing bacteria (AOB) over nitrite oxidizing bacteria (NOB) based on conversion rates. *Chemical Engineering, 304,* 953-961.

Yang, Q., Shen, N., Lee, Z. M.-P., Xu, G., Cao, Y., Kwok, B., Lay, W., Liu, Y., & Zhou, Y. 2016. Simultaneous nitrification, denitrification and phosphorus removal (SNDPR) in a full-scale water reclamation plant located in warm climate. *Water Science and Technology, 74 (2),* 448-456.

Yoo, K., Ahn, K.-H,. Lee, H.-J., Lee, K.-H., Kwak, Y.-J., & Song, K.-G. 1999. Nitrogen removal from synthetic wastewater by simultaneous nitrification and denitrification (SND) via nitrite in an intermittently-aerated reactor. *Water Research, 33 (1),* 145-154.

Zaman, M., Kim, M., & Nakhla, G. 2021. Simultaneous partial nitrification and denitrifying phosphorus removal (PNDPR) in a sequencing batch reactor process operated at low DO and high SRT for carbon and energy reduction. *Chemical Engineering Journal, 425,* 131881.

Zekker, I., Rikmann, E., Tenno, T., Saluste, A., Tomingas, M., Menert, A., Loorits, L., Lemmiksoo, V., & Tenno, T. 2012. Achieving nitritation and anammox enrichment in a single moving-bed biofilm reactor treating reject water. *Environmental Technology, 33 (4-6),* 703-710.

Zeng, R. J., Lemaire, R., Yuan, Z., & Keller, J. 2003. Simultaneous nitrification, denitrification, and phosphorus removal in a lab-scale sequencing batch reactor. *Biotechnology and Bioengineering, 84 (2),* 170-179.

Zhang, D., Li, Z., Lu, P., Zhang, T., & Xu, D. 2006. A method for characterizing the complete settling process of activated sludge. *Water Research, 40 (14),* 2637-2644.

Zhang, M., Wang, S., Ji, B., & Liu, Y. 2019. Towards mainstream deammonification of municipal wastewater: Partial nitrification-anammox versus partial denitrification-anammox. *Science of the Total Environment, 692,* 394-400.

Zhang, X. X., Zhao, D. Y., Wang, Z. X., Wu, B., Liw, X., & Cheng, S. P. 2009. Environmental biological model based on optimization of activated sludge process. *International Journal of Environmental Science & Technology, 61 (6)*, 69-76.

Zhang, X., Zhang, H., Ye, C., Wei, M., & Du, J. 2015. Effect of COD/N ratio on nitrogen removal and microbial communities of CANON process in membrane bioreactors. *Bioresource Technology, 189,* 302-308.

Zhang, Z., Zhang, Y., & Chen, Y. 2020. Recent advances in partial denitrification in biological nitrogen removal: From enrichment to application. *Bioresource Technology, 298,* 122444.

Zhao, Y., & Vanrolleghem, P. A. 2015. *Start-up of a highly instrumented pilot wastewater treatment plant with advanced process control.* Québec, QC, Canada: Internship Report, Université Laval.

Zheng, M., Wu, S., Zuo, Z., Wang, Z., Qiu, Y., Liu, Y.-C., Huang, X., & Yuan, Z. 2018. Predictions of the influent and operational conditions for partial nitritation with a model incorporating pH dynamics. *Environmental Science and Technology, 52,* 6457-6445.

Zhu, A., Guo, J., Ni, B.-J., Wang, S., Yang, Q., & Peng, Y. 2015. A novel protocol for model calibration in biological wastewater treatment. *Scientific Reports, 5,* 8493.

Appendix I – Reactive Settler Model Details

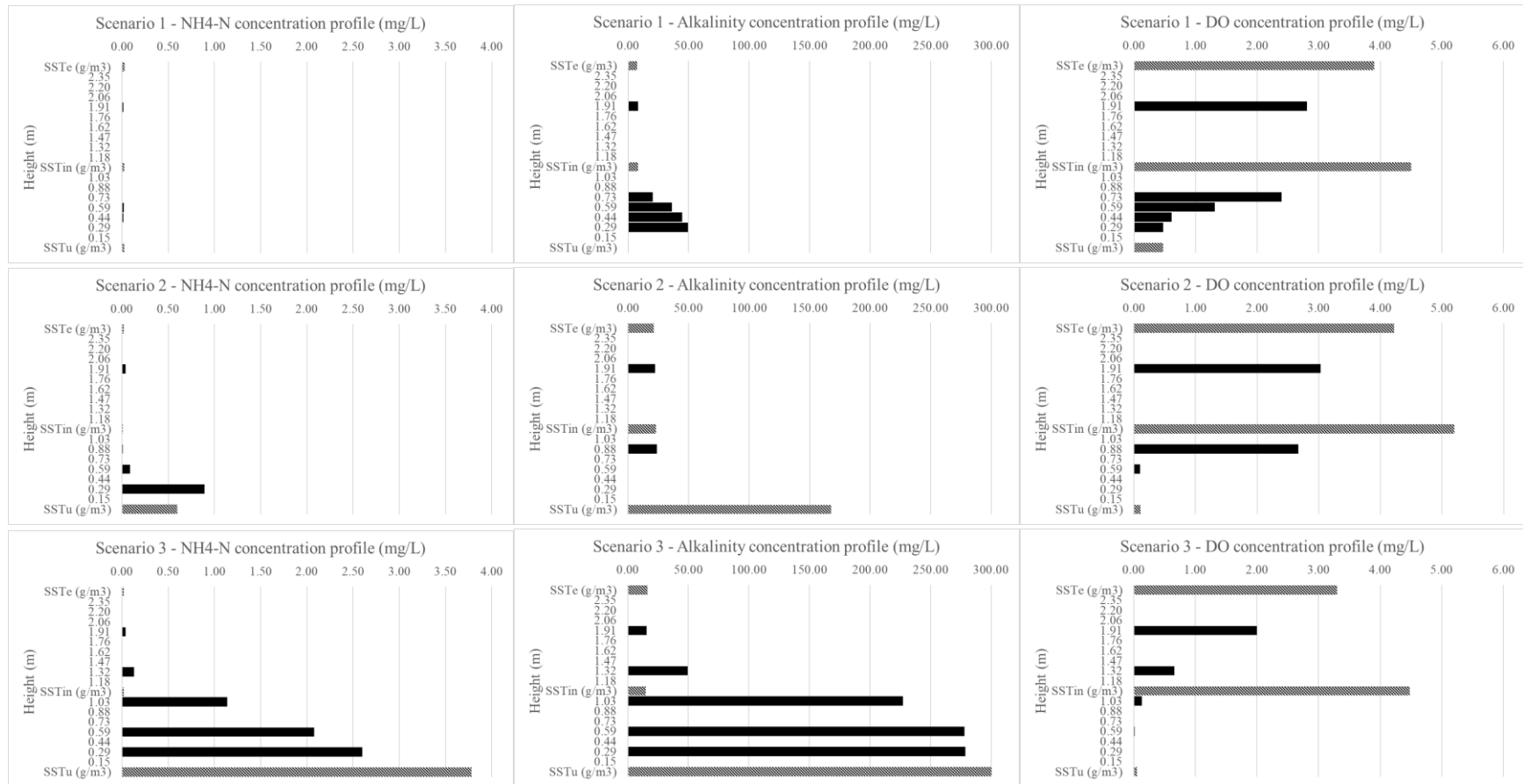## Reactive Settler Measurement Campaign Results

Figure 1. Measurement Results for NH₄-N* (left), alkalinity (middle) and DO (right) for the 3 Tested Operational Scenario**

*Missing measurements in Scenario 1 at heights 0.73 m. and 0.29 m.

**Missing measurements in Scenario 1 underflow and Scenario 2 at heights 0.59 m. and 0.29 m.

Clarifier Geometry Implementation

To improve model predictions, the actual clarifier geometry was implemented in the proposed settler model in order to correct for the model structural error originating from the constant area assumption. New model parameters were added to define the layer where the conic shape of the SST starts (N_c), the radius at the top cone layer (r) as well as the radius of the SST at the bottom outflow (r_b). The surface area and volume of the layers in the conic section of the bottom can now be calculated by considering their conical frustum geometry (Figure 2) as part of the model. The model first calculates the radius at the top of each layer (r_i) based on the radius (r) at the top cone layer (N_c), bottom layer (N_b) and the location of the relevant layer itself in between those two, then calculates its surface area (A_i) and volume (V_i). Thus, r, r_b, N_c, N_b are user-defined parameters that are used to calculate the surface area and volume of each layer in the conic part of the SST. For instance, for layer N_i, the radius of the relevant layer is r_i and the radius of the layer below becomes r_{i+1}. The volume of the layer is calculated as in Figure 2 (h is the height of each layer). The calculated surface area and volume for each layer can then be applied directly to the mass balance equations (Figure 3).
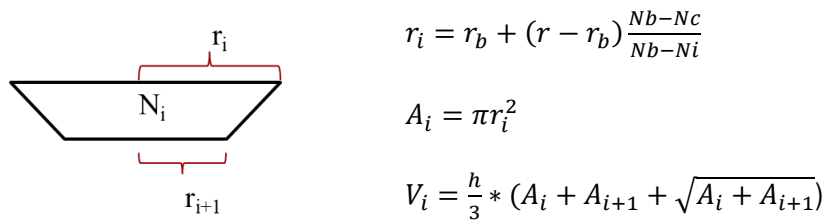

$$r_i = r_b + (r - r_b)\frac{Nb - Nc}{Nb - Ni}$$

$$A_i = \pi r_i^2$$

$$V_i = \frac{h}{3} * (A_i + A_{i+1} + \sqrt{A_i + A_{i+1}})$$

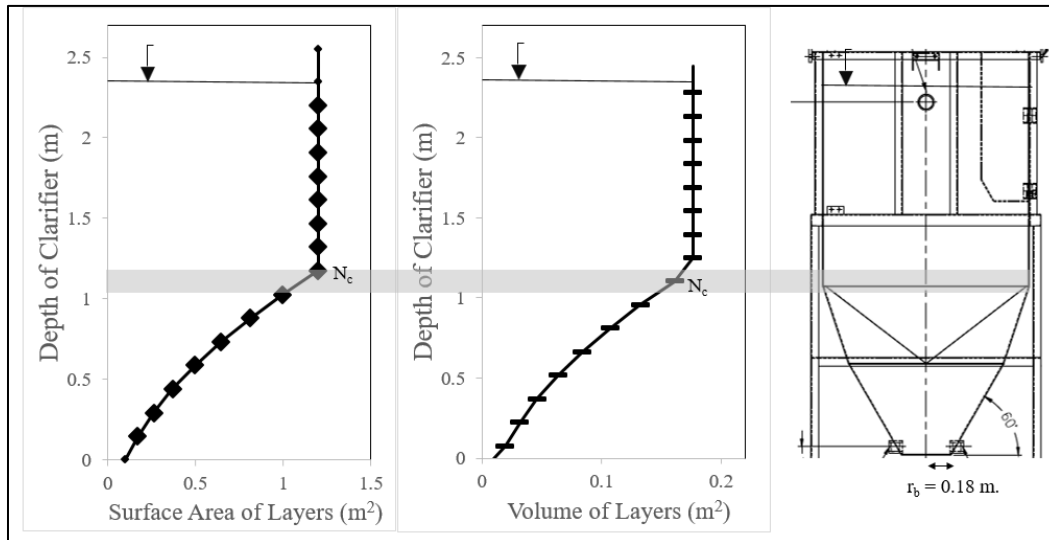**Figure 2. Volume Calculation for a Layer in the Conic Part of the SST**

Figure 3. Varying Surface Area and Volume of each Layer Calculated by the Model and Actual Shape of the SST of the Study

Mass Balance in Each Layer of the Reactive SST Model

N, j: Number of layer

i: Model component

A: Surface area of the layer

V: Volume of the layer

JG: Godunov flux

C: Concentration of the relevant model component

X: Sum of concentration of particulate model components

$f_{TSS/COD}$: Fraction TSS/COD

$Q_{outflow}$: Effluent flowrate

$Q_{underflow}$: Under flowrate

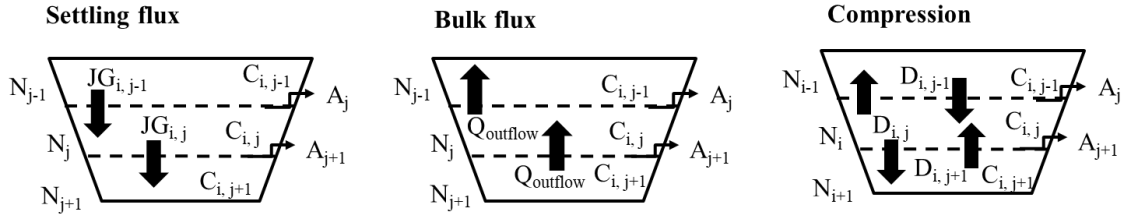r: Biokinetic reactions

- **Mass Balance Above Feed Layer:**

Figure 4. Schematic Representation of the Solids Mass Balance for Layers above the Feed Layer

Equation 1. Solids Mass Balance for Layers above the Feed Layer

$$\frac{dC_i}{dt} = \frac{1}{V_i} * \left(\begin{array}{c} \left(A_i * JG_{i-1} * \frac{C_{i-1}}{X_{i-1}} * f\frac{TSS}{COD} \right) - \left(A_{i+1} * JG_i * \frac{C_i}{X_i} * f\frac{TSS}{COD} \right) - (Q_{outflow} * C_i) + (Q_{outflow} * C_{i+1}) \\ + \left(\frac{1}{V_i} * \left(D_{i-1} * A_i^2 * \frac{C_{i-1}}{X_{i-1}} * f\frac{TSS}{COD} + D_{i+1} * A_{i+1}^2 * \frac{C_{i+1}}{X_{i+1}} * f\frac{TSS}{COD} - D_i * A_i^2 * \frac{C_i}{X_i} * f\frac{TSS}{COD} - D_i * A_{i+1}^2 * \frac{C_i}{X_i} * f\frac{TSS}{COD} \right) \right) \end{array} \right) + r_i$$
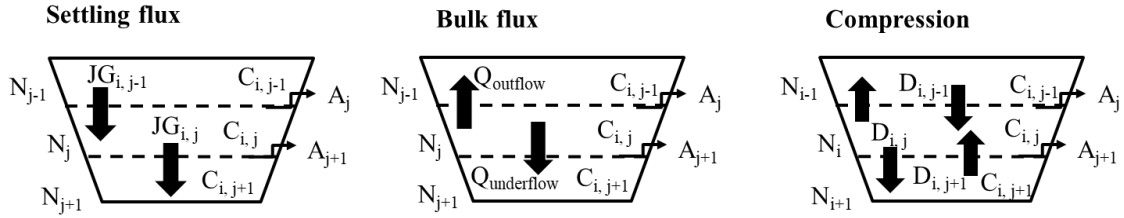
- **Mass Balance Of Feed Layer:**

Figure 5. Schematic Representation of the Solids Mass Balance for the Feed Layer

Equation 2. Solids Mass Balance for the Feed Layer

$$\frac{dC_i}{dt} = \frac{1}{V_i} * \left(\begin{array}{c} \left(A_i * JG_{i-1} * \frac{C_{i-1}}{X_{i-1}} * f\frac{TSS}{COD} \right) - \left(A_{i+1} * JG_i * \frac{C_i}{X_i} * f\frac{TSS}{COD} \right) - \left((Q_{outflow} + Q_{underflow}) * C_i \right) \\ + \left(\frac{1}{V_i} * \left(D_{i-1} * A_i^2 * \frac{C_{i-1}}{X_{i-1}} * f\frac{TSS}{COD} + D_{i+1} * A_{i+1}^2 * \frac{C_{i+1}}{X_{i+1}} * f\frac{TSS}{COD} - D_i * A_i^2 * \frac{C_i}{X_i} * f\frac{TSS}{COD} - D_i * A_{i+1}^2 * \frac{C_i}{X_i} * f\frac{TSS}{COD} \right) \right) \end{array} \right) + r_i$$
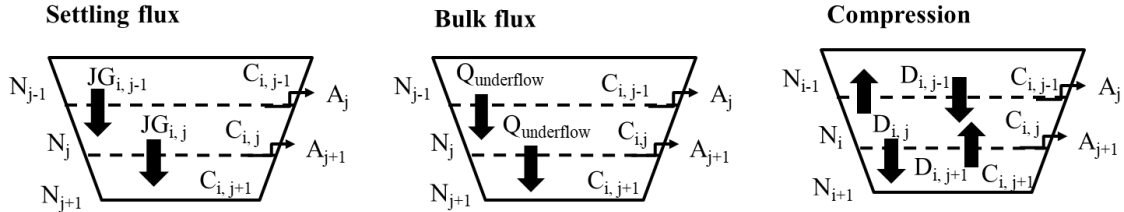
- **Mass Balance Below Feed Layer:**

Figure 6. Schematic Representation of the Solids Mass Balance for Layers below the Feed Layer

Equation 3. Solids Mass Balance for Layers below the Feed Layer

$$\frac{dC_i}{dt} = \frac{1}{V_i} * \left(\begin{array}{c} \left(A_i * JG_{i-1} * \frac{C_{i-1}}{X_{i-1}} * f\frac{TSS}{COD} \right) - \left(A_{i+1} * JG_i * \frac{C_i}{X_i} * f\frac{TSS}{COD} \right) + (Q_{underflow} * C_{i-1}) - (Q_{underflow} * C_i) \\ + \left(\frac{1}{V_i} * \left(D_{i-1} * A_i^2 * \frac{C_{i-1}}{X_{i-1}} * f\frac{TSS}{COD} + D_{i+1} * A_{i+1}^2 * \frac{C_{i+1}}{X_{i+1}} * f\frac{TSS}{COD} - D_i * A_i^2 * \frac{C_i}{X_i} * f\frac{TSS}{COD} - D_i * A_{i+1}^2 * \frac{C_i}{X_i} * f\frac{TSS}{COD} \right) \right) \end{array} \right) + r_i$$

Appendix II – Biokinetic Model Calibration Details

Pre-selection of the Model Parameters (5.6.1)

Table 1. Biokinetic Model Parameters (Pre-selected model parameters for calibration is shown in grey)

Name	Default Value	Description	Unit
Group: Composition			
i_N_BM	0.0583	Mass of Nitrogen Per Mass of COD in Biomass	gN/gCOD
i_N_XI	0.02	Mass of Nitrogen Per Mass of COD in Particulate Inert Products Formed	-
Group: Conversion factors			
F_BOD_COD	0.65	Fraction BOD/COD	-
F_TSS_COD	0.75	Fraction TSS/COD	-
Group: Kinetics			
K_HNO2_NO	0.000872	Nitrous Acid Half-Saturation Coefficient for NO Oxidizing Autotrophic Biomass	gCOD/m3
K_NH3_NH	0.75	Ammonia Half-Saturation Coefficient for NH4 Oxidizing Autotrophic Biomass	gNH3-N/m3
K_NH_AN	0.07	Ammonia Half-Saturation Coefficient for Anammox Biomass	gNH3-N/m3
K_NO2_AN	0.05	Nitrite Half-Saturation Coefficient for Anammox Biomass	gCOD/m3
K_NO2_AN_I	20	Nitrite Inhibition Coefficient for Anammox Biomass	g/m3
K_NO2_H	1	Nitrite Half-Saturation Coefficient for Denitrifying Heterotrophic Biomass	gCOD/m3
K_NO3_H	1	Nitrate Half-Saturation Coefficient for Denitrifying Heterotrophic Biomass	gNO3-N/m3
K_OH	0.2	Oxygen Half-Saturation Coefficient for Heterotrophic Biomass	gO2/m3
K_O_AN	0.01	Oxygen Inhibition Coefficient for Anammox Autotrophic Biomass	g/m3
K_O_NH	0.6	Oxygen Half-Saturation Coefficient for NH4 Oxidizing Autotrophic Biomass	gO2/m3
K_O_NO	1.5	Oxygen Half-Saturation Coefficient for NO Oxidizing Autotrophic Biomass	gO2/m3
K_SH	20	Substrate Half-Saturation Coefficient for Heterotrophic Biomass	gCOD/m3
K_X	0.03	Half Saturation Coefficient for Hydrolysis of Slowly Biodegradable Substrate	gCOD/gCOD
b_AN	0.0025	Decay Coefficient for Anammox Autotrophic Biomass	1/d
b_H	0.62	Decay Coefficient for Heterotrophic Biomass	1/d
b_NH	0.05	Decay Coefficient for NH4 Oxidizing Autotrophic Biomass	1/d
b_NO	0.033	Decay Coefficient for NO Oxidizing Autotrophic Biomass	1/d
k_h	3	Maximum Specific Hydrolysis Rate	gCOD/(gCOD*d)
mu_AN	0.019	Maximum Specific Growth Rate for Anammox Autotrophic Biomass	1/d
mu_H	6	Maximum Specific Growth Rate for Heterotrophic Biomass	1/d
mu_NH	0.8	Maximum Specific Growth Rate for NH4 Oxidizing Autotrophic Biomass	1/d
mu_NO	0.79	Maximum Specific Growth Rate for NO Oxidizing Autotrophic Biomass	1/d
n_NO2	0.6	Correction Factor for Anoxic Growth of Heterotrophs on Nitrite	-
n_NO3	0.6	Correction Factor for Anoxic Growth of Heterotrophs on Nitrate	-
Group: Operational			
pH_tank	7.9	pH	
Group: Stoichiometry			
Y_AN	0.159	Yield for Anammox (Anaerobic Ammonia Oxidisers) Biomass	-
Y_HNO2	0.44	Anoxic Yield for Heterotrophic Biomass on NO2 (nitrite)	-
Y_HNO3	0.44	Anoxic Yield for Heterotrophic Biomass on NO3 (nitrate)	-

Name	Default Value	Description	Unit
Y_HO	0.52	Yield for Heterotrophic Biomass on O2	-
Y_NH	0.15	Yield for Ammonium Oxidizing Autotrophic Biomass	-
Y_NO	0.041	Yield for Nitrite Oxidizing Autotrophic Biomass	-
f_XI	0.1	Fraction of Biomass Converted To Particulate Inert Matter	-
Group: Temperature correction			
Temp_Ref	20	Temperature	degC
theta_b_AN	0.096	Arrhenius constant for b_AN	
theta_b_H	0.113	Arrhenius constant for b_H	
theta_b_NH	0.094	Arrhenius constant for b_NH	
theta_b_NO	0.061	Arrhenius constant for b_NO	
theta_k_h	0.11	Arrhenius constant for k_h	
theta_kla	1.02	Temperature factor for the Kla	
theta_mu_AN	0.096	Arrhenius constant for mu_AN	
theta_mu_H	0.069	Arrhenius constant for mu_H	
theta_mu_NH	0.094	Arrhenius constant for mu_NH	
theta_mu_NO	0.061	Arrhenius constant for mu_NO	

Pre-screening of Model Parameters (5.6.2)

Calculation of Central Relative Sensitivity (CRS)

$$CRSi, j(t) = \frac{yi(t, \theta j + \Delta \theta j) - yi(t, \theta j - \Delta \theta j)}{2\Delta \theta j} * \frac{\theta j}{yi(t, \theta j)}$$

y: quantities; θ: variables; Δ: perturbation factor (chosen as 0.001); t: time; i: index of quantity; j: index of variable

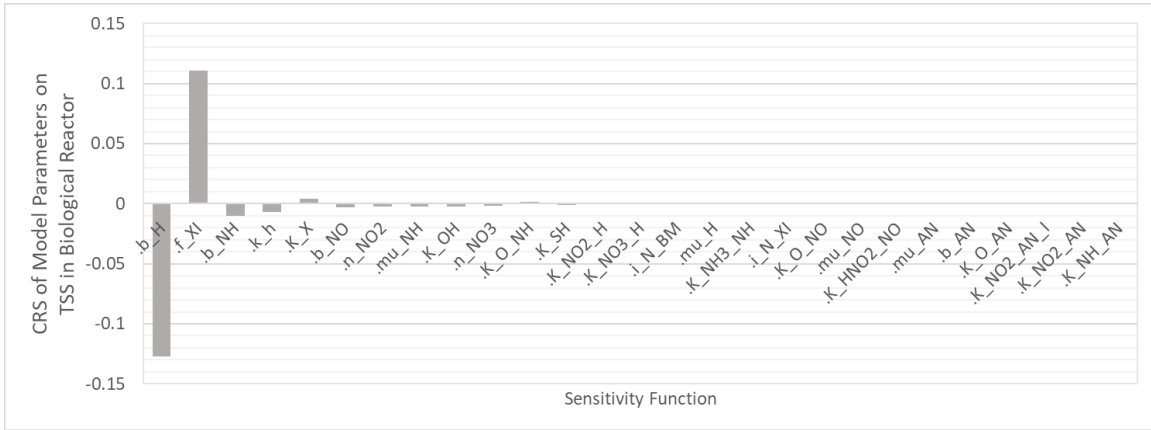|	
LSA evaluation criteria:	$|CRSi, j(t)| \geq 0.05$ on any model output
Model outputs/variables:	TSS concentration in biological reactors TSS concentration in underflow Air flowrate (Q_{air}) consumption in Basin 4 Effluent NH_4-N concentration Effluent NO_3-N concentration Effluent NO_2-N concentration
Model parameters:	27 model parameters (shown in grey in Table 1 above)

Figure 1. Calculated Central Relative Sensitivities of Model Parameters for TSS in Biological Reactors
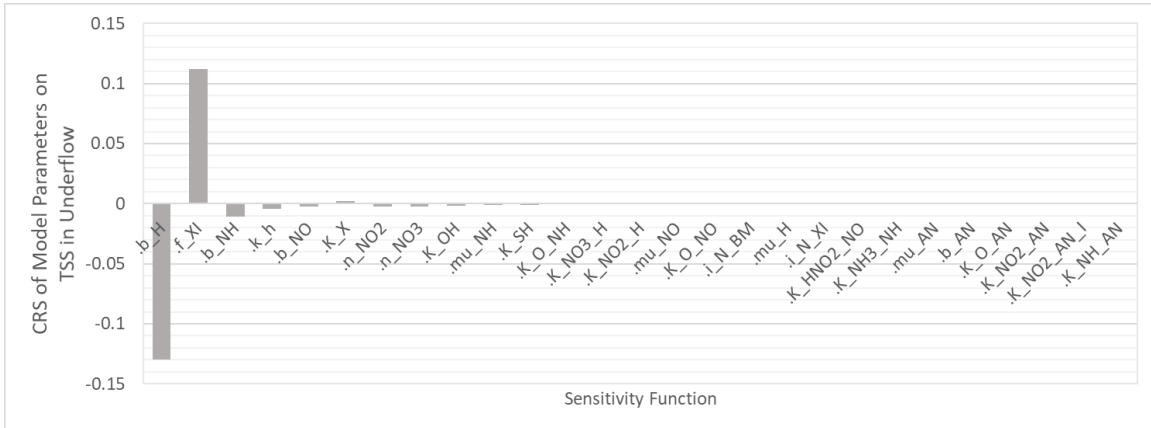

Figure 2. Calculated Central Relative Sensitivities of Model Parameters for TSS in Underflow
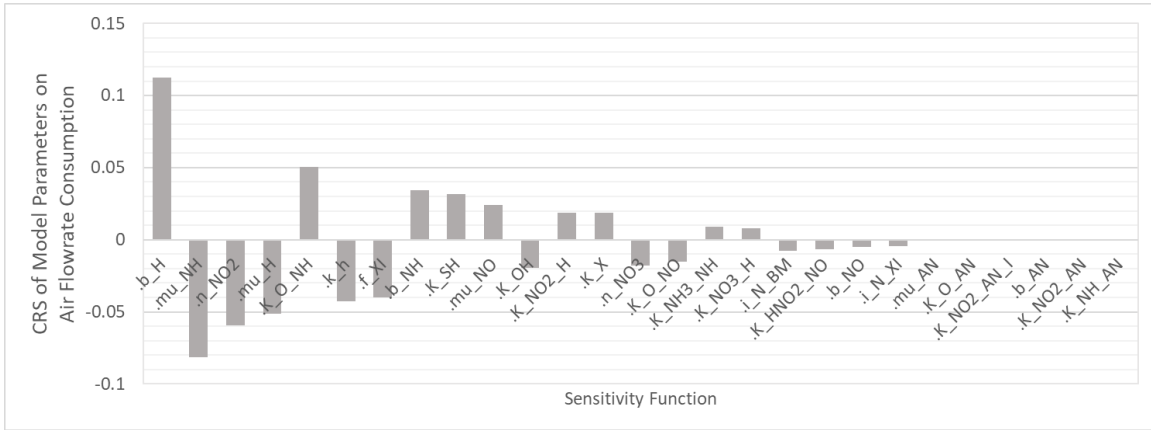
Figure 3. Calculated Central Relative Sensitivities of Model Parameters for Air Flowrate Consumption in Basin 4
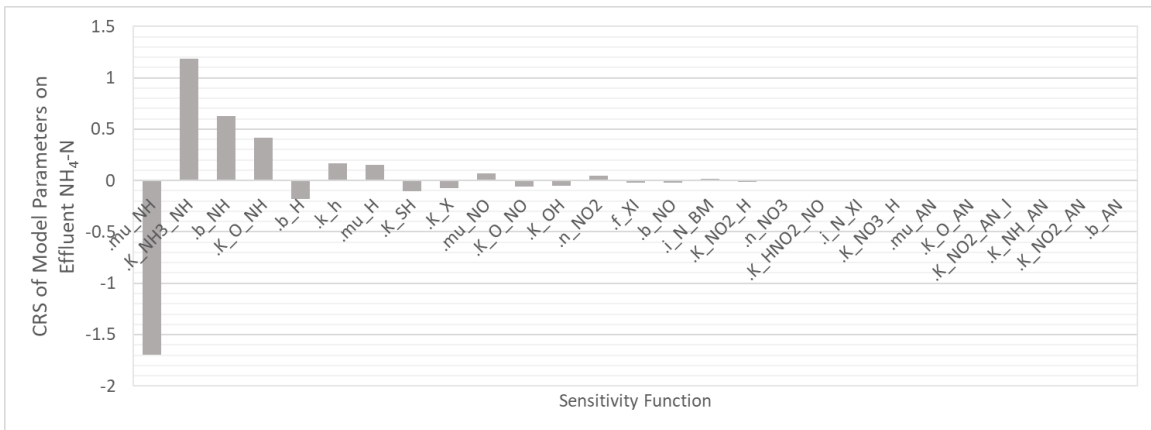

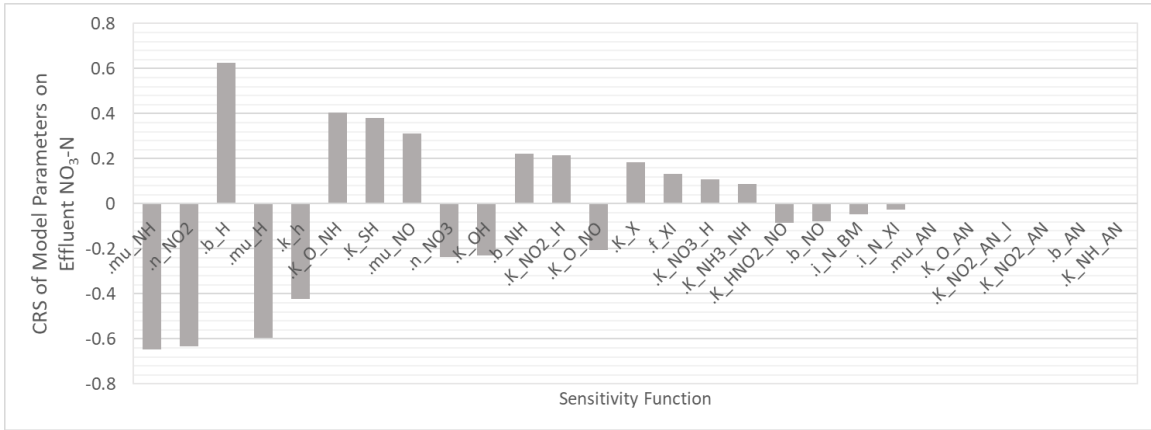**Figure 4. Calculated Central Relative Sensitivities of Model Parameters for Effluent NH$_4$-N**

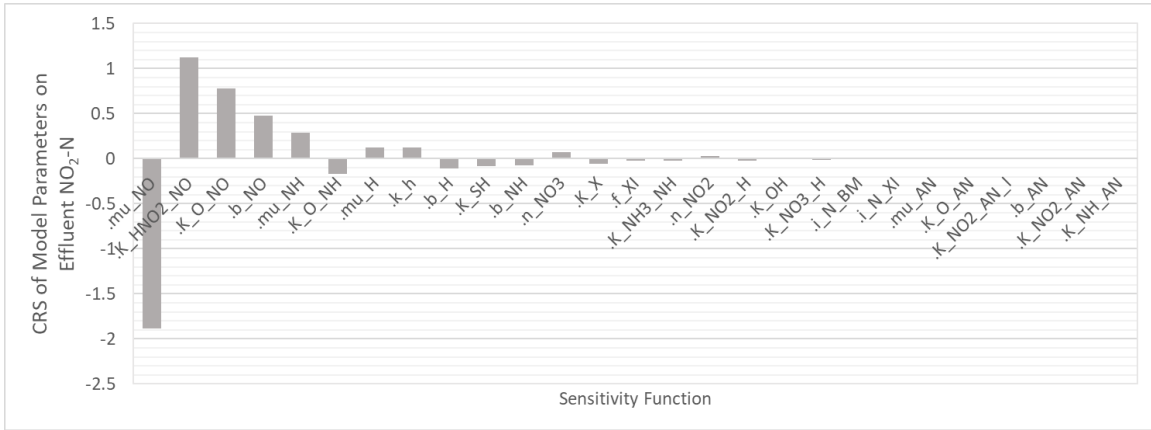**Figure 5. Calculated Central Relative Sensitivities of Model Parameters for Effluent NO$_3$-N**

Figure 6. Calculated Central Relative Sensitivities of Model Parameters for Effluent NO$_2$-N

Parameter Subsets Selection (5.6.3)

Table 2. Biokinetic Model Parameters Pre-screened for Calibration & Applied Parameter Value Ranges for Global Sensitivity Analysis

Parameters	Default (20ºC)	Literature Examples	Reference for Literature Examples	Uncertainty Range	Reference for Uncertainty Range	Applied Range for GSA
b_H	0.62	0.05–1.6 0.4-0.53 0.1-1.5	Jeppsson 1996 Hauduc et al. 2010 Weijers & Vanrolleghem 1997	2%	Hauduc et al. 2010	0.2-1.0
b_NH	0.05	0.15 0.05-0.2 0.071 0.08 0.07-0.17 0.04-0.2	Sin et al. 2008b Jeppsson 1996 Kampschreur et al. 2007 Jones et al. 2005 Hauduc et al. 2010 Weijers & Vanrolleghem 1997	25% 70%	Sin et al. 2009 Hauduc et al. 2010	0.02-0.1
b_NO	0.033	0.15 0.05-0.2 0.054 0.07-0.17 0.08 0.04-0.2	Sin et al. 2008b Jeppsson 1996 Moussa et al. 2004 Hauduc et al. 2010 Kampschreur et al. 2007 Weijers & Vanrolleghem 1997	25%	Sin et al. 2009	0.02-0.1
f_XI	0.1	0.08	Jeppsson 1996	-		0.05-0.15
k_h	3	2-5.2 3.0 2-4	Hauduc et al. 2010 Jeppsson 1996 Weijers & Vanrolleghem 1997	26 25%	Hauduc et al. 2010 Sin et al. 2009	1.0-5.0
K_HNO2_NO	0.000872	0.0014 0.27 0.05	Hellinga et al. 1999 Volcke et al. 2007 Jones et al. 2005	-		0.00002-0.0002
K_NH3_NH	0.75	0.1-0.5 1.0 0.468 0.75 0.8-10	Hauduc et al. 2010 Jeppsson 1996 Anthonisen et al. 1976 Van Hulle et al. 2007 Weijers & Vanrolleghem 1997	50% 25%	Sin et al. 2009 Hauduc et al. 2010	0.001-0.02
K_NO2_H	1	0.1-0.2 0.1-0.5 0.1-0.5	Hauduc et al. 2010 Jeppsson 1996 Weijers & Vanrolleghem 1997	80%	Hauduc et al. 2010	0.1-1.0

Parameters	Default (20ºC)	Literature Examples	Reference for Literature Examples	Uncertainty Range	Reference for Uncertainty Range	Applied Range for GSA
K_O_NH	0.6	0.2-0.75 0.4-2.0 0.5 0.25 0.1 0.1-1	Hauduc et al. 2010 Jeppsson 1996 Kampschreur et al. 2007 Jones et al. 2005 Sin et al. 2008b Weijers & Vanrolleghem 1997	0% 25%	Hauduc et al. 2010 Sin et al. 2009	0.1-0.75
K_O_NO	1.5	0.2-0.75 0.4-2.0 0.3 1.0 0.1-1	Hauduc et al. 2010 Jeppsson 1996 Sin et al. 2008b Kampschreur et al. 2007 Weijers & Vanrolleghem 1997	0% 25%	Hauduc et al. 2010 Sin et al. 2009	0.1-0.75
K_OH	0.2	0.05-0.1 0.01-0.2 0.1-1.0	Hauduc et al. 2010 Jeppsson 1996 Weijers & Vanrolleghem 1997	0% 50%	Hauduc et al. 2010 Sin et al. 2009	0.05-0.2
K_SH	20	5- 10 5-225 2.5-20	Hauduc et al. 2010 Jeppsson 1996 Weijers & Vanrolleghem 1997	50%	Hauduc et al. 2010	1.0-20.0
mu_H	6	4-5.7 0.6-13.2 2-10	Hauduc at al. 2010 Jeppsson 1996 Weijers & Vanrolleghem 1997	6% 25%	Hauduc et al. 2010 Sin et al. 2009	3.0-9.0
mu_NH	0.8	0.2-1.0 0.5 1.1 0.77-0.90 0.2-1.2	Jeppsson 1996 Kampschreur et al. 2007 Sin et al. 2008b Hauduc et al. 2010 Weijers & Vanrolleghem 1997	30% 5%	Hauduc et al. 2010 Sin et al. 2009	0.4-1.2
mu_NO	0.79	0.2-1.0 0.77-0.90 0.56 1.8 0.2-1.2	Jeppsson 1996 Hauduc et al. 2010 Kampschreur et al. 2007 Sin et al. 2008b Weijers & Vanrolleghem 1997	30% 5%	Hauduc et al. 2010 Sin et al. 2009	0.4-1.2
n_NO2	0.6	0.6-1.0 0.8	Jeppsson 1996 Hauduc et al. 2010	0%	Hauduc et al. 2010	0.2-1.0

Parameters	Default (20ºC)	Literature Examples	Reference for Literature Examples	Uncertainty Range	Reference for Uncertainty Range	Applied Range for GSA
n_NO3	0.6	0.6-1.0 0.8	Jeppsson 1996 Hauduc et al. 2010	0%	Hauduc et al. 2010	0.2-1.0

Standardized Regression Coefficient (SRC) Calculation

SRC method allows calculation of the SRC or slope of the multivariate linear regression model (Mannina et al. 2019; Saltelli et al. 2008).

$$y = b_0 + \sum_{i=1}^{n} b_i * x_i + \varepsilon$$

y: model output; x_i: model parameter; b_i: regression slope; ε: random error

$$SRC\ (x_i) = \beta_i = b_i * \frac{\sigma_i}{\sigma_y}$$

β_i: SRC of the relevant model parameter; σ_i: standard deviation of model parameter values; σ_y: standard deviation of model variable values

GSA evaluation criteria:	$|SRC\ (x_i)| \geq 0.1$ on any model output
Model outputs/variables:	TSS concentration in biological reactors TSS concentration in underflow Air flowrate (Q_{air}) consumption in Basin 4 Effluent NH_4-N concentration Effluent NO_3-N concentration
Model parameters:	17 model parameters (Table 2 above)
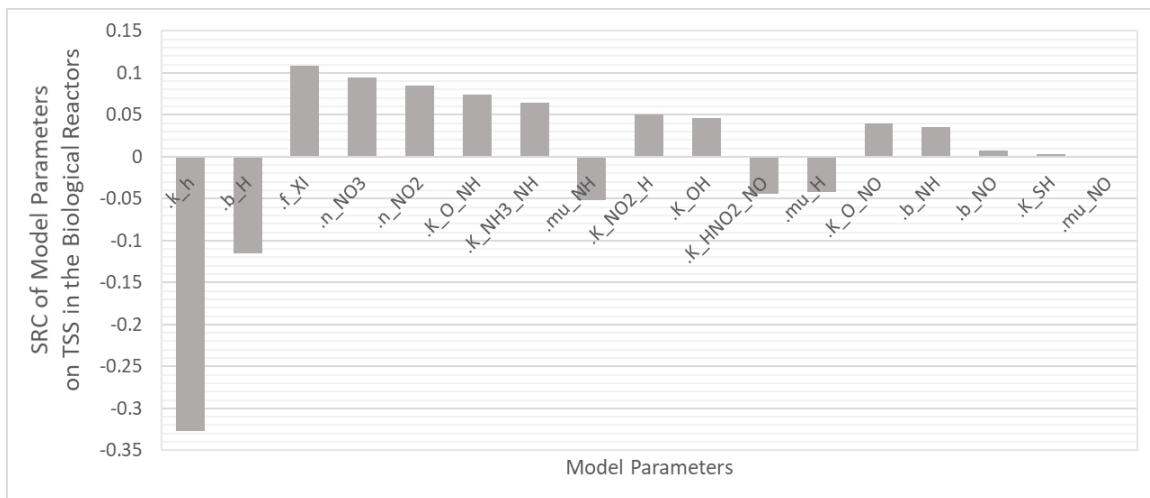
Figure 7. Calculated Standardized Regression Coefficients of Model Parameters for TSS in Biological Reactors
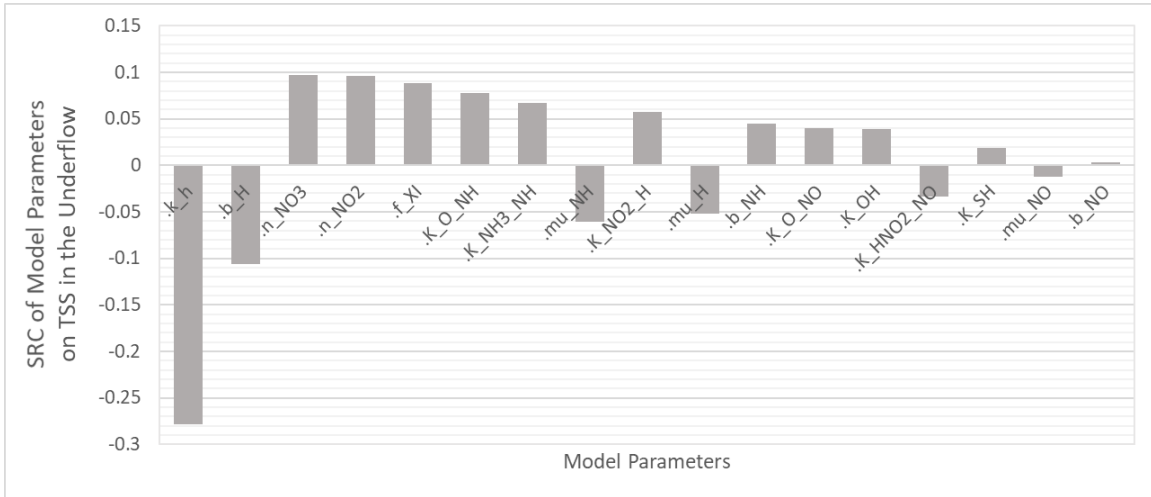

Figure 8. Calculated Standardized Regression Coefficients of Model Parameters for TSS in Underflow
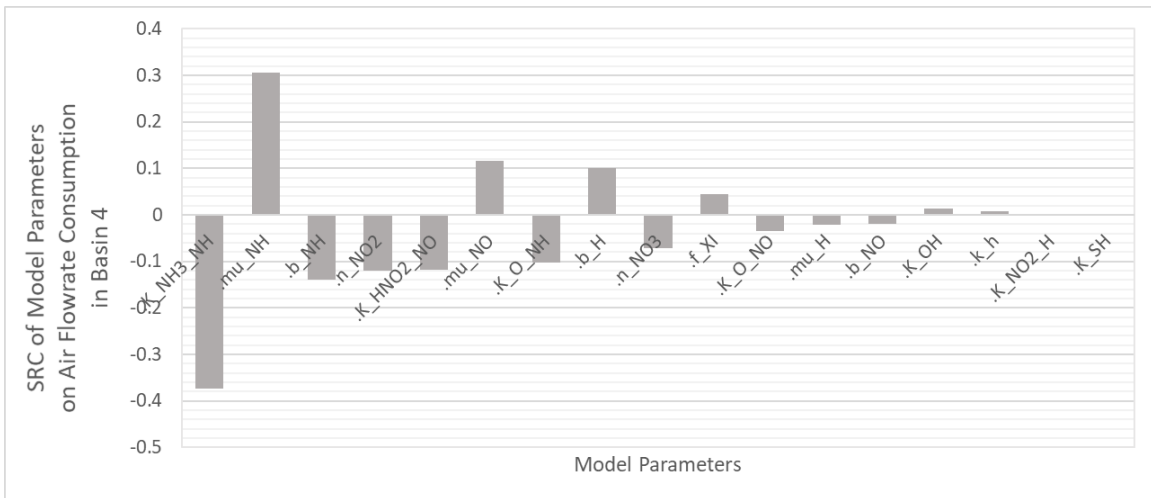

Figure 9. Calculated Standardized Regression Coefficients of Model Parameters for Air Flowrate Consumption in Basin 4
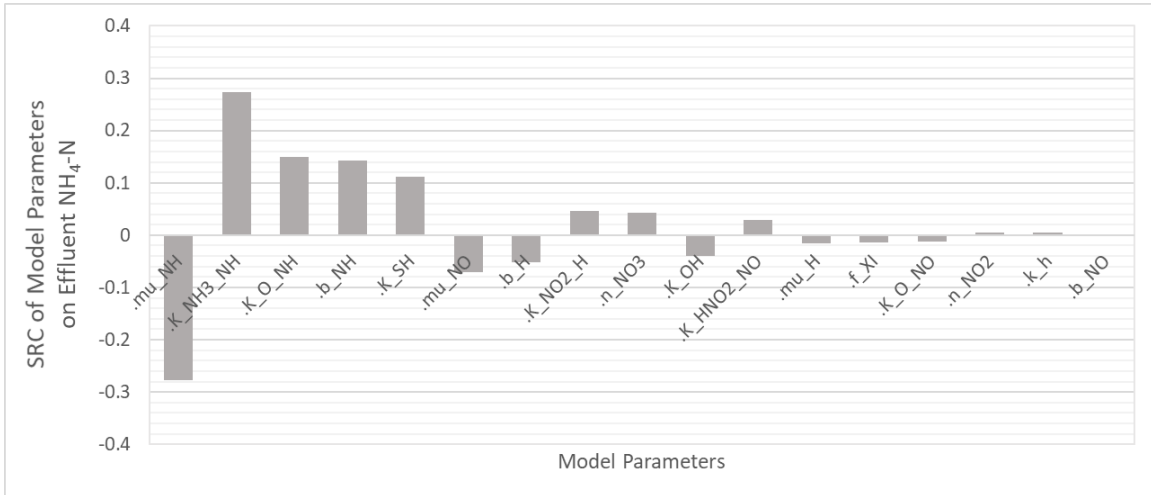
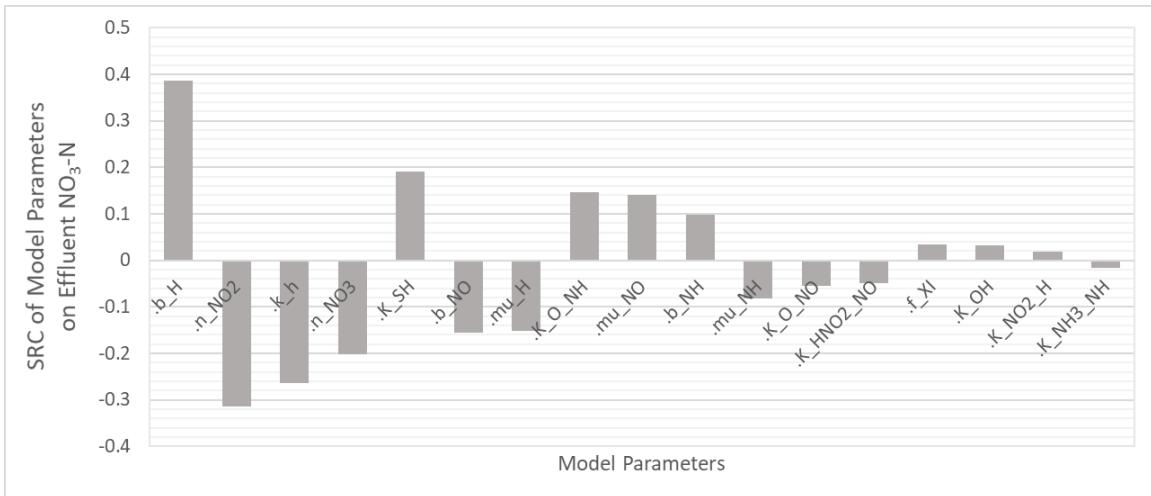**Figure 10. Calculated Standardized Regression Coefficients of Model Parameters for Effluent NH₄-N**

Figure 11. Calculated Standardized Regression Coefficients of Model Parameters for Effluent NO₃-N

Calibration of Parameter Subsets (5.6.4)

For the calibration of biokinetic model, the mean difference between the model predictions and measurement results of the relevant model variables (reference series) is calculated according to the equation below (Claeys 2008). Differences are calculated at each time point and then aggregated for the all model variables grouped for the relevant parameter subsets. For the difference calculation at each time points (objective function), sum of squared error (SSE) criterion is used. The weights for each model variable is chosen based on the average of measurement results to be able to normalize the calculated difference and make each variable equally weighted in the objective calculation. The parameter set that gives the minimum overall objective value is chosen as the optimal parameter set.

$$
J_{s_{i,l}}^{MeanDiff} = SSE = \sqrt{\frac{\sum_{m=1}^{n_{t_l}} w_{t_{l,m}} * \left(y_i(t_{l,m}) - \hat{y}_i(t_{l,m})\right)^2}{\sum_{m=1}^{n_{t_l}} w_{t_{l,m}}}}
$$

$J_s^{MeanDiff}$: Objective value for the parameter subset s

$w_{t_{l,m}}$: Weight of time point m of reference time series l

$\hat{y}_i$: Measurement of variable i

y_i : Model prediction of variable i

t : Time

n_t : Number of time points

Parameter Subset 1:

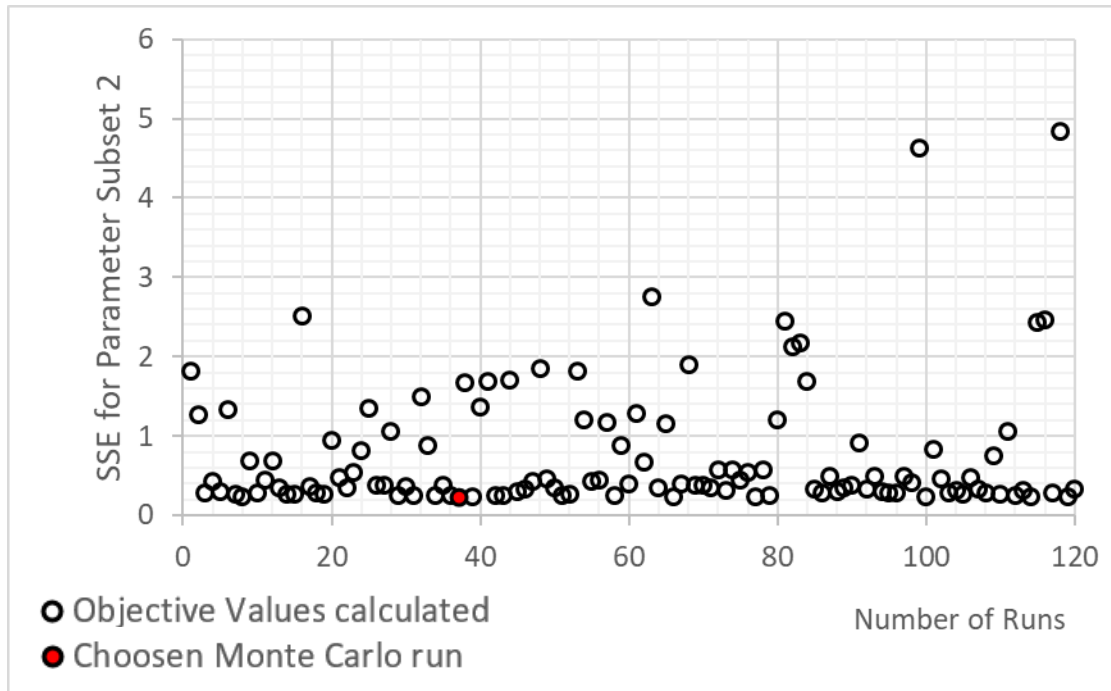| Evaluation criteria:	SSE		
Model outputs/variables:	TSS concentration in biological reactors TSS concentration in underflow		
Weights of variables	$w_{TSS \text{ concentration in biological reactors}} = 2$ $w_{TSS \text{ concentration in underflow}} = 1$		
Model parameters:	b_H	Decay Coefficient for Heterotrophic Biomass	
	f_XI	Fraction of Biomass Converted to Particulate Inert Matter	
	k_h	Maximum Specific Hydrolysis Rate	
Number of Monte Carlo Runs	80		
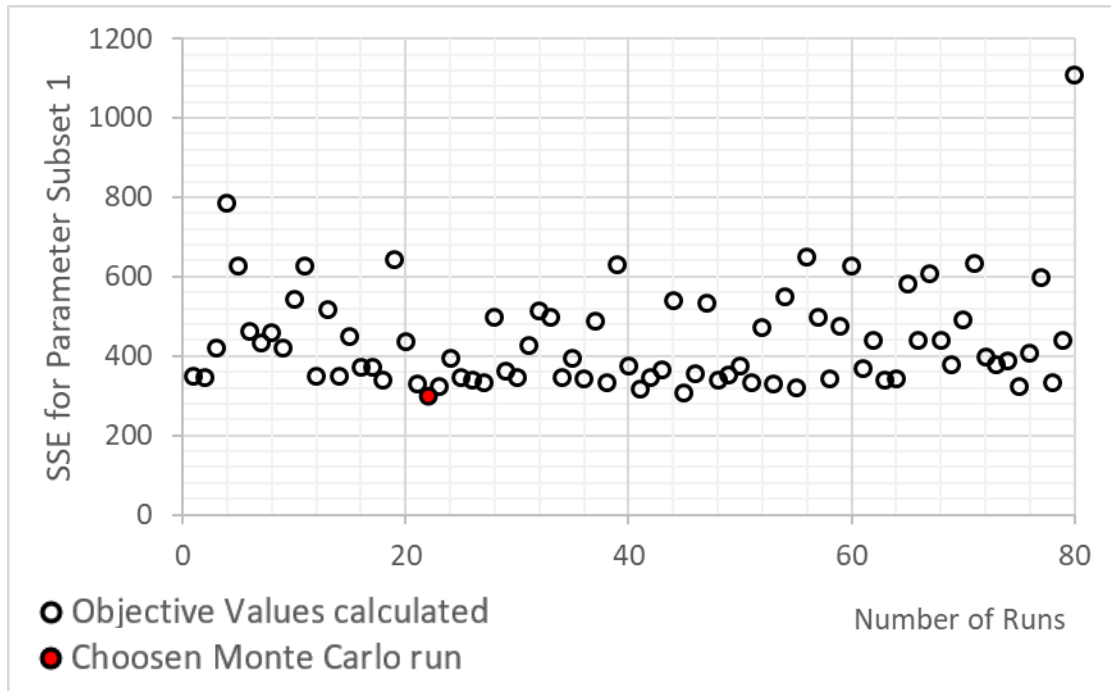
Figure 12. Calculated Sum of Squared Errors for each Monte Carlo run to calibrate Parameter Subset 1

Parameter Subset 2:

Evaluation criteria:	SSE	
Model outputs/variables:	Air flowrate (Q_{air}) consumption in Basin 4 Effluent NH$_4$-N concentration Effluent NO$_3$-N concentration	
Weights of variables	$w_{\text{Air flowrate (Qair) consumption in Basin 4}} = 0.03$ $w_{\text{Effluent NH4-N concentration}} = 40$ $w_{\text{Effluent NO3-N concentration}} = 1$	
Model parameters:	b_NH	Decay Coefficient for NH4 Oxidizing Autotrophic Biomass
	b_NO	Decay Coefficient for NO Oxidizing Autotrophic Biomass
	K_HNO2_NO	Nitrous oxide Half-Saturation Coefficient for NO Oxidizing Autotrophic Biomass
	K_NH3_NH	Ammonia Half-Saturation Coefficient for NH4 Oxidizing Autotrophic Biomass
	K_SH	Substrate Half-Saturation Coefficient for Heterotrophic Biomass
	mu_H	Maximum Specific Growth Rate for Heterotrophic Biomass
	mu_NH	Maximum Specific Growth Rate for NH4 Oxidizing Autotrophic Biomass
	mu_NO	Maximum Specific Growth Rate for NO Oxidizing Autotrophic Biomass
Number of Monte Carlo Runs	120	

185

Figure 13. Calculated Sum of Squared Errors for each Monte Carlo run to calibrate Parameter Subset 2

Parameter Subset 3:

|	
Evaluation criteria:	SSE
Model outputs/variables:	TSS concentration in biological reactors TSS concentration in underflow Air flowrate (Q_{air}) consumption in Basin 4 Effluent NH_4-N concentration Effluent NO_3-N concentration
Weights of variables	$w_{\text{Air flowrate (Qair) consumption in Basin 4}} = 0.03$ $w_{\text{Effluent NH4-N concentration}} = 40$ $w_{\text{Effluent NO3-N concentration}} = 1$
Model parameters:	K_NO2_H Nitrite Half-Saturation Coefficient for Denitrifying Heterotrophic Biomass K_O_NH Oxygen Half-Saturation Coefficient for NH4 Oxidizing Autotrophic Biomass K_O_NO Oxygen Half-Saturation Coefficient for NO Oxidizing Autotrophic Biomass K_OH Oxygen Half-Saturation Coefficient for Heterotrophic Biomass n_NO2 Correction Factor For Anoxic Growth of Heterotrophs on Nitrite n_NO3 Correction Factor For Anoxic Growth of Heterotrophs on Nitrate
Number of Monte Carlo Runs	200
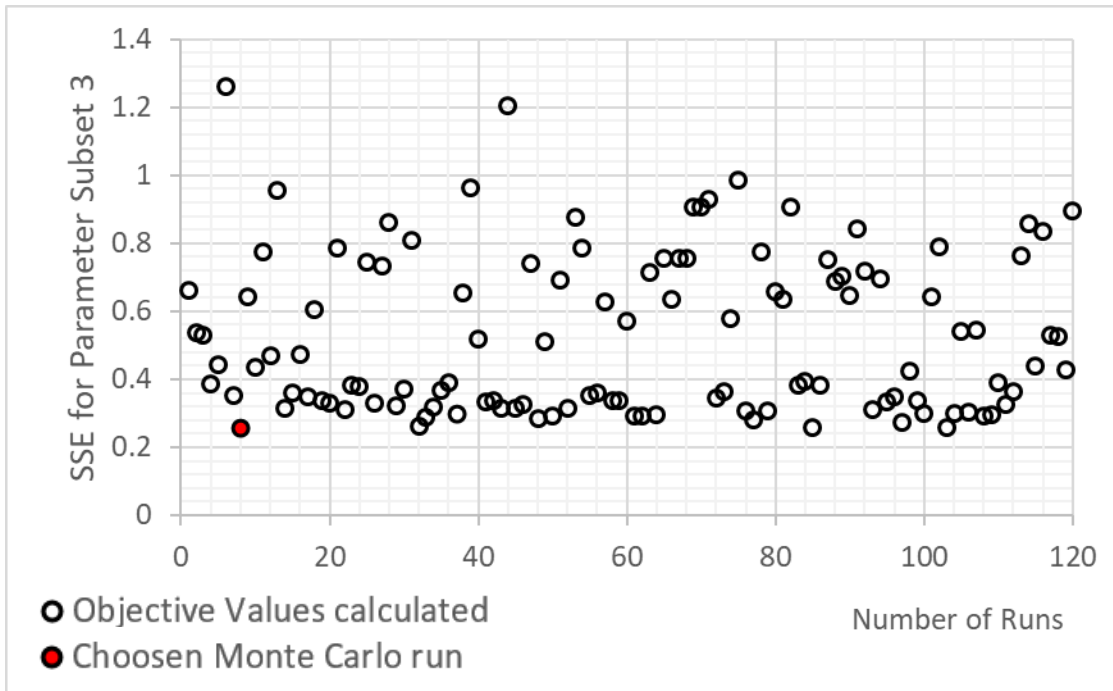
Figure 14. Calculated Sum of Squared Errors for each Monte Carlo run to calibrate Parameter Subset 3

Appendix III – Automatic AvN Control Results for the Time Periods that Successful Control Achieved
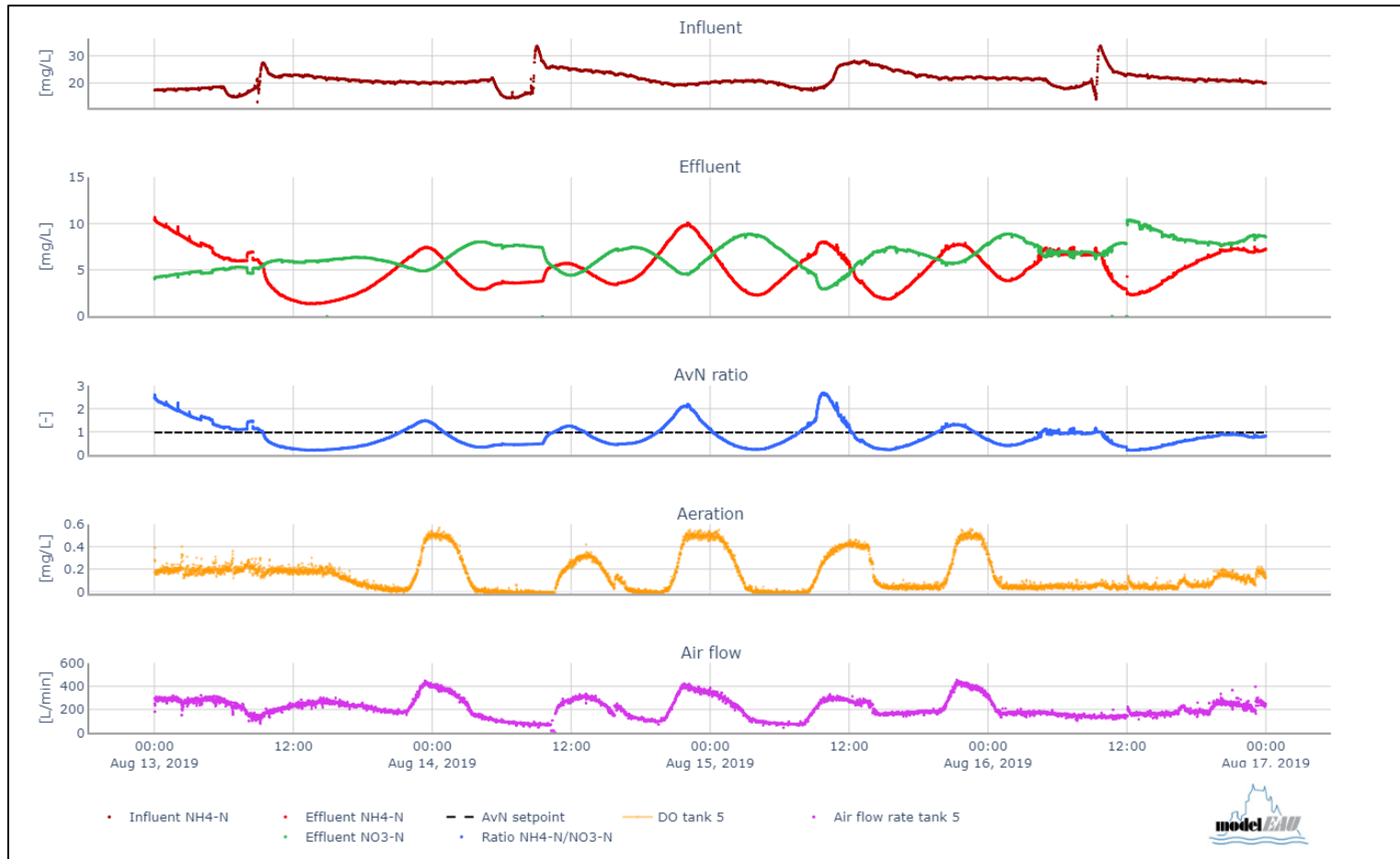
Continuous AvN

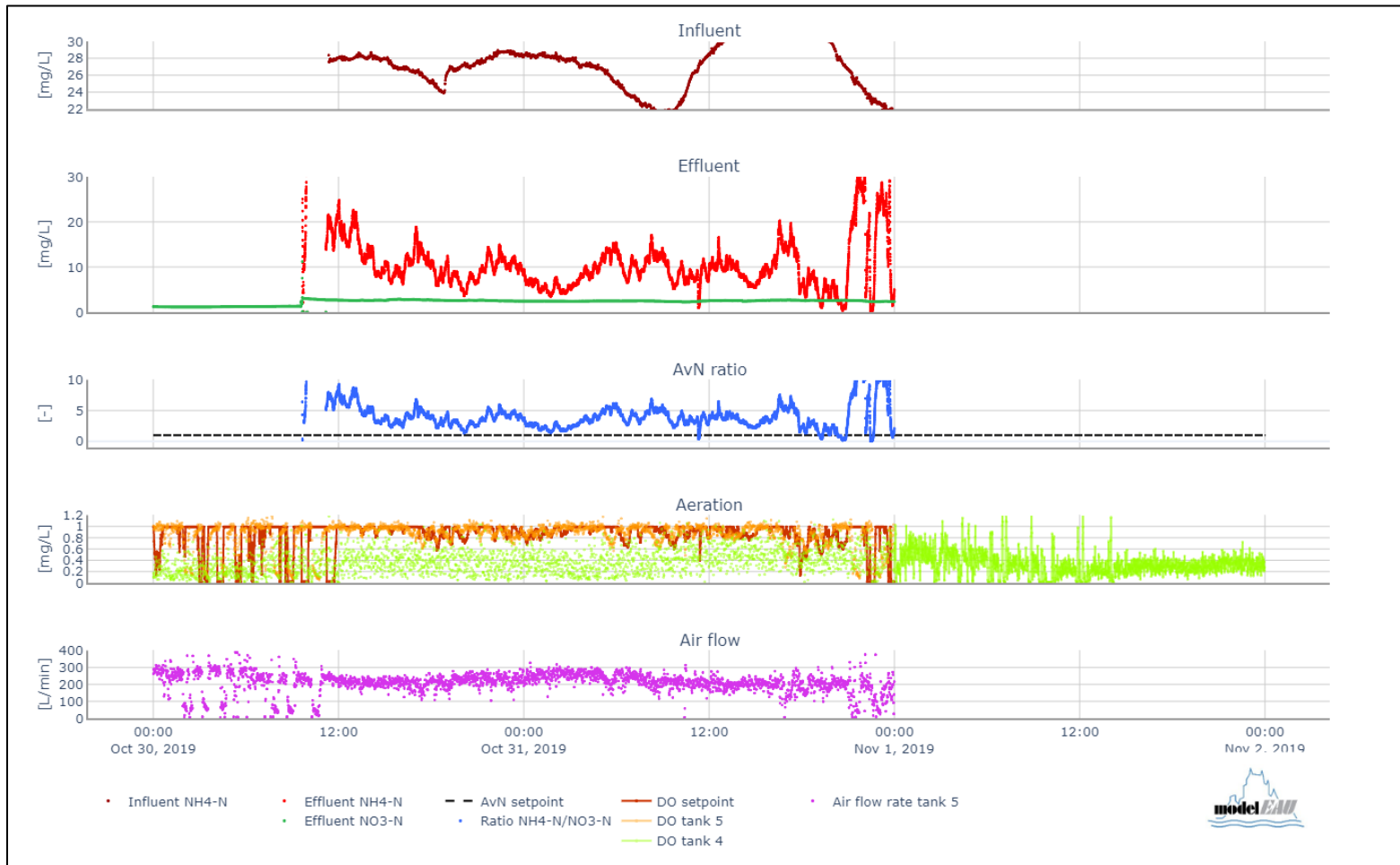**Figure 1. Continuous AvN Performance for the period 13th August – 17th August 2019**

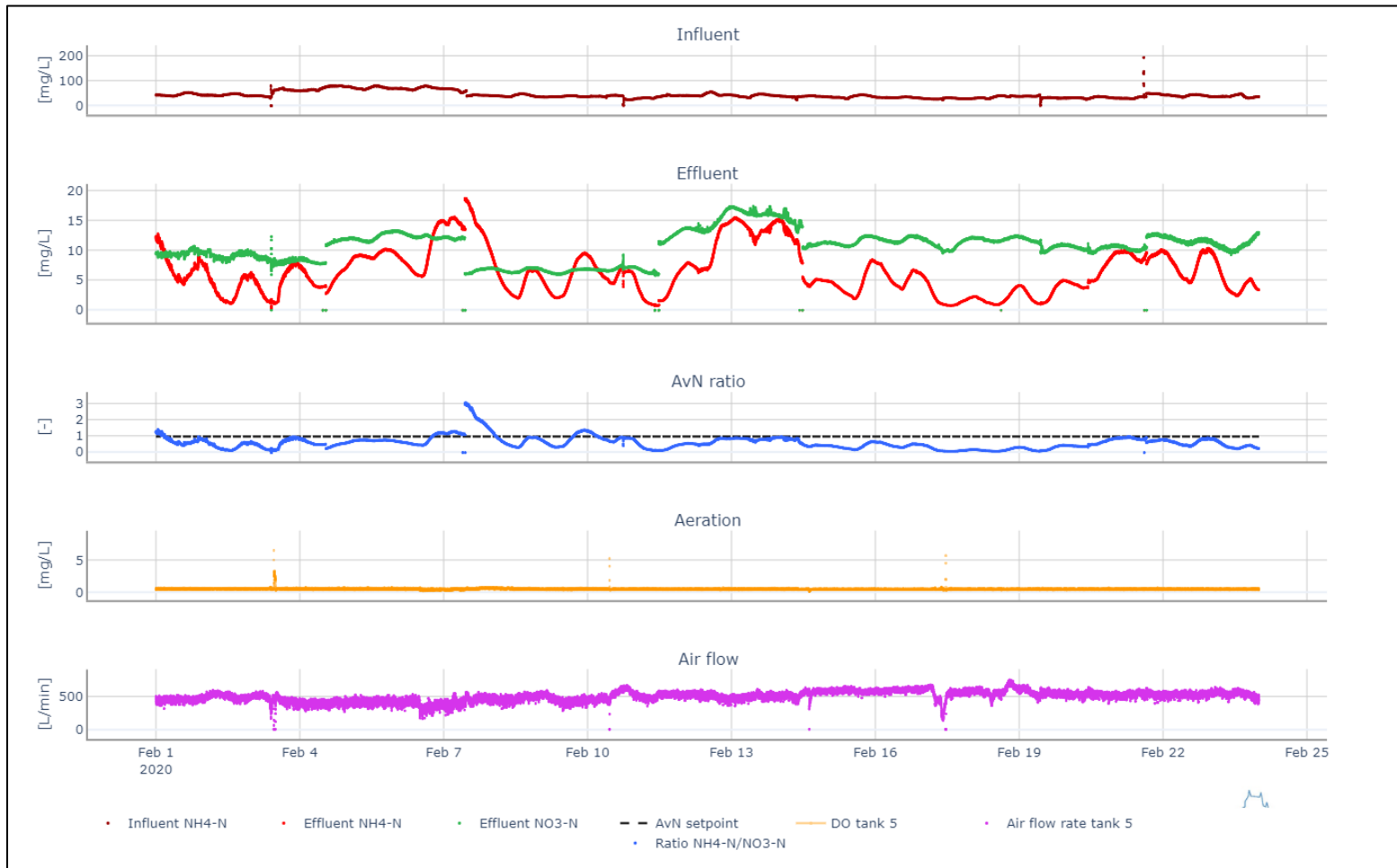**Figure 2. Continuous AvN Performance for the period 30th October – 1st November 2019**

Figure 3. Continuous AvN Performance for the period 1st February – 24th February 2020

Intermittent AvN

Figure 4. Intermittent AvN Performance for the period 30th November – 2nd December 2019

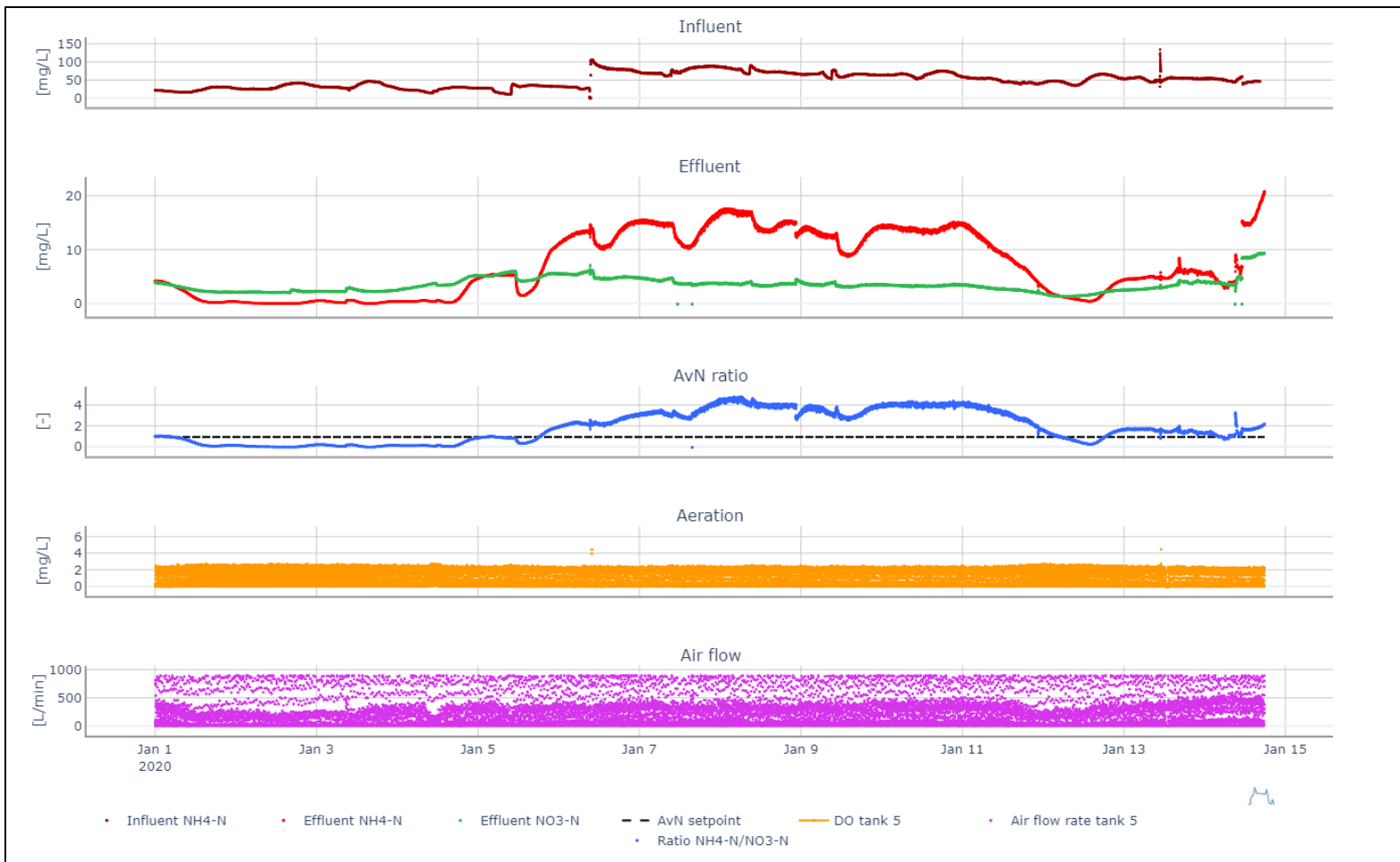**Figure 5. Intermittent AvN Performance for the period 2nd December – 14th December 2019**

Figure 6. Intermittent AvN Performance for the period 1st January – 15th January 2020
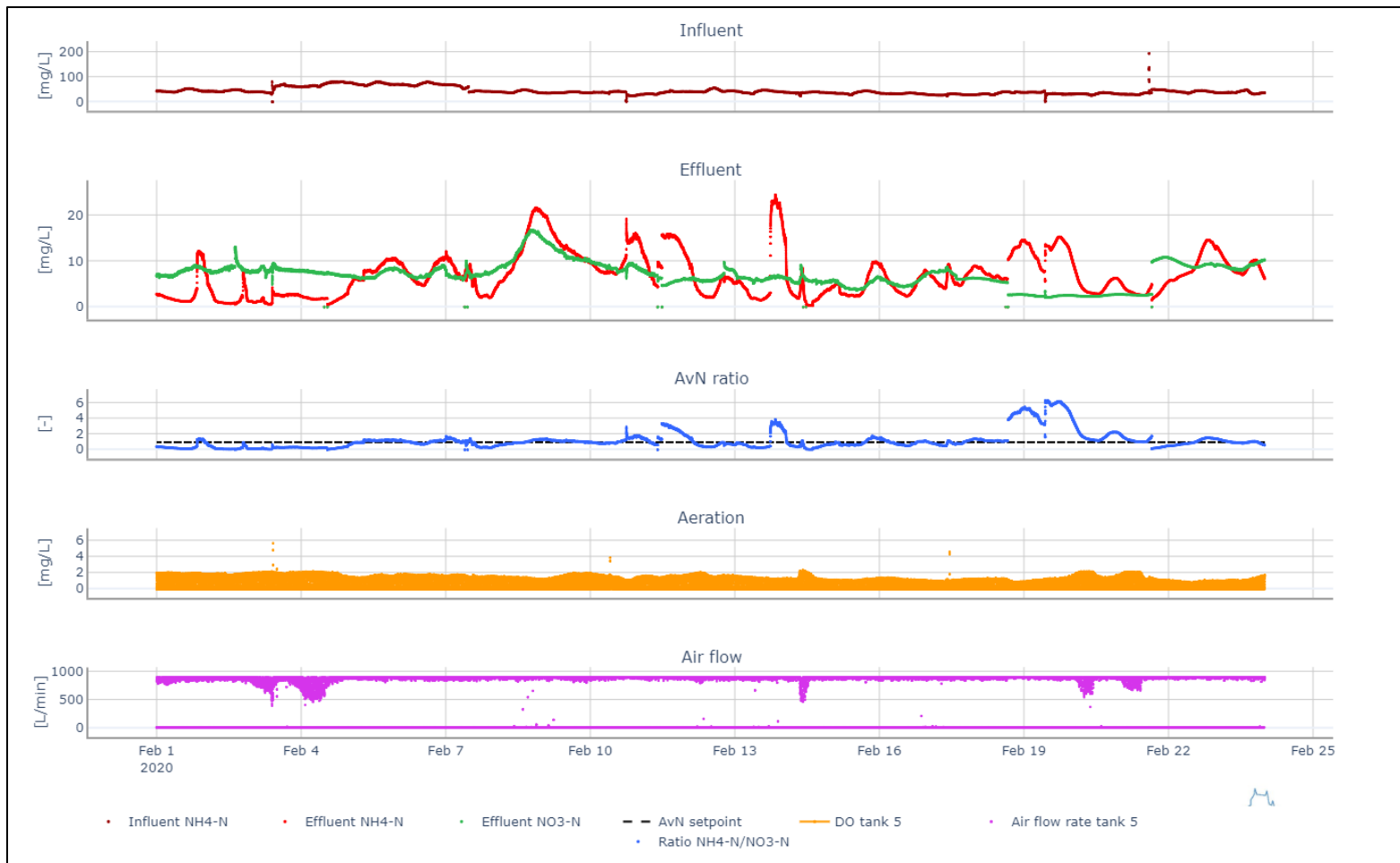
Figure 7. Intermittent AvN Performance for the period 1st February – 24th February 2020